First Principles Investigation of Thermoelectric Materials

SREEPARVATHY P. C.

A Thesis Submitted to

Indian Institute of Technology Hyderabad

In Partial Fulfillment of the Requirements for

The Degree of Doctor of Philosophy

भारतीय प्रौद्योगिकी संस्थान हैदराबाद

Indian Institute of Technology Hyderabad

Department of Physics

May 2019

Declaration

I declare that this written submission represents my ideas in my own words, and where ideas or words of others have been included, I have adequately cited and referenced the original sources. I also declare that I have adhered to all principles of academic honesty and integrity and have not misrepresented or fabricated or falsified any idea/data/fact/source in my submission. I understand that any violation of the above will be a cause for disciplinary action by the Institute and can also evoke penal action from the sources that have thus not been properly cited, or from whom proper permission has not been taken when needed.

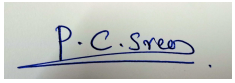

(SREEPARVATHY P. C.)

PH13P1007

Approval Sheet

This thesis entitled "First Principles Investigation of Thermoelectric Materials" by SREEPARVATHY P. C. is approved for the degree of Doctor of Philosophy from IIT Hyderabad

Prof. ZAKIR HOSSAIN
Professor
Dept. of Physics
IIT Kanpur
External Examiner

Prof. V. KANCHANA
Professor
Dept. of Physics
IIT Hyderabad
Adviser

IIT Hyderabad
Examiner

IIT Hyderabad
Chairman

Acknowledgements

From the beginning of the research work to the present thesis, i have been blessed to get enormous support from several people, without which i would not have carried out my research. Here i would like to mention few personalities, and show my gratitudes from the bottom of my heart.

Primarily, i would like to express my sincere acknowledgement to my supervisor **Prof. V. Kanchana** for unconditional support to fulfill this thesis work. Each step in this research work was carried out with her highly coherent suggestions and help, and i am sure these words are not sufficient to thank my supervisor. Highly organized discussions, and very healthy and homely atmosphere created by **Prof. V. Kanchana**, made my research working days in **Material Simulation and Design Lab** memorable. At this moment, i would like to recall all the support provided by my supervisor **Prof. V. Kanchana**, both professional and personal, and once again express the gratitude from my heart.

Apart from my supervisor, i would like to express my sincere gratitude to **Dr. G. Vaitheeswaran**, School of Physics, University of Hyderabad, for his unconditional support, valuable advices. Throughout my research work, i have received highly fruitful suggestions, help in finding promising literatures, and criticisms, which helped to elevate the research work, and once again i express sincere gratitude from heart.

Further, i would like to express my sincere gratitudes to **Prof. A. Svane**(deceased) and **Prof. N. E. Christensen**, Aarhus University, Denmark, **Prof. Chandan Mazumdar**, Saha Institute of Nuclear Physics, Kolkata, **Prof. Chandrabhas Narayana**, Jawaharlal Nehru Centre for Advanced Scientific Research, Bangalore and **Dr. P. Anees**, Indira Gandhi Centre for Atomic Research, Kalpakkam for the fruitful collaboration as a part of research work.

Here i use the opportunity to show the gratitude towards my doctoral committee members **Dr. Bhabani Shankar Mallik**, Department of Chemistry, and **Dr. J. Suryanarayana**, Department of Physics, for constructive criticism and valuable suggestions.

I would like to express my sincere acknowledgment to **Dr. Saket Asthana**, Head, Department of Physics, for providing helpful research atmosphere, and facilities. In addition, i thank all the faculty members of physics department, IIT Hyderabad.

Here i use the opportunity to show my sincere gratitude for **Prof. U. B. Desai**, the director of IIT Hyderabad for providing useful infrastructure for research and academic purposes, and i am extremely grateful for the financial support (for six months) to complete my thesis work. I would like to express my sincere thanks to Dean Academics, IIT Hyderabad.

I would like to acknowledge Ministry of Human Resource and Development (MHRD), New Delhi, India, for providing financial support for my research work without any difficulty. My sincere thanks to IIT Hyderabad for providing laptop for research work.

I would like to thank CDAC, National computing facility for computational support during my research work.

With huge pleasure i use this opportunity to show my gratitude to all the senior students in our lab, i cannot forget their constructive help and suggestions which help to me in each and ever step in my research work. Firstly i would like to thank **Dr. Swetarekha Ram**, for providing a helpful instructions for the work. Next i would like to thank **Dr. Vijay Kumar Gudelli**, for his unconditional support to understand my research field, and constructive criticism. Next i would like to thank **Dr. G. Shwetha** and **Dr. P. V. Sreenivasa Reddy** for their extreme help in

my research work. Once again i thank all my seniors for providing a homely atmosphere for me in the lab. Further i would like to thank few M.Sc students, **Mr. Anoop Chandran**, for fruitful discussions, and **Mr. Midhun**, **Mr. Kevin**. Next i would like to thank **Mr. P. Rambabu**, **Mr. Vineet Kumar Sharma**, **Ms. Karthika Menon** and **Ms. B. Anuroopa** for their great support and proving very healthy lab atmosphere.

Further, i would like to express my sincere thanks to all the research scholars of department of physics, IIT Hyderabad, and all staff members in Academics, Accounts, Library departments for their help throughout these years, and all the non-teaching staff in physics department, IITH.

Next i would like to mention my sincere acknowledgement to all the teachers who helped me to reach this stage. All the teachers in School of Physics, University of Hyderabad, and **Prof. D. Narayana Rao**, School of Physics, University of Hyderabad, for his great help and suggestions to fulfill my M.Sc project work. I use this opportunity to thank **Prof. Ashok Kumar Kapoor**, School of Physics, University of Hyderabad and **Prof. Ashok Chatterjee**, School of Physics, University of Hyderabad for their great support to understand the subject.

Further, i would like to mention few personalities who helped me to reach here. I would like to show my sincere acknowledgment to **Prof. Suresh Kumar**, Department of physics, Govt. College Madappally, **Prof. Ramakrishnan**, Govt. College Madappally, **Dr. G. Harikrishnan**, Govt. College Madappally, for their great support. Further i extend my sincere thanks to all faculty members in department of physics, Govt. College Madappally, and all the teachers in Memeunda Higher secondary school, Vadakara, and all the teachers in KRHS high school, Purameri, and all the teachers in VV LP School, Purameri.

I would like to thank all the friends in IIT Hyderabad, for providing homely feeling, and all the other friends for great support. I would like to mention few people for their help **Dr. Jishnu Suresh**, **Sapna Raveendran** and **Anjali**.

A special thanks to **Dr. Subramanyan Namboodiri Varanakkottu**, NIT Calicut, for his great support and useful suggestions.

I use this opportunity to show my sincere thanks to my parents, **E. K. Dhananjayan** and **P. C. Rajasree** for thier unconditional love and support, and my sister **Sreeranjini P. C.** I would like to show my special thanks to my husband **Nikhil Varma** for his great support to fulfill my research work, i am sure worlds are not enough to thank your patience. I would like to extend my gratitudes to my Father-in-law, **Rajan K.**, mother-in-law **Padmam K. C.**, brother-in-law **Neeraj Varma**, sister in-law **Anupama** for great support. I would like to thank all my family members for their unconditional support. A special thanks to my grandpa **Krishnan Namboodiri**, and all my other grandparents.

Dedication

To all my **Teachers** for their unconditional support
and **Family** and **Friends**

Abstract

The rapidly increasing energy demand in each and every domain of human life highlights the necessity of clean and renewable energy sources. Among them, thermoelectric (TE) energy conversion technique stands out due to the global availability of heat energy in the form of waste heat and find wide span of applications ranging from wrist watch to space applications. TE materials can play a major role in both power generation and waste heat recovery and can convert the heat energy to electricity. The search for better TE materials is still demanding due to the lesser efficiency of the same. The present thesis focuses on the search of novel TE materials fetching applications for a wide temperature range within the frame work of Density Functional Theory (DFT). DFT is a prominent tool for predicting the electronic structure and the diverse physical properties of materials and plays a leading role in computational condensed matter theory. Here in this thesis, we have investigated the TE properties of few interesting family of compounds and also tried to improve the TE properties by the application of hydrostatic/uni-axial strain and further attempted to explore the advantages of few exotic materials such as Dirac/topological insulator for TE applications. In the first chapter, we present a detailed investigation of electronic structure and TE properties of Zn based pnictide semiconductors in the form of $ZnXPn_2$ (X: Si, Ge, Sn; Pn: P, As, Sb). The entire compounds in this chapter belong to the well known chalcopyrite family and crystallize in tetragonal structure with space group $I\bar{4}2d$. The appropriate selection of exchange correlation functional is important and here the precise electronic structure of all the studied compounds are computed using Tran-Blaha modified Becke-Johnson (TB-mBJ) functional. The presence of a mixture of light and heavy bands in the band structure in general strengthen the TE properties, and the studied compounds shows this property. Computed TE properties unveils the p-type conduction to be favorable in $ZnXP_2$ (X: Si, Ge, Sn) and n-type conduction in $ZnGeP_2$ and $ZnSiAs_2$. Mechanical stability of the material is one of the criteria for device applications, and here we have confirmed the mechanical stability using the computed elastic constants. The TE properties such as thermopower, electrical conductivity scaled by relaxation time (will be addressing as electrical conductivity) and power factor for all the compounds are investigated by combining DFT with semi-classical Boltzmann transport theory. The thermopower of the investigated compounds are found to be higher compared with the prototype chalcopyrite TE materials, together with comparable values for electrical conductivity. In addition, the investigated compounds possess high thermopower compared to other established TE materials, which motivates further research in these compounds. Overall the considered compounds are found to possess appreciable TE coefficients, and we have analyzed the effect of hydrostatic strain on two of the investigated compounds $ZnGeSb_2$ and $ZnSnSb_2$. Among these, $ZnGeSb_2$ turned to be very promising TE material with huge power factor of the order of 3×10^{17} W m^{-1} K^{-2} s^{-1} due to the huge electrical conductivity around 8.5×10^{25} Ω^{-1} m^{-1} s^{-1}, observed in its massive Dirac state. The calculated electrical conductivity is higher than the well established Dirac materials, and is almost carrier concentration independent with similar behaviour for both 'n' and 'p' type carriers. Detailed analysis of the projected band structure reveals the 's', 'p' band inversion around Γ high symmetry point in the tensile strained state of $ZnGeSb_2$ and $ZnSnSb_2$. The possibility of low value for thermal conductivity is also evident from the phonon dispersion plot of $ZnGeSb_2$ and from Debye temperature. Application of systematic hydrostatic strain on $ZnGeSb_2$ and $ZnSnSb_2$ reveals the gradual phase change of $ZnGeSb_2$ from a normal semiconducting state, through massive Dirac states, to a topological semi-metal, whereas $ZnSnSb_2$ is transfered from normal semiconductor to metal to-

gether with a band inversion. The maximum power factor is observed in the massive Dirac states of $ZnGeSb_2$ compared to all other compounds. In the next chapter, we have investigated the electronic structure, mechanical and TE properties of few natural bulk super lattice materials, and report the high thermopower values together with the probability of low thermal conductivity in the studied series. The study includes BaXFCh (X: Cu, Ag, Ch: S, Se, Te), LaXSO (X: Cu, Ag) and SrCuTeF , and crystallize in tetragonal structure with space group P_4/nmm. The possibility of low thermal conductivity is predicted from the obtained elastic constants and few well established models such as Cahill's model and Slack's model. The huge difference in the band dispersion along the different crystallographic directions of the investigated compounds reveal the quasi two dimensional behavior of band structure in the valence band, and this is confirmed through effective mass calculations. The significant difference in effective mass along different crystallographic directions in valence band introduces an anisotropy in the transport properties. The properties along 'a' axis is found to be more favourable for hole doping. The magnitude of thermopower of these compounds are highly comparable with other established TE materials. In addition to these, the parameter A ($S^2\sigma/\tau$T/ κ_e/τ), which helps to decouple the relaxation time from our calculations is also calculated, and it reveals the potential TE properties of the considered compounds. Next chapter deals with a detailed electronic structure calculation, which reveals the strong topological insulating nature of a series of compounds CaSrX (X: Si, Ge, Sn, Pb), together with striking TE properties. The electronic structure of all the compounds are studied as a function of uni-axial strain and an emergence of Dirac semi-metallic state has been observed in CaSrX (X: Si, Ge, Sn, Pb), which is induced by uni-axial strain along 'b' axis. CaSrSi and CaSrGe evolved as normal semiconductor with uni-axial strain, and remaining compounds are found to preserve metallic states within the studied strain range. Since the investigated compounds preserve time reversal symmetry and inversion symmetry, the trivial and non-trivial topological phases are evaluated by band inversion and Z_2 topological invariants. An unusual thermopower oscillations has been observed at these Dirac semi-metallic states. Further the TE properties at strong topological insulating state and normal insulating state are summarized, which reveals the potential TE properties of these materials. In the last chapter of the results, we deal with the electronic and TE properties of few transition metal dichalcogenides, which are less investigated. We have chosen pyrite structure OsX_2 (X: S, Se, Te) and triclinic structure ReX_2 (X: S, Se). First we report the electronic structure and TE properties of OsX_2 (X: S, Se, Te), and find a giant value of thermopower of magnitude ranging from 600 μVK^{-1} to 800 μVK^{-1} for a wide temperature range of 100 K - 500 K for hole doping (at 10^{18}cm^{-3}), which is higher than the value found for well established TE materials. The optimized structural parameters are in good agreement with available experimental reports. The mechanical stability of OsX_2 is confirmed from the computed elastic constants. The band gap of the investigated compounds is examined by several exchange correlation functionals, and TB-mBJ with modified parameters is found to be the best for OsX_2. The heavy valence bands stimulates the thermopower value for hole doping and light conduction bands enhances the electrical conductivity values for electron doping, enabling both 'n' and 'p' type doping to be favourable for TE applications at higher concentrations (10^{20}cm^{-3}), which brings out the device application. Study on OsX_2 unveils the possibility of TE applications for all the examined compounds for a wide temperature range (100 K to 500 K), and OsS_2 specifically is a good alternate with the operating temperature ranging from 100 K - 900 K. Further, we have studied a highly versatile system ReS_2, which transforms from a semiconductor to a two dimensional

metal under uni-axial compressive strain along 'a' direction in both bulk and monolayer. The 2D nature is realised from highly flat Fermi surfaces and anisotropic transport properties. Moreover the layer independent electronic structure properties are revisited and TE properties of ReS_2 in bulk, monolayer and bilayer forms reveals the competing TE coefficients in each form. The in-plane power-factor shows an enhancement over 'c'-axis value as a function of strain, which is almost two orders of magnitude. In addition, strain induced tunable in-plane anisotropy of almost one order has been observed in both bulk and monolayer ReS_2 (around 20%), which further open up the possibility of TE application as nanowires. Our analysis reveals a wide range of application for ReS_2 in the field of thermoelectrics as bulk and thin films for a wide temperature range. The magnitude of TE coefficients are comparable with other well established transition metal dichalocogenides.

Overall, the present thesis addresses the potential TE properties in few compounds for a wide temperature range, and in each family of compounds we have attempted to enhance the power factor by the application of hydrostatic/uni-axial strain. In the case of $ZnGeSb_2$, we could enhance the power factor value to 3×10^{17} W m^{-1} K^{-2} s^{-1}, which is huge compared to normal power factor range. We believe that, the experimental realization of this potential TE material would be very fascinating and the understanding about thermal conductivity would further help in predicting the ZT. From our calculations, we could show that the super lattice structures possess low thermal conductivity, and if one can realize the potential TE application from experimental studies, it would be a great opening. Further, in the case of Ca based compounds, we could predict the coexistence of strong topological insulating nature and potential TE properties, and the exact benefit of strong topological nature with conducting surface states towards TE applications can be understood from the total electrical conductivity (from bulk and surface states), which is beyond the scope of present thesis, and we believe that this could be taken as future study. In the case of ReS_2, the layer independent TE properties can lead to several applications in thin film TE, and further strain induced in-plane anisotropy also can be taken as future study, where one can understand the TE properties in nano wire ReS_2. Altogether, the present thesis opens up new possibilities from the electronic structure point of view, but in reality for a TE device, the understanding of thermal conductivity, and figure of merit are very crucial. If one can utilize the predicted results, and calculate all the other vital parameters, we believe few of the compounds might turn out to be good TE materials.

Contents

Nomenclature

List of symbols

k_B	Boltzman's constant
h	Planck's constant
$\hbar$	Reduced Planck's constant (J. s)
V_{eff}	Interaction between the electrons
	mediated by the electron-phonon coupling
M	Atomic mass of ion
$N(E_F)$	Density of states at Fermi level
E_F	Fermi level
V_{ext}	External nuclear potential
$\widehat{H}$	Hamiltonian
m_i	Electronic mass
Z_I	Nuclear charges
M_I	Nuclear mass
$\widehat{T}_e$	Kinetic energy of the electron
$\widehat{V}_{ee}$	Potential energy of the electron
$\widehat{T}_n$	Kinetic energy of the nucleus
$\widehat{V}_{en}$	Potential energy of the electron and nucleus
$\widehat{V}_{nn}$	Potential energy of the nucleus
$\widehat{\theta}$	Time reversal operator
$\widehat{K}$	Conjugation operator
E_0	Ground state energy
E_{xc}	Exchange-correlation energy
V_{KS}	Kohn-Sham potential
j_l	Spherical Bessel functions
$n(r)$	Electronic density as a function of position
R_{MT}	Muffin-tin radius
K_{Max}	Plane wave cut-off
G_{max}	Charge-density Fourier expansion (a.u.$^{-1}$)
C_{ij}	Elastic constants (GPa)
G_H	Hill's shear modulus (GPa)
G_R	Reuss shear modulus (GPa)
G_v	Voigt shear modulus (GPa)
E	Young's modulus (GPa)
B	Bulk modulus (GPa)
A	Anisotropy factor
v_l	Longitudinal sound velocity (km/s)
v_t	Transverse sound velocity (km/s)
v_m	Mean sound velocity (km/s)
Θ_D	Debye temperature (K)
N_A	Avogadro's number
n_e	Electron concentration
n_h	Hole concentration

Greek Letters

ψ	wave function
σ	Electrical conductivity
τ	Relaxation time
ρ	Density
Ω	Ohm
κ	Thermalconductivity
κ_e	Electronic thermalconductivity
κ_l	Lattice thermalconductivity

Subscripts

i, j	Number of electron index
I, J	Number of nucleus index
e	Electron
n	Nucleus

Abbreviations

DFT	Density-functional theory
LDA	Local density approximation
GGA	Genelarized gradient approximation
TB-mBJ	Tran Blaha-modified Becke-Johnson
LAPW	Linearized augmented planewave
FP-LAPW	Full-potential linearized augmented planewave
SOC	Spin-orbit coupling
BZ	Brillouin zone
DOS	Density of states
HF	Hartree-Fock
AE	All electron
ps	Pseudo function
ZT	Figure of merit

Chapter 1

Introduction

The appropriate utilization of green and renewable energy sources can control the drastic changes induced by the global warming and balance the living conditions on earth. The need of renewable energy sources in the context of energy crisis and environmental pollution has been adequately studied and discussed in several articles[1, 2], and biomass, hydropower, wind energy, solar energy, thermoelectric energy etc, are few of the well accepted renewable energy sources. To balance the environmental issues such as climate changes, ozone layer depletion, air pollution, and the global energy consumption rate, the efficiency and large scale usage of green energy techniques have to be improved. A close analysis of the estimated usage of the above mentioned renewable energies disclose the fact that the power production by non-renewable energy is still higher than the same with the renewable energies. The availability of resources on time is one of the main challenge in using renewable energy source, which is very crucial in the case of wind and tidal energy sources, which eventually restrict the proper utilization of these green energy sources. Additionally, localized application also remains a challenge in utilizing these sources. The waste heat is considered to be the major global issue, which drastically affects the global climate system. Report says that more than 50% of energy is wasted as heat[3, 4, 5], ranging from house hold waste to industrial waste. Waste heat recovery is one of the major challenges and the process of waste heat recovery include extracting and transferring heat through the medium of gas, liquid or solid and convert to electrical or mechanical power. Several techniques such as Rankine cycle, Organic Rankine cycle, air preheaters, etc, have been proposed for this waste heat recovery and power generation[3, 4, 5]. Among these methods, solid state thermoelectric energy conversion technology gained additional attraction due to the absence of moving parts, lack of chemical reactions, sustainable life etc. Thermoelectric materials can convert heat in to electricity, which can play a major role in reducing the energy crisis by utilizing the heat. TE device is a solid state device, and it depends on material properties. Similar to any other device applications, materials for TE device also should satisfy certain qualities such as earth abundance, stability up to higher operating temperature, optimum mechanical properties, etc. The limitation of TE device is the efficiency, which is low around 15%, and the challenge in this field is to improve the efficiency by using several techniques, and the research on this energy conversion method is demanding. Since TE materials play the major role in this energy conversion technology, the exploration of potential materials with good TE properties can contribute to this field. The present thesis focuses on the TE properties of few novel materials, and we have analyzed

the possibilities of tuning the TE parameters of the same. Upcoming sections describe the history and development of TE materials, current status, etc.

1.1 Brief history

The footing of TE energy conversion technology is the TE effect, which explains the energy transformation between heat and electricity, and there are three basic effects which are Seebeck effect, Peltier effect and Thomson effect reported by three scientists, Seebeck, Peltier and Thomson. In this section, we would like to discuss the history and development of this field. The report says that the birth of TE phenomena had happened more than 15 decades ago, when a German physicist Thomas Johann Seebeck noticed the deflection of a compass magnet due to the circuit made from two different metals with their junctions kept at two different temperatures. In 1821, Seebeck reported this phenomena as Seebeck effect. Initially he thought that the deflection happened due to earth's magnetic field and very soon he had explained the reason as TE effect. The Seebeck effect is described as the emergence of a potential difference in a circuit, in which the junction of two dissimilar metals are kept at different temperatures, and this is a direct conversion of heat energy into electricity[6]. The amount of induced potential difference ∇V is directly proportional to the temperature difference between the junctions ∇T, and Seebeck coefficient is defined as the voltage generated by unit temperature difference α (or S) $= \nabla V/\nabla T$. Later in 1934, Jean Charles Athanase Peltier discovered the reverse process, where a reduction/increment in temperature had been observed due to the passage of current through a circuit with dissimilar metals. The change in temperature is proportional to the amount of electric current passing through it, and the coefficient is known as Peltier coefficient. Later in 1954, William Thomson came up with another thermoelectric effect, in which he described the ejection or absorption of heat when an electric current passes through a circuit made up of one single material with temperature difference along the length[7]. In addition to that, he had derived the relation between Seebeck and Peltier effect. The above mentioned three effects are considered to be fundamental TE effects. Seebeck effect is the basis of thermoelectric power generation and Peltier effect is the basis of thermoelectric refrigeration. After the invention of these three thermoelectric effects, Edmund Altenkirch put forward a model, and had derived the maximum energy conversion efficiency, for both power generation and cooling system[8]. His model could explain a dimensionless quantity named as figure of merit (ZT), which would decide the capability of a thermoelectric system, and identified that, the material parameters such as Seebeck coefficient, electrical conductivity and thermal conductivity will play a crucial role in deciding the figure of merit. High ZT needs high Seebeck coefficient, large electrical conductivity and low thermal conductivity. Later in 1949, Abram Fedorovich Ioffe invented the modern theory of thermoelectricity, in which he suggested the advantages of semiconductors for thermoelectric applications[9]. The first realization of thermoelectric cooling using Bi_2Te_3 system was by H. Julian Goldsmid[10], and he is the author of a book named as "Introduction to thermoelectricity", which explains the details of thermoelectricity. Over these years, several research groups have been actively working to get high efficient TE devices, for which high ZT materials are important, and the literatures clearly show the growth of research on thermoelectricity, focusing on mainly two ways, one is on achieving high ZT materials and the other is mainly on designing potential TE devices. The current thesis is mainly focusing on the first part which involve the high ZT TE materials,

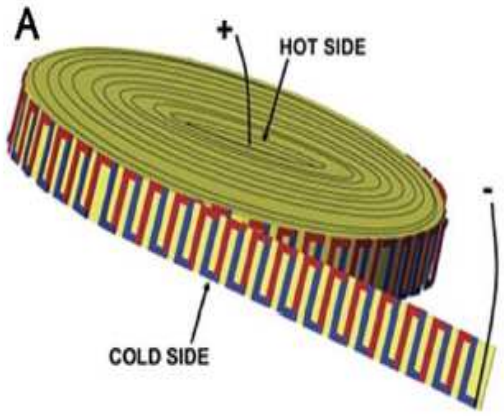

Figure 1.1: Schematic of a TE device (Figure has been taken from Ref[14])

where $ZT = \mathrm{S}^2\sigma/\mathrm{k}$, in which S is the Seebeck coefficient, σ is the electrical conductivity and k is the thermal conductivity (both electronic and lattice thermal conductivity terms are included in that), and T is the absolute temperature. Regarding the optimum ZT, several concepts have been discussed about enhancement of the power factor and suppressing the thermal conductivity. Eucken came up with an idea to reduce the thermal conductivity, where the point defects in alloys can cause the thermal conductivity reduction[11]. In 1990, Hicks and Dresselhaus addressed a new concept, which can be considered as the birth of new generation thermoelectric materials, and they explained the advantages of moving to low dimensional materials[12]. The traditional thermoelectric materials are Bi_2Te_3, PbTe, SiGe, etc, and ZT is reported to be below unity for these materials[13], and maximum efficiency estimated from this ZT is around 4% to 5%. Later on, the efficiency was enhanced by the size reduction and several nanostructured materials were explored and obtained ZT was approximately 1.7, and efficiency reached to 11% to 15%. Figure 1.1 represents a modern TE device, which is highly flexible consisting of metal films (Figure has been taken from Ref[14]. Now, several new methods are implemented to enhance the ZT value such as band engineering, connecting with other exotic properties like topological insulator etc. The upcoming section deals with the constituent parameters involved in ZT.

1.2 Constituent parameters involved in figure of merit

Obtaining a higher ZT value is considered to be a great challenge in this research field, which has been blocking the evolution of thermoelectric devices to a large scale production. The constituent parameters which decide the value of ZT are highly interrelated and the enhancement of one parameter may have a detrimental effect on other parameters. As we know, the figure of merit is defined as $ZT = S^2\sigma/k$, and for higher ZT value, we need higher value of thermopower, higher value of electrical conductivity and lower value of thermal conductivity. Each quantity discussed above depends on several material parameters, and the present section deals with the detailing of each quantity and aims at the improvement of each parameters. To begin with, we will discuss the Seebeck coefficient, which is also known as thermopower, then electrical conductivity followed by

thermal conductivity.

1.2.1 Seebeck coefficient (Thermopower)

As we discussed in the above section, Seebeck coefficient is the amount of voltage gained for an unit temperature gradient and the symbol is S with unit V/K. ZT is directly proportional to the square of thermopower, and it can be a deciding parameter for the performance of thermoelectric materials. Thermopower is a material dependent quantity, and the connection between thermopower and other parameters is defined using Mott formula, and it is given as

$$S = \frac{8\pi^2 k_B^2}{3eh^2} m^* T (\frac{\pi}{3m})^{2/3} \tag{1.1}$$

Here 'e' stands for the electron charge, 'k_B' represents the Boltzmann constant, 'h' is the Planck constant, 'n' is the carrier concentration , 'm' represents the effective mass and the absolute temperature is represented by 'T' . The thermopower is found to be directly proportional to effective mass and inversely proportional to carrier concentration. In addition, thermopower is directly proportional to temperature. Achieving higher value of thermopower implies the need for higher effective mass at low concentration range. In general, the presence of highly flat band and higher density of states near the Fermi level will help to enhance the thermopower.

1.2.2 Electrical conductivity

Unlike the thermopower, electrical conductivity is directly proportional to the carrier concentration and inversely proportional to effective mass, and this is evident from the Drude formula

$$\sigma = \frac{ne^2\tau}{m^*} \tag{1.2}$$

where 'n' is the carrier concentration, 'τ' is the relaxation time, and 'm*' is the effective mass. To achieve higher electrical conductivity, the band mass should be less, which is conflicting with the thermopower requirements. To examine the net thermoelectric properties from electronic structure, the quantity power factor is defined, which is the product of square of the thermopower and electrical conductivity. Increment of any of these quantities will be benefiting the power factor.

1.2.3 Thermal conductivity

Heat conduction is in general possible by electrons and phonons, and the net thermal conductivity can be defined as the sum of thermal conductivity due to electrons and thermal conductivity due to phonons. Electronic part of the thermal conductivity is related to the electrical conductivity by Wiedemann-Franz law, and $k_e = L\sigma T$, where 'k_e' is the electronic part of the thermal conductivity, 'L' is the Lorenz number, and 'σ' is the electrical conductivity, and enhancement of 'σ' will also enhance the 'k_e'. The studies proved that, at low temperature the total thermal conductivity is highly derived from the lattice part, and reducing the lattice thermal conductivity became a fruitful method to enhance the thermoelectric performance. The lattice thermal conductivity k_L can be defined as

$$k_L = \frac{1}{3} v l C_v, \tag{1.3}$$

where 'v', 'l' and 'Cv' represent the phonon velocity, mean free path and heat capacity respectively. This relation demands the need of low phonon veleocity and low mean free path for achieving lower value of lattice thermal conductivity. The low value of the mean free path implies the higher scattering rate, where mean free path can be considered as the distance between two successive phonon collisions. Another explicit equation for lattice thermal conductivity is

$$k_L = \frac{constant M \delta \gamma^2 \theta^3}{n^{2/3} T} \tag{1.4}$$

where 'M', 'δ^3', 'γ' and 'θ' indicate the average atomic mass, volume per atom, Gruneisen parameter and Debye temperature respectively. Further, 'n' indicates the number of atoms in the crystalline limit. From this relation, it is evident that, more the number of atoms in the unit cell lead to low lattice thermal conductivity. In addition, the Debye temperature and Gruneisen parameter are yet another quantities which are directly related to the lattice thermal conductivity. Next section deals with different ways, which helps to tune the constituent parameters of figure of merit.

1.2.4 Methods of tuning the parameters

The previous section discussed the conflicting interrelated parameters which are involved in the performance of a TE material, and the research pertaining to the search of compatible materials, which can provide high value of figure of merit ZT and hence the higher efficiency is still active. Thermoelectric device is a solid state device and the material which acts as the part of the device is preferred to be in a solid form. The well defined solid materials are metals, semiconductors, insulators and semi-metals. The concept of thermoelectricity, which is already discussed in the earlier section, was demonstrated first in metals, and then modern theories added the possibility of usage of the several other materials for TE applications, and in the current state, the researchers are working to connect thermoelectricity with very exotic material's properties such as topological insulators, Weyl/Dirac semi-metals etc. The strategy of this research field is to enhance the ZT and hence the efficiency. In general, any property of a material is the response to the external stimuli, and metal, semiconductor, insulators and semi-metals possess different ranges of thermopower, electrical conductivity and thermal conductivity values. In case of metals, the thermopower magnitude (5 - 10 μV/K) is very less compared to other materials, electrical conductivity in general is found to be very high in metals (around 10^6 Ω^{-1} cm^{-1}) and thermal conductivity can be found to be high around 50 W/m K. For semiconductors, the thermopower value will be higher than metals and can be around 200 μV/K, electrical conductivity, in general can be observed in the range of 10^3 Ω^{-1} cm^{-1} and the thermal conductivity shows 1-10 W/m K. Coming to insulators, the thermopower value will be very large (around 1000 μV/K), electrical conductivity will be very less around 10^{-12} Ω^{-1} cm^{-1}, and thermal conductivity is around 10 W/m K [15]. Compared to metals and insulators, semiconductors show better possibilities of TE applications with moderate thermopower and electrical conductivity values. The schematic of TE parameters as a function of carrier concentration is represented in Figure 1.2 (Figure is taken from Ref[16, 17]). In this section, we would like to discuss various methods which aim to enhance the ZT. To enhance the ZT, either one can concentrate on power factor or reduce the lattice thermal conductivity. The power factor is the product of thermopower and electrical conductivity and mostly depends on the electronic structure properties of the material, whereas the thermal conductivity will depend on both electronic and lattice parts. First, let us discuss

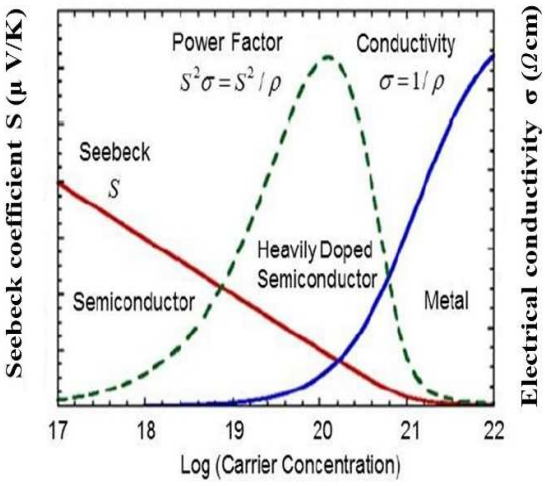

Figure 1.2: Schematic of the TE parameters as a function of carrier concentration

about the power factor. The conflicting dependencies of thermopower and electrical conductivity on effective mass demand the presence of light and heavy band mass near the Fermi level, since the bands near the Fermi level will be actively participating in transport properties. Effective mass can be understood in terms of the curvature of bands and flat band leads to higher effective mass and dispersive bands indicate low effective mass. When we look into the electronic structure, the materials which show the mixture of flat bands and light bands will be preferable. In general, chalcopyrite materials possess this kind of band structure[18], but one cannot expect similar band structure for every materials. Band engineering is considered to be one of the effective tools to enhance the power factor. The conflicting dependencies of thermopower and electrical conductivity constrained the enhancement of power factor, and this challenging task was addressed by several works in the literature[19, 20]. Huge increment in ZT is reported by enhancing the density of states through doping of thallium in PbTe [21], and in 2011, a higher value of ZT is achieved in doped PbTe structure by means of multiple valley degeneracy[22]. These results indicate the efficiency of this approach for getting better thermoelectric performance. In addition to doping, application of pressure and strain also alter the band profile and several studies have reported the enhancement of power factor as a function of pressure and strain[23, 24]. Sergeay *et. al.*, demonstrated the enhancement of power factor by the application of pressure in $(Bi, Sb)_2(Te, Se)_3$ system [23]. The modern research on thermoelectric materials explains the benefits of materials with low dimensional structures and nanostructuring emerged as a prominent tool for enhancing the power factor. In general, there are two type of nanostructures which are considered to be good thermoelectric materials, first kind is a single phase with the assembly of nano sized particles and the second is a system comprising of a major bulk phase with another minor nano particles in it. Vassilios *et. al.*, investigated the power factor increment of nanostructure using the nonequilibrium Greens function method[25], and they have reported 20% power factor improvement. Sabarinathan *et. al.*, studied the enhancement of power factor by the energy filtering effect in Bi based nanostructures[26]. Pichanusakorn *et. al.*, investigated the variation of Seebeck coefficient and hence power factor

with dimesion and length scale reduction and have shown the enhancement of power factor in nanostructures over bulk materials[27]. Further, several people have reported the role of quasi two dimensional bulk system in enhancing the Seebeck coefficient and hence power factor[28, 29]. Enhancement of electrical conductivity also leads to improvement in the power factor. The recent trend in thermoelectric research explored the benefits of topologically non trivial materials such as topological insulator, semimetals and Dirac/Weyl semi metals, where the non parabolic band profile of these compounds benefits the electrical conductivity. Te-Huan Liu *et. al.*, recently investigated the improved thermoelectric performance in Dirac materials[30]. Overall from the literatures, it is evident that band engineering, doping, pressure/strain, nanostructuring etc, are fruitful methods to enhance the power factor. Reduction of lattice thermal conductivity is yet another way to enhance the figure of merit, where lattice thermal conductivity is lying in the denominator of the figure merit expression. This idea is well explored and huge number of literatures, books, review articles explained this concept in detail. Here, we would like to point out few methods which are helpful in reducing lattice thermal conductivity. Alloying solid materials in general show the reduction of lattice thermal conductivity without decreasing the electrical conductivity, and Bi_2Te_3 family of compounds are well explored for the same[31, 19]. Since the reduction of lattice thermal conductivity is very crucial in thermoelectric materials, there are mainly three strategies existing for the same. Firstly by the means of phonon scattering, and this is achieved by using several method such as mass fluctuation scattering, grain boundary scattering etc. Second strategy is the reduction of thermal conductivity using complex crystal structures, where the concept of electron crystal and phonon glass has been proposed. The third strategy is the mixing of multi scale composites, which means alloying of solid solution. These three methods are studied for several family of compounds, where half Heusler materials are well investigated for mass fluctuation scattering methods[32, 33]. Clathrates, Skutterudites and Zintl phase are well established complex structures. The next section deals with the journey of thermoelectric materials.

1.3 The journey of thermoelectric materials

Countable number of materials only serve in a real thermoelectric industry and are realized as a part of thermoelectric devices, which are the materials invented in the early stage of research (in 1954) by Goldsmid and Douglas[10]. Bi-based tetradymite type materials are a class of materials which got several attraction in the field of thermoelectrics. From the early stage to the current research, one can clearly see the presence of this family in research field, and many techniques have been used to improve the thermoelectric properties of the same. The general formula for this compounds is $(Bi_{1-x}Sb_x)_2$ $(Te_{1-x}Se_x)_2$. The relevant electronic band structure and phonon dispersion made these series attractive for thermoelectric applications. All elements in this class of materials are heavy elements, enabling high spin orbit coupling interaction and hence low energy gap. Further most of these compounds provide low effective mass, which is fruitful for electrical conductivity. Coming to the phonon part, the presence of heavy elements in the compounds lead to low thermal conductivity and the higher size of the unit cell will help to reduce the thermal conductivity. The layered nature of these compounds further add benefits to it, where the anisotropic nature in conductivity and nearly two dimensional nature helps to enhance the figure of merit. Mishra *et.al.*, examined the electronic and thermoelectric properties of bismuth telluride and bis-

muth selenide[34], and several studies are reported aiming at the improvement of thermoelectric properties of these compounds by the application of pressure and strain[35, 36]. In the recent past, yet another exotic property was also associated with this family, when people realized that Bi_2Te_3 is a topological insulator[37, 38, 39]. This family of compounds attained attention in thin film form also. In 2001, a remarkable ZT around 2.4 at 300 K was reported by Venkatasubramanian for the super lattice thin film system of Bi_2Te_3/Sb_2Te_3[40]. Yet another fundamental thermoelectric material is PbTe, and similar to Bi-family, PbTe is also examined in various ways to extract the maximum efficiency and stay in forefront of thermoelectric device for last six decades. The studies on PbTe began in 1950's and the current research community also try to explore more from this compound[41, 42, 43]. The applications of PbTe is mainly on moderate temperature range from 600 K to 800 K[44, 45, 46], and the melting temperature is around 920^oC. Nanostructuring method in PbTe is found to be very promising for thermoelectric applications, and several literatures are discussing the same[45, 46, 47, 48, 49, 50]. Earth abundance of the material is essential for any application, and Mg_2Si and its solid solutions gathered attention for thermoelectric applications due to higher availability and low mass density. Doping with elements is found to be effective in this compound, and an improved TE properties were observed in Mg_2Si due to the effect of doping with external element Sb on Si site[51, 52]. Solid Solution of iso-structural Mg_2X (X: Si, Ge, Sn) such as Mg_2Si-Mg_2Sn systems show good improvement in thermoelectric properties, and several mixing obtained the ZT value above unity for a wide temperature range from 700 K to 800 K [53, 54, 55, 56]. Higher manganese silicide (HMS) compounds are yet another environmental friendly earth abundant materials, which show anisotropic electronic and thermoelectric properties[57, 58, 59]. Aoyama *et. al.*, studied $(Mn_{0.98}Mo_{0.02})(Si_{0.9865}Al_{0.0035}Ge_{0.01})_{1.74}$ and reported the ratio of ZT along 'a' and 'c' axes to be near 0.9 [60]. Several similar studies can be found in literatures[54], with huge anisotropic transport properties[61]. Technical application of HMS is tested in the very early stage itself and the thermogenrator of this HMS was patented in 1968 [62]. Kaibe *et. al.*, demonstrated a thermoelectric power generator using HMS and reported 6.5% efficiency[63], and enhanced the efficiency up to 15% by combining with bismuth telluride[64]. Overall HMS based thermoelectric studies are found to be very promising. Thermoelectricity using clathrate family of compounds are explored by several people, and significant number of compounds in this family which is derived from 14^{th} group elements are potential materials for thermoelectric applications, which obey the well known phonon glass electron crystal concept. The compound $Ba_{24}Ga_{15}Ge_{85}$ was explored for thermoelectric applications and ZT was reported around 1.25 at 670^oC[65], and the attraction of this family is the structure properties, which benefits thermoelectric applications[66, 67]. Half Heusler alloys contains large number of compounds with potential high temperature thermoelectric applications, and these compounds crystallize in cubic MgAgAs structure type. Significant number of half Heusler compounds including (Ti, Hf, Zr) NiSn and (Ti, Hf, Zr) CoSb are well known for potential thermoelectric applications. These compounds gathered attention towards thermoelectric applications due to several properties such as earth abundance, lightweight, low cost and the remarkable combination of high Seebeck coefficient and low electrical resistivity[68, 69, 70, 71] and the challenge in this compounds is the thermal conductivity value. To optimize the ZT value, in general doping studies were performed for power factor enhancement and alloying is performed for reduction of lattice thermal conductivity[72, 56, 69]. Other than normal bulk doping, nano-structuring and nano-inclusion are investigated in half Heusler alloys and an enhancement in thermoelectric properties is observed. In

addition to this, half Heusler compounds are well known for topological insulating nature. Cu based chalcogenides fascinated the researchers with potential thermoelectric applications. The signature of thermoelectric properties in Cu based chalcogenide was identified when Becquerel in 1827 noticed the generation of electricity in Copper wire circuit[73]. In 1866, Cu_2S thermoelectric battery was made[74]. Cu_2Se based radioisotope thermal generators were developed in 1960's - 1970's[75]. Further Ag doped Cu_2Se compound $Cu_{1.97}Ag_{0.03}Se_{1+y}$ (y <0.01) achieved a ZT value of 1.2 at 1000 K[76]. However the research on Cu_2Se had to stop in 1979 due to selenium evaporation issue and Cu -ion migrations[77]. Then three decades later, the interest on this compound regained due to the emergence of new concept called phonon-liquid-electron crystal[78]. Several work has reported the ZT value 1.3 to 2.1 in $Cu_{2-\delta}Se$[79, 80, 81, 82]. The main attraction in this compound is the low thermal conductivity due to its complex structural properties.

Layered ZrCuSiAs type 1111 compounds were highly investigated for superconducting properties and in the later stage, Pinsard-Gaudart *et. al.*, examined the thermoelectric properties of LaFeAsO and found large Seebeck coefficient at around 100 K. After this realization, several groups have extensively worked on this family of compounds for thermoelectric applications. Among that BiCuSeO secured the highest ZT in oxygen based thermoelectric materials[83]. The exceptional features of this layered structure is the stacking of conductive Cu-Se layer on insulating Bi-O layer along 'c' axis, which restrict the charge flow along 'c' axis leading to a super lattice type structure by itself. This naturally originated super lattice type crystal structure opened a wide range of possibilities in thermoelectric field. In general, super lattice structuring is one of the prominent method to reduce the lattice thermal conductivity, where additional phonon scattering will be happening in the interface and lead to lesser thermal conductivity. The process of creating a heterostructure is very challenging where the lattice of two layers should match properly, here comes the importance of the natural super lattice structures. In its original form, the Seebeck effect is in general found to be high for these compounds and electrical conductivity is moderate, which lead to a moderate value of power factor. To enhance the thermoelectric performance for these compounds, doping study is found to be effective and it has been reported that due to doping with Mg, C, Sr elements in BiCuSeO, the ZT value is increased from 0.5 to 1.1[84]. The contribution of zintl phase compounds towards thermoelectric filed is worth discussing, and these compounds are the intermetallic compounds and are recognized by covalently bonded anionic substructures coordinated by highly electropositive cations[85, 86]. The structure of these compound are highly complex due the significant combination of covalent and ionic bonding, enabling a very good platform for thermoelectric applications. The reported ZT value for few zintl phase compounds $YbZn_2Sb_2$, Zn_4Sb_3 are found to be unity[87, 88]. The compound $Yb_{14}MnSb_{11}$ gathered special attention and evolved as a thermoelectric module from the study performed in Jet Propulsion Laboratory[89], and the attraction towards Zintl phase compounds increased further [90, 91]. A glass like lattice thermal conductivity is reported for these compounds[92], and became main attraction for thermoelectric applications. Wide variety of materials with diverse structural properties have been adequately investigated for thermoelectric applications through experimental and theoretical studies and few are explained above. Several books, review articles described the development of TE materials. It is quite evident that for a large scale production of TE device, these efforts has to continue and in this scenario the search of potential materials is worth investigating.

1.4 Applications of thermoelectric materials

Power generation and refrigeration are the main applications of thermoelectric materials. The solid state environmental friendly thermoelectric devices can be useful in industries, transportation facilities, space applications, military equipments, waste heat recovery, biomass gasifiers etc[93, 94]. Due to the increase of population and life style of our generation, large number of automobiles are in use and lot of energy is getting wasted as heat form these vehicles. Thermoelectric modules can be used to extract these waste heat and can convert the same to useful electricity. The main heat wastage is happening in the exhaust pipe and the radiator of the vehicle. Thermoelectric power generators can be kept at different spots in vehicles to extract electric power from heat wastage. It is understood that the low temperature TE application is also possible from automotive exhaust pipes using Bi_2Te_3 and its derivatives. The TEG device has been tested for power generation and cooling in electric vehicles, and the generated power is able to manage the sound system in the vehicle[95]. It is proved that a TEG device can extract heat from a table lamp[96]. Thermoelectric cooling devices are in general known as Peltier coolers. These coolers are important for few applications where the conventional cooling system is inadequate for the removal of heat. For the utilization of these wide range of applications, we have to enhance the efficiency of TE device.

1.5 Disadvantages of thermoelectric materials

From the earlier section, it evident that TE materials have plenty of applications, but the large scale usage of TE device is restricted due to the poor efficiency. The current thermoelectric materials which are used for applications are having efficiency only around 15%, which is very less compared to other energy sources. Large scale waste heat recovery demand higher value of ZT and high efficiency, and the material which shows higher ZT at high temperature is very limited. Over these years, researchers have improved the ZT and efficiency by using several techniques, and reported the efficiency up to 20% [97]. These two limitations demands the need for the search of potential novel thermoelectric materials.

1.6 Overview of the thesis

The importance of the search of novel thermoelectric materials is presented clearly in the previous sections. Computational study of thermoelectric materials are further helpful to predict the optimum thermoelectric materials and hence can be proposed for practical applications, which can be verified experimentally. The present thesis analyzes the thermoelectric properties of few series which belong to well established material families such as chalcopyrites, zintl phase, transition metal dichalcogenides etc, within the frame work of Density Functional Theory. Moreover the present study focuses on the tuning of thermoelectric coefficients such as thermopower and electrical conductivity by the application of hydrostatic and uni-axial strain and reported the possibilities of enhancement of thermoelectric coefficients. The present thesis contains seven chapters including introduction, methodology , results and discussions and conclusions. The current chapter discussed the history of thermoelectric materials and basic thermoelectric effects. The upcoming chapters are organized as follows. The second chapter deals with the methodology used for the present thesis, which explains

the introduction of many body theory, and several methods which were established to solve the many body equations and the role of Density Functional Theory. Further, we have explained the details of our calculations. All the electronic structure calculations are based on full potential linearized augmented plane wave method as implemented in Wien2k package, and geometry optimizations were performed using pseudo potential methods as implemented in VASP and PWscf programme. The thermoelectric properties are calculated by the combination of Density Functional Theory and semi-classical Boltzmann transport theory. The results of the present thesis are organized as four chapters (chapter 3 - chapter 6) and the thermoelectric properties of Zn based pnictides are presented in third chapter. Zn based pnictides in the form $ZnXPn_2$ (X: Si, Ge, Sn, Pn: P, As, Sb) are mostly earth abundant and are having high melting temperature. Our results reveal the potential thermoelectric properties of these compounds and are proposed for high temperature applications. Among them, $ZnGeSb_2$ is observed as a very fruitful material for thermoelectric applications due to its peculiar electronic structure. Chapter 4 deals with very interesting layered materials which are known as natural super lattice materials. We have examined the possibility of low thermal conductivity in these compounds. The huge thermopower values is also an attraction in these compounds. Chapter 5 presents few Ca based zintl phase compounds, which shows very good thermoelectric properties together with strong topological insulting nature. Further chapter 6 deals with two types of transition metal dichalcogenies and its thermoelectric properties. First series (OsX_2 (X: S, Se, Te) crystallizes in cubic structure, and the second series ReX_2(X: S, Se) crystallizes in triclinic structure. Giant thermopower is observed in p-type OsX_2 (X: S, Se, Te), and layer independent TE properties is observed in ReS_2. In totality the present thesis deals with four diverse family of compounds and its potential TE properties. In chapter 7, we have concluded all the vital points from each study.

Chapter 2

Methodology

The present chapter briefly discusses the methodology of entire calculations performed to fulfill the present study. The discussion starts with the physical interpretation of many body problem. Subsequently, we discuss the emergence of Density Functional Theory (DFT), one of the prominent methods for solving many particle system. In addition to that, the necessary explanation of exchange correlation functionals has been included. A concise explanation for the calculations such as Z_2 topological invariant and surface states, which are performed for the topological non-trivial states in few of the investigated compounds is also presented. The thermoelectric properties of all the studied system are computed by the combination of DFT and the semi-classical Boltzmann transport theory, and the later part of this chapter discusses the basics of semi-classical transport theory.

2.1 A brief introduction to the problem

The remarkable description of many electron system is comprised in Schrödinger equation (SE), which was proposed in 1926 by Erwin Schrödinger in his paper entitled "Quantization as an Eigenvalue Problem" which dealt with hydrogen atom, and evolved as the foundation of quantum mechanics. Solids can be considered as a many body system with interacting electrons and ions, and by solving the Schrödinger equation, the physical observables of the system can be obtained. The expected sets of interactions in a many body Hamiltonian are provided below.

$$\widehat{H} = \widehat{T}_N + \widehat{T}_e + \widehat{V}_{N-e} + \widehat{V}_{N-N} + \widehat{V}_{e-e} \tag{2.1}$$

where $\widehat{H}$ represents the Hamiltonian operator of the system, $\widehat{T}$ and $\widehat{V}$ represent the kinetic and potential energy operators respectively. The symbol 'N' stands for nucleus and 'e' represents electrons. The operators $\widehat{V}_{N-N}$ and $\widehat{V}_{e-e}$ are nucleus-nucleus $(N-N)$ and electron-electron $(e-e)$ interactions respectively. The operator $\widehat{V}_{N-e}$ represents the nucleus and electron interaction.

The explicit form of each operator in the above Hamiltonian of a system which contains M number of nuclei and N number of electrons can be written as

$$\widehat{H} = -\frac{1}{2}\sum_{I=1}^{M}\frac{\bigtriangledown_I^2}{M_I} - \frac{1}{2}\sum_{i=1}^{N}\frac{\bigtriangledown_i^2}{m_i} - \sum_{I=1}^{M}\sum_{i=1}^{N}\frac{Z_I e^2}{|R_I - r_i|} + \sum_{\substack{i,j=1 \\ i\neq j}}^{N}\frac{e^2}{|r_i - r_j|} + \sum_{\substack{I,J=1 \\ I\neq J}}^{M}\frac{Z_I Z_J e^2}{|R_I - R_J|} \tag{2.2}$$

where capital symbols in the summation 'I', 'J' represent the nuclei terms and small letters 'i' 'j' represent the electrons terms, Z_I is the atomic number M_I and m_i are the atomic masses of the nuclei and electrons respectively. R_I and R_J indicate the positions of nuclei, and r_i and r_j represent the positions of electrons. Reaching a complete solution for the above equation becomes hard, when we evolve from hydrogen to a complex solid. Various approximations have been proposed to obtain the solution of a many body problems, and the present chapter deals with the method, which solves the many body system within the frame work of DFT.

2.1.1 Born-Oppenheimer approximation

Due to the huge number of interacting particles in a system (around $\sim 10^{23}$), the exact solution to the above mentioned SE will be difficult. Born and Oppenheimer in 1927, came up with an approximation which helps to decouple the electronic and nuclei part in a many body Hamiltonian. The idea behind this approximation was the huge mass difference between electron and the ion, and the motion of the ions will be very less compared to the motion of electrons [98]. In other words, it can be seen in such a way that the electrons are moving in a frozen ion background at every instant. According to this approximation, the nuclei kinetic energy in the Hamiltonian can be considered to be zero and potential energy term ($\widehat{V}_N + \widehat{V}_{N-e} \approx \widehat{V}_{ext}$) can be considered as a constant. The modified Hamiltonian is given below.

$$\widehat{H} = \widehat{T}_e + \widehat{V}_{e-e} + \widehat{V}_{ext} \tag{2.3}$$

Even though the complexity of the many body problem has been reduced little bit, solving the above Hamiltonian is still a tiring task. More approximations are needed to get a reasonable solution to this problem, which are adequately discussed in the upcoming sections.

2.1.2 Hartree approximation

In 1928, Hartree proposed a method to solve the electronic part of the above mentioned Hamiltonian, where he has considered the electrons to be non-interacting particles and the total wave function of the system can be obtained as the product of all individual electron wave function, $\psi(r_1, r_2, r_3, ...r_N) = \phi_1(r_1) \times \phi_2(r_2) \times \phi_3(r_3) \times ..... \times \phi_N(r_N)$. Further, using variational principles, total energy term will be minimized and he tried to extract the exact ground state properties of the system. From this approximation, Hartree potential term is derived, which is defined as the average electrostatic potential created by all other electrons. The Hartree potential is defined as follows

$$V_H = \sum_{i=1}^{N} V_{r_i} \tag{2.4}$$

Yet another name of this approximation is individual particle approximation. Modified Hamiltonian can be written as,

$$\widehat{H} = \widehat{T}_e + \widehat{V}_{ext} + \widehat{V}_H \tag{2.5}$$

where $\widehat{V}_H$ represents the Hartree potential as discussed in the equation 2.4. In reality, the solid is a many electron system, and this approximation failed to incorporate the anti-symmetric character of electrons (Fermionic) and also did not consider the proper electron-electron interaction. These failures demand further understanding and approximations which will include the fermionic character of the electron wave function.

2.1.3 Hartree-Fock approximation

In 1930 Fock modified the wave function by including the concept proposed by Slater. To include the anti-symmetric nature to the wave function, Fock represented the total wave function as Slater determinant, which is given below.

$$\psi(r_1, r_2, r_3, ...r_N) = \frac{1}{\sqrt{N!}} \begin{vmatrix} \phi_1(r_1) & \phi_2(r_1) & \phi_3(r_1) & ... & \phi_N(r_1) \\ \phi_1(r_2) & \phi_2(r_2) & \phi_3(r_2) & ... & \phi_N(r_2) \\ . & . & . & ... & . \\ . & . & . & ... & . \\ \phi_1(r_N) & \phi_2(r_N) & \phi_3(r_N) & ... & \phi_N(r_N) \end{vmatrix} \tag{2.6}$$

This expression helps to give an anti-symmetric nature for the wave function, where by interchanging the positions of two particles a negative sign will be induced, eventually taking in to account the

anti-symmetric nature. The wave function for two electron system can be written as

$$\psi(r_1, r_2) = \frac{1}{\sqrt{2}} \left[\phi_1(r_1)\phi_2(r_2) - \phi_1(r_2)\phi_2(r_1)\right]. \tag{2.7}$$

The inclusion of anti-symmetric nature to the interacting particle causes an extra term in the total energy calculations which is known as exchange energy. The modified Hamiltonian is

$$\widehat{H} = \widehat{T}_e + \widehat{V}_{ext} + \widehat{V}_{HF} (2.8)$$

where the V_{HF} represents the modified version of the HF approximation potential. $\widehat{V}_{HF}$ is given by

$$V_{HF} = \int v_x(r, r')\phi_i(r_i')dr' = -\sum_j^N \int \frac{\phi_j(r)\phi_j^*(r')}{|r_i - r_j|}\phi_i(r_i')dr' \tag{2.9}$$

The exchange energy term overcome the first drawback of Hartree equation, still the H-F equation is in the mean-field approximation, where the electrons are considered to move in an average potential generated by the other electrons. This approximation is fruitful for several system but strongly correlated solids are difficult to be considered using this method.

2.2 Introduction to density functional theory

Attaining the proper solution of a many body system through the assumption of wave function is highly complicated since the wave function depends on 3N variables, where N is the number of electrons. To reduce the complexity, Hohenberg and Kohn [99] in 1964, came up with a theory which is rooted on the electron's density, and evolved as Density Functional Theory (DFT). The method involves Hohenberg-Kohn theorem [99] and the Kohn-Sham [100] equations. While replacing the wave function with electron density the dependent variables are reduced from 3N to 3, which eventually narrow down the complexity of many body Hamiltonian. Many articles and books have discussed the DFT methods in details [101, 102, 103, 104, 105, 106, 107, 108]. Here we have discussed a brief journey of the same. Before going to the details, let us see the expression of the electron density, which is given as below,

$$n(r) = N \int d^3r_2 d^3r_3 .... d^3r_N \psi(r, r_2, ...r_N)\psi^*(r, r_2, ...r_N) \tag{2.10}$$

The upcoming section deals with the Thomas-Fermi theory, which is the footing of DFT.

2.2.1 Thomas-Fermi theory

The first attempt to solve the many body Hamiltonian based on electron density was proposed in two independent work by Thomas and Fermi [109, 110]. The kinetic energy of the system was expressed as a function of electron density $n(r)$, which is given below,

$$T[n(r)] = C_F \int n^{5/3}(r)dr \tag{2.11}$$

where $C_F = \frac{3}{10}(3\pi^2)^{2/3}$=2.871, $n(r)$ define the electron density and total number of electrons N van be obtained by the integration

$$\int n(r)dr = N \tag{2.12}$$

The expression of kinetic energy in this model was developed for only a homogeneous system, and total energy of the system can be written as follows

$$E_{TF}[n(r)] = C_F \int n^{5/3}(r)dr - Z \int \frac{n(r)}{r}dr + \frac{1}{2}\int\int \frac{n(r)n(r')}{|r-r'|}drdr' \tag{2.13}$$

Thomas-Fermi has laid the first step to reduce the complexity of the many body Hamiltonian by replacing the wave function with electron density, which is a crude way of an approximation for the kinetic energy term alone. They have considered homogeneous electron gas and imposed classical interaction terms for electrons, which was the drawback of the theory, however they have contributed the great idea of replacing the wave function with electron density.

2.2.2 Hohenberg-Kohn theorems

Hohenberg and Kohn (HK) [99] elaborated the idea proposed by Thomas and Fermi, and constructed two theorems, which are the basis of DFT. The two theorems are described as follows.

Theorem-I states that, the external potential $v_{ext}(r)$ is a unique functional of electron density $n(r)$, and hence the total ground state energy is also a unique functional of electron density $n(r)$.

Theorem-II states that, for any external potential $v_{ext}(r)$, an universal functional for the energy in terms of the density $n(r)$ can be defined and also the global minimum of this functional gives the exact ground state energy of the system. The density $n(r)$ that minimizes this functional is known as the exact ground state density $n_0(r)$. According to this, the Hamiltonian of the interacting particles of the system is given by,

$$\begin{aligned} \widehat{H} &= -\frac{1}{2}\sum_i {\nabla_i}^2 - \sum_i v_{ext}(r_i) + \sum_{i\neq j}\frac{1}{|r_i - r_j|} \\ where \quad v_{ext}(r_i) &= -\sum_I \frac{Z_I}{|r_i - R_I|} \end{aligned} \tag{2.14}$$

Here $v_{ext}(r_i)$ represents the external potential which includes the interaction between electrons and nuclei. Overall, the two theorems proved the one-to-one relation between external potential $v_{ext}(r)$ and the ground state density $n_0(r)$. The exact ground state energy of system can be calculated by minimizing the total energy functional. The proof of these theorem can be found in Ref[99, 111]. Next section deals about the Kohn-Sham method, a practical way of solving many body equation using density functional theory.

2.2.3 Kohn-Sham method

A systematic way of solving the many body problem within the frame work of DFT is developed by Kohn and Sham[100], and known as Kohn Sham equation. The equation is,

$$E_{KS} = T[n] + V_{ext}[n] + V_H[n] + E_{xc}[n] \tag{2.15}$$

While looking into the individual terms, $T[n]$ represents the independent particle kinetic energy which is given by,

$$T[n] = -\frac{1}{2}\sum_{i=1}^{N}\langle\psi_i|\delta|\psi_i\rangle. \tag{2.16}$$

$V_{ext}[n]$ is the external potential energy which has the form,

$$v_{ext}[n] = \int v_{ext}(r)n(r)dr. \tag{2.17}$$

V_H is the Hartree potential due to the electron-electron Coulomb interaction which is given by,

$$v_H = \int \frac{n(r')}{|r-r'|}dr' \tag{2.18}$$

Finally E_{xc} represents the exchange-correlation energy which goes beyond the Hartree - Fock approximation. In general the Schrödinger form of the Kohn-Sham equation is given as follows:

$$H_{KS}\psi_i = E_{KS}\psi_i \tag{2.19}$$

where H_{KS} and v_{eff} are the Kohn-Sham Hamiltonian and effective potential which are defined by

$$\begin{aligned} H_{KS} &= [-\frac{1}{2}\nabla^2 + v_{eff}(r)] \\ v_{eff} &= v_{ext} + v_H + v_{xc}. \end{aligned} \tag{2.20}$$

An iterative approach has been used to solve the many body problem, and reach up to the ground state energy and the density of the system. All physical quantities can be extracted from this ground state energy values. The term v_{xc} is still not defined properly, which takes in to further approximations.

2.3 Exchange-correlation functionals

The many body problem still remains unsolved without knowing the exact form of exchange correlation functional E_{xc}, which is the key parameter in DFT. The challenging task here is to predict the exact form of the exchange correlation functional, which is the combination of both exchange and correlation parts. Several approximations have been developed to explain the form such as LDA, GGA, TB-mBJ etc, and few are explained here. The exchange energy can be defined as the induced energy change due to the exchange of the position of two particle, which is the consequence of the

anti-symmetric nature of the wave function. The exchange energy of the two particles can be defined as

$$E_x = -\frac{1}{2}\sum_{ij}\int\int \frac{\psi_i^*(r)\psi_i(r')\psi_j^*(r')\psi_j(r)}{|r-r'|}drdr' \tag{2.21}$$

and the correlation energy is defined as the collective interaction on one electron due to all other electrons in the system.

Since there is no exact expression for correlation energy, one can think of the difference between exact non-relativistic energy and Hartree-Fock energy. The combination of the above discussed two forms is known as exchange-correlation energy

$$E_{xc} = E_x + E_c \tag{2.22}$$

To tackle real many body systems, the forms of exchange correlation energy should be proper. Few of them are discussed below.

2.3.1 The local-density approximation (LDA)

To attain a meaningful solution to the many body problem, Kohn and Sham in 1965 proposed an approximation for exchange correlation functional known as local density approximation[100]. Based on this approximation, the electron density in a system varies very slowly with respect to space coordinates, enabling a locally uniform electron density. The form of exchange correlation defined in this approximation is

$$E_{xc}^{LDA}[n(r)] = \int n(r)\epsilon_{xc}^{hom}(n(r))dr. \tag{2.23}$$

Here ϵ_{xc}^{hom} is exchange-correlation energy per particle of the interacting homogeneous electron gas of density $n(r)$. This approximations is capable enough to predict the electronic structure of molecules and few less interacting solids. LDA is proved successful for several cases, such as prediction of lattice parameters, charge density etc. In the case of solids, LDA results are found to be improved from H-F method.

2.3.2 The generalised gradient approximation (GGA)

The concept of locally uniform electron density is not appropriate for several highly correlated systems, where one should expect the variation of electron density as a function of spatial coordinates. In 1969, Herman *et. al.*, [112] came up with an idea such that the electron density might vary with spatial coordinates and the corresponding exchange correlation energy can be expressed as the gradient of electron density, and the method is known as generalised gradient approximation (GGA). The form of exchange correlation functional in this approximation is

$$E_{xc}^{GGA}[n(r)] = \int n(r)\epsilon^{xc}[n(r), \delta n(r)]dr. \tag{2.24}$$

In few cases such as ground state properties and magnetic properties, GGA achieved better results than LDA. In the case of ferroelectric calculations, GGA failed to give proper results. Both LDA and

GGA failed to provide the band gap of semiconductor, which is important for transport calculations. In the next section, we deal with a convenient method, which predicts an improved band gap over LDA and GGA.

2.3.3 Tran-Blaha modified Becke-Johnson potential (TB-mBJ)

In 2009, Tran and Blaha proposed an efficient form of exchange correlation functional, and tested in several solids such as wide band gap insulators, 's,p' semiconductors, and few strongly correlated 3d transition metal oxides, and have shown the proper prediction of band gap which is comparable with experimental values[113]. There are several methods such as LDA +U, GW etc, proposed after the traditional exchange correlation functional LDA, GGA. The TB-mBJ functional gained more attraction as it is computationally less expensive. This method is a modification over the exchange correlation proposed by Becke and Johnson[114], and can be expressed as follows

$$v_{x,\sigma}^{MBJ}(r) = cv_{x,\sigma}^{BR}(r) + (3c-2)\frac{1}{\pi}\sqrt{\frac{5}{12}}\sqrt{\frac{2t_{\sigma(r)}}{\rho_\sigma(r)}} \tag{2.25}$$

where $\rho_\sigma = \sum_{1,N} |\psi_{i,\sigma}|^2$is the electron density $\mathrm{t}_\sigma = \frac{1}{2}\sum_{1,N_\sigma} \nabla\psi_{i,\sigma}^*.\nabla\psi_{i,\sigma}$
is the kinetic energy density and

$$v_{x,\sigma}^{BR}(r) = -\frac{1}{b_\sigma(r)}(1 - e^{-x_\sigma(r)} - \frac{1}{2}x_\sigma(r)e^{-x_\sigma(r)}) \tag{2.26}$$

is the Becke-Roussel potential which was proposed to model the Coulomb potential created by the exchange hole. x_σ is determined from an equation involving ρ_σ, $\nabla\rho_\sigma$,$\nabla^2_{\rho_\sigma}$ and t_σ
and then 'b$'_\sigma$
is calculated with

$$b_\sigma = [x_\sigma^3 e^{-x_\sigma}/8\pi\rho_\sigma]^{1/3} \tag{2.27}$$

'c' was chosen to depend linearly on the square root of the average of $|\nabla\rho|/\rho$,

$$c = \alpha + \beta(\frac{1}{V_{cell}}\int \frac{|\nabla\rho(r^{'})|}{\rho(r^{'})}d^3r^{'})^{1/2}. \tag{2.28}$$

where 'α' and 'β' are two free parameters V_{cell} is the unit cell volume.

he band gap of the compounds included in the present thesis has been calculated using TB-mBJ and few are reported with TB-mBJ with improved parameters, where the value of α is found to be different. We have performed electronic structure calculations using Wien2k code, which is based on full-potential linearized augmented plane wave method (FP-LAPW). Few of the geometry optimizations are calculated using pseudo potential method. In next section, we have discussed the vital points of above mentioned methods.

2.4 Methods

Here we would like to discuss few basic methods which are developed to estimate the electronic structure of a real solid. This method in general divide the entire electrons as valence and core

electrons, since the core electrons are mostly inactive for physical properties of the material. It is very important to implement the form of potential in these core region and valence region, and we briefly explain few methods which are used in this thesis.

2.4.1 Linearized Augmented Plane Wave (LAPW) Method

Before discussing the LAPW method, we have to understand the basic Augmented plane wave method (APW), which is explained below

Augmented plane wave method (APW)

The unit cell of a periodic solid can be divided into two, one is core region and the other is interstitial region. The core region is also known as Muffin-Tin spheres[115]. The potential in these two regions are identified as different and given below.

$$V(r) = \begin{cases} \sum_{lm} V_{lm}(r) Y_{lm}(r) & (r \in MT) \\ \\ \sum_{G} V_G e^{iG.r} & (r \in I) \end{cases} \tag{2.29}$$

Hence the basis of two regions also will be different. In the atomic region the wave function vary rapidly, whereas in the interstitial region the wave functions are smoothly varying and expressed as below

$$\phi_{k_n}^{APW}(r, \epsilon_l) = \begin{cases} \sum_{lm} A_{lm,k_n} u_l(r,\epsilon_l) Y_{lm}(r) & (r \in MT) \\ \\ \frac{1}{\sqrt{V}} e^{ik_n.r} & (r \in I) \end{cases} \tag{2.30}$$

where $k_n = k + G_n$, G_n are the reciprocal lattice vectors, k is the wave vector inside the first Brillouin zone and V is the volume of unit cell. The coefficients A_{lm} are calculated by matching the wave functions of the atomic sphere and the interstitial regions. Further the augmented plane wave function will act as the basis of the Kohn-Sham wave function (ψ) as follows:

$$\psi_k(r) = \sum_n c_n \phi_{k_n(r)} \tag{2.31}$$

APW method is very slow due to the unknown energy parameter included in the radial part of the wave function. Next we will discuss the Linearized APW method

Linearized Augmented Plane Wave (LAPW) method

Through the linearizion method, LAPW helps to reduce the problems which appeared in APW method due to the non-linearity of $u_l(r, \epsilon_l)$. Taylor series is used to expand ϵ_l in LAPW method as shown below:

$$u_l(r, \epsilon_l) = u_l(r, \epsilon_l^1) + (\epsilon_l - \epsilon_l^1)\dot{u}_l(r, \epsilon_l^1) + O((\epsilon_l - \epsilon_l^1)^2) \tag{2.32}$$

where $\dot{u}_l = \partial u_l / \partial \epsilon_l$. The ϵ_l^1 is a fixed point energy around which the Taylor expansion is carried out. The basis set for the LAPW method defined as:

$$\phi_{k_n}^{LAPW}(r) = \begin{cases} \sum_{lm}[A_{lm,k_n}u_l(r,\epsilon_l)+B_{lm,k_n}\dot{u}_l(r,\epsilon_l)]Y_{lm}(r) & (r\in MT) \\ \\ \frac{1}{\sqrt{V}}e^{ik_n\cdot r} & (r\in I) \end{cases} \tag{2.33}$$

From the above mentioned equation, it is evident that both APW and LAPW share the same basis set in the case of interstitial region. and the main difference stems only from the Muffin-Tin spheres, in which the basis set will depend both on energy u_l and its energy derivative, $\dot{u}_l$. The inclusion of energy and its derivative in LAPW method will enhance the accuracy compared to the APW method.

APW+lo method

The inclusion of local orbitals (lo) to the linearization of APW method is the next method to improve the solutions. The basis set for the APW+lo method is defined as follows:

$$\phi_{lm}^{APW+lo}(r) = \begin{cases} [A_{lm}u_l(r,\epsilon_l)+B_{lm}\dot{u}_l(r,\epsilon_l)]Y_{lm}(r) & (r\in MT) \\ \\ 0 \quad (r\in I) \end{cases} \tag{2.34}$$

The accuracy of this method is similar as LAPW method, and the advantage of this method is the small basis set like APW method. The process of normalisation is used to extract the coefficients A_{lm} and B_{lm} using the condition that the local orbital is zero at the Muffin-Tin boundary. The present thesis examines the electronic structure properties using full-potential LAPW (FP-LAPW) and APW+lo methods as implemented in WIEN2k code [115].

2.4.2 Pseudopotential method

We have used pseudopotential method to reduce the computational time involved in the full-electron methods, where all electrons will be taken care, for calculating the dynamical properties. A clear division of core and valence electrons is observed in every solid. The valence electrons are considered to be the reason for most of the physical properties, and core electrons are considered to be inactive. In pseudo potential method only valence electrons are considered. The wave functions in this method are selected in such as way that, within the core region the wave function may not match with the real wave function and after the cut off region the pseudo wave function becomes equal to the real wave function. The main criteria that need to be satisfied in this method is that both pseudo wave function and potential should exactly match to the full potential terms out side the core region. The second condition is that pseudo wave functions and its first and second derivatives should be continuous at the boundary, where core and valence regions are separated. The Schrödinger equation in pseudopotential method will be,

$$(\frac{1}{2}\nabla^2 + V)\psi = \varepsilon\psi \tag{2.35}$$

Here ψ is the wave function for the all electron (AE) atomic system with angular momentum component l. The pseudo wave function is of the form

$$\psi_l^{ps} = \sum_{i=1}^{n} \alpha_i j_l \tag{2.36}$$

Here α_i is the fitting parameter and j_l are the spherical Bessel functions. In the present thesis, we have used the pseudopotential method to evaluate the structural optimization and phonon dispersion calculations as implemented in PWSCF [116] code.

2.5 Z_2 topological invariant: Method of calculations

We have extended our electronic structure calculations up to Z_2 topological invariant for few system which preserve both time reversal symmetry and inversion symmetry. Here we would like to discuss the theory behind this calculation and method of calculation. In 2007, Fu and Kane proposed a method for Z_2 topological invariant, where they have connected the parity of occupied Bloch wave function to Z_2 topological invariant for a system which preserve time reversal symmetry and inversion symmetry[117]. First let us discuss the concept of time reversal symmetry in condensed matter physics.

2.5.1 Time Reversal Symmetry

Like any other symmetry, the invariance of a physical law under time reversal transformation is known as time reversal symmetry, this can be considered as a general definition. The time reversal operator is defined as

$$\widehat{\theta} = i\sigma_y \widehat{K} \tag{2.37}$$

where σ_y is Pauli spin matrix and K is complex conjugation operator. The time reversal operator is the product of a unitary operator and complex conjugate operator, enabling an antiunitary nature for this operator. Any periodic crystal can be described by Bloch theorem, and the Schrödinger equation can be written as

$$H(k)|u_{nk}> = E_{nk}|u_{nk}> \tag{2.38}$$

If the Hamiltonian satisfy the time reversal symmetry,

$$H(-k) = \theta H(k)\theta^{-1} \tag{2.39}$$

This implies that, at particular momenta k , where k = -k + G, G is the reciprocal vector, two bands will have same energy, which is known as Kramers pairs. The corresponding spatial momenta is known as TRIM (Time reversal invariant momenta) point.

2.5.2 Z_2 topological invariant

For the compounds which preserve time reversal symmetry and inversion symmetry, we have calculated Z_2 topological invariant by combining with parity of Bloch wave functions as explained by Fu and Kane[117]. For a three dimensional system there are eight TRIM points in the BZ, and four

topological invariant parameters such as ν_0, ν_1, ν_2, ν_3. The definition of ν_0 is as follows,

$$(-1)^{\nu_0} = \prod_{i=1}^{8} \delta(i) \tag{2.40}$$

where δ(i) is defined as the parity at each TRIM point. A non-zero value of ν_0 represent strong topological insulator. For the other three parameters, we have to consider TRIM points in corresponding planes.

2.6 Surface states

In present thesis, we have calculated the surface states of few of the investigated compounds by the combination of Wien2k and Wannier90 packages. The details regarding Wien2k and its FP-LAPW method is discussed in the above section. In this section, we would like to outline the bridge between these two methods for the surface states computation. Wannier90 package is based on maximally-localised Wannier functions, (MLWF)[118], which is an alternative method to understand the electronic properties of material. Using first principles slab calculations, one can calculate the surface electronic structure, but this method needs huge computational resources. Wannier based approach for surface states is more convenient, and here we have used the same. The method can be describe as follows. Firstly a well converged calculations have to to performed for a bulk crystal (here we have used Wein2k). After selecting the range of energy which cover the upper valence bands and lower conduction bands, disentangled WFs spanning the upper valence and low-lying conduction bands will be generated, and the corresponding TB Hamiltonian matrix will be constructed. The augmented TB parameters are then used to construct sufficiently thick free-standing tight-binding slabs by a simple truncation of the effective TB model[119]. In present thesis, we have plotted the surface spectral function using the same.

2.7 Boltzmann transport theory: Method to calculate the thermoelectric properties

In general, any kind of transport in a material can be understood as the response of this carriers to any external perturbations. The external stimuli can be electric or magnetic field, temperature, etc. The transport theory explains all possible ways of response of the carriers to the stimuli. Two transport theories are well established, one is Boltzmann transport theory[120] and the other is Green Kubo theory[121]. The thermoelectric properties of investigated compounds in the present thesis are performed using semi-classical Boltzmann transport theory implemented in BoltzTraP code[122]. Here we would like to discuss the semi-classical Boltzmann theory and few assumptions included in the same.

Boltzmann transport equation starts with the definition of the electron distribution function $f(r,k,t)drdk$ (here the carriers are considered to be electrons), which is the number of electrons at point r with wave number k in the small phase space volume $drdk$. The core of this problem is the time evolution of the electron distribution function $f(r,k,t)$. The total number of electrons in the system can be calculated by integrating the electron distribution function in k and r space. To

understand the variation of the distribution function in time, the knowledge of the stimuli is needed, in general external field, temperature gradient and scattering are considered as the cause of carrier transport, which cause diffusion, drift and collision. After incorporating all these perturbations, the variation of $f(r,k,t)$ in time can be seen as

$$\frac{f(r,k,t)}{\partial t} = \frac{f(r,k,t)}{\partial t}_{diffusion} + \frac{f(r,k,t)}{\partial t}_{drift} + \frac{f(r,k,t)}{\partial t}_{collision} \tag{2.41}$$

Each term in the above equations can be understood separately, To understand the diffusion term, let us fix the 'k' point, and see how the carriers vary as function of 'r', and 't'. If v_k is the velocity, the particles in a small volume dr at r and at time t are considered to be same as were at the point $r - \mathrm{v}_k dt$ and at time $t - dt$. Then the variation of the distribution function in time due to diffusion can be written as

$$\frac{f(r,k,t)}{\partial t}_{diffusion} = -v_k . \frac{\partial f(r)}{\partial r} \tag{2.42}$$

In similar way, at a fixed 'r' electrons with wave number k were same with wave number $k - dtdk/dt$, the change of distribution function due to drift

$$\frac{f(r,k,t)}{\partial t}_{drift} = -k . \frac{\partial f(k)}{\partial k} \tag{2.43}$$

The challenge here is to address the collision term, in general collision depends on all the scattering mechanism and the form will be very complicated. Here we have used the simplest case, where the change in distribution function due to collision is considered as

$$\frac{f(r,k,t)}{\partial t}_{collision} = -\frac{f(k) - f^0(k)}{\tau(k)} \tag{2.44}$$

After substituting the exact form of all the terms, the Boltzmann transport equation can be written as

$$\frac{f(r,k,t)}{\partial t} = -v_k . \frac{\partial f(r)}{\partial r} - k . \frac{\partial f(k)}{\partial k} - \frac{f(k) - f^0(k)}{\tau(k)} \tag{2.45}$$

At the steady state, the time derivative of the distribution function will be zero, and then

$$-v_k . \frac{\partial f(r)}{\partial r} - k . \frac{\partial f(k)}{\partial k} - \frac{f(k) - f^0(k)}{\tau(k)} = 0 \tag{2.46}$$

The knowledge of the electron distribution function helps to compute several transport properties. The transport coefficients can be obtained by solving the current density equation, the equation for electric current density is

$$J_e = \frac{2e}{8\pi^3} \int v(k) f(k) dk \tag{2.47}$$

Further heat current density due to electrons can be written as

$$J_Q = \frac{2}{8\pi^3} \int v(k)[E - \mu] f(k) dk \tag{2.48}$$

where μ is the chemical potential. After substituting the electron distribution function obtained

from Boltzmann transport theory, the above two equations become

$$J_e = \frac{2e}{8\pi^3}\int v(k)v(k)\tau(k)(\frac{-\partial f^0}{\partial E})[e\epsilon - \nabla\mu + \frac{E-\mu}{T}(-\nabla T)]dk \tag{2.49}$$

Then

$$J_Q = \frac{2}{8\pi^3}\int v(k)v(k)\tau(k)(\frac{-\partial f^0}{\partial E})[e\epsilon - \nabla\mu + \frac{E-\mu}{T}(-\nabla T)][E-\mu]dk \tag{2.50}$$

To minimize the complexity, response function has been defined

$$I_n = \frac{1}{4\pi^3}\int v(k)v(k)\tau(k)(\frac{-\partial f^0}{\partial E)[E-\mu]dk} \tag{2.51}$$

Both the current densities can be expressed in terms of response function

$$J_e = e^2 I_0\epsilon + e\frac{I_1}{T}(-\nabla T) \tag{2.52}$$

$$J_Q = eI_1\epsilon + \frac{I_2}{T}(-\nabla T) \tag{2.53}$$

When the temperature gradient is zero, $J_e = \sigma\epsilon$ where σ is the electrical conductivity. The electrical conductivity can be calculated using $\sigma = e^2 I_0$ Similarly, by switching off the electric filed and allow a temperature gradient, the equation for J_Q becomes $J_Q = k(-\nabla T)$ where k represents the thermal conductivity due to electrons. 'k' can be calculated using

$$k = \frac{1}{T}[I_2 - \frac{I_1^2}{I_0}] \tag{2.54}$$

The equation for Seebeck coefficient, where the temperature gradient is non-zero and in absence of electric current,

$$S = \frac{I_1}{eTI_0} \tag{2.55}$$

Using Boltzmann transport theory, one can find electrical conductivity, Seebeck coefficient (thermopower) and electronic part of thermal conductivity. The calculation of these transport properties in the present thesis was performed using BoltzTraP code, which is based on two assumptions, which are discussed here. Constant Scattering Time Approximation (CSTA), which assumes that the relaxation time is a constant. Another approximation is rigid band approximation, and in this approximation, the small change in the number of valence electrons does not effect the electronic structure profile, and bands are considered to be rigid, and are explained below.

2.7.1 Constant Relaxation Time Approximation

In the previous section, we have discussed the three main perturbation which cause carrier transport, among that collision involves several scattering processes such as electron-electron scattering, electron-phonon scattering, scattering with boundary spaces. To simplify the collision term in BTE, constant scattering time approximation (CSTA) was introduced. After imposing this approximation

one can write the change in electron distribution function due to collision as

$$\frac{f(r,k,t)}{\partial t}_{collision} = -\frac{f(k) - f^0(k)}{\tau(k)} \tag{2.56}$$

where 'τ(k)' is defined as the relaxation time. The physical meaning of the relaxation time can be explained as follows. Consider at time t =0, both external field and temperature gradient perturbations are switched off, the change in electron distribution function will be only due to collision, and the relaxation time is defined as the characteristic time for a system to set back to its equilibrium state.

2.7.2 Rigid band Approximation

The aim of the present thesis is to explore the thermoelectric properties of few prospective materials within the frame work of first principles calculations, where one should understand the TE properties as a function of hole and electron doping. To perform the hole and electron doping calculations, large super cells are needed which is computationally very expensive. A feasible approximation known as rigid band approximation (RBA) is introduced to overcome the above issue. Considering the number of valence electron in the system as 'N_0', and change in the valence electron after doping as 'δn', the total number of electrons can be written as

$$N_e = \int N(E) f(T,\mu) dE \tag{2.57}$$

where 'μ' represents the chemical potential for the doped material with carrier concentration N_e = N_0 + δn. It is assumed that, the electronic structure properties such as band profile and density of states remains rigid for small change in valence electrons. In the present thesis, the thermoelectric properties have been calculated based on RBA. Several studies proved that doping with the elements Sb and Bi does not effect the band structure[123, 124]. The validity of RBA has been verified for optimum doping range and significant number of TE materials are successfully predicted using this approximation [125, 126].

2.8 Computational Details

The electronic structure properties of all the studied compounds were calculated using FP-LAPW method as implemented in Wien2k package. Few of the geometry optimization and phonon dispersions were calculated by using pseudo potential method as implemented in Pwscf program and VASP package. Thermoelectric properties were calculated using DFT and BoltzTraP code. Electronic properties such as band structure, density of states and Fermi surfaces were calculated, and thermoelectric coefficients like thermopower, electrical conductivity scaled by relaxation time (will be addressing as electrical conductivity throughout the thesis) and power factor were calculated. Surface state were calculated by the combination of Wien2k and Wannier90 and Wannier-tools. All the calculations were well converged. In each chapter we have included computational details, which were used for that particular set of calculations.

Chapter 3

Thermoelectric properties of $ZnXPn_2$ (X: Si, Ge, Sn: Pn: P, As, Sb), and tunable ultra high conductivity in $ZnGeSb_2$

We present a detailed first principles study of electronic and TE properties of Zn based pnictide series in this chapter. Compounds considered in this chapter crystallize in tetragonal structure with space group $I\bar{4}2d$, and fall into a well known chalcopyrite family. Precise electronic structure of all the studied compounds is computed using Tran-Blaha modified Becke-Johnson (TB-mBJ) functional. We find the existence of a mixture of light and heavy bands in the band structure which in general strengthen the TE properties. Computed TE properties unveils the p-type conduction to be favorable in $ZnXP_2$ (X: Si, Ge, Sn) and n-type conduction in $ZnGeP_2$ and $ZnSiAs_2$. Mechanical stability of all the studied compounds are verified using elastic constants. The thermopower of the investigated compounds are found to be higher than the prototype chalcopyrite TE materials, together with comparable values for electrical conductivity. In addition, the investigated compounds are found to possess higher thermopower than the well known traditional TE materials at room temperature and above, which motivates further research in these compounds. Among these investigated compounds, $ZnGeSb_2$ turned out to be very promising TE material with huge power factor of the order of 3×10^{17} W m^{-1} K^{-2} s^{-1} due to the huge electrical conductivity around 8.5×10^{25} Ω^{-1} m^{-1} s^{-1}, observed in its massive Dirac state. The calculated electrical conductivity is higher than the well established Dirac materials, and is almost carrier concentration independent with similar behaviour for both n and p type carriers. Detailed analysis of the projected band structure reveals the s, p band inversion around Γ high symmetry point in the tensile strained state of $ZnGeSb_2$ and $ZnSnSb_2$. The possibility of low range of thermal conductivity is also evident from the phonon dispersion plot of $ZnGeSb_2$ and Debye temperature. Application of systematic hydrostatic strain on $ZnGeSb_2$ and $ZnSnSb_2$ reveals the gradual phase change of $ZnGeSb_2$ from a normal semiconducting state, through massive Dirac states, to a topological semi-metal, whereas $ZnSnSb_2$ is transfered from normal semiconductor to metal together with a band inversion. The maximum power factor is observed in the massive Dirac

states of $ZnGeSb_2$ compared to all other compounds.

3.1 Introduction

Exploring potential TE materials is challenging, and for this purpose one has to find promising materials which show desired properties which are already discussed in the previous chapter. Chalcopyrite and pnictide semiconductors of the form ABC_2 have attracted researchers due to diverse physical properties such as high melting point, high refractive index, high nonlinear optical susceptibility and many more[127, 128, 129]. As a result of these properties, both the chalcopyrites and pnictides are identified as promising materials for several device applications like electronic devices [130], nonlinear optical devices [131, 132], photo-voltaic cell [133], thermoelectric applications[134] etc. The investigated compounds are known to be the ternary analogue of zinc blende structure. A significant number of 'Zn' and 'Cd' based pnictides are found to be promising material for nonlinear optical applications, as observed in $ZnGeP_2$ and $CdSiP_2$[135, 136], and $ZnSnP_2$ is identified as a good material for solar cell applications[137]. The structural, electronic and optical properties of these compounds are well explored by experimentalist as well as theoreticians [138, 139, 128]. The TE applications of these compounds are less investigated, even though the prototype compounds have shown good TE properties[140, 141, 142]. The prototype compound $CuGaTe_2$ showed a figure of merit around 1.4 from experiment[143], and theoretical study on this material also confirmed the same [141]. Another 'Ag' based compound $AgGaTe_2$ was also investigated for TE properties [140]. As we have seen in first chapter, earth abundance, stability up to high temperatures and semiconducting electronic properties are fruitful for TE application and the investigated compounds are highly earth abundant and stability of these compounds is reported up to 1000 K[144]. The band structure calculations of these series is quite appreciable with it's remarkable combination of heavy and light bands that can help for TE properties[140]. Here we would like to examine the TE properties of 'Zn' based pnictides. Further, we have studied the possibilities of improving the TE properties by applying strain. To enhance the performance of a TE material we have to either increase the power factor, which highly depends on the electronic structure or suppress the lattice thermal conductivity. Since the power factor is highly dependent on the electronic structure, the enhancement of the power factor can be controlled by tuning the electronic structure of the material, and this can be achieved by the application of pressure or strain[145, 146]. The recent research on TE materials are connected with different quantum states of matter like topological insulators, semi-metals, Dirac materials etc, and studies proved that significant number of TE materials are topological insulators[147, 148]. One such example is the potential applications of graphene, a 2D Dirac material[149] which influenced the material research, and it became a dominant research area in condensed matter theory and experiment. There are several studies reported on the thermoelectric properties of graphene[150, 151], and the latest study revealed the enhancement of power factor in graphene/hBN (hexagonal boron nitride) device[152]. Apart from graphene and graphene like materials, topological insulators like $TlBiSe_2$[153] and Bi_2Te_3 [154] etc, also host surface Dirac states. Subsequently some of the 3D materials like Cd_3As_2 and Na_3Bi show Dirac cone in the bulk [155, 156, 157] form, and this discovery accelerated the research in 3D Dirac materials. In 3D Dirac materials, the conduction and valence band will touch each other at a particular point, and from that point we can observe linearly dispersive energy eigen states in all momentum directions. This can be described by a pseudo relativistic Dirac equation, and these materials can be considered as a 3D analogue of graphene. The spin orbit coupling plays a crucial role in these materials, and in addition to that small perturbations like strain and chemical potential, can help in tuning the 3D bulk Dirac

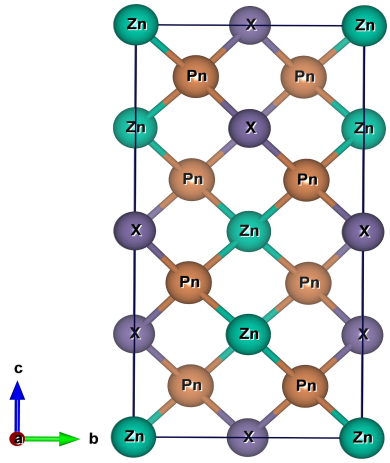

Figure 3.1: Crystal structure of investigated compounds.

states in these compounds. In Dirac materials themselves, massless and massive Dirac fermions are observed, and graphene has massless Dirac fermions, and the compound like $Pb_{1-x}Sn_xTe$ has massive fermions also[158], and this arises due to the small opening between the Dirac points. Current studies on graphene showed that a small band gap between Dirac points are helpful for good device applications[159, 160], which enabled further studies to improve the application of graphene by opening a gap between the Dirac cones. The wide range of applications of the materials which carry massless or massive Dirac fermions has motivated the scientists to explore further. To the best of our knowledge, there are only very few studies available, which are connecting the Dirac states and transport properties.[161] This further encourage us to examine how a massive Dirac state will influence the thermoelectric properties. In this chapter, we have analyzed the electronic and TE properties of $ZnXPn_2$ (X:Si, Ge, Sb; Pn: P, As), $ZnSiSb_2$, $ZnGeSb_2$ and $ZnSnSb_2$, and the effect of hydrostatic strain on electronic structure and TE properties of $ZnGeSb_2$. This chapter is organized as follows, section 3.2 describes the computational details used for the present study, section 3.3 contains the results and discussions which include structural, electronic and thermoelectric properties and section 3.4 concludes the vital points in this chapter.

3.2 Computational details

Present calculations are based on the first principles density functional theory. We have used full potential linearized augmented plane wave (FP-LAPW) method as implemented in WIEN2k package [162, 163]. Experimental lattice parameters are used as an input for our calculations and we have optimized the structure using generalized gradient approximation of Perdew, Burke, and Ernzerhof (GGA-PBE) functional[164]. The optimized lattice parameters are used for further calculations. In general the traditional exchange functionals like local density approximation (LDA) and generalized gradient approximation (GGA) underestimate the band gap of semiconductors and insulators, so we have used Tran-Blaha modified Becke-Johnson (TB-mBJ) functional[165, 166] which is found to be quite successful in reproducing the experimental band gaps[167, 168]. Due to the presence of heavy elements in the investigated compounds, we have included spin orbit coupling in our calculations.

For total energy calculations, band structures and density of states, we have used 10×10×10 k-points in the full Brillouin zone. Transport coefficients such as thermopower and electrical conductivity were calculated using BoltzTraP code[169] with a dense k-mesh of the order of 50×50×50 k-points. The BoltzTraP code is based on rigid band approximation (RBA) [170, 171, 172] and the constant scattering time approximation (CSTA), and these approximations have been successfully applied for several thermoelectric materials[173, 174, 175, 176, 177]. The structural optimization and phonon calculations of $ZnGeSb_2$ are carried out using pseudopotential method as implemented in the Plane wave self-consistent field (Pwscf) program[178]. The hydrostatic strain was applied by changing the lattice parameter by corresponding percentage and further for each strained state, we have optimized the position of atoms.

3.3 Results and discussion

3.3.1 Structural properties

The crystal structure of the investigated Zn-based pnictides in the form $ZnXPn_2$ (X: Si, Ge, Sn; Pn: P, As), $ZnSiSb_2$, $ZnGeSb_2$ and $ZnSnSb_2$ is shown in Figure 3.1, and these compounds possess tetragonal structure with space group $I\bar{4}2d$. The present crystal structure in general can be identified as the ternary analogue of zinc blende structure with slight tetragonal distortion. For all the investigated compounds, each anion Pn (Pn: P, As, Sb) is coordinated by two Zn-type cations and two X-type (X: Si, Ge, Sn) cations and each cation (Zn, Si, Ge, Sn) is tetrahedrally coordinated by four Pn anions (Pn: P, As, Sb). The optimized lattice parameters of $ZnXPn_2$ (X: Si, Ge, Sn; Pn: P, As), $ZnSiSb_2$, $ZnGeSb_2$ and $ZnSnSb_2$ along with the available experimental and other theoretical values are reported in Table 3.1. It is quite evident that the calculated lattice parameters are in good agreement with the experimental and other theoretical reports. In the next section, we have examined the electronic structure properties of $ZnXPn_2$(X: Si, Ge, Sn; Pn: P, As), $ZnSiSb_2$ and $ZnSnSb_2$

3.3.2 Electronic properties of $ZnXPn_2$ (X: Si, Ge, Sb; Pn: P, As), $ZnSiSb_2$ and $ZnSnSb_2$

Figure 3.2 shows the electronic structure of $ZnXPn_2$ (X: Si, Ge, Sn; Pn: P, As), $ZnSiSb_2$ and $ZnSnSb_2$ calculated using TB-mBJ functional. To estimate the range of band gap of all the investigated compounds, we have plotted the calculated band gaps of $ZnXPn_2$(X: Si, Ge, Sb; Pn: P, As), $ZnSiSb_2$ and $ZnSnSb_2$ together with experimental and other reported values, and are given in Figure 3.3. From this figure, it is quite clear that our values are in good agreement with the experimental and other theoretical reports. Among the studied compounds $ZnSiAs_2$, $ZnSiSb_2$ and $ZnGeP_2$ exhibit an indirect band gap, and other compounds are direct gap semiconductors (See Figure 3.2). Previous theoretical study predicted an indirect band gap in $ZnGeP_2$ by comparing it with its binary analogue GaP[179],whereas the present study confirms the indirect band gap nature of $ZnGeP_2$ using TB-mBJ functional along Γ-X direction. In the case of $ZnSiP_2$, Kumar and Tripathy reported the pseudo-direct band gap nature using LDA[129], while the present calculations using TB-mBJ functional reveals the direct band gap nature of $ZnSiP_2$, which might be due the improved band gap obtained using TB-mBJ functional over LDA functional. In the case of 'Si' compounds $ZnSiP_2$, $ZnSiAs_2$ and

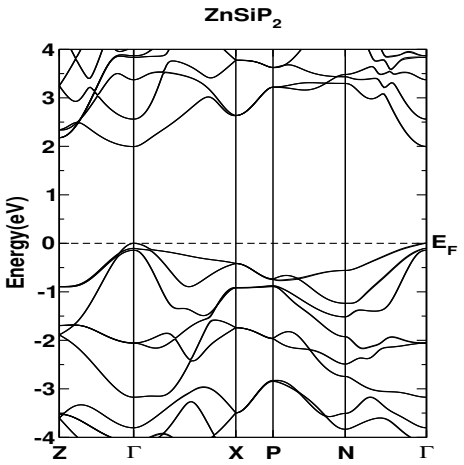
ZnSiP2
Energy(eV)
4
3
2
1
0
-1
-2
-3
-4
EF
Z
Γ
X
P
N
Γ

(a)

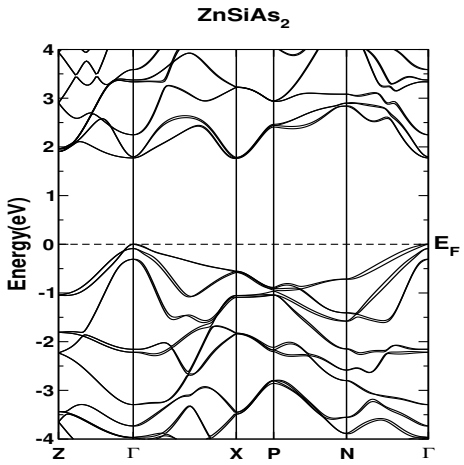
ZnSiAs2
Energy(eV)
4
3
2
1
0
-1
-2
-3
-4
EF
Z
Γ
X
P
N
Γ

(b)

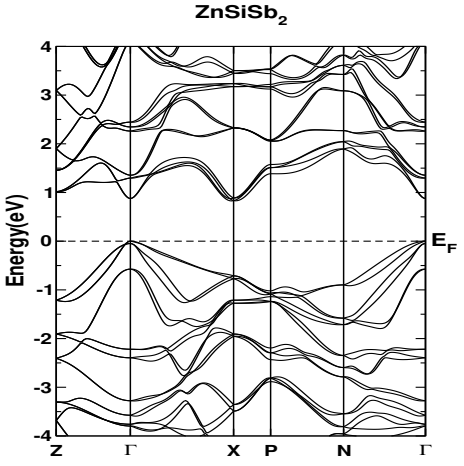
ZnSiSb2
Energy(eV)
4
3
2
1
0
-1
-2
-3
-4
EF
Z
Γ
X
P
N
Γ

(c)

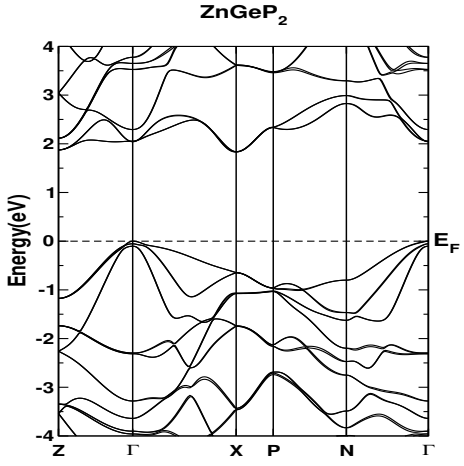
ZnGeP2
Energy(eV)
4
3
2
1
0
-1
-2
-3
-4
EF
Z
Γ
X
P
N
Γ

(d)

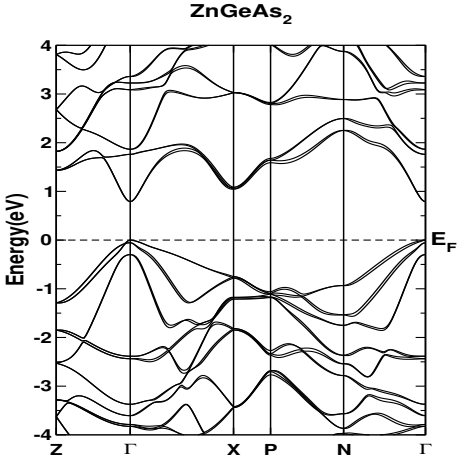
ZnGeAs2
Energy(eV)
4
3
2
1
0
-1
-2
-3
-4
EF
Z
Γ
X
P
N
Γ

(e)

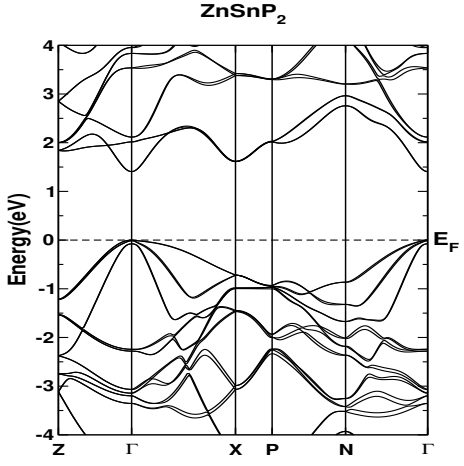
ZnSnP2
Energy(eV)
4
3
2
1
0
-1
-2
-3
-4
EF
Z
Γ
X
P
N
Γ

(f)

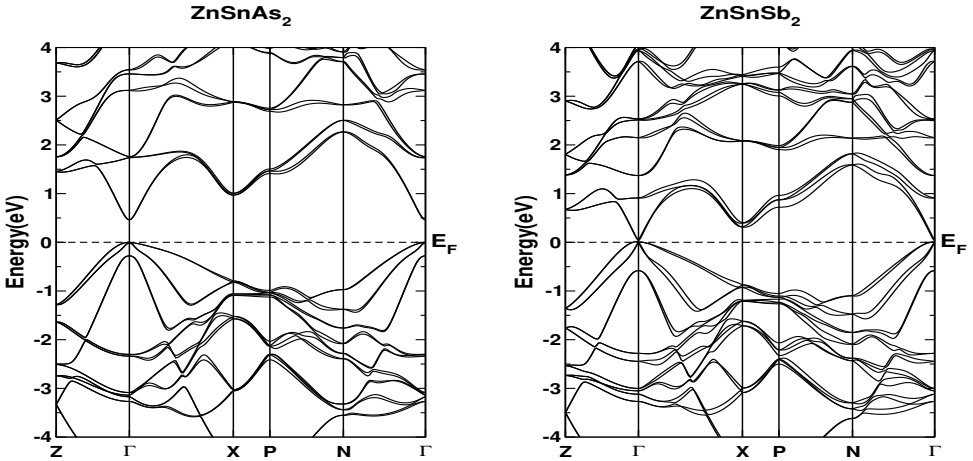

Figure 3.2: Calculated band structures using TB-mBJ functional with optimized lattice parameters a) $ZnSiP_2$ b) $ZnSiAs_2$, c) $ZnSiSb_2$, d) $ZnGeP_2$, e) $ZnGeAs_2$, f) $ZnSnP_2$, g) $ZnSnAs_2$, h) $ZnSnSb_2$

$ZnSiSb_2$, the band gap is found to decrease from $ZnSiP_2$ to $ZnSiSb_2$. A similar reduction in band gap is found in the case of 'Ge' and 'Sn' compound as we move from 'P' to 'As'. The decremental trend in band gap going down the column in periodic table might be due to the increase in size of the atom. Further we have examined the band profile of all the compounds in detail. The dispersion of bands along Γ-Z direction (along c axis) is little higher than the dispersion of bands along Γ-N direction (planar direction) in valence band, whereas in conduction band, dispersion of band along Γ-N direction is more pronounced than Γ-Z direction, which is confirmed through effective mass calculations in all the compounds as given in Table 3.2. To perceive the contribution from each atom near the Fermi level, we have examined the total and partial density of sates of $ZnXPn_2$ (X: Si, Ge, Sn; Pn: P, As), $ZnSiSb_2$ and $ZnSnSb_2$, and are reported in Figure 3.4. In the case of $ZnXPn_2$ (X: Si, Ge, Sn; Pn: P, As), near the Fermi level (E_F) in valence band, the main contribution stems from the Pn-p state, Zn- p and d states, whereas in conduction band X-s, p and Pn-s, p states are dominating more. For $ZnSiSb_2$ and $ZnSnSb_2$, Sb-p states and Zn-p, Zn-d are dominating in valence band edge, whereas in conduction band, (Si,Sn) and Sb p and s states play a major role. Compared to valence band, the extent of hybridization between X and Pn states is more in the conduction band for all the investigated compounds (see Figure 3.4). This shows that the electrical conductivity in the case of electron doping may dominate a little than hole doping for all the investigated compounds. We observed a sharp increment in density of states around valence band edge for all the studied compounds, and this trend is more pronounced in $ZnXP_2$ compounds compared to 'As' compounds. From this, we infer that hole doped $ZnXP_2$ compounds might show higher value of thermopower than 'As' compounds. For 'Si' compounds in conduction band, we observed the Si-s state to shift towards the Fermi level when the anion 'P' is replaced with 'As' and 'Sb', causing a reduction of band gap from 'P' to 'Sb'. The same scenario is observed in other 'Ge' and 'Sn' compounds when 'P' is replaced with 'As'. Similar increment in density of states at both valence band and conduction band indicate good TE properties for both the carriers, in all the investigated compounds. Mechanical stability is yet another important criteria for any device applications. Here we have confirmed the

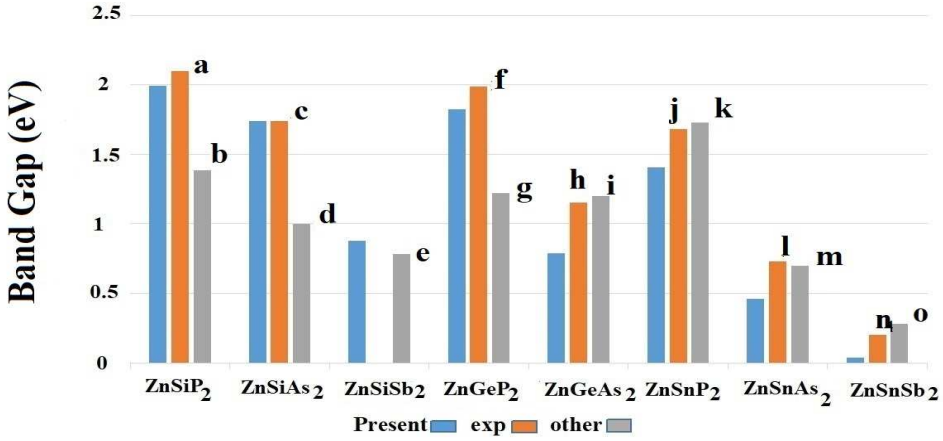

Figure 3.3: Calculated band gaps for all investigated compounds along with available experimental and other theoretical reports a: Ref.[[190]], b: Ref.[[129]], c: [Ref.[191]], d: [Ref.[192]], e: Ref.[[193]], f: Ref.[[194]], g: Ref.[[179]], h,i: Ref.[[195]], j: Ref.[[201]], k: Ref.[[202]], l,m: Ref.[[203]], n: Ref.[[204]], o: Ref.[[205]]

mechanical stability of all the compounds using elastic constants. Computed elastic constants of the investigated compounds are reported in Table 3.3. All the compounds are found to be mechanically stable. Debye temperature of all the compounds are reported in same table. In the case of 'Si' based compounds, $ZnSiP_2$ has highest value of Debye temperature and 'As' and 'Sb' compounds show smaller value. In line with 'Si' compounds, 'Ge' and 'Sn' compounds also follow the similar trend. The lower Debye temperature values of 'As' and 'Sb' compounds indicate the possibility of low thermal conductivity in these compounds. Further we have studied the TE properties which are explained in the succeeding section.

3.3.3 Thermoelectric properties of $ZnXPn_2$ (X: Si, Ge, Sn; Pn: P, As), $ZnSiSb_2$ and $ZnSnSb_2$

Thermoelectric properties of all the investigated compounds were calculated for temperatures ranging between 300 K to 900 K. The thermopower, electrical conductivity and power-factor are calculated as functions of both carrier concentration and temperature. We have investigated the transport properties for the concentrations lying between 1×10^{18} to 1×10^{21} cm^{-3} for all the investigated compounds, which is an optimum carrier concentration range for better thermoelectric performance. As mentioned earlier, the investigated compounds crystallize in tetragonal structure, and it is very important to observe the variation of transport properties along different crystallographic directions. For this purpose, we have investigated the thermoelectric properties along the crystallographic *'a'* and *'c'* axes. We have plotted the variation of thermopower as a function of both hole and electron concentrations at different temperatures along the *'a'* and *'c'* axes of all the compounds and are presented in Figure 3.5. For all these cases except $ZnSnAs_2$, the magnitude of thermopower is decreasing with increasing concentrations for both the carriers, which is a regular trend in TE

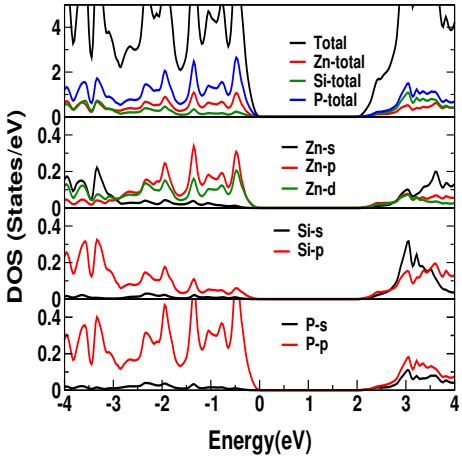
Total
Zn-total
Si-total
P-total
Zn-s
Zn-p
Zn-d
Si-s
Si-p
P-s
P-p
DOS (States/eV)
Energy(eV)

(a)

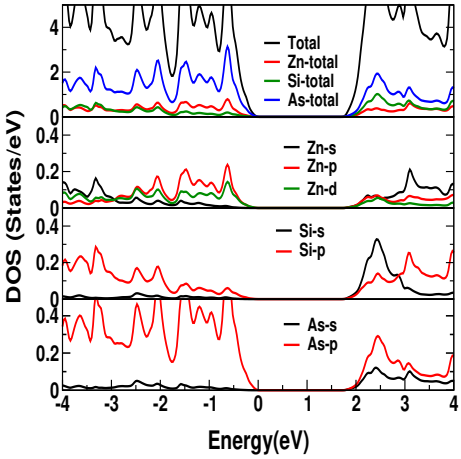
Total
Zn-total
Si-total
As-total
Zn-s
Zn-p
Zn-d
Si-s
Si-p
As-s
As-p
DOS (States/eV)
Energy(eV)

(b)

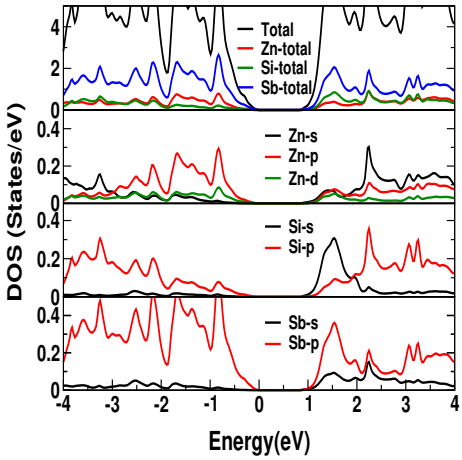
Total
Zn-total
Si-total
Sb-total
Zn-s
Zn-p
Zn-d
Si-s
Si-p
Sb-s
Sb-p
DOS (States/eV)
Energy(eV)

(c)

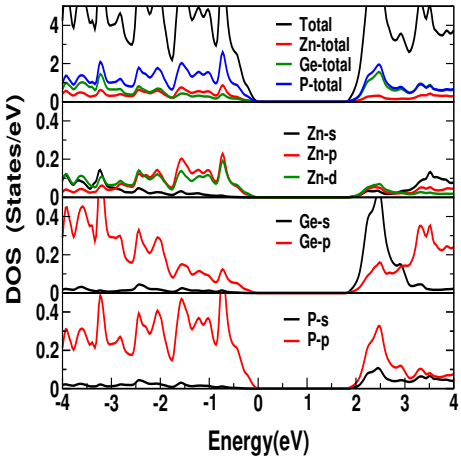
Total
Zn-total
Ge-total
P-total
Zn-s
Zn-p
Zn-d
Ge-s
Ge-p
P-s
P-p
DOS (States/eV)
Energy(eV)

(d)

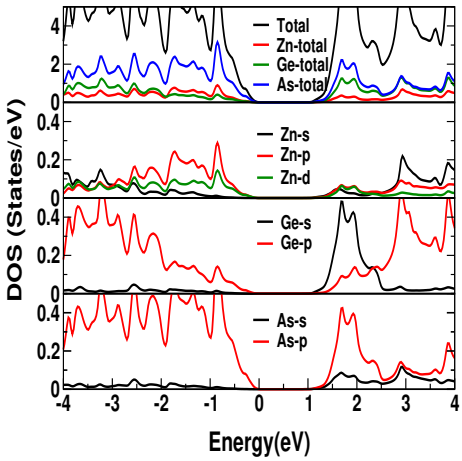
Total
Zn-total
Ge-total
As-total
Zn-s
Zn-p
Zn-d
Ge-s
Ge-p
As-s
As-p
DOS (States/eV)
Energy(eV)

(e)

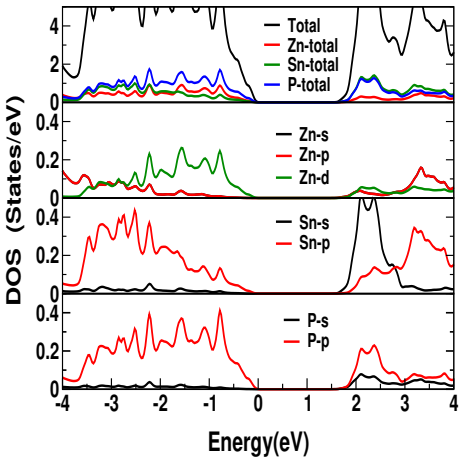
Total
Zn-total
Sn-total
P-total
Zn-s
Zn-p
Zn-d
Sn-s
Sn-p
P-s
P-p
DOS (States/eV)
Energy(eV)

(f)

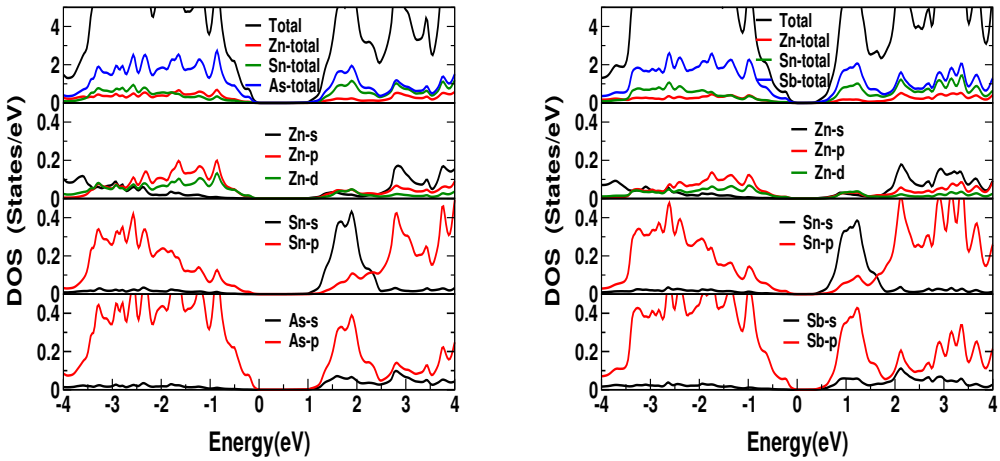

Figure 3.4: Calculated density of states of all the investigated compounds a) $ZnSiP_2$ b) $ZnSiAs_2$, c) $ZnSiSb_2$, d) $ZnGeP_2$, e) $ZnGeAs_2$, f) $ZnSnP_2$, g) $ZnSnAs_2$, h) $ZnSnSb_2$

materials. From the analysis of thermopower plots, we found all the compounds to possess higher thermopower values for holes compared to electrons. This might be due to the bands being less dispersive in the case of valence band maximum compared to the conduction band minimum. For all the compounds we did not observe any significant difference in thermopower along *'a'* and *'c'* directions which confirms the isotropic nature in thermopower along *'a'* and *'c'* crystallographic directions. The maximum thermopower is found in hole doped $ZnSiP_2$ compared to all other compounds. For hole doped $ZnSnAs_2$ we observed a bipolar conductivity at 900 K and for $ZnSiSb_2$ from 300 K onwards bipolar conductivity is observed at low concentration range around (1×10^{18} cm^{-3}),which might be due to the lesser band gaps of these compounds. For $ZnSiSb_2$ promising thermopower values are observed at higher concentration range from 1×10^{19} cm^{-3} to 1×10^{21} cm^{-3}, which is accepted as a considerable range. Further we have addressed electrical conductivity as a function of both holes and electrons along different crystallographic directions at different temperatures in Figure 3.6. For all the compounds electrical conductivity is increasing with increasing carrier concentration for both holes and electrons. A similar type of isotropic nature is found in electrical conductivity also, implying the investigated compounds to possess isotropic nature of TE properties. To understand the net TE properties, we have plotted the variation of power factor as a function of carrier concentrations at different temperatures for all the compounds, and the same is given is in Figure 3.7, and from the figure it is clear that the power-factor values are higher for all the investigated compounds for the range of optimum carrier concentrations(1×10^{18} to 1×10^{21} cm^{-3}). For hole doping, power-factor value is decreasing down the column, and for electron doping also a similar trend is observed except for $ZnSiPn_2$, where $ZnSiAs_2$ has secured enhanced value than $ZnSiP_2$. Another vital point to be mentioned about the investigated compounds is that the reported lattice thermal conductivity is higher compared to other TE materials[180], which is evident from the Debye temperature values. If one can reduce the lattice thermal conductivity by some techniques (such as superlattice, nano-structuring, etc), all the investigated compounds would be promising materials for TE applications.

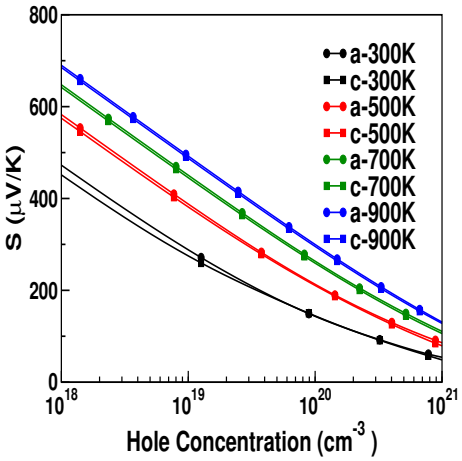
S (μV/K)
Hole Concentration (cm-3)
a-300K
c-300K
a-500K
c-500K
a-700K
c-700K
a-900K
c-900K

(a)

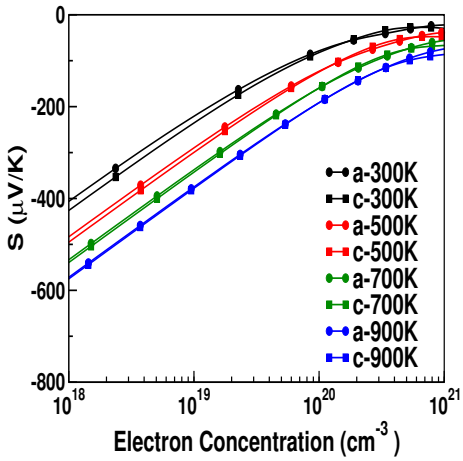
S (μV/K)
Electron Concentration (cm-3)
a-300K
c-300K
a-500K
c-500K
a-700K
c-700K
a-900K
c-900K

(b)

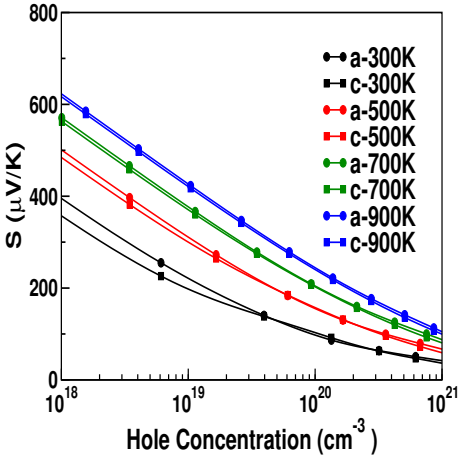
S (μV/K)
Hole Concentration (cm-3)
a-300K
c-300K
a-500K
c-500K
a-700K
c-700K
a-900K
c-900K

(c)

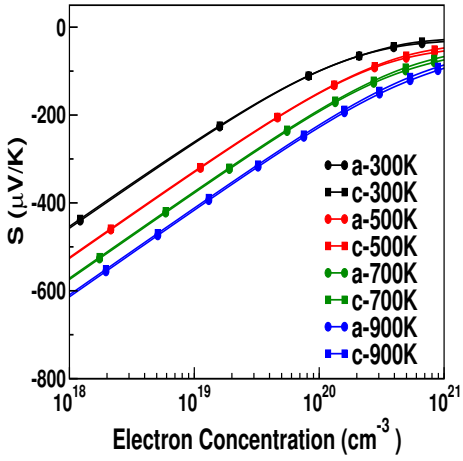
S (μV/K)
Electron Concentration (cm-3)
a-300K
c-300K
a-500K
c-500K
a-700K
c-700K
a-900K
c-900K

(d)

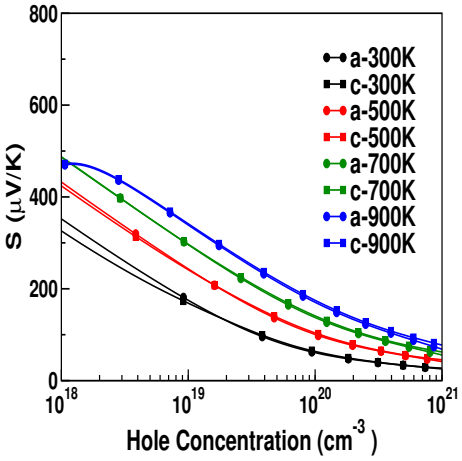
S (μV/K)
Hole Concentration (cm-3)
a-300K
c-300K
a-500K
c-500K
a-700K
c-700K
a-900K
c-900K

(e)

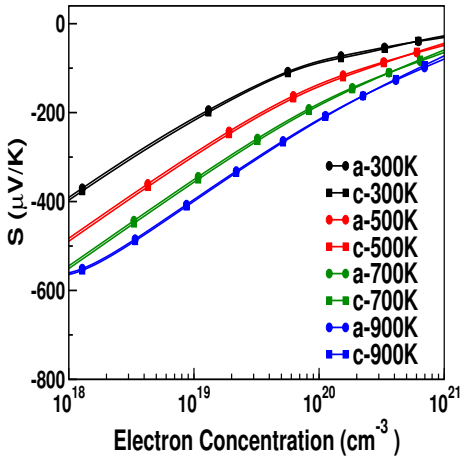
S (μV/K)
Electron Concentration (cm-3)
a-300K
c-300K
a-500K
c-500K
a-700K
c-700K
a-900K
c-900K

(f)

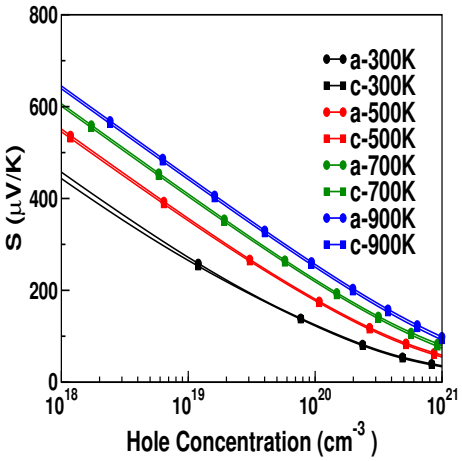
S (μV/K)
Hole Concentration (cm-3)
a-300K
c-300K
a-500K
c-500K
a-700K
c-700K
a-900K
c-900K

(g)

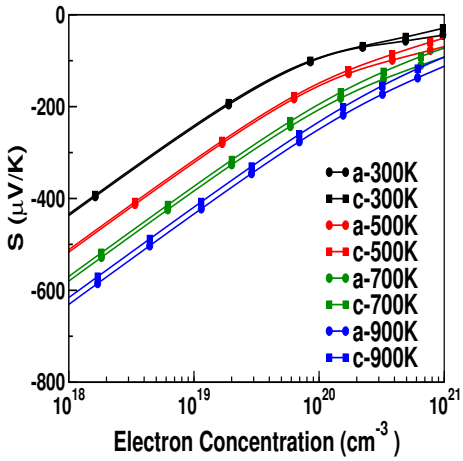
S (μV/K)
Electron Concentration (cm-3)
a-300K
c-300K
a-500K
c-500K
a-700K
c-700K
a-900K
c-900K

(h)

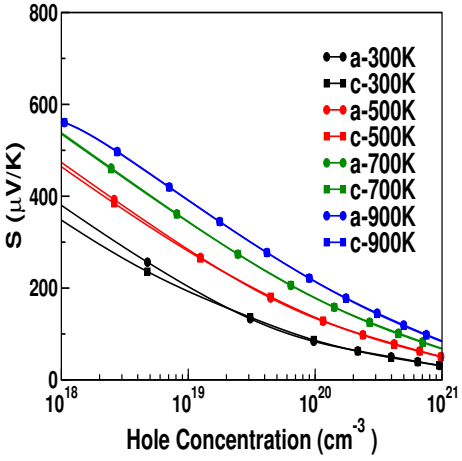
S (μV/K)
Hole Concentration (cm-3)
a-300K
c-300K
a-500K
c-500K
a-700K
c-700K
a-900K
c-900K

(i)

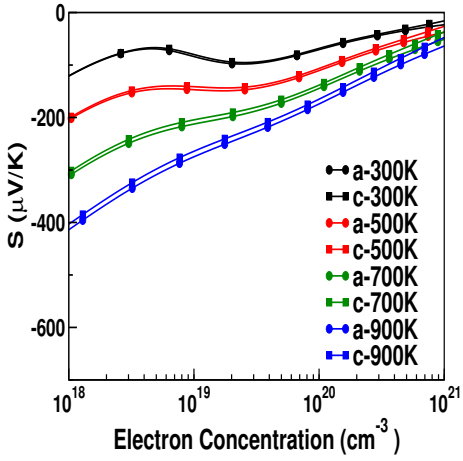
S (μV/K)
Electron Concentration (cm-3)
a-300K
c-300K
a-500K
c-500K
a-700K
c-700K
a-900K
c-900K

(j)

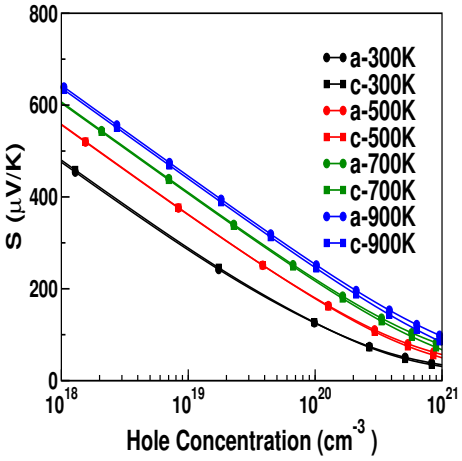
S (μV/K)
Hole Concentration (cm-3)
a-300K
c-300K
a-500K
c-500K
a-700K
c-700K
a-900K
c-900K

(k)

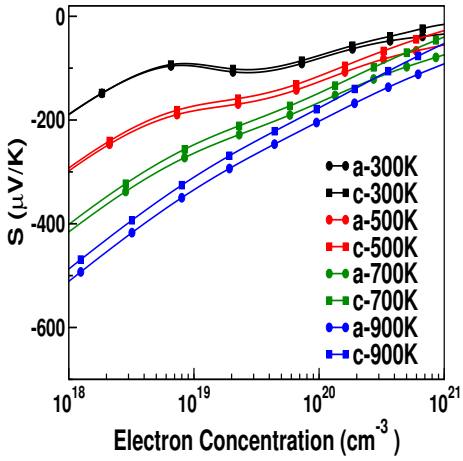
S (μV/K)
Electron Concentration (cm-3)
a-300K
c-300K
a-500K
c-500K
a-700K
c-700K
a-900K
c-900K

(l)

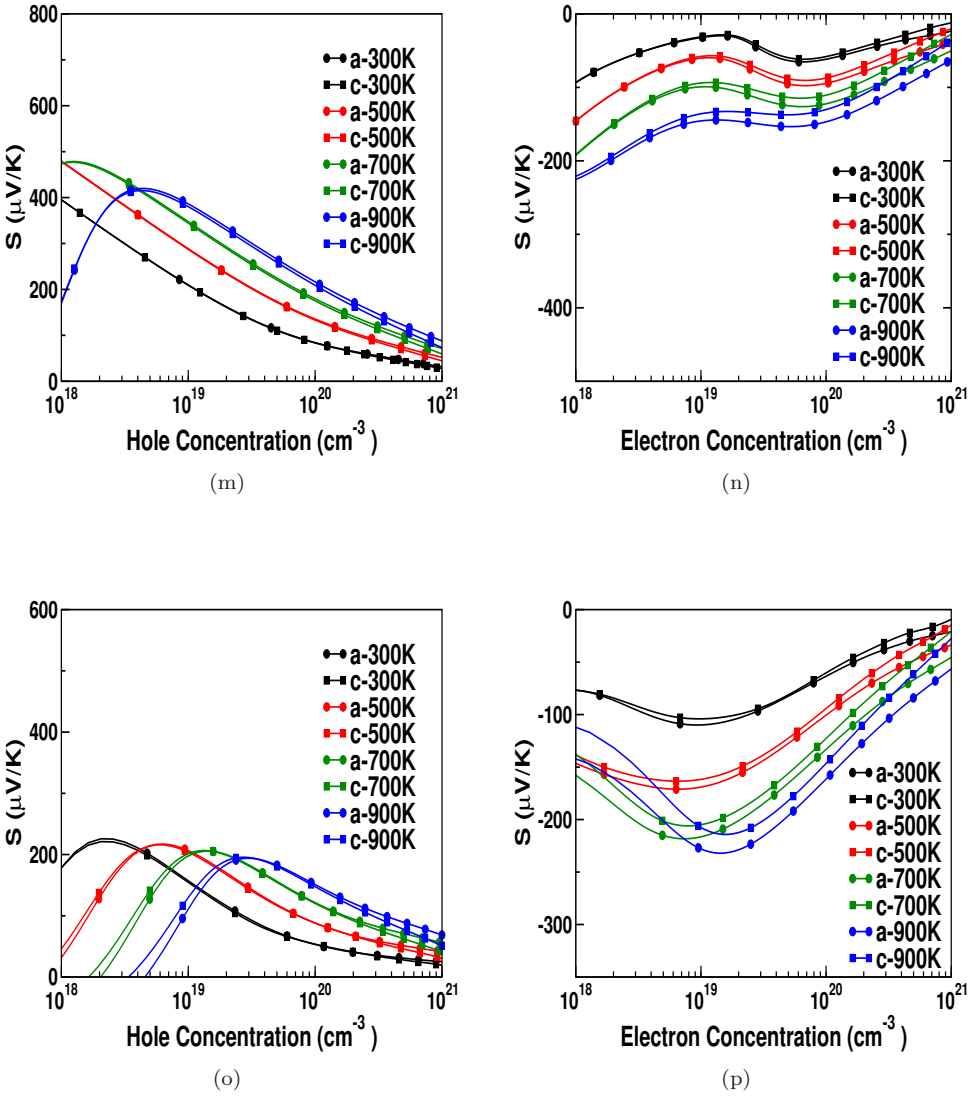

Figure 3.5: Variation of thermopower as a function of hole and electron concentrations for all the compounds at different temperature, (a,b) $ZnSiP_2$, (c,d) $ZnSiAs_2$, (e,f) $ZnSiSb_2$, (g,h) $ZnGeP_2$, (i,j) $ZnGeAs_2$, (k,l) $ZnSnP_2$, (m,n) $ZnSnAs_2$, (o,p) $ZnSnSb_2$

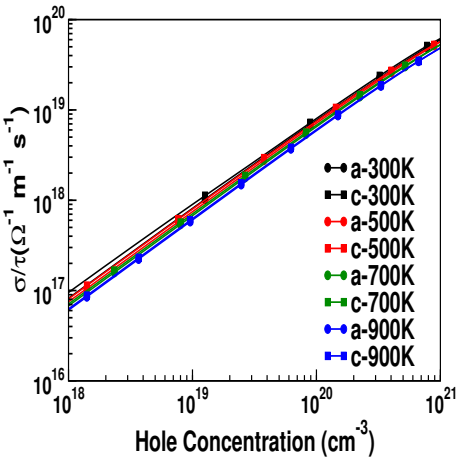
σ/τ(Ω⁻¹ m⁻¹ s⁻¹)
Hole Concentration (cm⁻³)
a-300K
c-300K
a-500K
c-500K
a-700K
c-700K
a-900K
c-900K

(a)

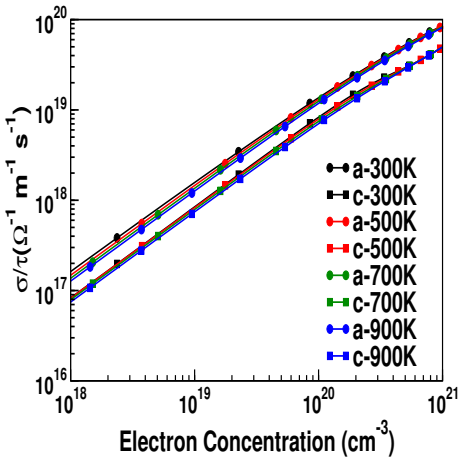
σ/τ(Ω⁻¹ m⁻¹ s⁻¹)
Electron Concentration (cm⁻³)
a-300K
c-300K
a-500K
c-500K
a-700K
c-700K
a-900K
c-900K

(b)

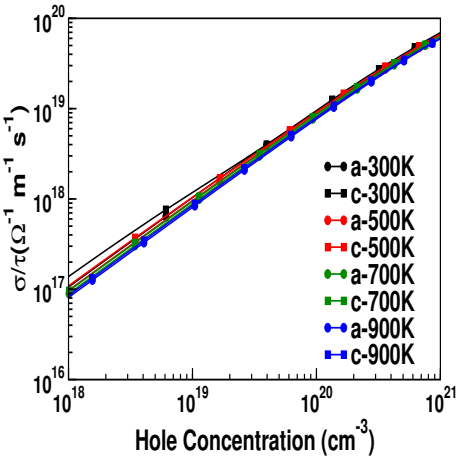
σ/τ(Ω⁻¹ m⁻¹ s⁻¹)
Hole Concentration (cm⁻³)
a-300K
c-300K
a-500K
c-500K
a-700K
c-700K
a-900K
c-900K

(c)

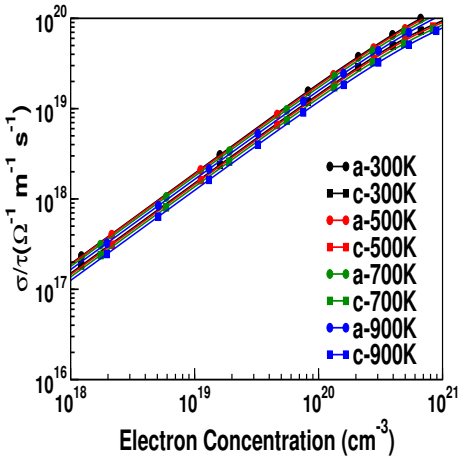
σ/τ(Ω⁻¹ m⁻¹ s⁻¹)
Electron Concentration (cm⁻³)
a-300K
c-300K
a-500K
c-500K
a-700K
c-700K
a-900K
c-900K

(d)

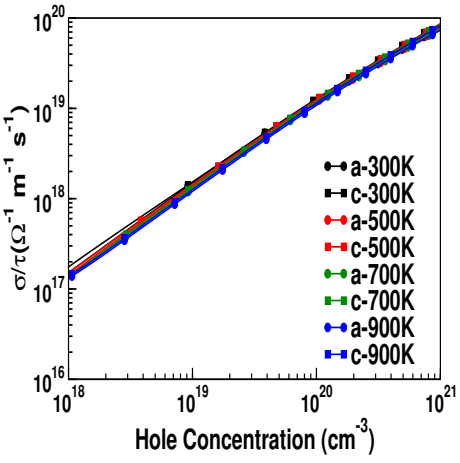
σ/τ(Ω⁻¹ m⁻¹ s⁻¹)
Hole Concentration (cm⁻³)
a-300K
c-300K
a-500K
c-500K
a-700K
c-700K
a-900K
c-900K

(e)

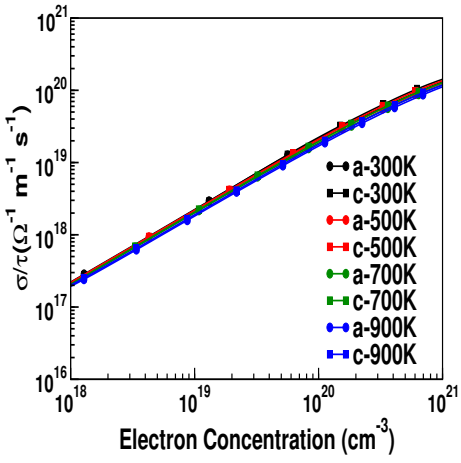
σ/τ(Ω⁻¹ m⁻¹ s⁻¹)
Electron Concentration (cm⁻³)
a-300K
c-300K
a-500K
c-500K
a-700K
c-700K
a-900K
c-900K

(f)

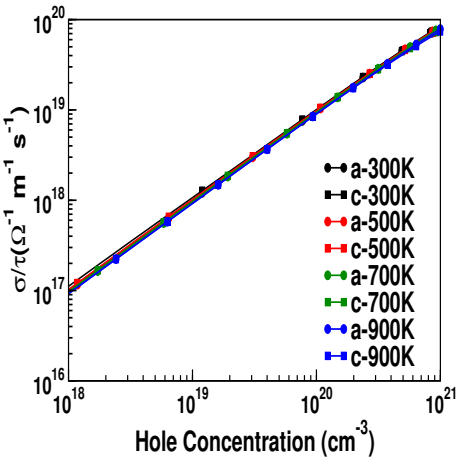
σ/τ(Ω⁻¹ m⁻¹ s⁻¹)
Hole Concentration (cm⁻³)
a-300K
c-300K
a-500K
c-500K
a-700K
c-700K
a-900K
c-900K

(g)

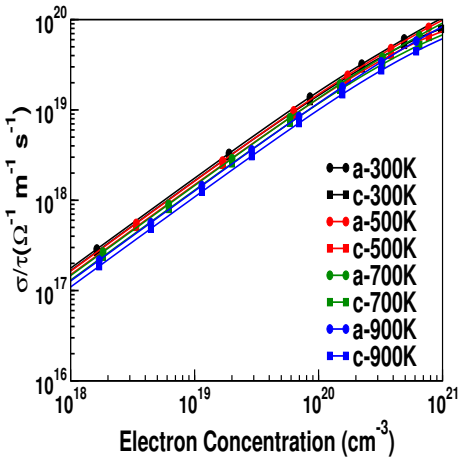
σ/τ(Ω⁻¹ m⁻¹ s⁻¹)
Electron Concentration (cm⁻³)
a-300K
c-300K
a-500K
c-500K
a-700K
c-700K
a-900K
c-900K

(h)

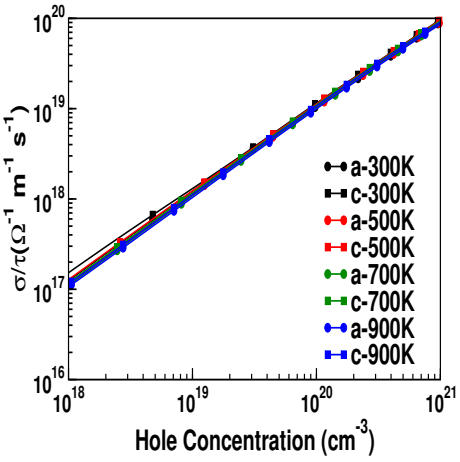
σ/τ(Ω⁻¹ m⁻¹ s⁻¹)
Hole Concentration (cm⁻³)
a-300K
c-300K
a-500K
c-500K
a-700K
c-700K
a-900K
c-900K

(i)

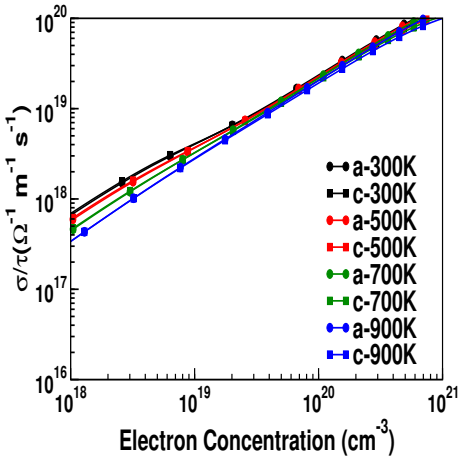
σ/τ(Ω⁻¹ m⁻¹ s⁻¹)
Electron Concentration (cm⁻³)
a-300K
c-300K
a-500K
c-500K
a-700K
c-700K
a-900K
c-900K

(j)

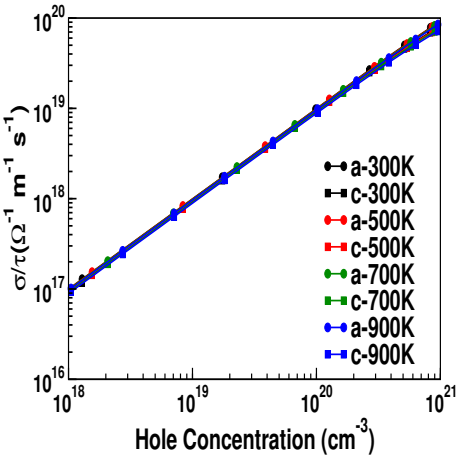
σ/τ(Ω⁻¹ m⁻¹ s⁻¹)
Hole Concentration (cm⁻³)
a-300K
c-300K
a-500K
c-500K
a-700K
c-700K
a-900K
c-900K

(k)

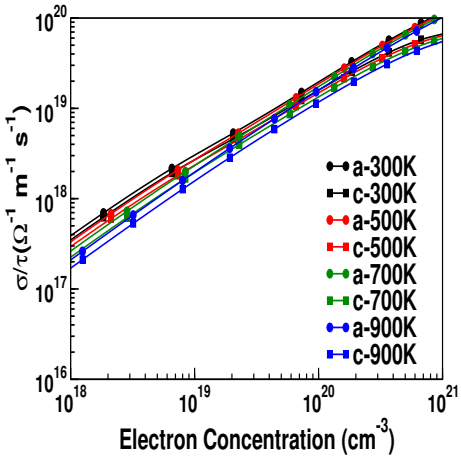
σ/τ(Ω⁻¹ m⁻¹ s⁻¹)
Electron Concentration (cm⁻³)
a-300K
c-300K
a-500K
c-500K
a-700K
c-700K
a-900K
c-900K

(l)

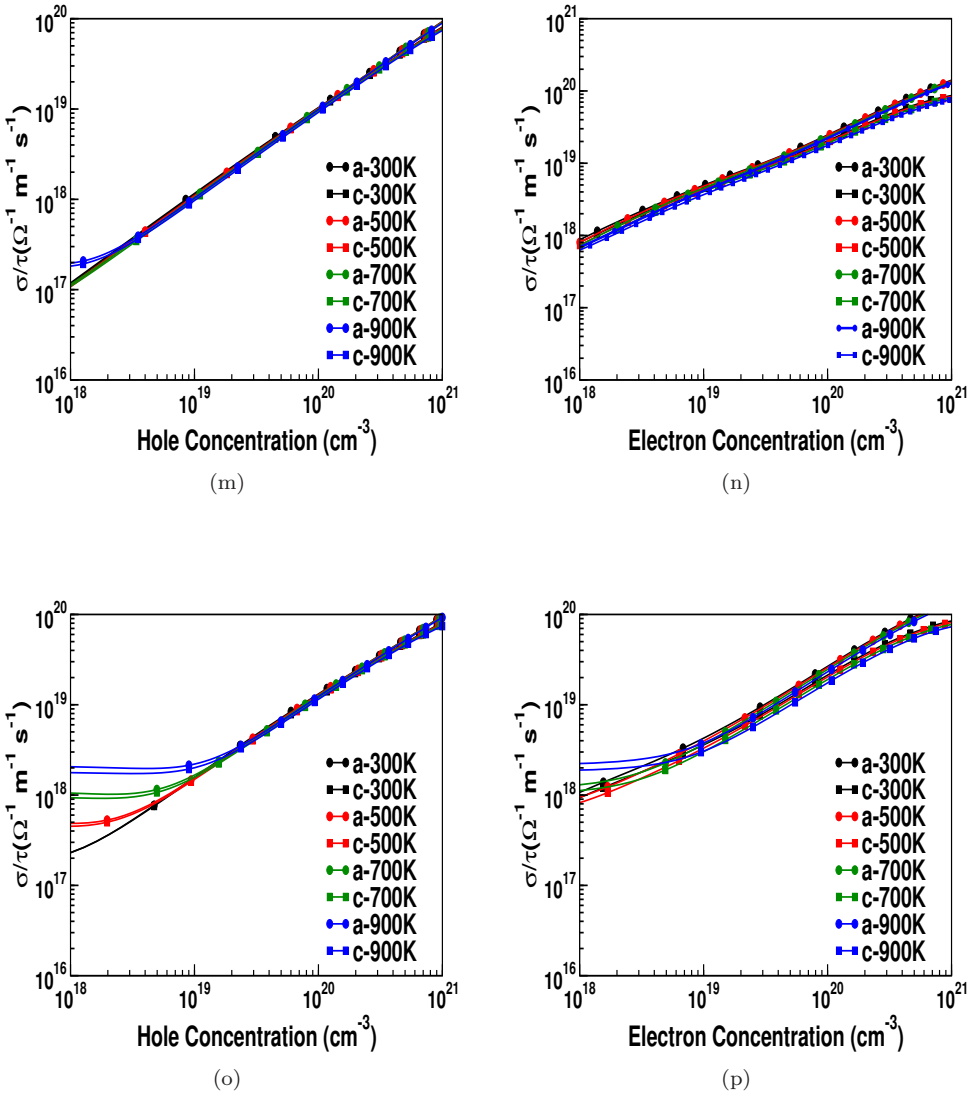

Figure 3.6: Variation of electrical conductivity as a function of hole and electron concentration for all the compounds at different temperature (a,b) $ZnSiP_2$, (c,d) $ZnSiAs_2$, (e,f) $ZnSiSb_2$, (g,h) $ZnGeP_2$, (i,j) $ZnGeAs_2$, (k,l) $ZnSnP_2$, (m,n) $ZnSnAs_2$, (o,p) $ZnSnSb_2$.

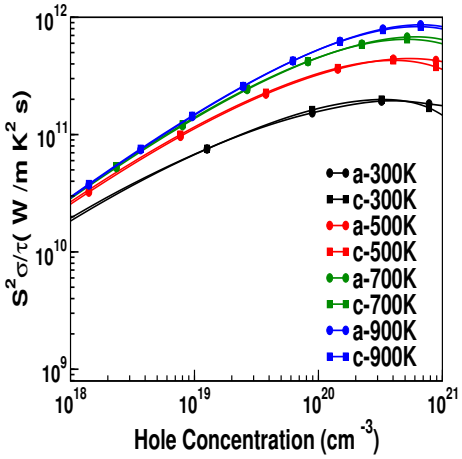
10^{12}
10^{11}
10^{10}
10^{9}
$S^2\sigma/\tau$(W /m K^2 s)
a-300K
c-300K
a-500K
c-500K
a-700K
c-700K
a-900K
c-900K
10^{18}
10^{19}
10^{20}
10^{21}
Hole Concentration (cm^{-3})

(a)

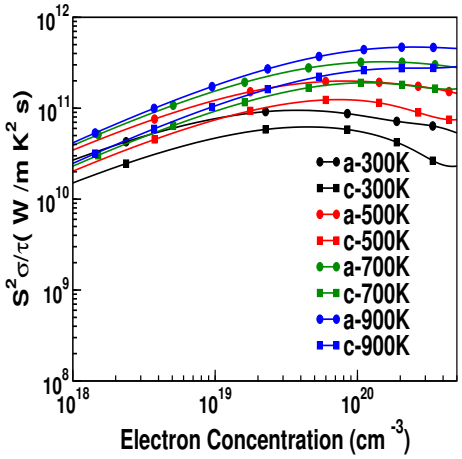
10^{12}
10^{11}
10^{10}
10^{9}
10^{8}
$S^2\sigma/\tau$(W /m K^2 s)
a-300K
c-300K
a-500K
c-500K
a-700K
c-700K
a-900K
c-900K
10^{18}
10^{19}
10^{20}
Electron Concentration (cm^{-3})

(b)

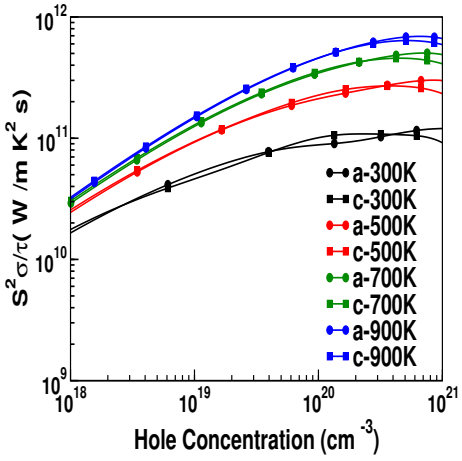
10^{12}
10^{11}
10^{10}
10^{9}
$S^2\sigma/\tau$(W /m K^2 s)
a-300K
c-300K
a-500K
c-500K
a-700K
c-700K
a-900K
c-900K
10^{18}
10^{19}
10^{20}
10^{21}
Hole Concentration (cm^{-3})

(c)

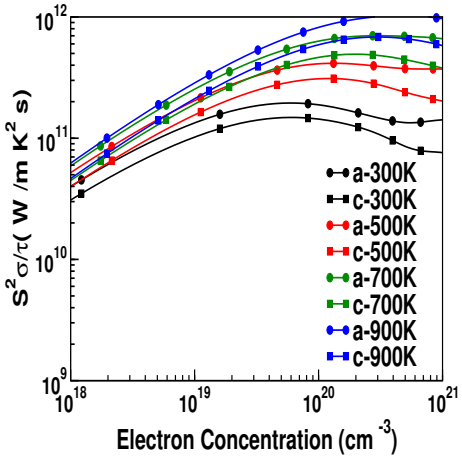
10^{12}
10^{11}
10^{10}
10^{9}
$S^2\sigma/\tau$(W /m K^2 s)
a-300K
c-300K
a-500K
c-500K
a-700K
c-700K
a-900K
c-900K
10^{18}
10^{19}
10^{20}
10^{21}
Electron Concentration (cm^{-3})

(d)

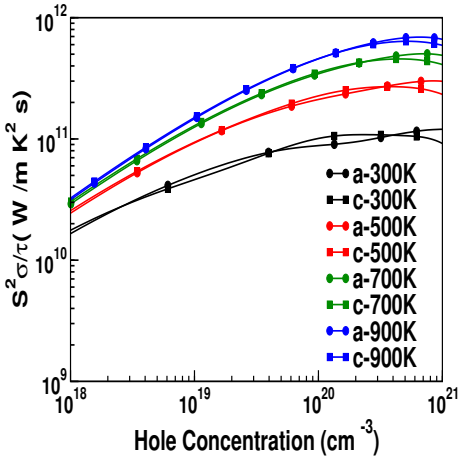
10^{12}
10^{11}
10^{10}
10^{9}
$S^2\sigma/\tau$(W /m K^2 s)
a-300K
c-300K
a-500K
c-500K
a-700K
c-700K
a-900K
c-900K
10^{18}
10^{19}
10^{20}
10^{21}
Hole Concentration (cm^{-3})

(e)

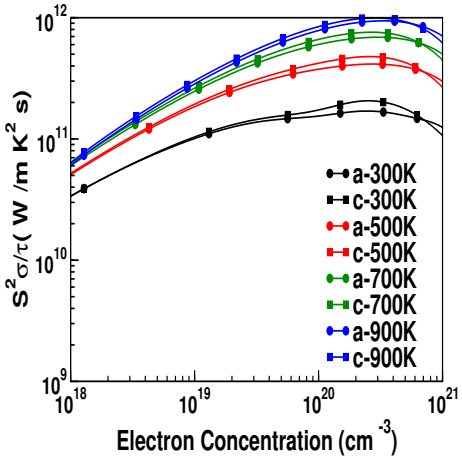
10^{12}
10^{11}
10^{10}
10^{9}
$S^2\sigma/\tau$(W /m K^2 s)
a-300K
c-300K
a-500K
c-500K
a-700K
c-700K
a-900K
c-900K
10^{18}
10^{19}
10^{20}
10^{21}
Electron Concentration (cm^{-3})

(f)

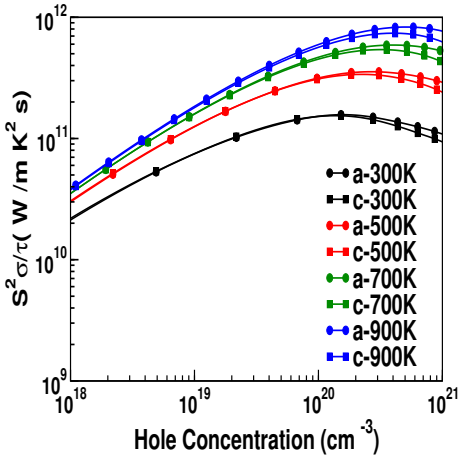
$S^2\sigma/\tau$(W /m K^2 s)
Hole Concentration (cm^{-3})
a-300K
c-300K
a-500K
c-500K
a-700K
c-700K
a-900K
c-900K

(g)

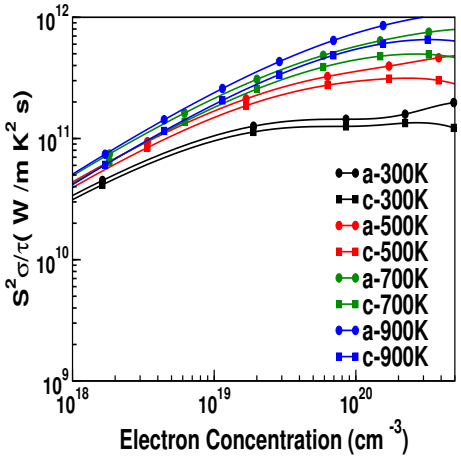
$S^2\sigma/\tau$(W /m K^2 s)
Electron Concentration (cm^{-3})
a-300K
c-300K
a-500K
c-500K
a-700K
c-700K
a-900K
c-900K

(h)

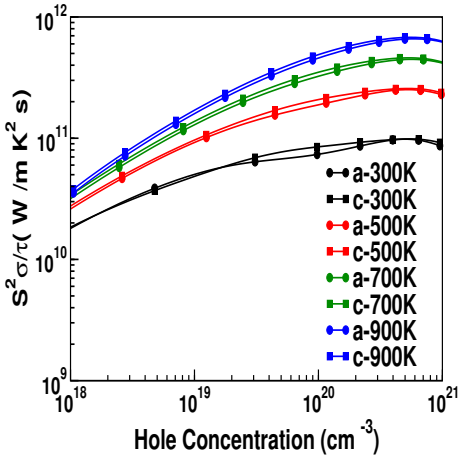
$S^2\sigma/\tau$(W /m K^2 s)
Hole Concentration (cm^{-3})
a-300K
c-300K
a-500K
c-500K
a-700K
c-700K
a-900K
c-900K

(i)

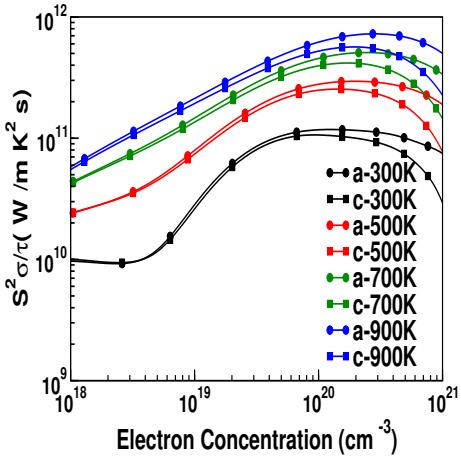
$S^2\sigma/\tau$(W /m K^2 s)
Electron Concentration (cm^{-3})
a-300K
c-300K
a-500K
c-500K
a-700K
c-700K
a-900K
c-900K

(j)

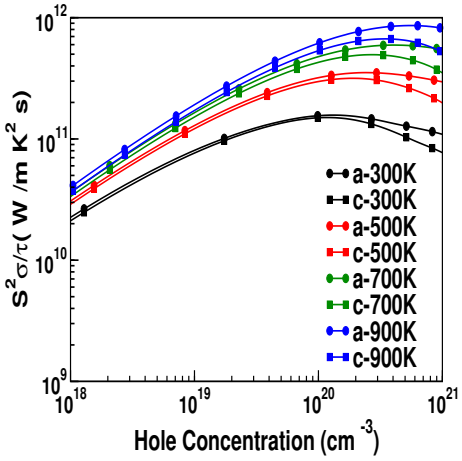
$S^2\sigma/\tau$(W /m K^2 s)
Hole Concentration (cm^{-3})
a-300K
c-300K
a-500K
c-500K
a-700K
c-700K
a-900K
c-900K

(k)

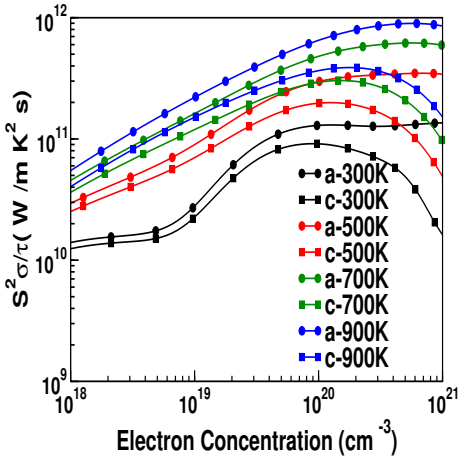
$S^2\sigma/\tau$(W /m K^2 s)
Electron Concentration (cm^{-3})
a-300K
c-300K
a-500K
c-500K
a-700K
c-700K
a-900K
c-900K

(l)

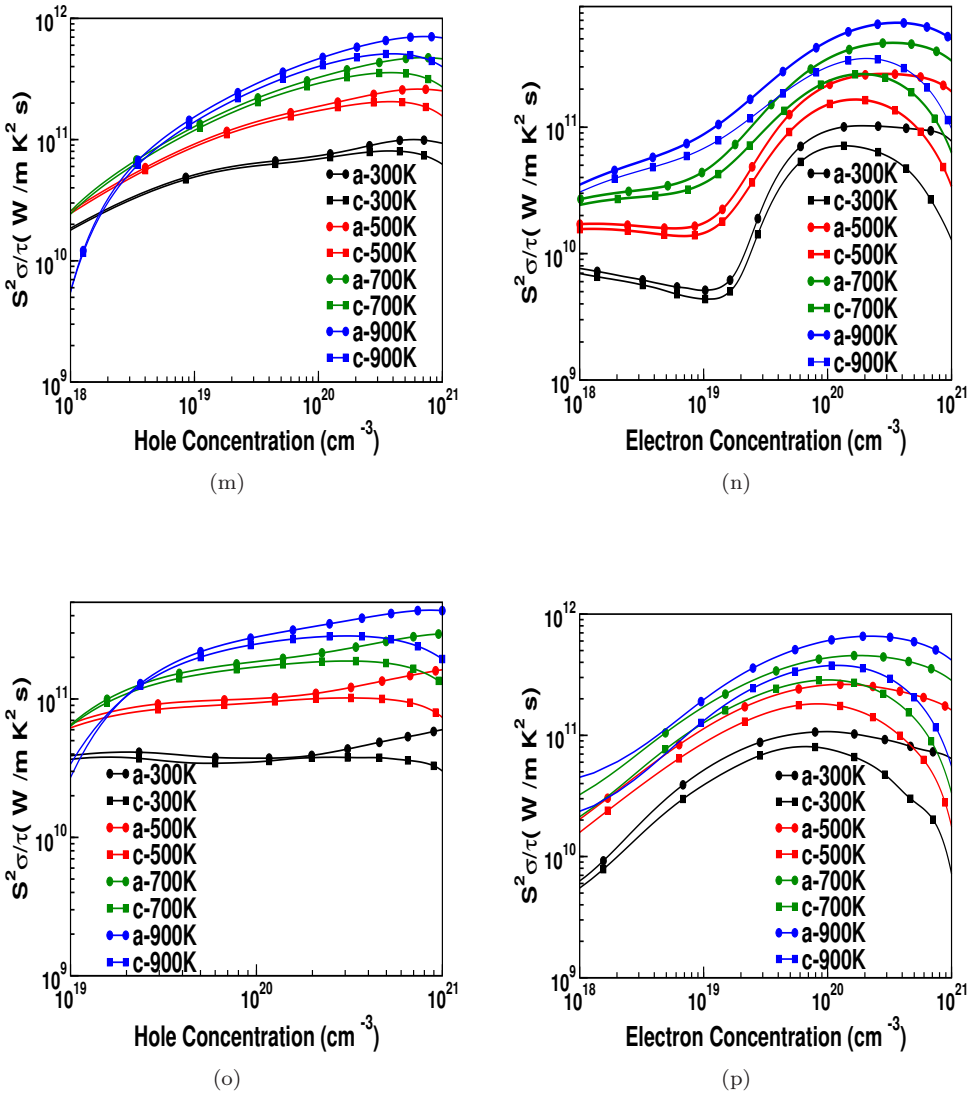

Figure 3.7: Variation of power factor as a function of hole and electron concentrations for all the compounds at different temperature (a,b) $ZnSiP_2$, (c,d) $ZnSiAs_2$, (e,f) $ZnSiSb_2$, (g,h) $ZnGeP_2$, (i,j) $ZnGeAs_2$, (k,l) $ZnSnP_2$, (m,n) $ZnSnAs_2$, (o,p) $ZnSnSb_2$.

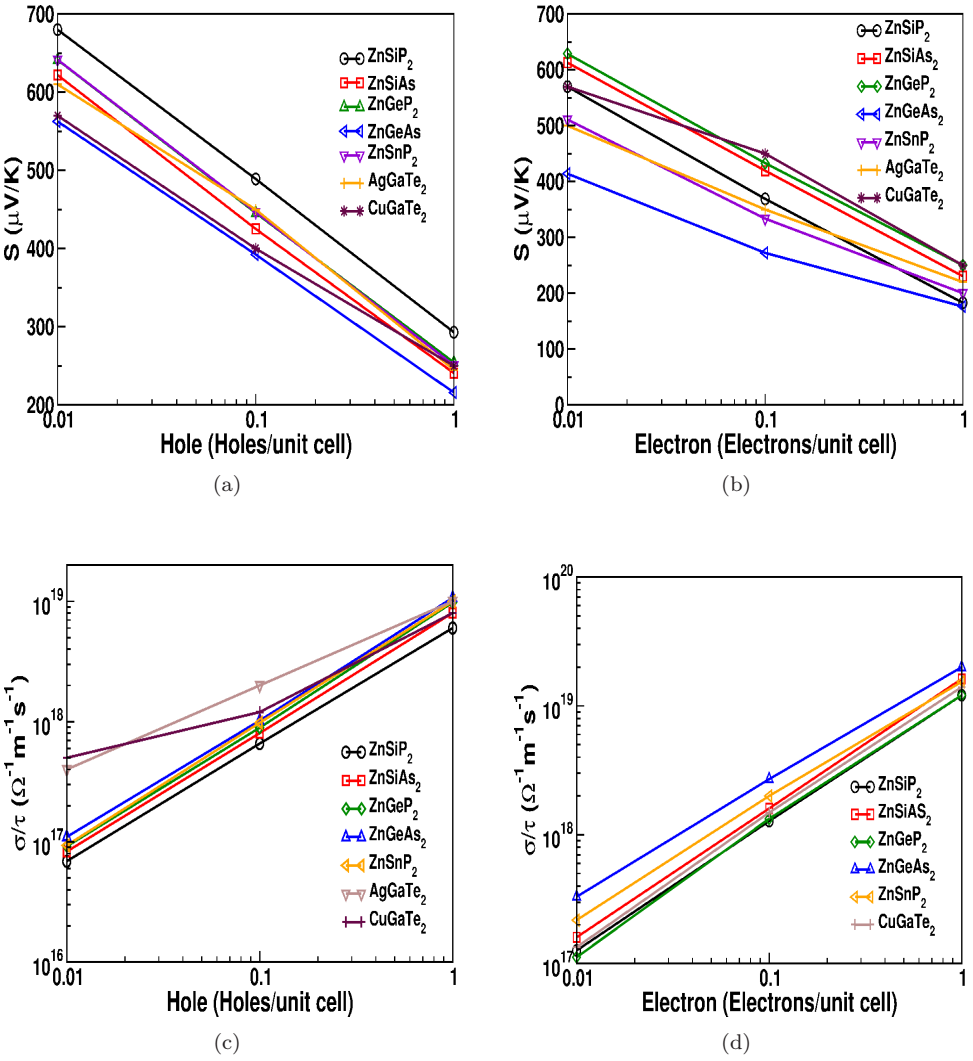

Figure 3.8: Comparison of thermopower (a,b) and electrical conductivity (c,d) with $AgGaTe_2$ and $CuGaTe_2$ along planar axis, at 900 K. One hole per unit cell is considered as $1{\times}10^{20}$ cm^{-3}.

Table 3.1: Lattice parameters of all the investigated compounds along with available experimental and other theoretical values

Compounds	a_{pre}(Å)	a_{exp}(Å)	a_{Other}(Å)	c_{pre}(Å)	c_{exp}(in Å)	c_{other}(inÅ)	u_{pre}	u_{exp}
$ZnSiP_2$	5.44	5.4072[a]	5.398[d]	10.56	10.4539[a]	10.435[d]	0.268	0.26948[a]
$ZnSiAs_2$	5.68	5.60[b]	5.584[e]	11.07	10.88[b]	10.95[e]	0.262	0.26575[b]
$ZnSiSb_2$	6.13	-	6.077[f]	12.08	-	11.68[f]	0.254	-
$ZnGeP_2$	5.52	5.46[b]	5.465[f]	10.88	10.71[b]	10.70[f]	0.252	0.25816[b]
$ZnGeAs_2$	5.75	5.672[c]	5.663[e]	11.35	11.153[c]	11.22[e]	0.247	0.264[c]
$ZnGeSb_2$	6.2	-	-	12.01	-	-	0.244	-
$ZnSnP_2$	5.72	5.651[c]	5.71[g]	11.48	11.303[c]	11.43[g]	0.226	0.264[c]
$ZnSnAs_2$	5.93	5.852[c]	5.851[h]	11.95	11.703[c]	11.702[h]	0.223	0.239[c]
$ZnSnSb_2$	6.28	-	-	12.56	-	-	0.25	-

a: ref.[186], *b*: ref.[128], *c*: ref.[187], *d*: ref.[129], *e*: ref.[189], *f*: ref.[207], *g*: ref.[133], *h*: ref.[127].

Table 3.2: Calculated effective masses of all the investigated compounds along the crystallographic directions in the unit of electron mass

Compounds	Γ-N(VB)	Γ-Z(VB)	Γ-N(CB)	Γ-Z(CB)
$ZnSiP_2$	2.89	2.20	0.38	1.17
$ZnSiAs_2$	2.01	1.59	0.54	1.43
$ZnSiSb_2$	3.07	0.92	0.16	0.68
$ZnGeP_2$	1.54	0.70	0.18	0.19
$ZnGeAs_2$	1.0	0.71	0.21	0.16
$ZnGeSb_2$	0.09	0.02	0.03	0.02
$ZnSnP_2$	1.91	0.97	2.02	0.82
$ZnSnAs_2$	1.03	0.90	1.04	0.71
$ZnSnSb_2$	0.44	1.32	0.315	0.39

In order to understand how better are the TE properties of the investigated compounds, we have compared it with well-known chalcopyrite TE materials. The comparison between few of the studied compounds, which secured good thermoelectric properties ($ZnSiP_2$, $ZnSiAs_2$, $ZnGeP_2$, $ZnGeAs_2$, $ZnSnP_2$) with prototype chalcopyrite compound $CuGaTe_2$ (which has a high figure of merit of 1.4 from experiment[143]) and $AgGaTe_2$ is shown in Figure 3.8. From this figure it is quite evident that the investigated systems are appreciable similar to the well known TE materials $CuGaTe_2$ and $AgGaTe_2$ for both electrons and holes. At 900 K, $ZnSiP_2$ possess a higher thermopower in the case of holes, which is even higher than hole doped $AgGaTe_2$ and $CuGaTe_2$. We also found that the electrical conductivity is also very similar to that of the compared compounds, and it is imperative that the power factor value might be higher or comparable with other prototype compounds. This shows that the investigated pnictide compounds almost show better thermoelectric properties compared to well known chalcopyrite materials $CuGaTe_2$ and $AgGaTe_2$[140, 141]. In addition to this, we have

Table 3.3: Elastic constants of all the compounds and Debye temperature (Θ), at optimized volume

Compounds	C_{11}(GPa)	C_{12}(GPa)	C_{13}(GPa)	C_{33}(GPa)	C_{44}(GPa)	C_{66}(GPa)	Θ(K)
$ZnSiP_2$	444.7	347.5	205.0	130.4	150.68	154.7	585.3
$ZnSiAs_2$	104.5	46.4	47.0	103.2	54.6	64.7	363.57
$ZnSiSb_2$	78.0	33.5	35.3	78.97	38.0	39.1	350.5
$ZnGeP_2$	118.2	50.14	51.92	119.4	60.9	61.7	500.0
$ZnGeAs_2$	122.5	36.9	32.9	87.6	55.9	70.3	358.4
$ZnGeSb_2$	75.2	35.2	37.5	72.3	34.1	33.9	238.9
$ZnSnP_2$	105	43	45	100	50	70	320.3
$ZnSnAs_2$	74.3	43.3	44.3	92.9	38.7	49.3	265.44
$ZnSnSb_2$	78	30	36	70	45	60	230.4

also compared the thermopower values of the present studied systems with traditional TE material, Bi_2Te_3. At room temperature, and around a carrier concentration of 4×10^{18} cm^{-3}, Bi_2Te_3 has a thermopower of 313 $\mu V/K$ for p-type and 196 $\mu V/K$ for n-type, while for our compound (we have chosen $ZnSiP_2$) at the same conditions, it is 358 $\mu V/K$ for p-type and 292 $\mu V/K$ for n-type [181]. This shows that the investigated compounds are found to have higher value of thermopower compared with well known traditional TE materials, which lead us to claim the investigated compounds as potential materials for TE applications.

3.3.4 Electronic and thermoelectric properties of $ZnGeSb_2$ at ambient

Crystal structure of $ZnGeSb_2$ also fall into the tetragonal symmetry, and the optimized lattice parameters of this compound is included in Table 3.1. Since there is no experimentally reported values, we have confirmed the dynamical stability of $ZnGeSb_2$ by using phonon dispersion plot (See Figure 3.9). The primitive cell of $ZnGeSb_2$ has 8 atoms in the unit cell which results in 24 phonon modes for each wave vector in this compound. From the phonon dispersion plots, it is clear that the low frequency optical modes interact with the acoustic modes in the frequency around 50 cm^{-1}, which indicate the strong phonon phonon scattering, and might lead to low thermal conductivity in this compound[208]. For further investigation we have calculated the electronic structure properties using TB-mBJ functional. The calculated band structure at the optimized volume along different high symmetry directions, Γ-Z, Γ-N are given in Figure 3.10. From the figure, one can clearly see the highly linearly dispersive band structure near Fermi level around Γ point, which levitate the interest towards $ZnGeSb_2$ compared to other $ZnXPn_2$. To capture the proper nature of this band structure, we have given the three dimensional representation of band projection in k_x, k_y and k_y k_z plane (see Figure 3.10(b,c,e,f)). Now one can see the dispersion, which exactly represents a gapped Dirac states in the low energy region, with small anisotropy along different high symmetric directions(Γ-Z and Γ-N). The three dimensional representation of the projection along different momentum directions gives a clear idea that the dispersion along the different momentum directions are same, indicating the presence of 3D Dirac cone in the band structure. If we recall the band structure of $ZnSnSb_2$ (See Figure 3.2), one can observe similar linear band structure around Γ high symmetry point, but

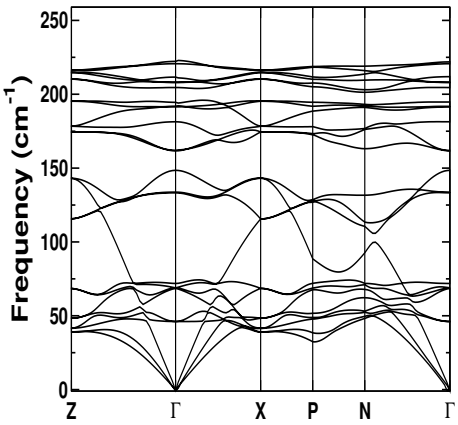

(a)

Figure 3.9: Phonon dispersion of $ZnGeSb_2$

in addition, a parabolic band lies in between these highly linearized band in the low energy region, which might annihilate the Dirac kind of band nature. Coming back to $ZnGeSb_2$, the band gap of the compound is direct. The presence of time reversal symmetry has been verified using spin-polarised calculations. Highly linearly dispersed bands imply the carriers to exhibit low band mass, which we have confirmed using effective mass calculations (see Table.3.2). Calculated elastic constants of $ZnGeSb_2$ at the optimized volume are represented in Table 3.3, and this confirmed the stability of this compound. Calculated Debye temperature is comparable with the other chalcopyrite materials and with few zintl phase compounds[210, 211], and the low value of Debye temperature indicates the possibility of low thermal conductivity in this compound. The thermoelectric properties of a material are derived from it's transport coefficients like thermopower, electrical conductivity and thermal conductivity. The parameters like thermopower and electrical conductivity at ambient is shown in Figure 3.11. The magnitude of thermopower is found to vary slowly as a function of carrier concentration. This behaviour is different from the normal semiconducting nature where the magnitude of thermopower is found to decrease with carrier concentrations. In order to compare the behaviour of $ZnGeSb_2$ with semiconductor, we have represented the variation of thermopower of $ZnGeAs_2$ in the same figure. We have observed the electrical conductivity to shoot by several orders of magnitude (around $3\times10^{25}\ \Omega^{-1}m^{-1}s^{-1}$) compared to normal semiconductor, and it showed almost same value for all the studied concentrations. Both thermopower and electrical conductivity show unusual response compared to normal semiconductors, which also indicate the highly linearized dispersion in this compound. In $ZnSnSb_2$, we could not observe this behavior, which might be due to the presence of a parabolic band in between two highly linearized bands around Fermi level. The carrier independent nature of thermopower and electrical conductivity of $ZnGeSb_2$ open up the possibility of TE application for a wide range of concentration, which may attract the experimentalists. The huge value of electrical conductivity in $ZnGeSb_2$ will play very crucial role in the thermoelectric properties of this compound, which will be discussed in the upcoming section. The fine tuning of these kind of compounds using some perturbations like spin orbit coupling, strain, chemical substitutions can lead to different states in this compound, which motivated us to check the electronic and thermoelectric properties in a range of volumes slightly higher and lower than our

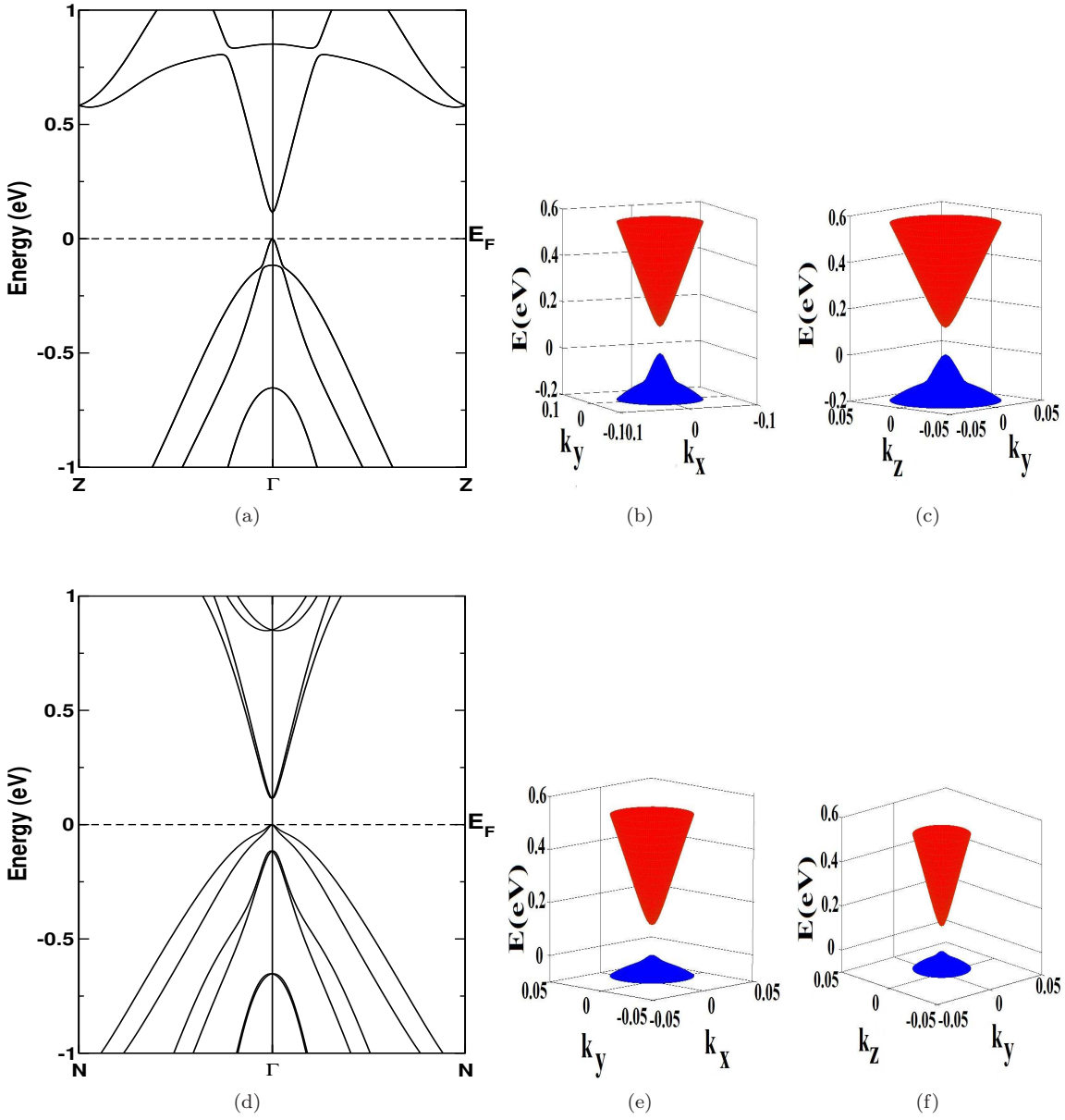

Figure 3.10: Band structure of $ZnGeSb_2$. (a) band structure using optimized parameters along Z -Γ -Z direction, (b) and (c) three dimensional representation of the k_x, k_y and k_z, k_y projection along Z -Γ -Z direction, (d) band structure using optimized parameters along N -Γ -N direction, (e) and (f) three dimensional representation of the k_x, k_y and k_z, k_y projection along N -Γ -N direction

optimized volume.

3.3.5 Electronic and thermoelectric properties of $ZnGeSb_2$ under strain

Now it is curious to examine how the band profile of $ZnGeSb_2$ changes by the application of strain (hydrostatic strain has been applied with respect to the optimized volume). The band gap is found to decrease under tensile strain, and increased for compressive strain. The band structure along Γ - Z together with projection along k vector directions at compressive strained volume (around -4.6%) are presented in Figure 3.12. The calculated band gap at this compressive volume (-4.6 %) is 0.33 eV, and the parabolic nature of band structure observed here certainly reveal the volume dependent electronic properties of this compound. By increasing the volume, the band gap is decreasing, and it is found to close at 2.4% strain and for further strains it starts opening again around 3.2%. The band structure for few strains are represented in Figure 3.13 (a,b,c,d). The band profile at 1.6% strain is represented here, and it shows similar behavior as the optimized structure, with lesser band gap. This kind of highly linearly dispersive nature is an indication of Dirac states, but here the valence and conduction band tips are not touching each other indicating this state to be a massive Dirac state. For further strain, around 2.4%, the band gap is found to be closed, and in this state the conduction band is just touching the Fermi level. For 2.6% strain also band nature is same but the conduction band starts dipping down to the valence band, by maintaining a small gap between the conduction band tip and valence band tip. Around 2.6% strain, the dispersive nature of the band is observed similar to 2.4% strain, but we have observed that the conduction band is further moving towards valence band. The details of the relative conduction and valence band tip positions from the Fermi level along with the gap between the conduction and valence band tip are given in Table 3.4. For further strain around 3.2%, the band nature has changed, that is the conduction band is lifted upward, and valence band started crossing the Fermi level. The band structure of this strained state is given in Figure 3.13(d), where we can observe the crossing of valence band through the Fermi level along Γ-X. The closing and opening of the bulk band gap, and the change of band nature from indirect band gap to direct band gap along with the application of hydrostatic strain further motivate us to check the topology change in this compound. For this purpose we have plotted the band structure at different strains together with total 's' character, see Figure 3.13 (e,f,g,h). At a compressive volume corresponding to -4.6% strain, $ZnGeSb_2$ is found to be an indirect band gap semiconductor with band gap around 0.33 eV. At this state *'s'* like (Γ_6) bands are dominating near CBM (conduction band minimum) and *'p'* like (Γ_8) bands are dominating near VBM (valence band maximum). The parameter E_0 is defined as the energy difference between *'s'* like Γ_6 bands and *'p'* like Γ_8 bands ($E_0 = E(\Gamma_6) - E(\Gamma_8)$). At this volume (compressive strained state), E_0 is around +0.35 eV, and this positive value, indicate the presence of 's' states above 'p' states, and this value confirm the normal semiconducting nature at compressive strain, and this is in good agreement with the previous study.[209] At 2.4% strain the band order is found to be reversed, at Γ point, where the *'s'* like bands are shifted below VBM and aligned below the *'p'* like bands (see Figure 3.13(f)). The size of the circle represent the *'s'* character, and upon hydrostatic expansion, one can easily observe the size of the circle at the Γ point in the conduction band to reduce and in the valence band it is found to increase. This is an indication of band inversion which is crucial in topological insulating behaviour. At this expanded state, we found that the value E_0 turned to be negative around -0.07 eV, where the *'s'* like Γ_6 band aligned 0.07 eV below the

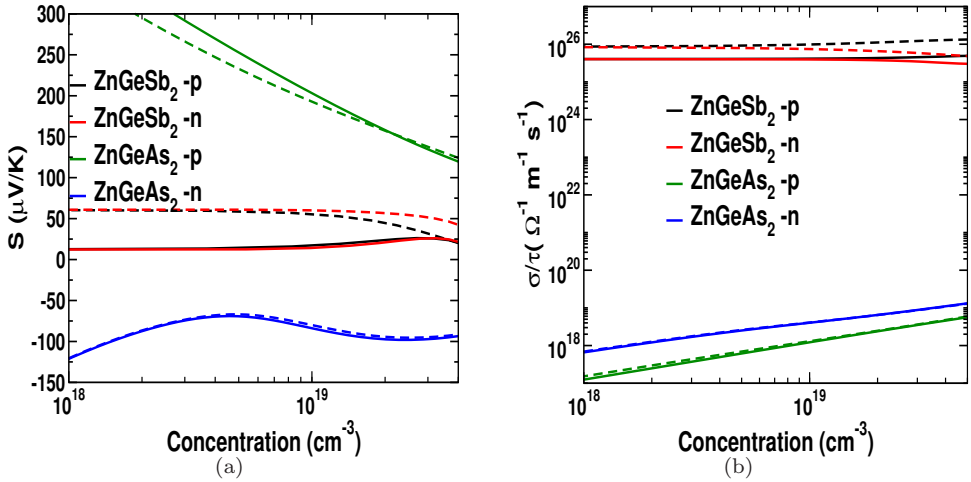

(a) (b)

Figure 3.11: Variation of thermopower and electrical conductivity as a function of carrier concentration for optimized structure $ZnGeSb_2$ and $ZnGeAs_2$. Solid line for 'a' axis, and dashed line for 'c' axis

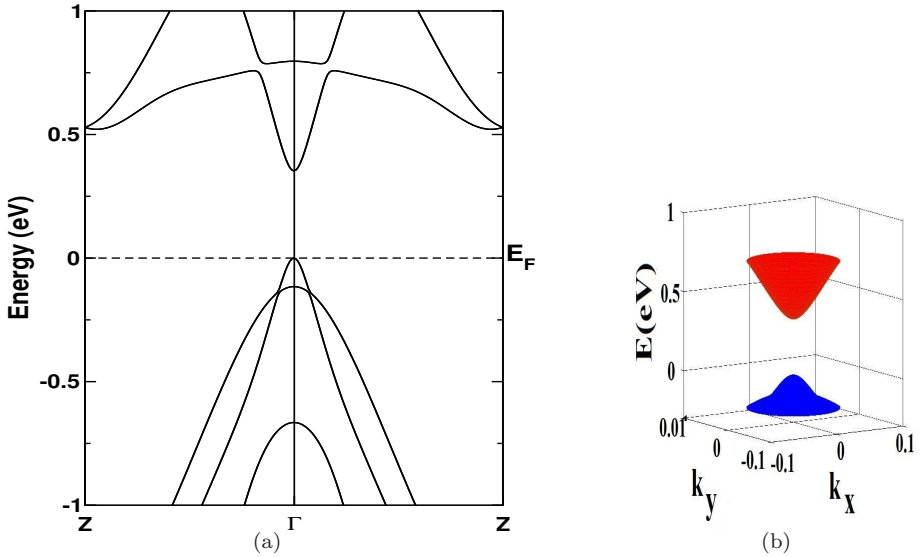

(a) (b)

Figure 3.12: Band structure of $ZnGeSb_2$ at -4.6% strain (a) along Γ -Z high symmetric direction, (b) three dimensional representation of the k_x, k_y projection along Z -Γ -Z direction.

VBM. The schematic of electronic structure over a range of volume is given in Figure 3.14. While analysing the band structure systematically, it is evident that at compressive strain (around 4.6 %), the compound is a normal semiconductor, around optimized volume, the compound possesses massive Dirac state, where it shows highly linearly dispersive band profile, and above 3.2 % tensile strain, the compound shows topological semi-metallic state. This clearly indicate the three states of this compound: normal semiconductor, massive Dirac states and topological semi-metal. In addition to this, tuning of massive Dirac states can be observed by the application of expansive strain. In a similar line we have analysed $ZnSnSb_2$, and we could see that the band gap is closing at 8% tensile strain and remains the same up to 20% tensile strain. A band inversion is observed at the strained state, and the projected band structure of ambient and 8% strained state are given in Figure 3.15. Further we have concentrated only on $ZnGeSb_2$. In the following paragraph we discuss the transport properties in these states.

The interesting part of the electronic structure of this compound is already discussed, and now one can analyse the thermoelectric properties, and this is summarised in Figure 3.16. In this figure, we have given the variation of transport coefficients as a function of strain at carrier concentration around 5.0×10^{19} cm^{-3} at 300 K, and as function of carrier concentrations from 1.0×10^{18} cm^{-3} to 1.0×10^{20} cm^{-3}. As we expected from the electronic structure, peculiar behaviour of thermoelectric coefficients are observed. The magnitude of thermopower is found to be decreased for tensile strain and increased for compressive strain, which indicate that at the compressive strained states, the compound has normal semiconducting nature, where the thermopower is high compared to ambient and expanded states are the ones where system has massive Dirac states. The reduction of magnitude of thermopower might be due to the small band mass near the Fermi level. The thermopower has a local peak at 2.4% strain, where the electronic topology is changing. The electrical conductivity exhibits a huge increment (in the order of 1×10^{25} $\Omega^{-1}m^{-1}s^{-1}$) in the Dirac states compared to normal semiconducting states. Figure 3.16 shows that for negative strains the electrical conductivity is lesser than ambient and expanded states(massive Dirac states). To understand the overall thermoelectric properties, we have given the power factor also (see Figure 3.16), where one can clearly observe that around the optimized volume, there is a huge increment in power factor, with a subsequent decrease, and after 2.4% it starts increasing. Among massive Dirac states, one can clearly see that the strained states which hold the Fermi level far from the Dirac points are more favourable. Similar observations are mentioned in graphene based studies.[212] From the figure it is evident that the magnitude of power factor is almost similar for both holes and electrons, which indicate the possibility of device application in this compound. There is a huge anisotropy in power factor observed in the Dirac states, the 'c' axis is more beneficial than the 'a' axis for optimized volume. One point we would like to mention here is that all the Dirac states observed in this study were massive Dirac states, where we have observed a gap between two Dirac points, which is beneficial for device applications, unlike the massless state in graphene. Recent research in graphene is evolving in a direction where people are trying to open a small gap between the degenerate Dirac point.[213] This shows the significance of the investigated material. Overall, the maximum power factor observed at the optimized state is several orders of magnitude higher than the power factor observed for the normal semiconducting state, and also the magnitude of power factor observed in the Dirac state is higher than the power factor of well known thermoelectric materials.[214] In figure 3.16(f), we have compared the power factor of our investigated compound at it's massive Dirac

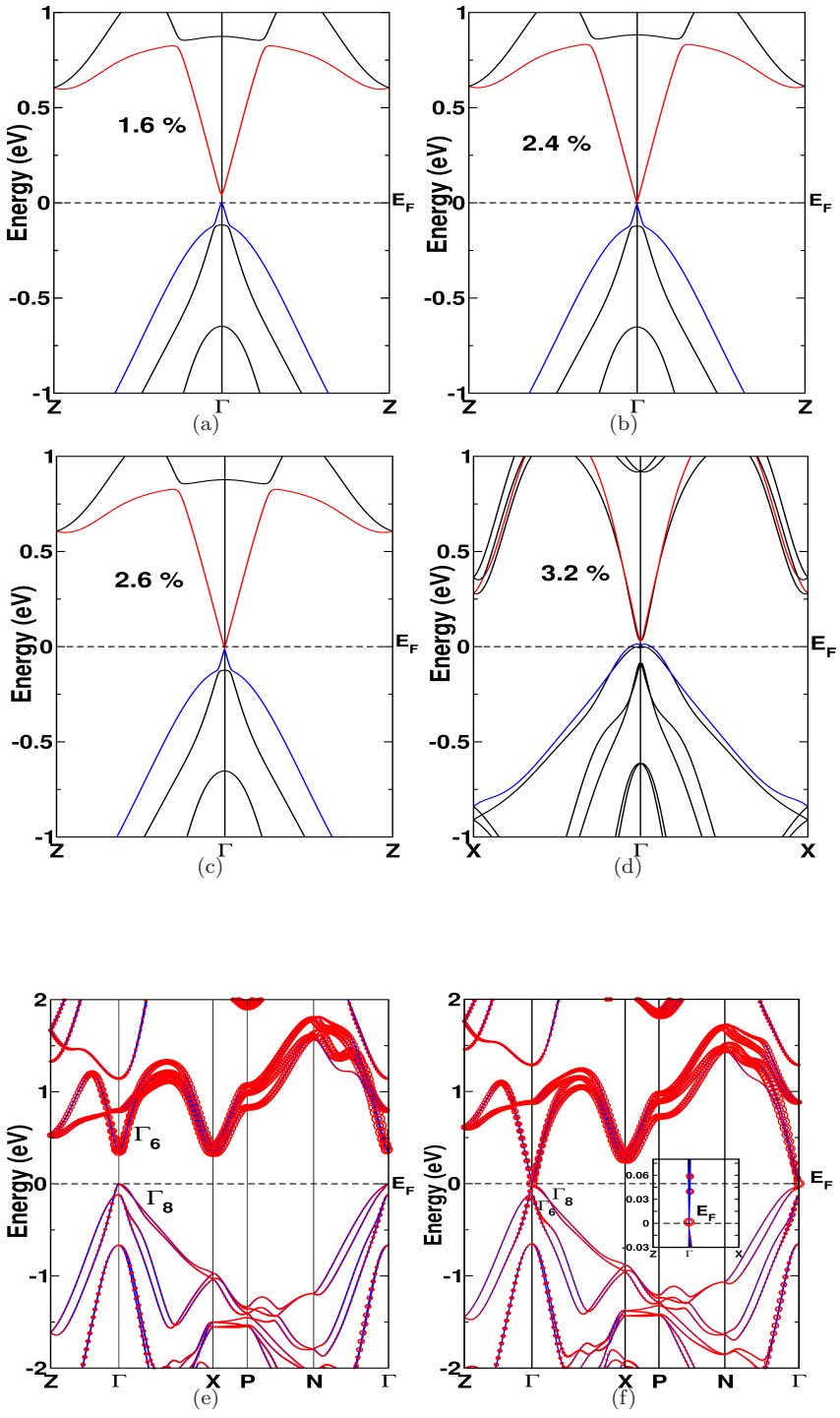
1.6 %
2.4 %
2.6 %
3.2 %
Energy (eV)
E_F
Z
Γ
X
P
N
Γ6
Γ8
(a)
(b)
(c)
(d)
(e)
(f)

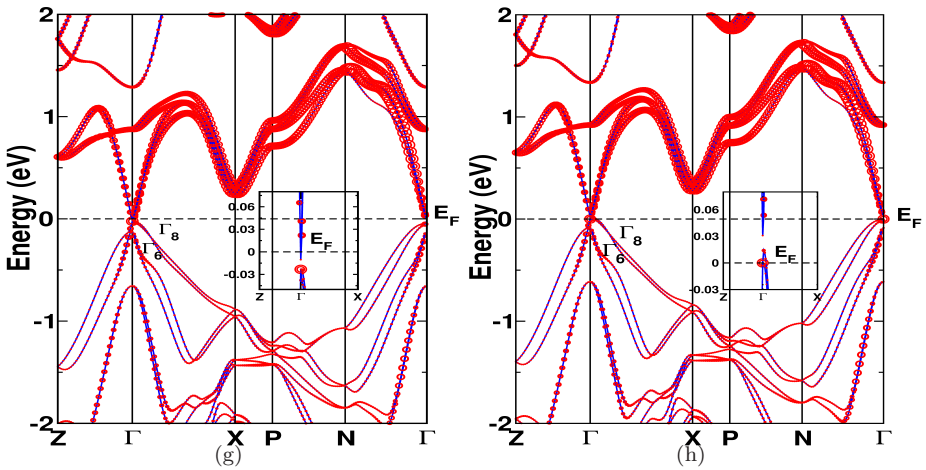

Figure 3.13: Band structure of $ZnGeSb_2$ (a) band structure at 1.6% strain along Z -Γ -Z direction, (b) band structure at 2.4% strain along Z-Γ -Z direction, (c) band structure at 2.6 % strain along Z -Γ -Z direction,(d) band structure at 3.2% strain along X -Γ -X direction, Calculated s, p projected band structure for different strains (black circle represent 's' bands, red circle represent 'p' bands): e) -4.6% strain f) 2.4% strain g)2.8% strain h) 3.2% strain

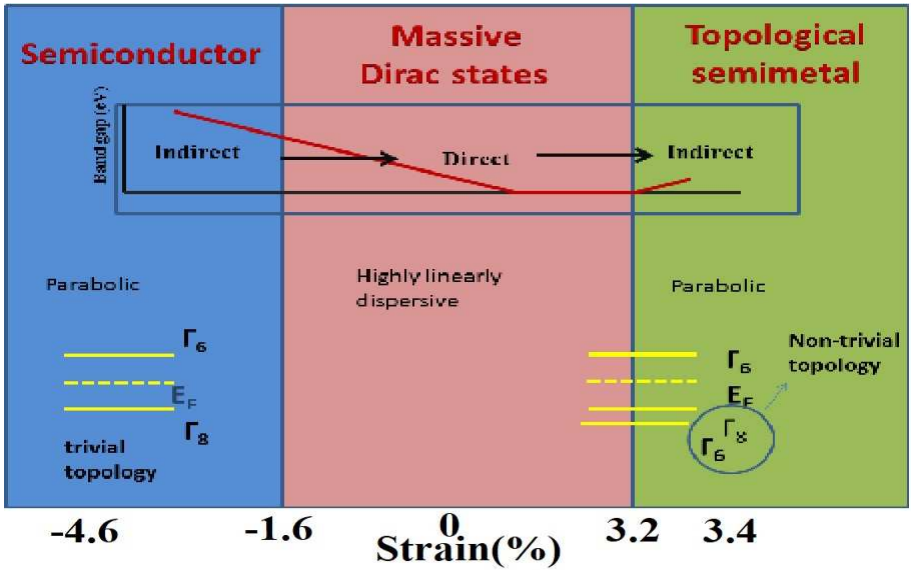

(a)

Figure 3.14: The schematic of electronic structure as a function of strain

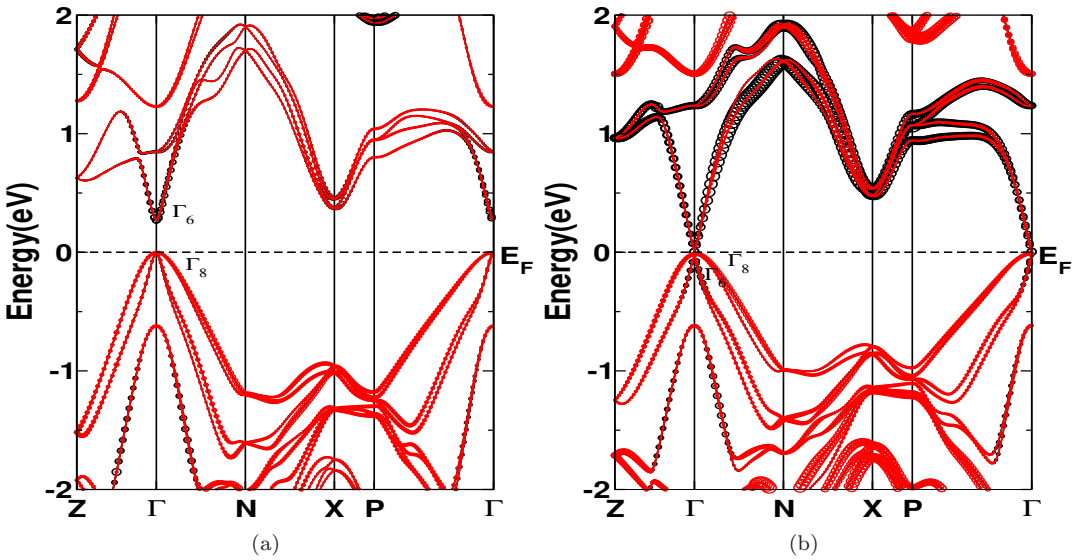

Figure 3.15: Projected band structure for $ZnSnSb_2$ at a) ambient and b) 8% hydrostatic strain, (black circle represent 's' bands, red circle represent 'p' bands)

state with other materials. The magnitude of thermal conductivity also plays crucial role in the performance of thermoelectric materials. The investigated phonon dispersion and calculated Debye temperature gave strong evidence of low lattice thermal conductivity. The magnitude of thermal conductivity of chalcopyrite family is previously investigated[180], and they have reported that the prototype structure $ZnGeP_2$ and $ZnGeAs_2$ have lattice thermal conductivity of 158 $mW(cmK)^{-1}$ and 117 $mW(cmK)^{-1}$ respectively. As we know that the magnitude of lattice thermal conductivity will reduce if one replace As with Sb, the magnitude of lattice thermal conductivity of $ZnGeSb_2$ can be expected to be lesser than that of $ZnGeAs_2$. To estimate the range of power factor ($S^2\sigma$), which is independent of relaxation time, we have assumed the relaxation time as 1×10^{-14} s and 1×10^{-15} s , and the calculated electrical conductivity (σ) and power factor ($S^2\sigma$) are given in Table 3.5. We have observed high power factor due to the ultra high conductivity. The conductivity values observed for both the relaxation time are very high compared to other established materials, and the comparison is given in Table 3.5. In addition to this, conductivity value is higher than the reported conductivity of the Dirac semi-metal Cd_3As_2[215]. In Figure 3.17, we have summarised the TE properties of $ZnGeSb_2$ in schematic way. In the era of thermoelectric materials, we have observed the enhancement of power factor ($S^2\sigma$) due to some external effect like pressure or in low dimensional materials. Here in the present study, the bulk optimized structure itself showed a huge power factor. To predict the exact figure of merit, the knowledge of the relaxation time is needed. The relaxation time of graphene is predicted to be in the order of 1×10^{-15}.[216] If one can experimentally verify the lattice thermal conductivity and relaxation time of $ZnGeSb_2$, it will turn out to be an excellent thermoelectric material.

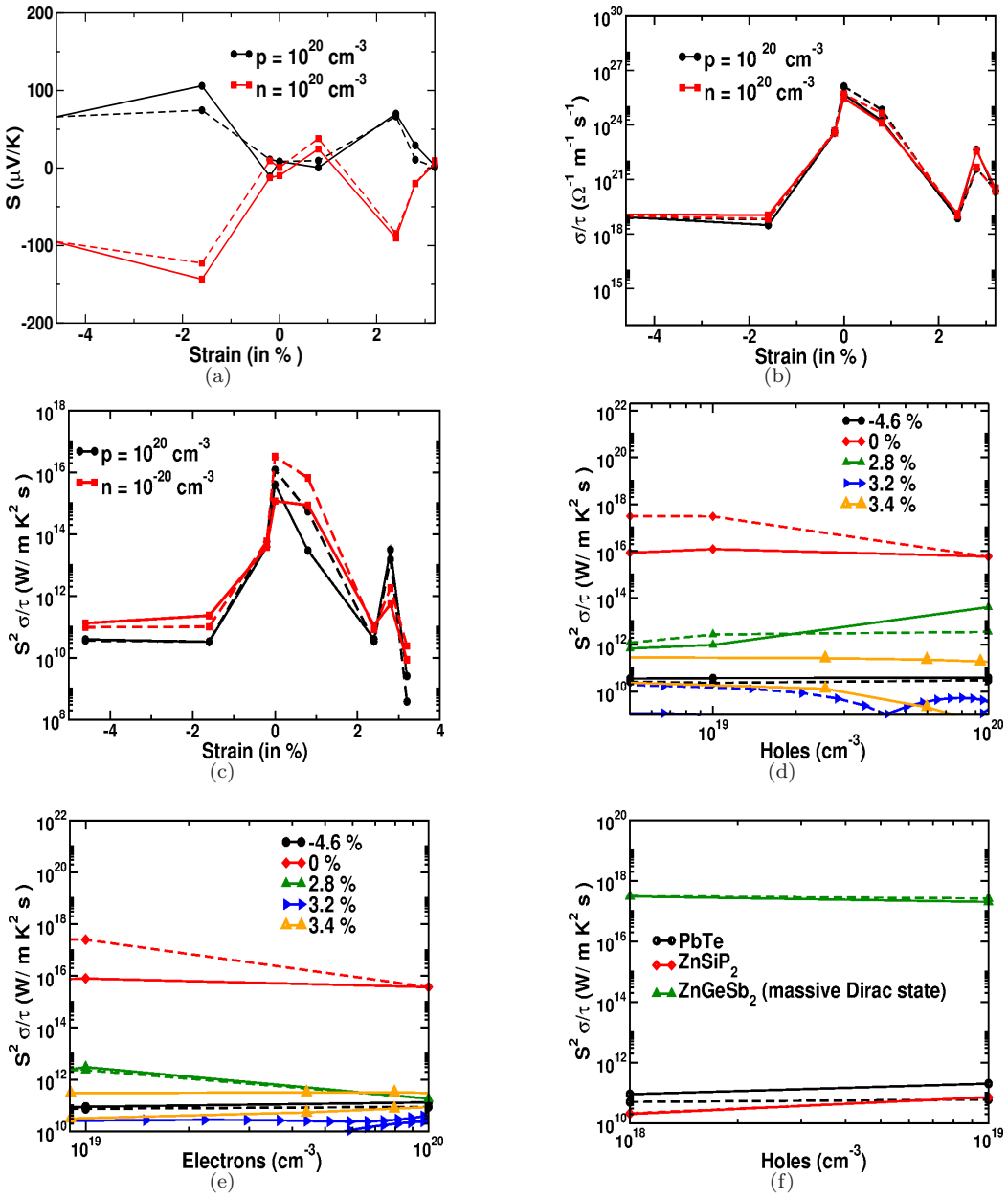

Figure 3.16: (a,b,c) Variation of thermopower, electrical conductivity and power factor as a function of strain. Solid line for 'a' axis, and dashed line for 'c' axis, (d,e) Variation of power factor as a function of concentration, f) Comparison of power factor with other materials PbTe[214], solid line for p -type and dashed line for n- type.

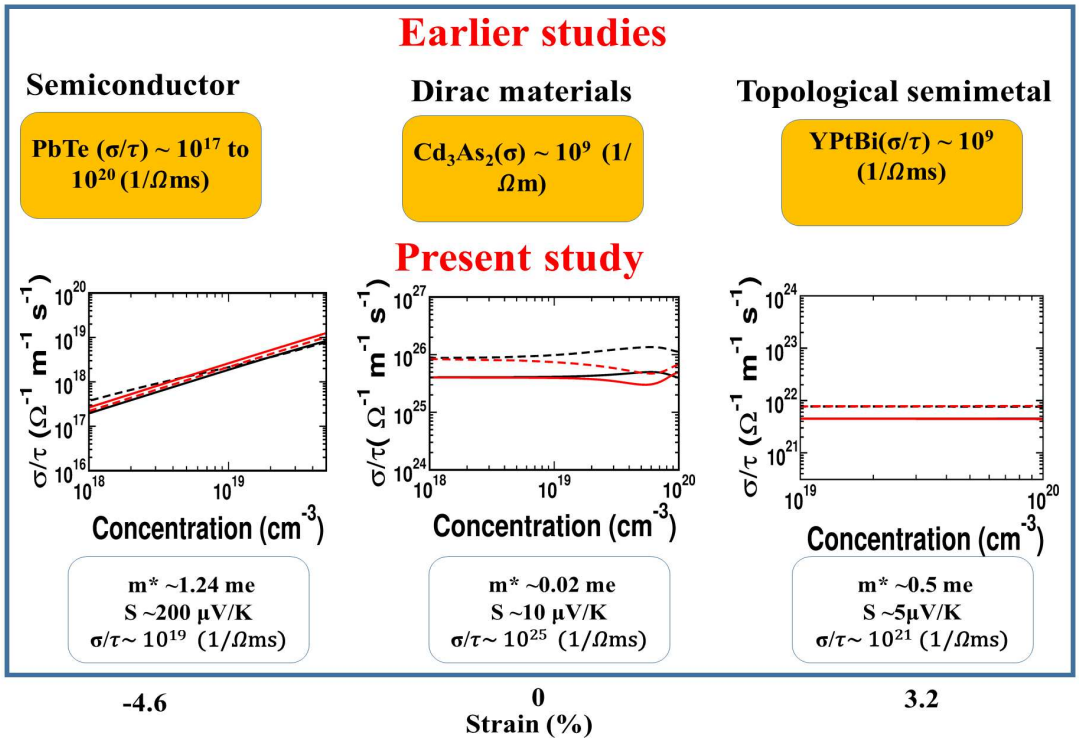

Figure 3.17: Schematic of phase change and comparison with well established compounds, PbTe[214], Cd_3As_2[215], YPtBi[221]

3.4 Conclusions

The band structure of $ZnXPn_2$ (X: Si, Ge, Sn: Pn: P, As: Sb) is studied, where $ZnSiAs_2$, $ZnSiSb_2$ and $ZnGeP_2$ show indirect band gap nature and other investigated compounds are direct band gap semiconductors. From the transport properties, it is quite clear that most of the investigated compounds are favorable for TE applications for temperatures ranging from 300 K to 900 K. The investigated pnictide compounds show almost comparable thermoelectric properties with the well-known TE materials of chalcopyrite structures. Among the studied compounds, p-type $ZnSiP_2$, $ZnGeP_2$ and $ZnSnP_2$ and n-type $ZnGeP_2$ and $ZnSiAs_2$ are found to have good TE properties. Present study reveal the potential thermoelectric properties of Zn based pnictides, and can be best used, if one could reduce the thermal conductivity by alloying or nano-structuring. Highly tunable massive Dirac states and their transport properties were discussed systematically. The investigated compound is found to be an excellent material for thermoelectric application due to massive Dirac states, which lead to a huge power factor, ultra high conductivity and low thermal conductivity. In addition to that, the band inversion in this compound is also analysed. The mechanical and dynamical properties revealed the stability and low thermal conductivity of this compound. Compared to other chalcopyrite thermoelectric materials, the present compound exhibits a huge power factor in it's stable massive Dirac states. The electrical conductivity and thermopower are found to be almost carrier concentration independent, which may certainly fetch device applications and need to be verified experimentally.

Table 3.4: Alignment of bands near Fermi level of $ZnGeSb_2$ at different strains

Strain(in %)	CBtip	VBtip	gap
0.6	0.089(+)	0	0.089
0.8	0.076(+)	0	0.076
1	0.068(+)	0	0.068
1.2	0.059(+)	0	0.059
1.4	0.047(+)	0	0.047
1.6	0.037(+)	0	0.037
1.8	0.026(+)	0	0.026
2.4	0.00145(+)	0.0058(-)	0.00725
2.6	0.00725(-)	0.0114(-)	0.00415
2.8	0.0104(-)	0.0235	0.01312
3	0.0087(-)	0.024(-)	0.0153

Table 3.5: Comparison of electrical conductivity, thermal conductivity and power factor with other compounds (The lattice thermal conductivity of $ZnGeAs_2$ is 11.7 (W/mK)[180], and lattice thermal conductivity of $ZnGeSb_2$ is assumed to be of the order of 10.0 (W/mK))

compounds	$\sigma(1/\Omega m)$	κ (W/mK)	P.F (W/mK^2)
$ZnGeSb_2$(τ=1×10^{-14} s)	8.5×10^{11}	10.0	3×10^3
$ZnGeSb_2$(τ=1×10^{-15} s)	8.5×10^{10}	10.0	3×10^2
$Bi_2Se_{0.5}Te_{2.5}$[217]	8.7×10^4	0.96	4×10^{-3}
SnSe(c-axis)[251]	1×10^3	0.68	3.8×10^{-4}
$Sn_{0.93}Mn_{0.04}Te$[219]	2×10^5	-	2×10^{-3}
$Hf_{0.75}Zr_{0.25}NiSn_{0.99}Sb_{0.01}$[220]	1.5×10^5	4.5	50×10^{-4}

Chapter 4

Novel natural super lattice materials with low thermal conductivity for thermoelectric applications

The present chapter deals with the electronic structure, mechanical and TE properties of few superlattice materials, which possess high thermopower values together with the probability of low thermal conductivity. The investigated compounds BaXFCh (X: Cu, Ag, Ch: S, Se, Te), LaXSO (X: Cu, Ag) and SrCuTeF crystallize in tetragonal structure with space group P_4/nmm. The possibility of low thermal conductivity is predicted from the obtained elastic constants and from Slack's model and Cahill's model. Electronic structure properties of the investigated series reveal the quasi two dimensional nature in the valence band, and this is confirmed through effective mass calculations. The significant difference in effective mass along different crystallographic directions in valence band introduces an anisotropy in the transport properties, where the properties along 'a' axis is found to be more favourable for hole doping. The magnitude of thermopower of these compounds are highly comparable with other established TE materials. Further we have extended our analysis to decouple the relaxation time through the parameter 'A' ($S^2\sigma/\tau T/\ \kappa_e/\tau$), which further helps to predict the TE properties better, and the investigated compounds possess higher value of 'A' parameter than the other well established materials.

4.1 Introduction

As we have discussed in the introduction, the structural complexity might play a vital role in deciding the TE properties of materials, and in this chapter we have chosen a series of compounds which have inherent hetero-layer type structure, and are known as superlattice structures. Diverse methods have been adapted to enhance the efficiency of a TE material, and these methods predominantly focus either on increasing the power-factor or aim at suppressing the lattice thermal conductivity. Superlattice/heterostructures creation is one of the emerging techniques which can elevate the performance. In the early stages of research itself, attention towards two dimensional quantum well structures for TE properties were significant[223]. There would be increased number of controlling parameters to tune the value of ZT compared to normal bulk structures, which includes the thickness of these structures. Superlattice of multi layers helps to strengthen the TE properties since the charge carriers are more confined in one plane[223]. In general the phonon scattering would be higher in these multi-layer materials, where scattering from the interface of two layers also contribute, thereby reducing the lattice thermal conductivity[223]. In addition to this, the thermopower value for these systems are found to be higher, which further attracts the researchers. The origin of the high thermopower is discussed in one of the early study by Kuroki, and they explained that the peculiar band model referred as "pudding-mold" which contain the mixture of highly flat and dispersed band[224], could be the reason for the same. In spite of having these advantages of low thermal conductivity and huge thermopower, the attraction towards hetero-layer TE system is very less due to practical difficulties. The lattice mismatch (the lattice parameters of the constituent systems should comparable) and reproducibility in general, constrain the production. The realization of materials which possess inherent hetero-layer/superlattice structures could resolve the practical issues and the search of novel materials in this direction becomes highly demanding. A study on Na_xCoO_2 revealed the potential TE property [225], which mainly emerged due to two dimensional electronic structure [226]. Electron doped $FeAs_2$ revealed the huge Seebeck coefficient due to quasi one dimensional band structure[227]. There are several types of layered materials which are explored and are always interesting to examine. The diverse properties of these materials are decided by the bonding within the layers and the bonding between two layers and specifically the weak bonding nature between two layers of the system introduce dimensional reduction. The high temperature superconductivity in La based layered material is one of the example[228]. Later on, this approach is generalized as new chemistry for zintl-phase compounds, which involves construction of crystal structures out of, charge compensating layers, specifically a stable cationic layer, e.g. SrF or LaO, and an anionic functional layer, e.g. FeAs, to make compounds like LaFeAsO [228] or SrFeAsF [229]. A Coulombic interaction can be found between these two adjacent layers. The hetero-layered '1111' type compounds have attracted attention due to various properties, like ionic conductivity, moderate temperature super conductivity and many more[230, 228]. The compounds such as BiCuSeO[231], SrAgSF[232] have drawn attention due to potential TE properties. Here in this chapter, we present the investigation on '1111' type of compounds to explore the possible TE applications. An ideal TE material for device application should have, high mechanical strength, high melting point, high Seebeck coefficient, high electrical conductivity and low thermal conductivity. From this point of view, we have done an extensive study on this present compounds, which reveals the mechanical, electronic and transport properties of zintl-type compounds BaCuChF (Ch=S, Se, Te), BaAgFCh (Ch= S, Se, Te), SrCuTeF, LaCuSO, LaAgSO.

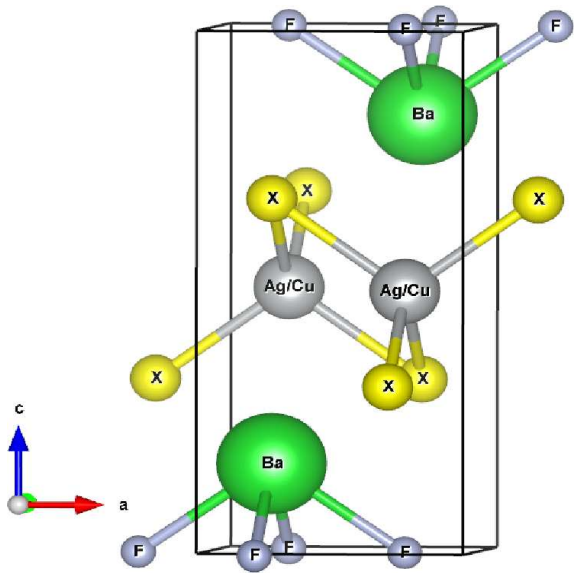

Figure 4.1: Crystal structure of investigated compounds

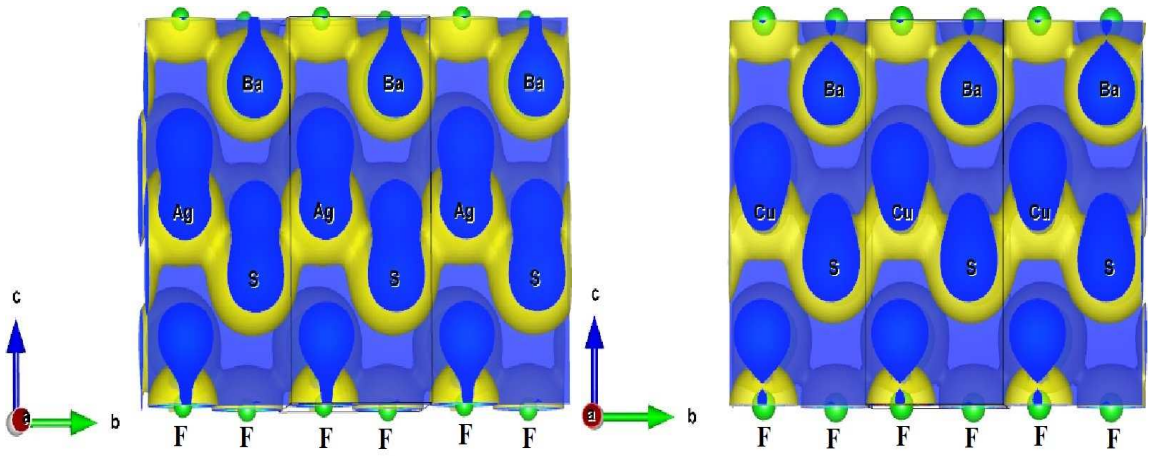

(a) (b)

Figure 4.2: (a)Charge density plots of BaFAgS and BaFCuS along [100] plane. Yellow colour surface shows the charge flow.

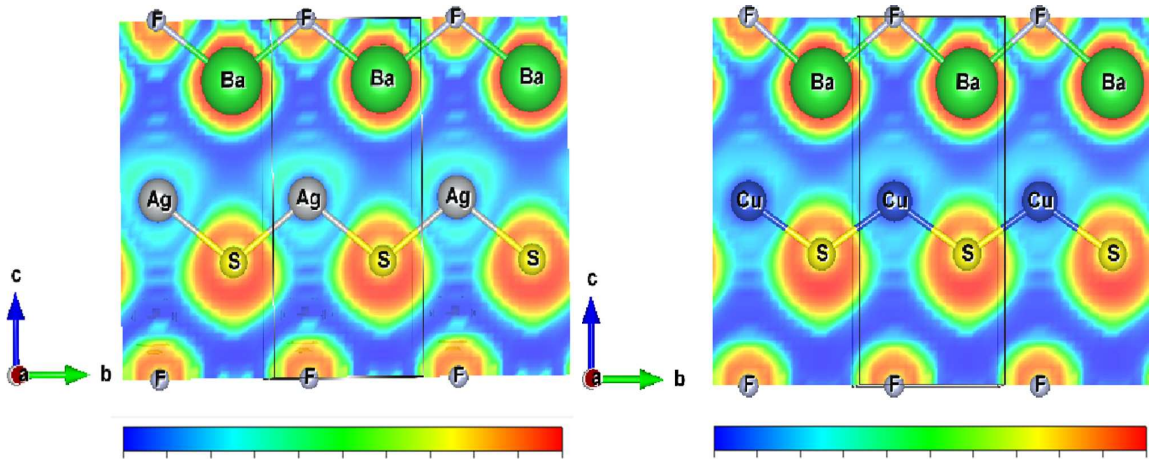

Figure 4.3: (a)Electron localization function of BaFAgS and BaCuFS along [100] plane. ELF value is high for red and low for blue colour in the diagram

4.2 Computational details

The electronic band structures were calculated by means of full-potential linear augmented plane wave (FP-LAPW) method based on first-principles density functional theory as implemented in the WIEN2k code.[233] The structural optimisation was carried out to compute the ground state properties within the generalized gradient approximation (GGA) of the Perdew-Burke-Ernzerhof (PBE) potential,[234] using the experimental parameters with an energy convergence of 10^{-6} Ry per formula unit. The traditional exchange-correlation potential of LDA or GGA schemes underestimate the band gaps of semiconductors, and we have used the modified GGA known as the Tran-Blaha modified Becke-Johnson[165] potential (TB-mBJ) [235]. For k-space integrations a $12\times12\times5$ k-mesh was used. The self-consistent calculations included spin-orbit coupling. The carrier concentration (p for holes and n for electrons) and temperature (T) dependent TE properties like thermopower, electrical conductivity were calculated using the BoltzTraP[236] code, within the Rigid Band Approximation (RBA)[170, 171] and the constant scattering time (τ) approximation (CSTA). In the RBA, the band structure is assumed unaffected by doping, which only leads to a shift of the chemical potential. For semiconductors, it is a good approximation for the calculation of transport properties, when the doping level is not too high.[171, 172, 237, 238, 239, 240] In CSTA, the scattering time of electrons is assumed to be independent of the electron energy. A detailed discussion of the CSTA is given in Refs. [241],[242] and [243], and references therein. The phonon dispersion of investigated compounds was calculated using pseudo potential method as implemented in Quantum espresso program[244]. Electron localization function (ELF) is calculated using VASP[245].

Table 4.1: Ground state properties of BaXChF (X: Cu, Ag; Ch: S, Se, Te), SrCuTeF, LaCuSO and LaAgSO with GGA functional along with the available experimental and other theoretical results

compounds	a(Å)(present)	a(Å)(Exp[a])	c(Å)(present)	c(Å)(Exp[a])	Gap(eV)(PBE)	Gap(eV)(TB-mBJ)
BaCuSF	4.23	4.123	9.14	9.0327	1.6	2.24
BaCuSeF	4.25	4.239	9.18	9.1217	1.44	2.06
BaCuTeF	4.43	4.4297	9.36	9.3706	0.99	1.52
BaAgSF	4.33	4.24	9.23	9.30	1.44	2.65
BaAgSeF	4.39	4.34	9.57	9.40	1.262	2.36
BaAgTeF	4.58	-	9.75	-	1.56	2.43
SrCuTeF	4.27	4.2474	9.39	9.2003	1.18	2.06
LaCuSO	3.87	3.9962	8.52	8.5174	1.6	2.27
LaAgSO	3.92	4.050	8.99	9.039	1.32	2.33

[a][254]; [b][255]; [c][256]

Table 4.2: Calculated bond lengths of all the investigated compounds

Compounds	A-F(O)(Å)	X-Ch(Å)	F-Ba-F(deg)	Ch-X-Ch(deg)
BaCuSF	2.63	2.44	67.26	106.73
BaCuFSe	2.65	2.55	69.07	107.77
BaCuTeF	2.65	2.69	72.38	108.89
BaFAgS	2.67	2.71	69.97	111.07
BaFAgSe	2.69	2.79	70.43	112.53
BaFAgTe	2.72	2.92	72.87	112.8
LaCuOS	2.36	2.42	73.49	108.67
LaAgOS	2.35	2.51	72.06	113.24
SrCuTeF	2.53	2.7	73.15	111.93

4.3 Results and discussions

4.3.1 Structural properties

Alternative layers of conducting X_2Ch_2 (X: Cu Ag, Ch: S, Se, Te) and insulating Ba_2F_2 segments results in the robustness of the investigated compounds. The crystal structure is provided in Figure 4.1, and all system possess tetragonal structure. The computed lattice parameters agree well with the experimental values as seen in Table 4.1. The computed bond lengths and bond angles of all the investigated compounds can provide more insight into the structural properties, and the same is presented in Table 4.2. For BaCuSF, the bond length of Cu-S bond is comparable with the sum of the radius of these two atoms, implying ionic character of this bond, whereas Ba-F bond is observed to be less ionic in character, and the trend is similar for BaCuSeF and BaCuTeF. Among these three compounds, Cu-Te bond in BaCuTeF is found to be more ionic. In the case of BaFAgS, Ag-S bond is found to be of higher ionic character compared to Ba-F bond, and the same trend is followed

down the column from S to Te in periodic table. While comparing BaCuSF and BaAgSF, it is observed that all bond lengths are higher for BaFAgS, and same trend is observed for Se and Te based compounds. In addition to this, Ba-Cu distances in BaCuChF compounds are lesser than Ba-Ag distances in BaAgFS compounds, which might be due to the weak bonding nature of Ag in these compounds, and this is further discussed in the upcoming section. Estimation of bond angle will help us to understand the bond distortions, and are represented in Table 4.2. It is found that in BaCuSF, the bond angle of Ba-F bond is more tetragonally distorted compared to Cu-S bond, where ideal tetragonal bond is 109.5^o, and Cu-S bond angle has almost same angle as tetragonal. Bond angles for Ba-F, and X-Ch are found to increase from S to Te, and compared to Cu compounds Ag based compounds have higher bond angle for all the bonds as seen in Table 4.2. The more distorted bonds may lead to soft lattice and introduce more anharmonicity in lattice thermal conductivity[246].

Table 4.3: Calculated effective mass for all the investigated compounds in the unit of electron mass.

Effective mass (me)	BaCuSF		BaCuSeF		BaCuTeF	
	VB	CB	VB	CB	VB	CB
m_z	30.78	1.85	39.61	1.53	32.88	0.96
m_x	5.29	0.68	4.50	0.59	3.48	0.58
Effective mass (me)	SrCuTeF		LaCuSO		LaAgSO	
	VB	CB	VB	CB	VB	CB
m_z	30.78	1.85	39.61	1.53	32.88	0.96
m_x	5.29	0.68	4.50	0.59	3.48	0.58
Effective mass (me)	BaFAgS		BaFAgSe		BaFAgTe	
	VB	CB	VB	CB	VB	CB
m_z	28.91	0.75	21.97	1.10	13.5	1.26
m_x	2.90	1.42	6.02	0.54	3.7	0.64

Further we have examined the charge flow in these compounds, and for this we have presented the charge density of two compounds BaCuFS and BaFAgS along [100] plane (See Figure 4.2). The charge flow in 'xy' plane is found to be higher compared to the charge flow along 'z' direction, and this might lead to a significant anisotropy in the physical properties. For further analysis, we have calculated the electron localization function (ELF) for the investigated compounds and in Figure 4.3 we have shown the ELF for BaFAgS and BaCuFS. ELF can help to identify the chemistry of bonds, and a value close to unity indicate the more covalent nature. In Figure 4.3, we could see that Ba, S, and F atoms shows this (see the red colour), but around Ag/Cu atoms we found very less ELF value, which indicate the weak Ag/Cu bonds in this series. Our results are in line with the previous results for prototype compounds[246].

Moving to electronic structure, we have calculated the band structure using TB-mBJ functional to predict the better band gap values of the investigated compounds. In Table 4.1, we have given the band gap using both PBE and TB-mBJ functionals, and from this it is quite clear that the PBE functional underestimate the band gap, and further calculations are performed using TB-mBJ functional only. Figure 4.4 represent the band structure of all the investigated compounds. The

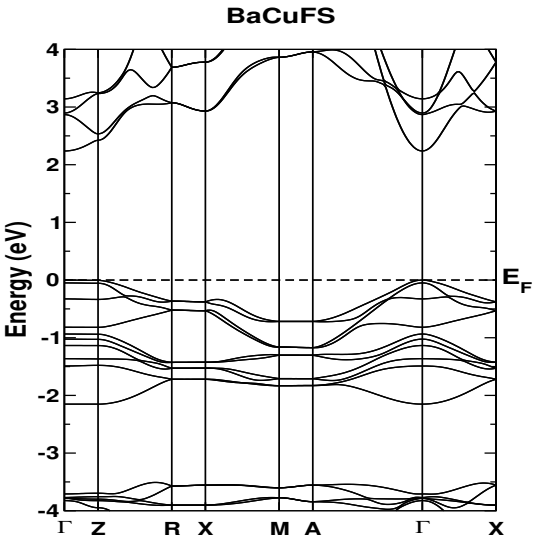
BaCuFS
Energy (eV)
E_F
Γ Z R X M A Γ X

(a)

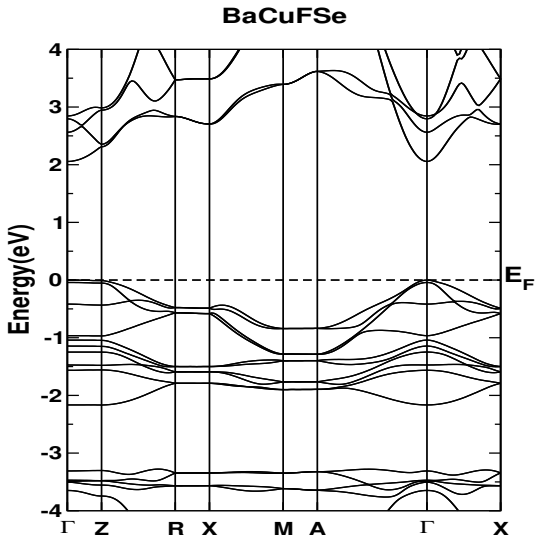
BaCuFSe
Energy(eV)
E_F
Γ Z R X M A Γ X

(b)

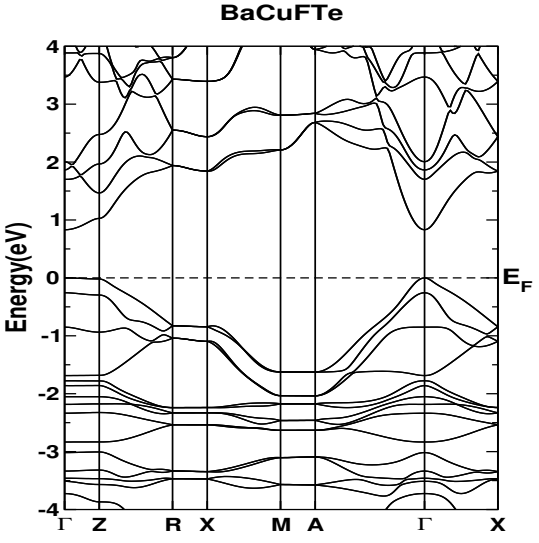
BaCuFTe
Energy(eV)
E_F
Γ Z R X M A Γ X

(c)

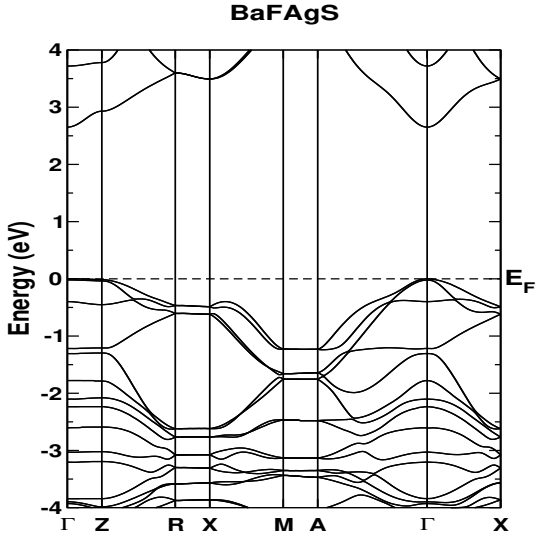
BaFAgS
Energy (eV)
E_F
Γ Z R X M A Γ X

(d)

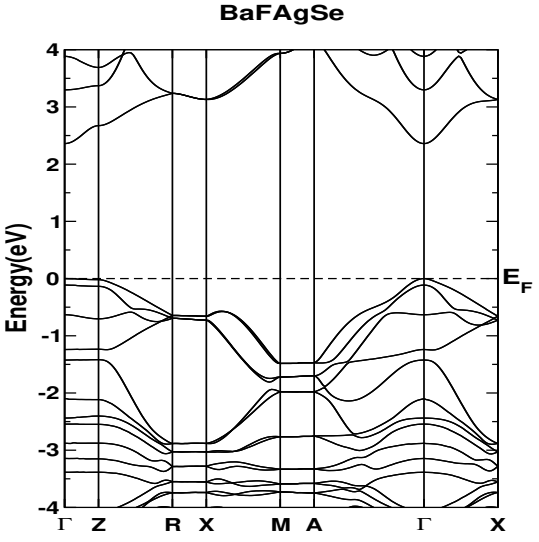
BaFAgSe
Energy(eV)
E_F
Γ Z R X M A Γ X

(e)

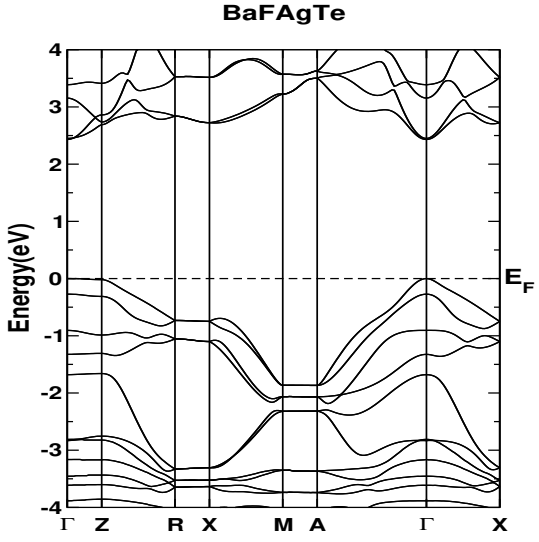
BaFAgTe
Energy(eV)
E_F
Γ Z R X M A Γ X

(f)

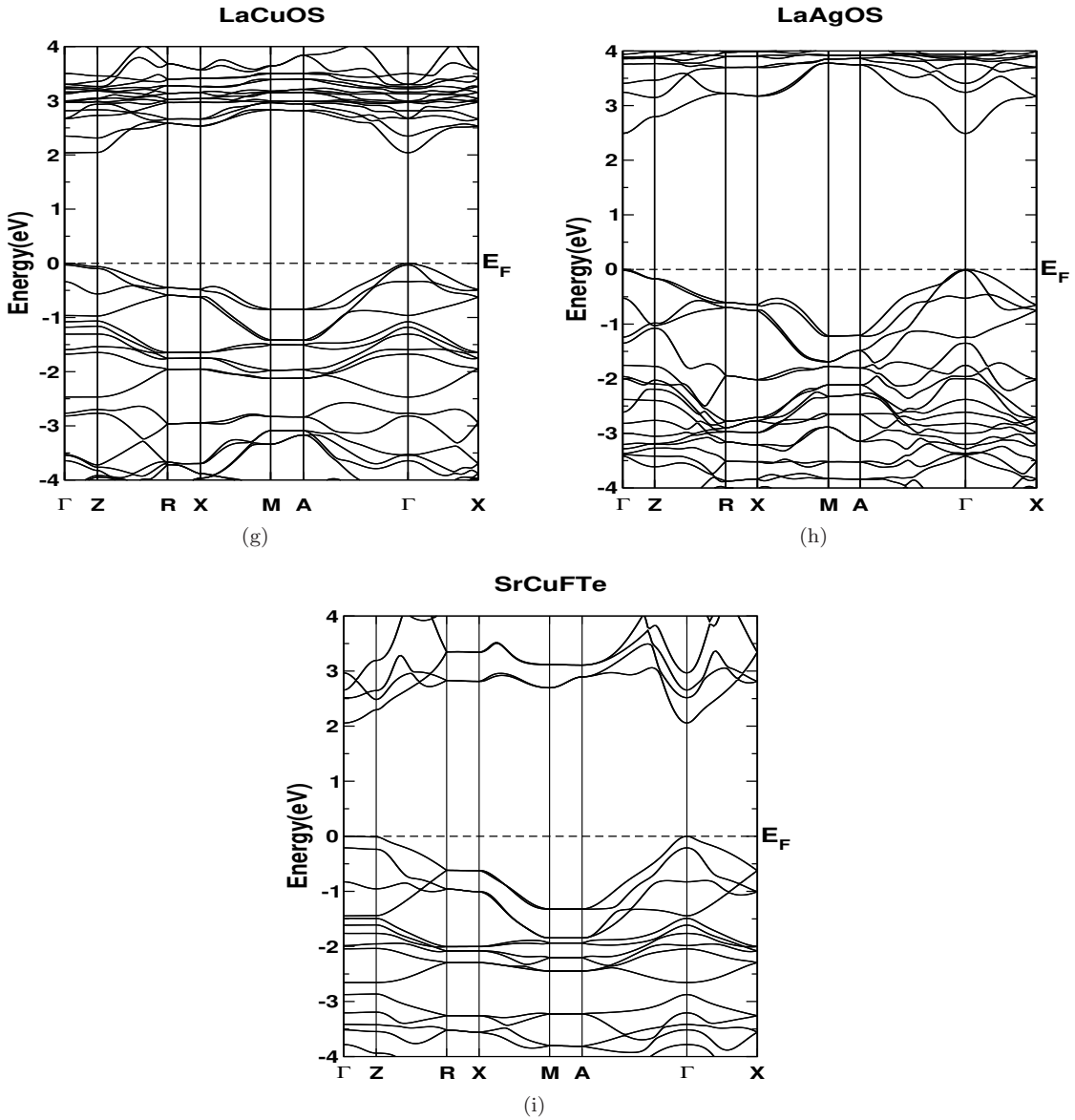

Figure 4.4: Calculated band structure for all the investigated compounds, a) BaCuFS, b) BaCuFSe, c) BaCuFTe, d) BaFAgS, e) BaAgFSe, f) BaAgFTe, g) LaCuOS, h) LaAgOS, i) SrCuFTe

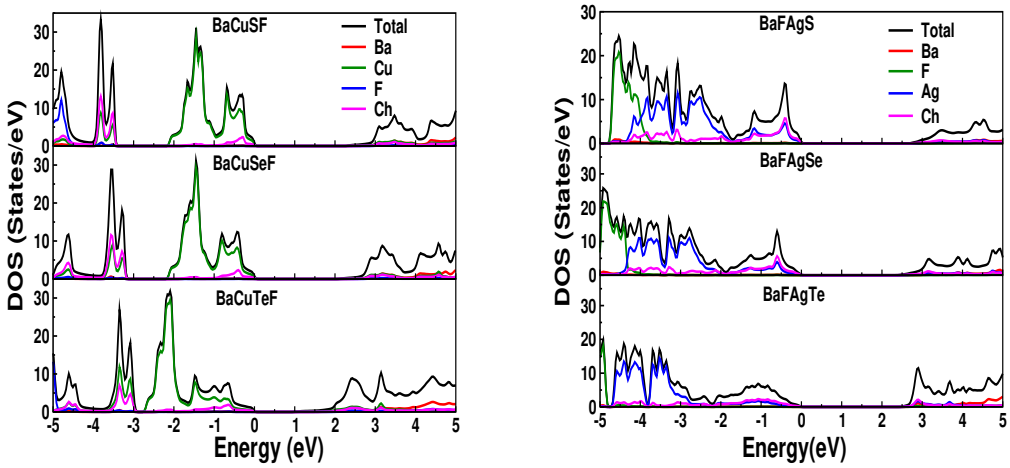

(a)

(b)

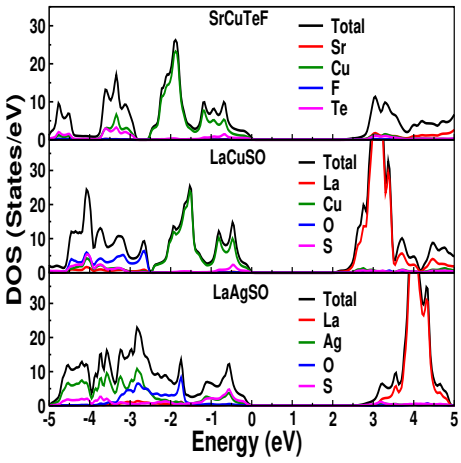

(c)

Figure 4.5: Calculated density of states of all the investigated compounds, a) BaCuFCh (Ch: S, Se, Te), b) BaAgFCh (Ch: S, Se, Te), c)LaCuOS, LaAgOS and SrFCuTe

earlier study on these compounds revealed the role of spin-orbit coupling[247], and our calculations also considered the effect of spin-orbit coupling. As we discussed earlier, the investigated compounds crystallize in the tetragonal structure, the high symmetry $\Gamma - X$ direction indicates the crystallographic 'ab' plane and $\Gamma - Z$ direction indicates the 'c' axis of the tetragonal crystal structure. The band gap values are found to decrease down the column in periodic table except for BaFAgTe. All the compounds fall in the range of wide band gap semiconductors. The band structure investigation of this '1111' type compounds are quite interesting because of the highly anisotropic character, and this causes dimensional reduction in these compounds. From the band structure, we can clearly see that along the high-symmetry directions $\Gamma - Z$, $R - X$, $M - A$, bands are completely flat, which indicate the heavy mass carriers, whereas the dispersive band along $\Gamma - X$ and $\Gamma - A$ indicate the lighter band mass carriers. The inherent nature of the combination of highly flat and dispersed band may lead to the quasi two dimensional structure, which is highly recommended for thermoelectric applications. The prototype compounds have already emerged as good thermoelectric materials [232]

The huge difference in the calculated effective mass confirm the quasi two dimensional nature in the band structure and the values are given in Table 4.3. For further analysis, we have plotted the density of states, which is given in Figure 4.5. In the case of BaCuChF compounds, Cu-d states are dominating in valence band, whereas in conduction band we can see the mixture of Ba-d and Cu-s states. For SrCuTeF, the Cu states are more dominant in valence band, and Sr and Cu states are prominent in conduction band. For LaCuSO, Cu states are significant in valence band, whereas La states are dominating in the conduction band. For LaAgSO, we can see a strong hybridisation of Ag and S states in valence band, whereas in conduction band La states are dominating. In the case of BaFAgCh, in valence band Ag and Ch states are dominating and in the conduction band we can see the combination of Ba, Ag and Ch states. Overall for all the compounds, the quasi two dimensional bands present in the upper valence band is derived from Cu or Ag 'd' states. Compared to valence band, the states are more hybridised in the conduction band, which may lead to enhanced conduction for electron doping compared to hole doping. In the next section, we have discussed the thermoelectric properties of the investigated compounds.

4.3.2 Thermoelectric properties

To predict the TE properties of a material, we need to have the knowledge of the value of thermopower, electrical conductivity and thermal conductivity of the compound. Here using the combination of DFT and Boltzmann transport theory, we have calculated thermopower, electrical conductivity and power-factor of all the compounds, for temperatures ranging between 300 K - 900 K, and for carrier concentration range between $1 \times 10^{18} cm^{-3}$ to $1 \times 10^{21} cm^{-3}$. The discussion regarding the range of thermal conductivity has been taken up separately. Calculated TE properties of all the investigated compounds as a function of both hole and electron concentrations at different temperatures are represented in Figure 4.6 to Figure 4.14. A decremental behavior is observed in the thermopower value as a function of carrier concentration for all the investigated compounds, which is the usual trend in semiconductors. Further from the same figures, it is evident that the thermopower values are increasing as function of temperature. The trend of thermopower for all the investigated compounds are the same, and we have reported the range of magnitude of thermopower for both holes and electrons for temperatures between 300 K- 900 K as represented in Figure. 4.15 for all the

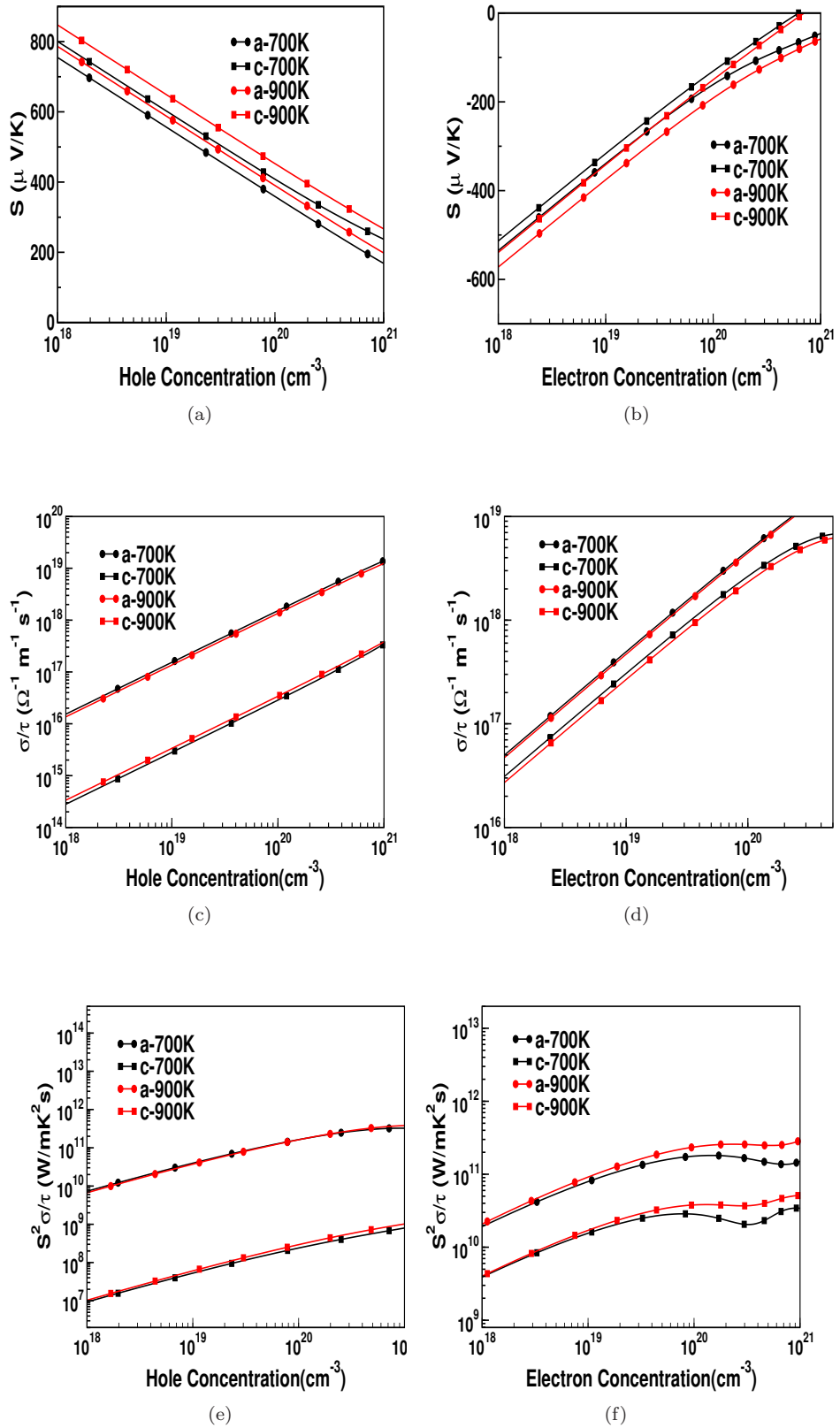

Figure 4.6: Calculated thermopower, electrical conductivity and power factor as a function of hole and electron concentration for BaCuFS

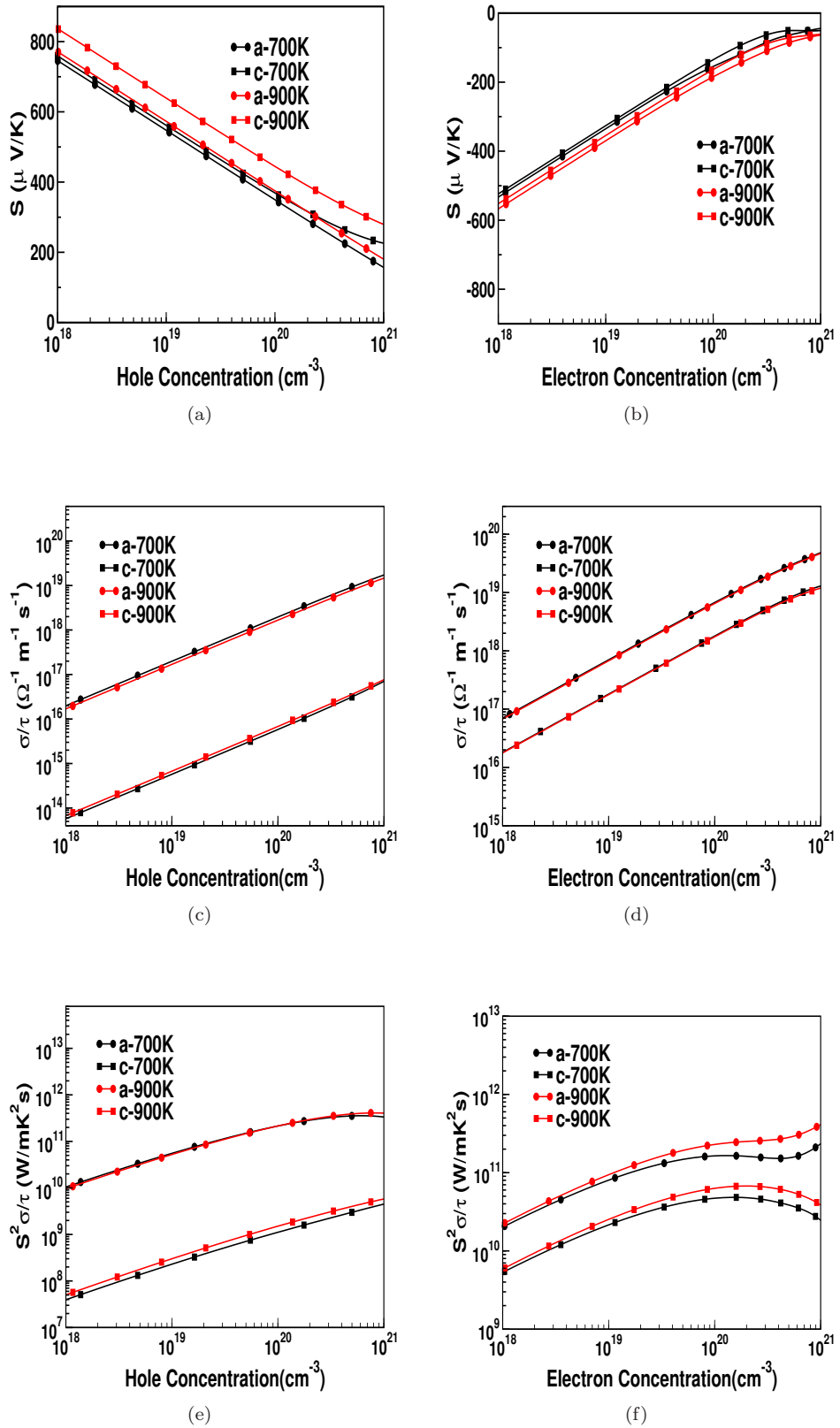

Figure 4.7: Calculated thermopower, electrical conductivity and power factor as a function of hole and electron concentration for BaCuFSe

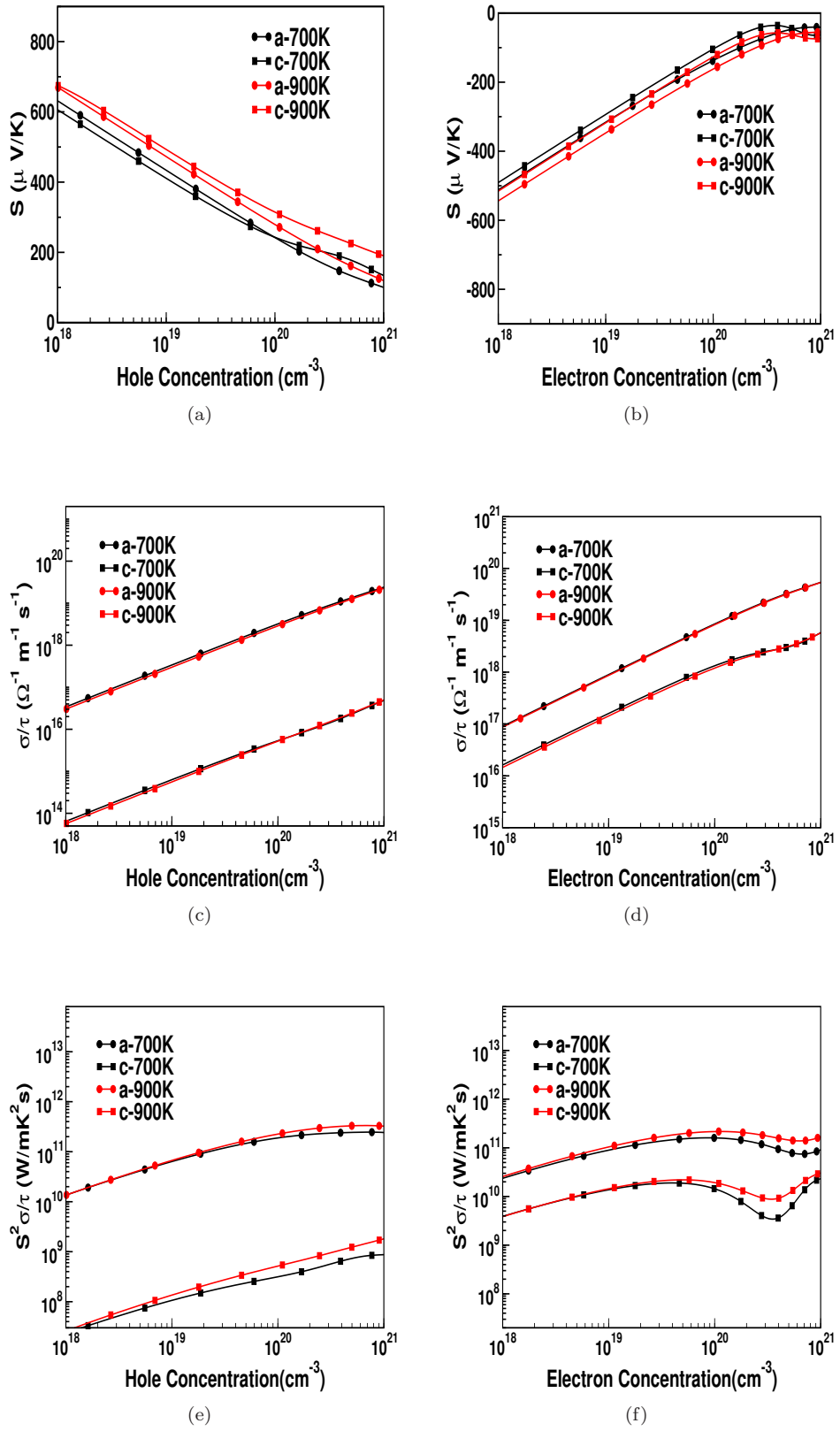

Figure 4.8: Calculated thermopower, electrical conductivity and power factor as a function of hole and electron concentration for BaCuFTe

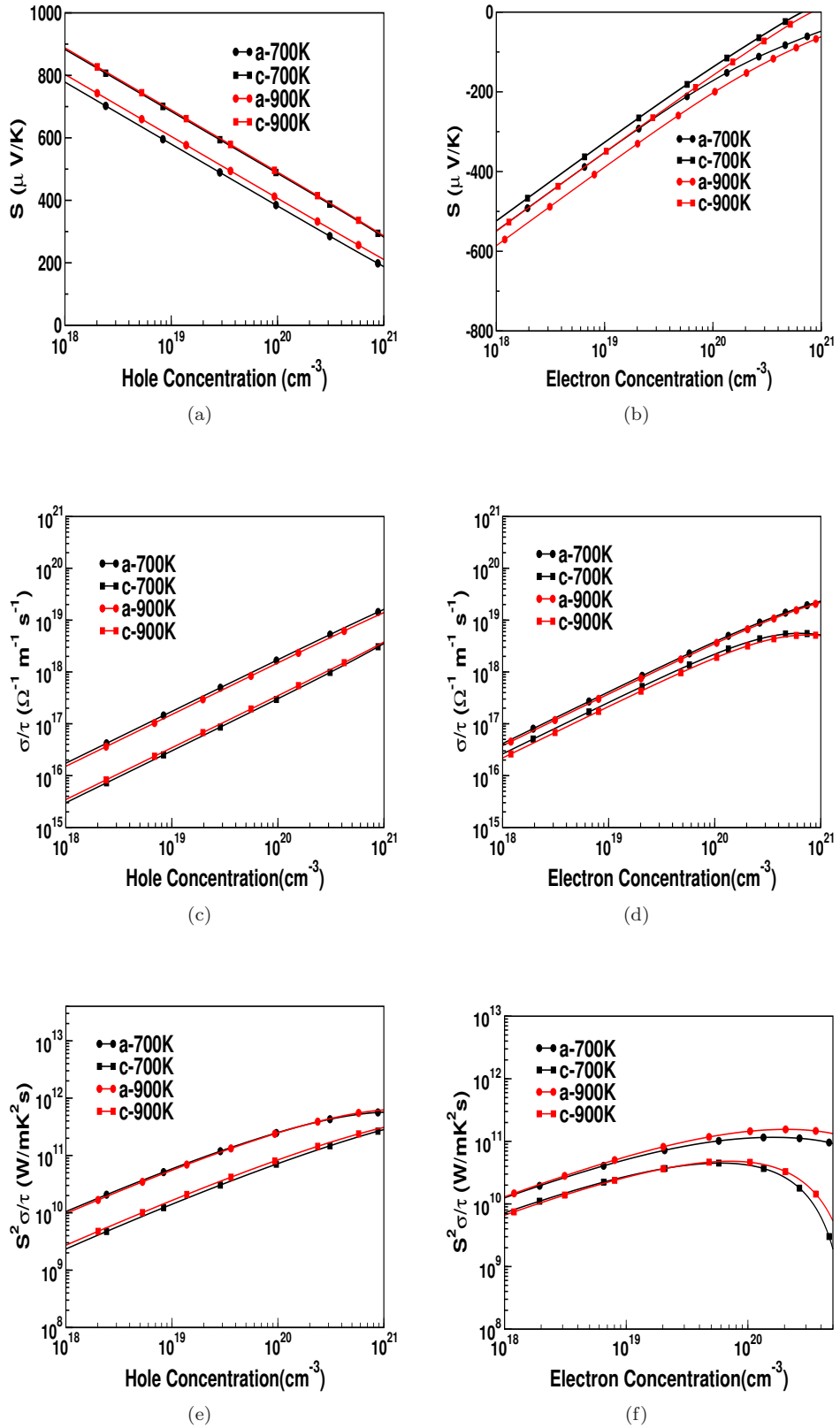

Figure 4.9: Calculated thermopower, electrical conductivity and power factor as a function of hole and electron concentration for BaFAgS

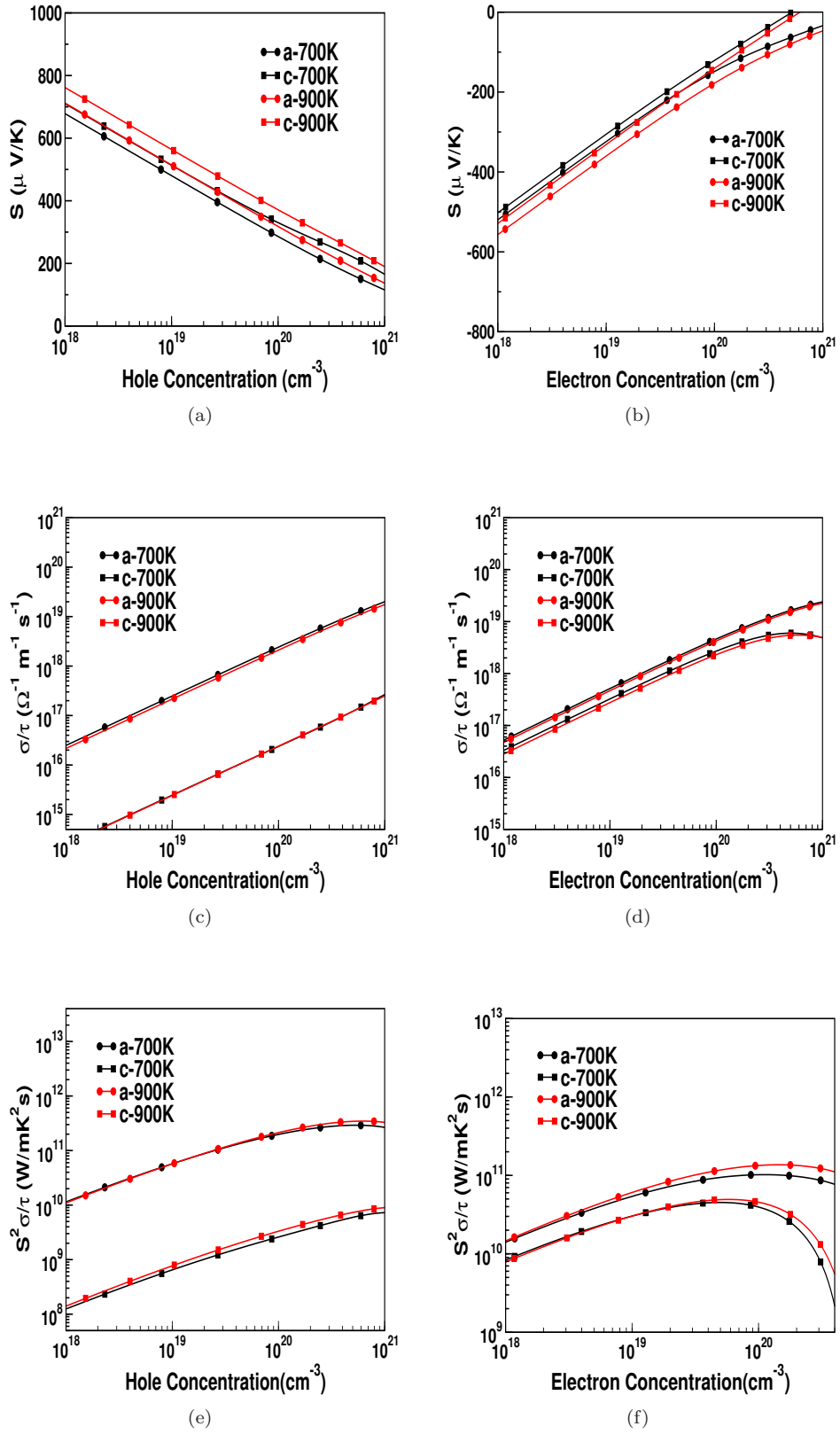

Figure 4.10: Calculated thermopower, electrical conductivity and power factor as a function of hole and electron concentration for BaFAgSe

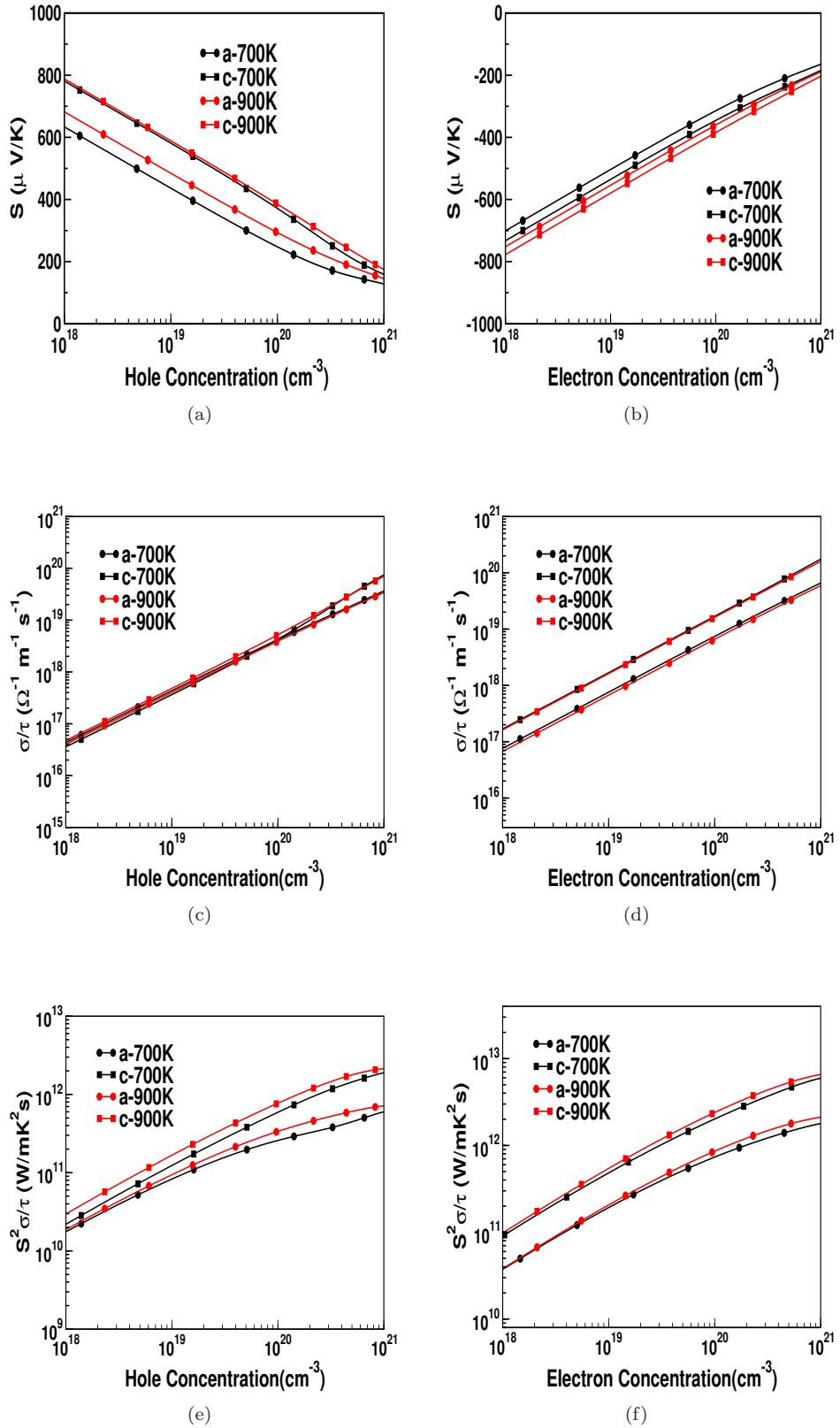

Figure 4.11: Calculated thermopower, electrical conductivity and power factor as a function of hole and electron concentration for BaFAgTe

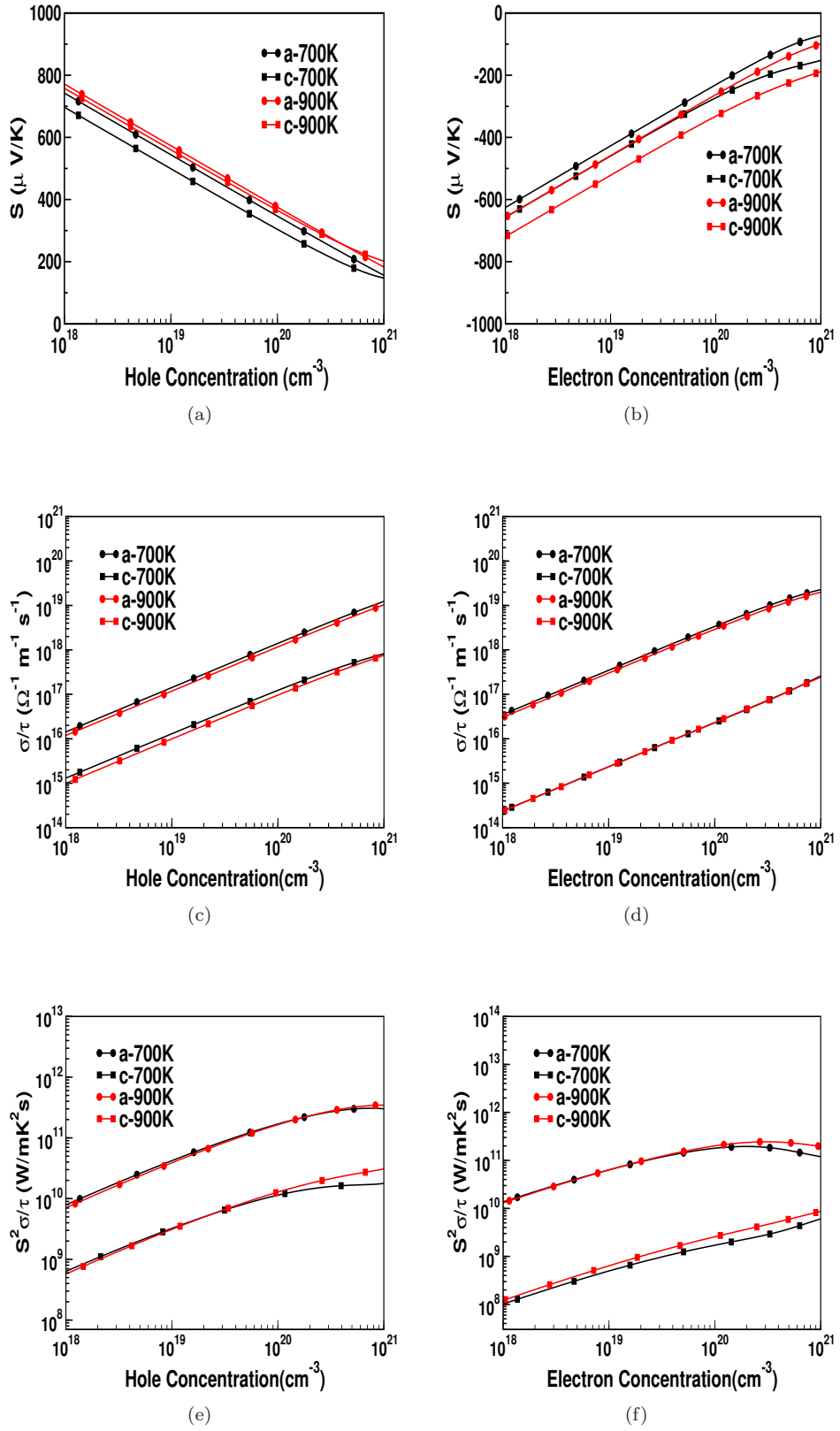

Figure 4.12: Calculated thermopower, electrical conductivity and power factor as a function of hole and electron concentration for LaCuSO

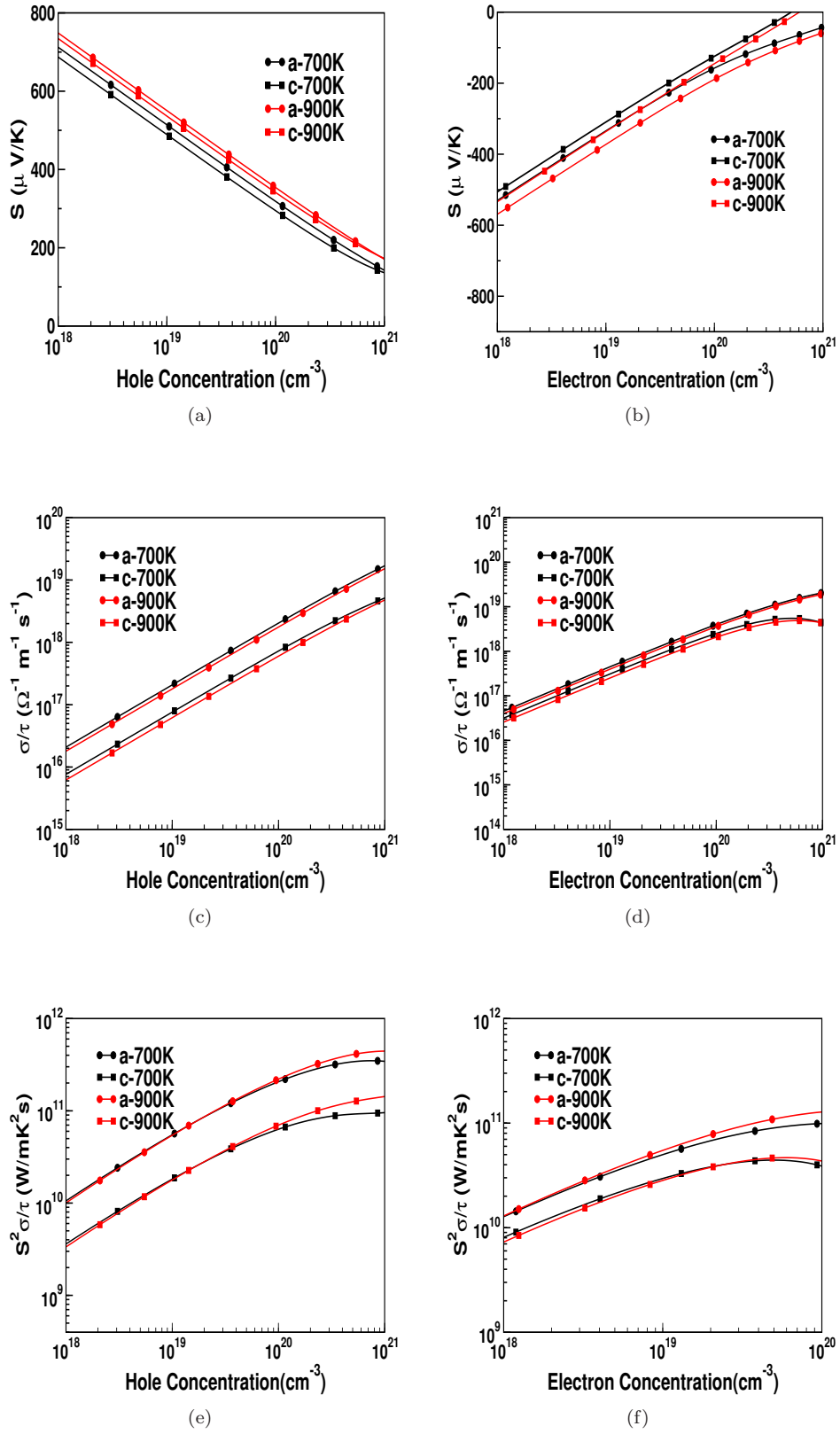

Figure 4.13: Calculated thermopower, electrical conductivity and power factor as a function of hole and electron concentration for LaAgSO

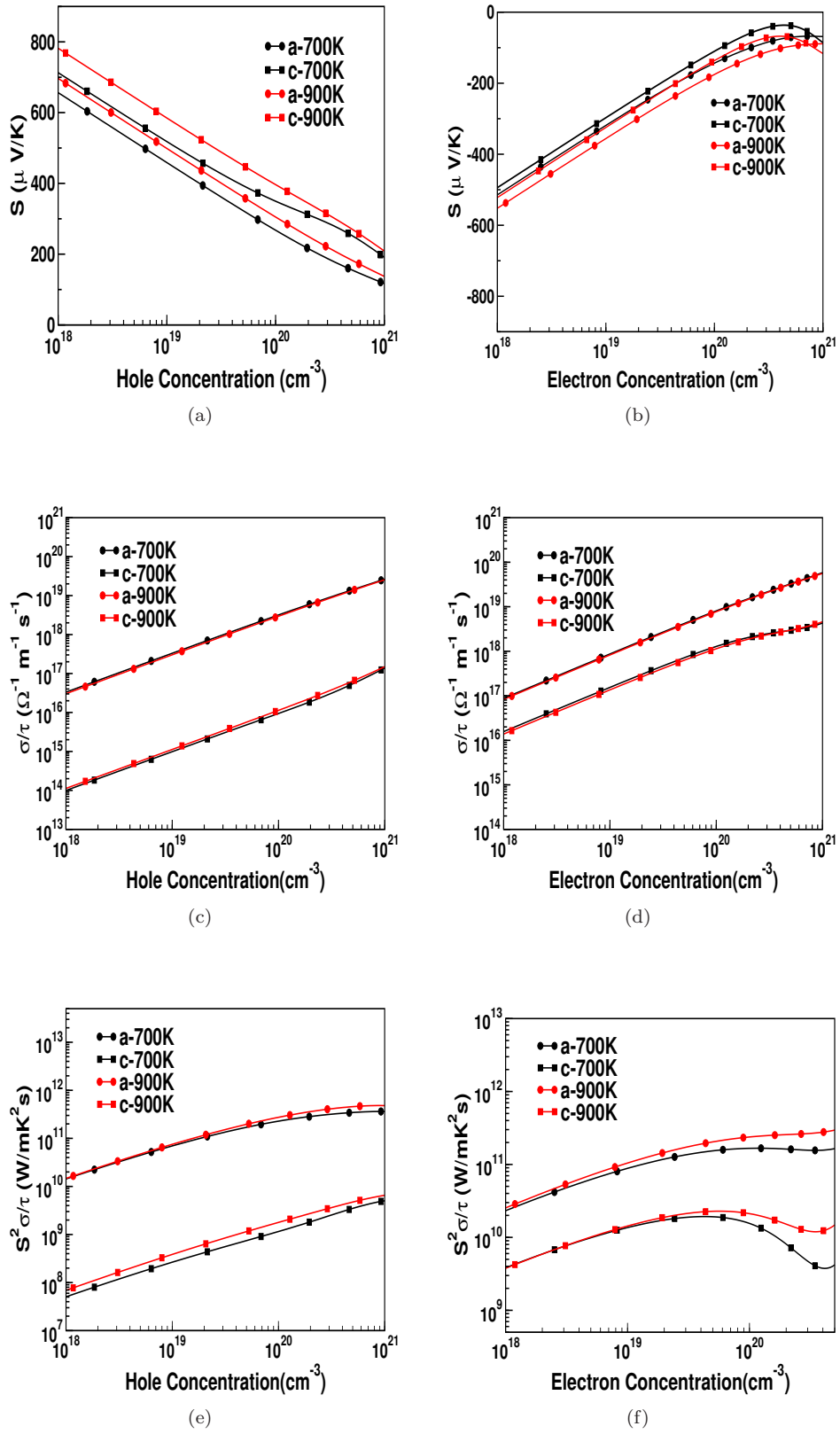

Figure 4.14: Calculated thermopower, electrical conductivity and power factor as a function of hole and electron concentration for SrCuTeF

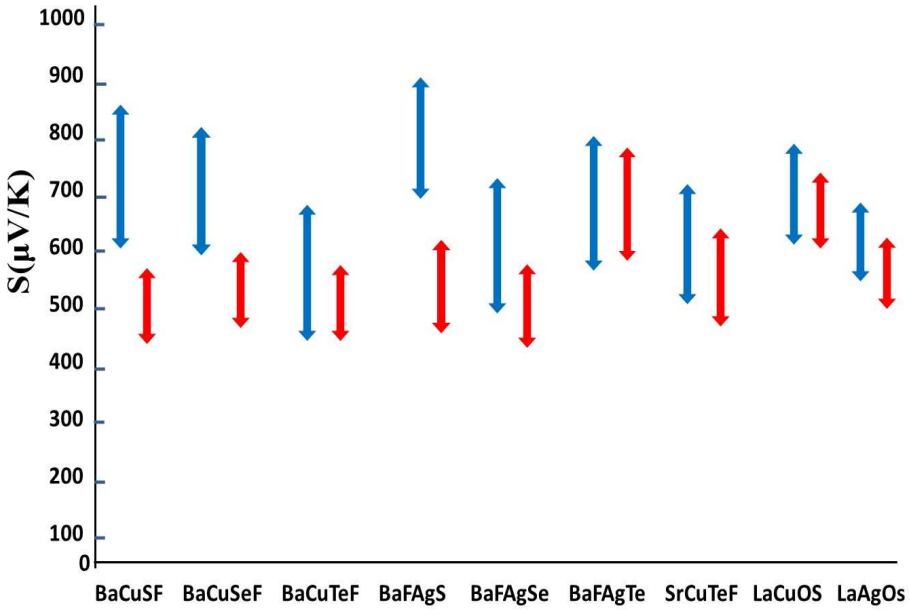

(a)

Figure 4.15: Calculated thermopower values of all the investigated compounds for temperature range 300 K to 900 K, and foe carrier concentrations ranging between $1\times\ 10^{18}$ to $1\times\ 10^{21}$ cm^{-3}

investigated compounds. Thermopower for hole doping is found to be higher than electron doping for all the cases, and this might be due to the presence of highly flat bands in valence band. Among the investigated compounds, BaCuSF and BaFAgS are found to have maximum value of thermopower. The quasi two dimensional nature in valence band introduce anisotropy in thermopower values for holes along 'a' and 'c' axis.

The electrical conductivity for both the electron and hole concentration is calculated for all the investigated compounds. All the studied compounds have almost similar behaviour and we have represented the variation of electrical conductivity as a function of carrier concentration for the temperature range of 300K to 900 K for all the investigated compounds. As we expected from the band structure, the electrical conductivity for the holes is higher along the 'a' axis compared to the 'c' axis, due to the dispersion along the $\Gamma - X$ being higher compared to that along $\Gamma - Z$. As there is no great difference in the conduction band dispersion, we can find lesser anisotropy in the case of electrons. We also found the electrical conductivity to be higher in case of electron doping compared to hole doping which is approximately of two orders. The electrical conductivity is found to increase as we move down the group from S to Te in all the compounds, which is expected.

In order to pick out the best compound among the investigated series, we have plotted the power factor $S^2\sigma/\tau$ in Figure 4.16. We can see a clear difference among the power factor along 'a' and 'c' directions from this figure. The power factor along the 'a' directions is more dominating than 'c' direction. The position of the peak in this transport function provides an upper bound on the possible optimum doping level, and this is below $\sim 10^{21} cm^{-3}$ holes for all investigated compounds. Among the investigated compounds, the power factor of BaCuSeF is found to be higher for hole doping. The present studied compounds have comparable value of thermopower and electrical conductivity

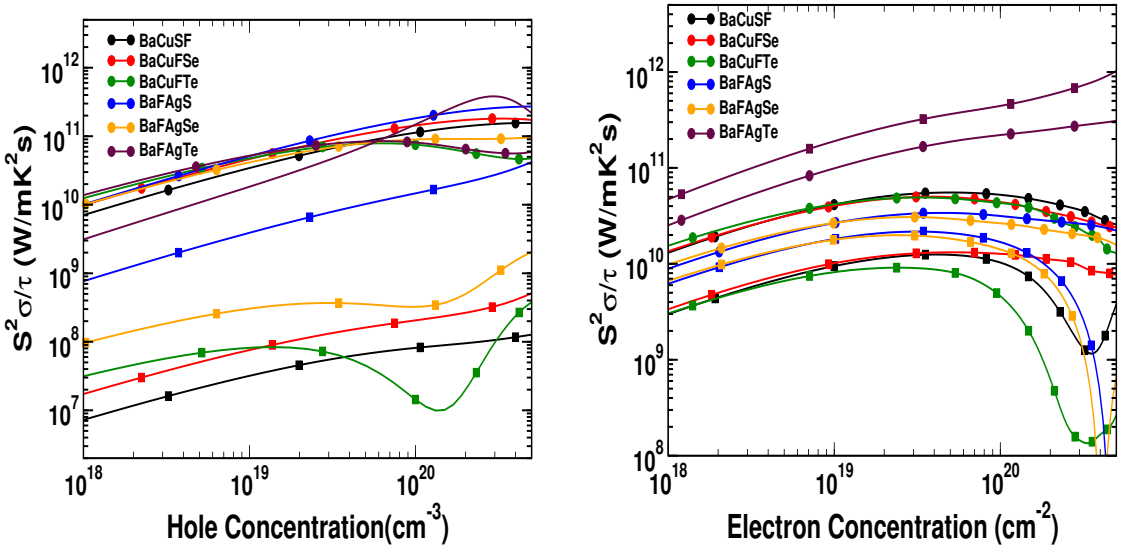

Figure 4.16: Calculated power factor of all the investigated compounds

as that of the prototype compound SrAgSF[232], which is realized as a natural superlattice. The figure of merit depends on thermopower, electrical conductivity, thermal conductivity and absolute temperature. In our calculations, the value of electrical conductivity is coupled with the relaxation time. Now let us examine the decoupling of relaxation time in order to comment more about the figure of merit. For this purpose we are following the method proposed by Takeuchi[248] to decompose ZT in two parts 'A' and 'B', where 'A' is purely dependent on electronic part and 'B' contains the lattice thermal conductivity part.

ZT= ($S^2\sigma T/ \kappa_e+\kappa_l$) = AB, A = ($S^2\sigma T/ \kappa_e$),

B= $1/(1+\kappa_l/\kappa_e)$

Since the value of 'B' is less than unity, 'A' can be considered as the maximum possible value of ZT. The parameter 'A' is defined as ($S^2\sigma T/ \kappa_e$). In our case both electrical conductivity and electronic part of thermal conductivity are coupled with relaxation time, and by using this formula we can decouple it. The range of 'A' parameter for all investigated compounds are given in Figure 4.17. Since both electrical conductivity scaled by relaxation time and electronic part of thermal conductivity scaled by relaxation time have anisotropy along 'a' and 'c' axis, there is no much anisotropy observed in 'A' parameter. Since the thermopower and electrical conductivity values are good enough within the studied temperature range of 300K to 900K, the investigated compounds find promising TE applications for a wide temperature range.

4.3.3 Lattice dynamics

Here we have examined the elastic properties and mechanical stability of the investigated compounds. We start with the analysis of six elastic constants of the investigated compounds, and calculated elastic constants are given in Table 4.4 to Table 4.6, which satisfy the Born criteria [250] for stability. To understand the stiffness along different crystallographic directions, we have compared the elastic constants along these directions. As we know for the tetragonal system, C_{11} and C_{22} will be same (along 'a' and 'b' axis) and C_{33} is along 'c' axis, and it is observed that C_{11} is higher than C_{33},

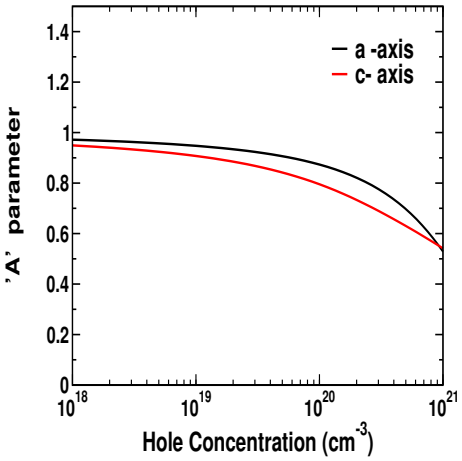
a -axis
c- axis
'A' parameter
Hole Concentration (cm^{-3})

(a)

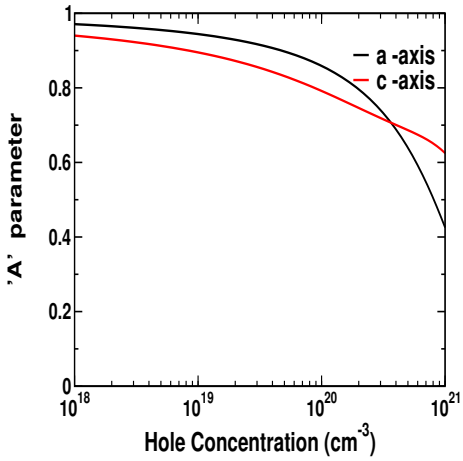
a -axis
c -axis
'A' parameter
Hole Concentration (cm^{-3})

(b)

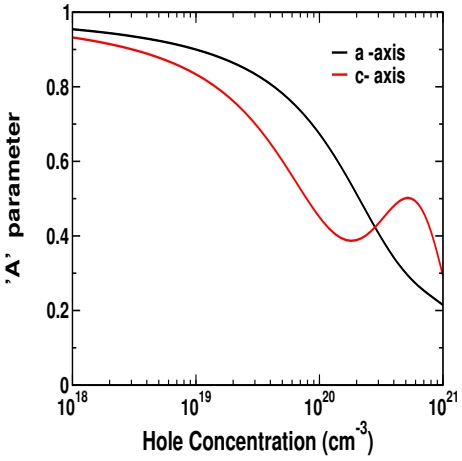
a -axis
c- axis
'A' parameter
Hole Concentration (cm^{-3})

(c)

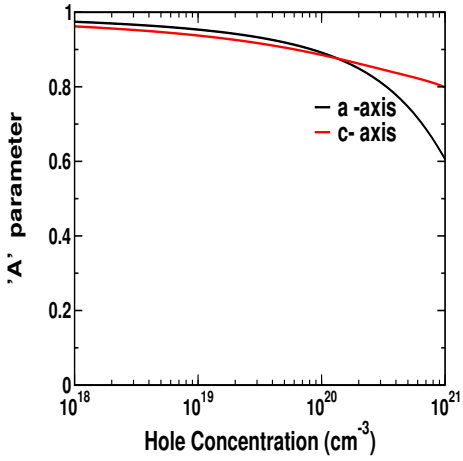
a -axis
c- axis
'A' parameter
Hole Concentration (cm^{-3})

(d)

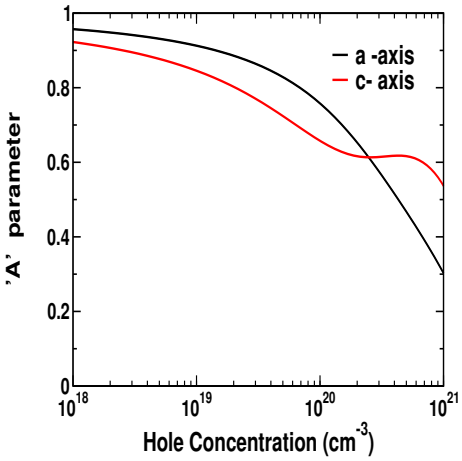
a -axis
c- axis
'A' parameter
Hole Concentration (cm^{-3})

(e)

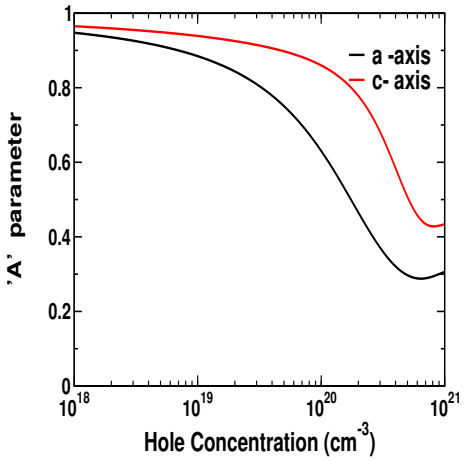
a -axis
c- axis
'A' parameter
Hole Concentration (cm^{-3})

(f)

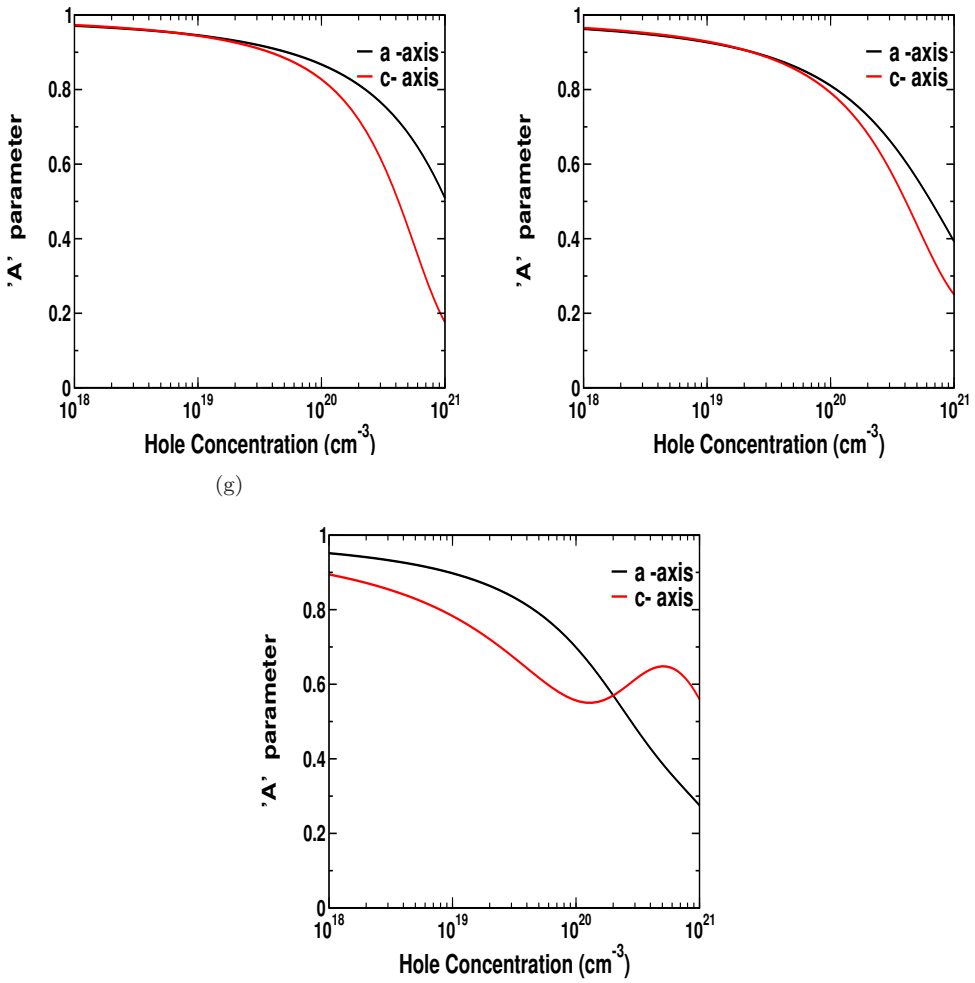

Figure 4.17: Calculated 'A' parameter for a) BaCuSF, b) BaCuSeF, c) BaCuSTe, d) BaFAgS, e) BaFAgSe, f) BaFAgTe, g) LaCuSO, h) LaAgSO, i) SrCuTeF

which indicates that 'a' axis is more stronger than c axis, which again is obvious from the bonding itself, as the distance between Ba-Ch is higher compared to other bond lengths in the system, and this may lead to easy compression along 'c' axis. Further we have observed that magnitude of elastic constants of Ag based compounds are lesser than Cu based compounds, and this indicate the weak Ag bonding in these compounds, and the same we have observed in ELF calculations also. In addition, the large shear modulus ((C_{11}-C_{12})/2) in Cu based compounds indicate the higher mechanical strength. The magnitude of C_{12} is further related with the bonding in 'x' and 'y' plane, so the large value of C_{12} in Cu based compounds indicate the stronger bond in 'x' and 'y' plane of this series compared to Ag based compounds, which was also obvious from the bond length calculations, where we have observed the higher bond length for Ag based compounds compared to Cu based compounds. From elastic constants, we have further calculated other mechanical properties like bulk modulus, shear modulus etc, and are represented in Table 4.4 to Table 4.6, which indicate all the compounds to be ductile materials. Bulk modulus is found to decrease from S to Te in both Cu and Ag based compounds, and is observed that the range of bulk modulus is comparable with well known prototype materials BiOCuSe [246], and SrAgChF [232]. We also found that the oxygen based chalcogen have higher bulk modulus values compared to the fluro based chalcogens (see Table 4.4 to Table 4.6). Longitudinal and transverse sound velocities are calculated and observed that for all the compounds there is an anisotropy in these compounds. Further, calculated Debye temperature (see Table 4.4 to Table 4.6) indicate the possibility of very low thermal conductivity in these investigated compounds, and have almost comparable values with prototype materials. The Grünesian parameter relates the phonon frequencies and crystal volume, and by calculating this, we can comment about the rate of anharmonicity in phonon conduction. Here we have calculated the average Grünesian parameter of investigated compounds and are given in Table 4.7, and from table it is clear that the investigated compounds have Grünesian parameter lesser than prototype material BiOCuSe, and other TE material SnSe[251], which indicate the lesser anharmonicity in phonon conduction. In this scenario, the prediction of lattice thermal conductivity from calculated Debye temperature and Grünesian parameter is worthy. One of the pioneering work regarding thermal conductivity by G. A. Slack [252]has been adapted here to predict the thermal conductivity of investigated compounds. The main assumption used here is that the heat is only conducted by acoustic phonons. The Slack's equation for thermal conductivity is

$k = 3.1\times10^{-6}\ (M\theta^3\ \delta\ /\ \gamma^2\ n^{2/3}\ T\ )$ in W m^{-1} K^{-1}

where 'M' is average atomic mass in amu, 'θ' is Debye temperature in K, '$\delta^{\,3}$' is volume per atom in $Å^3$, 'n' is number of atoms in the primitive cell, γ is average Grünesian parameter. Since the contribution of optical modes of phonons towards thermal conductivity is lower compared to acoustic phonons, this equation is worthy to be used for predicting the range of the thermal conductivity. Calculated values of thermal conductivity of investigated compounds using Slack's equation are given in Table 4.7. From the table, it is quite clear that all the compounds possess very low thermal conductivity. The exact value of thermal conductivity may differ from the calculated values little bit because of the exclusion of anharmonic effects, which has be to verified further by future studies. The low value of Debye temperature confirms the higher atomic mass and weak inter atomic bonding, while the range of Grünesian parameter indicate the moderate anharmonicity in these compounds[252]. This confirms that the investigated compounds can emerge as good thermoelectric materials which can be realized by future experimental studies. For further proof, we have used Cahill

model[253] to find the range of minimum thermal conductivity in studied compounds. According to Cahill model, the equation of minimum thermal conductivity is

$k_{min} = k_B/2.48\ (n^{2/3}\ (v_l + 2v_t)$

where k_B is the Boltzmann constant, n is the density of number of atoms per volume, v_l and v_t are average longitudinal and transverse velocities. Calculated values of k_{min} are given in Table 4.4 to Table 4.6. Further we have also related the anisotropy in lattice thermal conductivity values by using Young's modulus. Since lattice thermal conductivity is proportional to v^3, and v is proportional to Y (Yong's modulus). We have estimated the anisotropy in lattice thermal conductivity in a crude way by comparing with Young's modulus along different axis.

$Y_c = C_{33}$ -$(2C_{13}2C_{13}/c_{11}+c_{12})$

$Y_a = ((C_{11}\text{-}C_{12})(C_{11}C_{13}+C_{12}C_{33}\text{-}\ 2C_{13}C_{13}))/(C_{11}C_{33}\text{-}C_{13}c_{13})$

From our calculations it is observed that lattice thermal conductivity also possess anisotropy along different crystallographic direction and found to be more along 'a' axis than 'c' axis.

For further analysis we have calculated the phonon dispersion of the investigated compounds. The phonon dispersion relation of few compounds are presented in Figure 4.18 to understand the behaviour of phonon modes, and the dynamical stability of the investigated compounds. The positive values of frequencies confirmed the dynamical stability of the investigated compounds. To understand about the thermal conductivity, we have to examine the interaction between acoustic and optical modes of the dispersion plots. We have observed that the optical branches intersect the acoustic branches around 60 cm^{-1} for BaFAgS, around 65 cm^{-1} for BaCuFS, and around 81 cm^{-1} for LaCuOS. The trend indicate that for all investigated compounds, the interaction between low frequency optical modes and acoustic modes are higher. We know that to reduce the lattice thermal conductivity we need higher phonon scattering, which might be possible through the interaction between acoustic and optical phonon modes. Further we can see the flat acoustic branches, which again indicate the low thermal conductivity in these compounds. Here we would like to recall the bonding and electronic structure analysis, where we have noticed that the highly quasi flat band nature was derived from the X-Ch states. The remarkable structure of these family of compounds showed a combination of high thermopower and low thermal conductivity, and further the electrical conductivity can be enhanced by band engineering techniques, which eventually project this series to be promising thermoelectric materials.

4.4 Conclusions

The electronic, mechanical and transport properties of BaXChF (X: Cu, Ag, Ch: S, Se, Te), LaXOS and SrCuTuF were calculated using density functional theory. The calculations revealed the low thermal conductivity in these compounds. The quasi two dimensional nature of band structure is identified, and all the investigated compounds can be considered as natural super-lattice structures. The calculated thermopower values are found to be higher for all the compounds. Huge anisotropy is observed for electrical conductivity for hole doping, which again confirms the quasi two dimensional nature in these compounds. The transport properties of all the investigated compounds are comparable with the prototype material SrAgSF. The low value of Debye temperature and highly interacting acoustic and optical phonon modes confirm the possibility of low thermal conductivity in these compounds. The calculated 'A' parameter have higher values than traditional TE materials.

The emergence of high power factor and low thermal conductivity can site these compounds for better TE applications.

Table 4.4: Calculated elastic constants of BaCuChF (Ch = S, Se, Te)

Parameters	BaCuSF	BaCuSeF	BaCuTeF
C_{11} (GPa)	106.20	98.91	88.20
C_{33} (GPa)	98.40	99.91	53.05
C_{44} (GPa)	34.73	33.52	29.54
C_{66} (GPa)	17.94	17.75	17.27
C_{12} (GPa)	27.94	25.26	15.60
C_{13} (GPa)	45.73	42.22	29.76
Bulk Modulus(B) (GPa)	60.50	41.11	43.7
V_l(km/s)	4.28	3.99	3.43
V_t(km/s)	2.31	2.14	1.96
V_m (km/s)	2.58	2.39	2.18
θ_D (K)	286.67	260.57	228.03
k_{min}(W/mK)	0.43	0.38	0.29

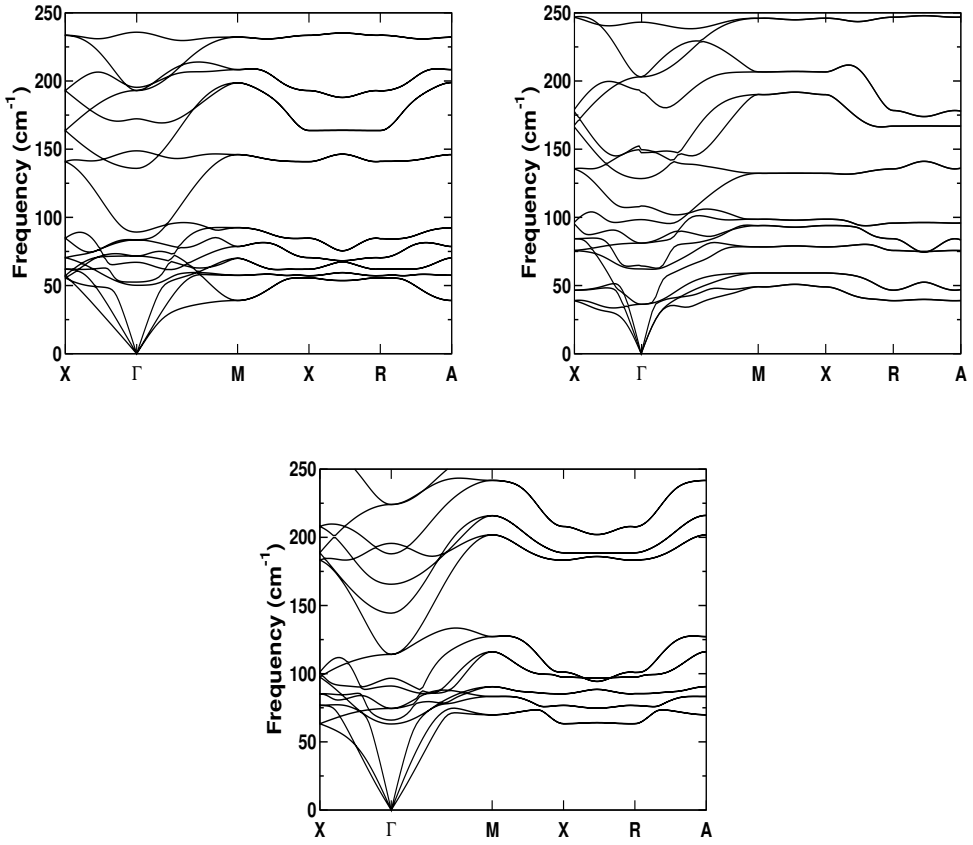

Figure 4.18: Calculated phonon dispersion of a) BaFAgS, b)BaCuSF, c) LaCuOS

Table 4.5: Calculated elastic constants of BaAgChF (Ch = S, Se, Te)

Parameters	BaAgSF	BaAgSeF	BaAgTeF
C_{11} (GPa)	106.20	98.91	88.20
C_{33} (GPa)	98.40	99.91	53.05
C_{44} (GPa)	34.73	33.52	29.54
C_{66} (GPa)	17.94	17.75	17.27
C_{12} (GPa)	27.94	25.26	15.60
C_{13} (GPa)	45.73	42.22	29.76
Bulk Modulus(B) (GPa)	60.50	41.11	43.7
V_l(km/s)	4.28	3.99	3.43
V_t(km/s)	2.31	2.14	1.96
V_m (km/s)	2.58	2.39	2.18
θ_D (K)	286.67	260.57	228.03
k_{min}(W/mK)	0.43	0.38	0.29

Table 4.6: Calculated elastic constants of LaCuSO, LaAgSO and SrCuTeF

Parameters	SrCuTeF	LaCuSO	LaAgSO
C_{11} (GPa)	94.45	216.58	215.51
C_{33} (GPa)	60.69	104.61	101.08
C_{44} (GPa)	27.48	44.56	35.94
C_{66} (GPa)	18.40	57.04	64.21
C_{12} (GPa)	17.61	80.71	57.12
C_{13} (GPa)	32.68	66.04	57.18
Bulk Modulus(B) (GPa)	45.42	92.34	85.42
V_l(km/s)	3.74	5.05	4.76
V_t(km/s)	1.92	2.57	2.47
V_m (km/s)	2.15	2.88	2.74
θ_D (K)	230.80	341.48	315.41
k_{min}(W/mK)	0.29	-	0.51

Table 4.7: Calculated Grünesian parameter and lattice thermal conductivity at 300 K of all compounds

Compounds	γ	k (W m^{-1} K^{-1})
BaFAgS	1.97	1.84
BaFAgSe	1.82	2.05
BaFAgTe	2.26	0.79
BaCuSF	1.74	3.469
BaCuSeF	1.73	3.27
BaFCuTe	1.53	3.23
LaCuOS	1.94	4.31
LaOAgS	1.87	4.4
SrCuTeF	1.91	1.7

Chapter 5

Evidence of strong topological insulating nature in CaSrX (X: Si, Ge, Sn, Pb) together with potential thermoelectric properties

The present chapter deals with a detailed electronic structure calculation, which reveals the strong topological insulating nature of series of compounds CaSrX (X: Si, Ge, Sn, Pb), together with striking TE properties. The electronic structure of all the compounds are studied as a function of uni-axial strain and an emergence of Dirac semi-metallic states has been observed in CaSrX (X: Si, Ge, Sn, Pb), which is induced by uni-axial strain along *'b'* axis. CaSrSi and CaSrGe evolved as normal semiconductor with uni-axial strain, and remaining compounds are found to preserve metallic states within the studied strain range. Since the investigated compounds preserve time reversal symmetry and inversion symmetry, the trivial and non-trivial topological phases are evaluated by band inversion and Z_2 topological invariants. An unusual thermopower oscillation has been observed at these Dirac semi-metallic states. Further the TE properties at strong topological insulating state and normal insulating state have been summarized, which reveals the potential TE properties of these materials.

5.1 Introduction

As mentioned in the introduction part, the evolution of research on TE materials recently is inclined towards several quantum states of matter such as topological insulators, topological semi-metals, Dirac materials, etc. It has been noticed that, a large quantity of the TE materials are having topological non-trivial states either at ambient or with some external perturbations, and transition metal chalcogenides, Bi_2Te_3 family, PbTe family and many more fall in this category[154, 257, 258, 209]. The co-existence of TE (thermoelectric) and TI (Topological insulator) properties in materials were examined previously, and was proposed that small band gap, and complex band profile near the Fermi level could be fruitful for both the properties[259, 147]. First principles calculations have successfully predicted significant number of thermoelectric and topological materials[260, 261, 262]. Both TE and TI materials are vastly in demand, where TE materials permit the conversion of waste heat to electricity and TI materials can be useful for quantum computing. The capability of TE material has been quantified using figure of merit (ZT), which is a dimensionless quantity, and the detailed discussion has already been presented in the introductory chapter. In the case of topological insulators, the band inversion, topologically invariant parameter such as chern number, Z_2 topological invariant, and exotic surface states need to be analyzed for better understanding. Both TE and TI properties can be tuned by the prominent tool such as strain/pressure, and there are literatures which report that several compounds have turned from trivial to non-trivial states and vice versa as function of strain/pressure, which projects the significance of these calculations[263, 264]. It is understood that the iso-structural topological transitions are possible by closing and opening of the band gap, and the transition states are interesting due to the presence of Dirac/weyl semi-metallic state. Understanding of electronic structure in these states is worth investigating, and here we would like to examine the same. Usually thermopower is considered as a parameter for thermoelectric energy conversion, and in addition, several literatures have explored the thermopower to understand the response of the system at some exotic states [265, 266, 267, 268]. The fluctuation of thermopower as a function of temperature has been analysed by Yong Lu *et. al.*, and they explored the possibility of thermopower fluctuation above superconducting transition temperature[267]. Later, the thermopower fluctuations in the presence of magnetic filed has been connected to quantum oscillations[269]. In the recent past, the thermopower fluctuations as a function of chemical potential/ carrier concentrations has been observed and studies proposed the same to be possible for quantum oscillation in thermopower in the absence of magnetic field, and the Fermi surface topology change or strain can very well play a major role in these materials[270, 271]. From this point of view, the role of Dirac semi-metallic state, and disconnected Fermi arcs, and the relation with the thermopower fluctuation will be very interesting, and here we would like to examine the thermoelectric response at the transition stage from a non-trivial insulator to trivial insulator. For this purpose, we have analysed four zintl phase compound, which in general shows good thermoelectric properties. Zintl phase compounds are well recognized for possessing complex crystal structure, and are having inherent property which are helpful for TE applications [272, 273]. Significant number of zintl phase compounds fall under narrow band gap semiconductors. The huge difference in electronegativities among the constituent elements, make these compounds more rich in chemistry. The main attraction towards these compounds is that, they generally possess high melting point and low thermal conductivity. Zintl phase compounds mostly consists of alkali, alkaline earth metals with the combination of post transition metal group elements (such as pnictides and chalcogenides). One

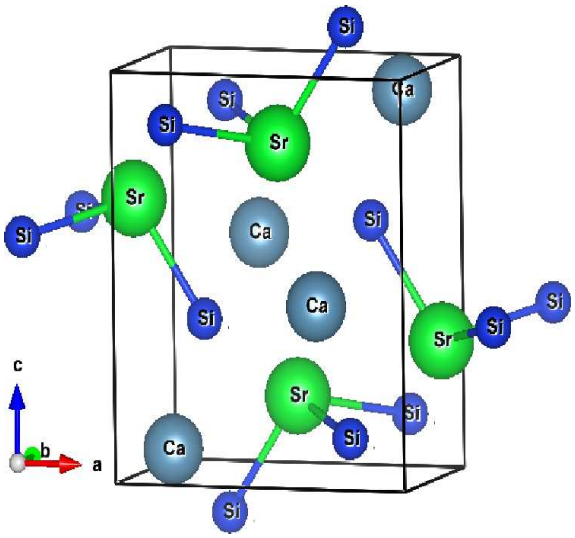

(a)

Figure 5.1: Crystal structure of investigated compounds

of the prototype compound SrLiAs has been investigated[272], and reported as good thermoelectric material with very low thermal conductivity. The present investigated compounds are less explored, and here we wish to analyse the electronic structure, topological and thermoelectric properties of orthorhombic zintl phase compounds at ambient and as a function of strain.

Table 5.1: Ground state properties of CaSrX (X: Si, Ge, Sn, Pb)

parameter	CaSrSi	CaSrGe	CaSrSn	CaSrPb
a(Å)	7.99	8.05	8.35	8.42
a_{exp}(Å)	8.108	8.124	8.421	8.509
b(Å)	4.88	4.93	4.92	5.13
b_{exp}(Å)	4.944	4.949	5.168	5.189
c(Å)	9.18	9.24	9.71	9.79
c_{exp}(Å)	9.170	9.184	9.685	9.740
E_g(eV(with GGA))	0.37	0.40	0.27	0.09
E_g(eV(with TB-mBj))	0.64	0.713	0.561	0.49
E_g(previous)[279](eV (with GGA))	0.331	0.326	0.252	0.029

5.2 Computational details

The structural optimization and phonon dispersion were calculated using Plane Wave self consistent field (Pwscf) program[274], which is based on pseudo potential method. Further calculations were carried out using optimized lattice parameters. We have performed the electronic structure calculations by using Wien2k package [162, 163], which is based on FP-LAPW (full potential linearised

augmented plane wave) method. The improved band gap of investigated compounds was achieved using Tran-Blaha modified Becke-Johnson (TB-mBJ) functional[165, 166], since the exchange correlation functional such as local density approximation (LDA) and generalized gradient approximation (GGA) underestimate the band gap of semiconductors and insulators. The spin orbit effect is incorporated using second variational method in present calculations. The k-point mesh of 8×14×7 in the full Brillouin zone was used to study the electronic properties. The BoltzTraP code[169] was used to extract the thermoelectric coefficients including thermopower, electrical conductivity with dense k-mesh. The rigid band approximation (RBA) [170, 171, 172] and the constant scattering time approximation (CSTA), are incorporated in BoltzTraP code[169], and several materials have been successfully predicted using the same[173, 174, 175, 236, 177]. The parity analysis was performed using VASP, and all the occupied bands are taken into account for the same. Topological surface states have been calculated by combining Wien2k and Wannier90 package. Well converged Wien2k outputs are used as inputs to Wannier90 and Wannier-tools were used to plot the spectral functions [275, 276]. The strain calculations were performed by changing the lattice parameters, and atomic positions of each strained state were optimized.

5.3 Results and discussions

5.3.1 Properties at ambient conditions

The structure of the studied compounds is given in Figure 5.1, and these compounds crystallize in orthorhombic structure with space group P_{nma} in the form CaSrX (X: Si, Ge, Sn, Pb). Computed ground state properties of all the studied materials are reported in Table 5.1, which indicate the compatibility between the present values and other reported theory and experimental values. In order to examine the electronic structure properties in detail, we have calculated the band structure with several exchange correlation functionals such as GGA and TB-mBJ, together with inclusion of spin orbit coupling. From the analysis, we have observed that spin orbit effect is negligible in the studied compounds. Band gaps of all the compounds are reported in Table 5.1, and all the compounds show semiconducting nature. The band structure calculated along different high symmetry directions for all the investigated compounds are presented in Figure 5.2. For CaSrSi, we have represented the band structure by combining two cases, with spin-orbit coupling and without spin-orbit coupling (see red dot and black solid lines in Figure 5.2(a)), and from the figure, it is evident that spin-orbit effect is very minimum in this compound. The band profile of all the compounds is almost similar, and band gap is found to decrease from CaSrSi to CaSrPb. A direct band gap is observed at Γ high symmetry point. Along all crystallographic directions, 'a','b', 'c', the bands are observed to be dispersive in the valence band, with dispersion being little higher along 'b' axis. A similar scenario can be observed in conduction band. A flat band is observed along R-S high symmetry direction in valence band in all the compounds. A thorough investigation of the band structure of these compounds reveal a highly linearised Dirac like band profile along Γ - Y direction in conduction band. Figure 5.3 represents the projected band structure, which confirms the domination of Si-p states near valence band and a competing Si-p and Sr-d states in the conduction band. Figure 5.4 presents the total density of states of all the compounds and partial density of states of CaSrSi, which also indicate similar contributions from Si-p and Sr-d states near Fermi level. The calculated elastic

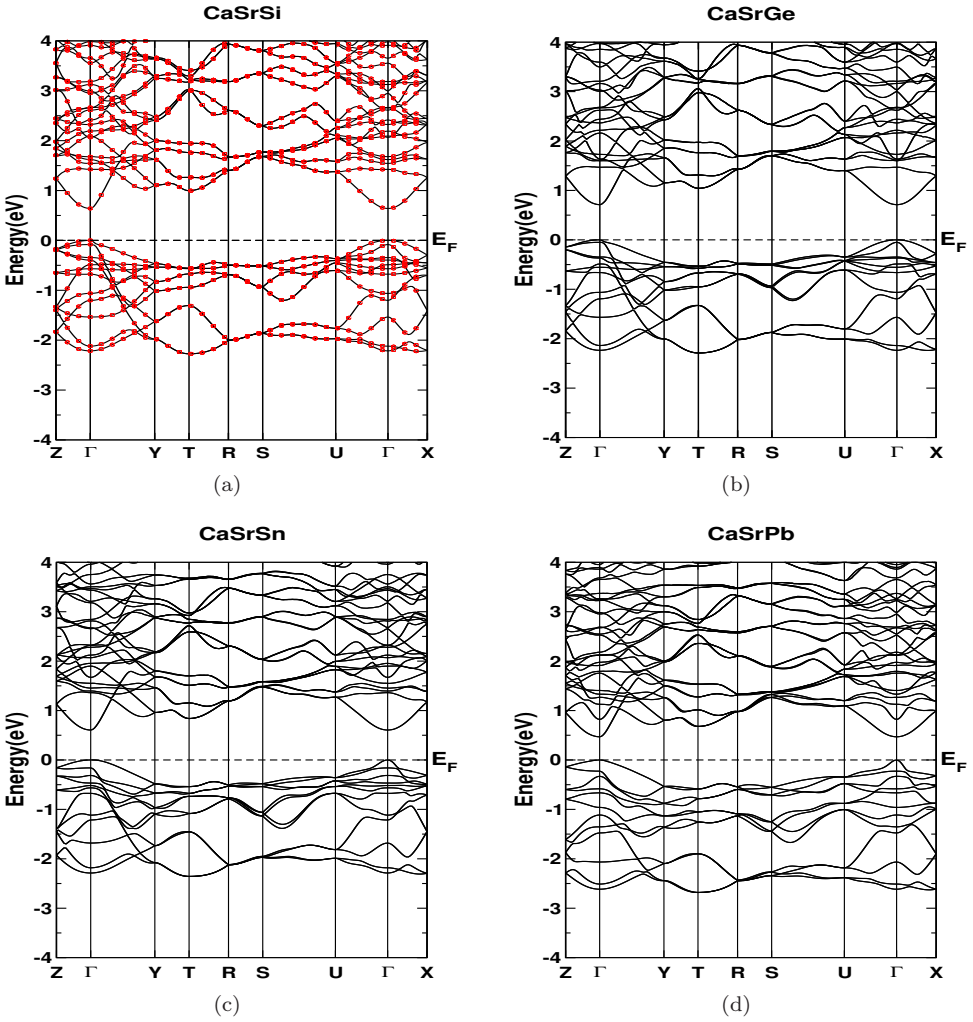

Figure 5.2: Band structure of investigated compounds, a) CaSrSi with and without inclusion of spin orbit coupling, solid lines represent band structure with spin orbit coupling and red dots represent the band structure without spin-orbit coupling, b) CaSrGe, c) CaSrSn d) CaSrPb with spin orbit coupling

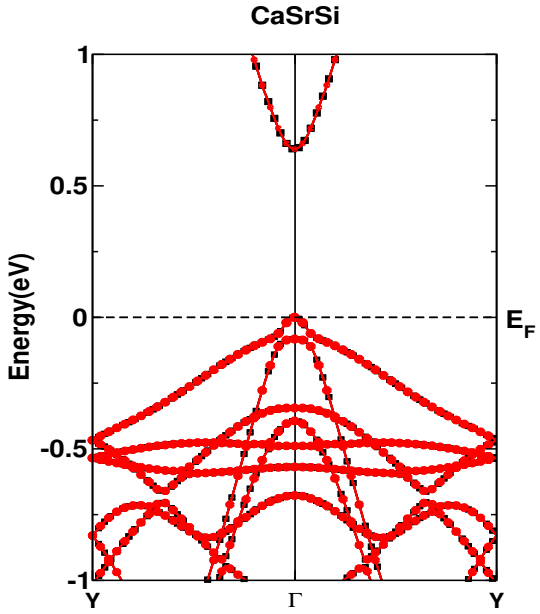

(a)

Figure 5.3: Projected band structure of CaSrSi, black circle represents Si-p states and red circle represents Sr-d states

constants of all the investigated compound are presented in Table 5.2. The born stability criteria is found to be satisfied for all the compounds, confirming the mechanical stability of these compounds. The elastic constants are comparable with iso-structural materials. In Table 5.2 we have reported the bulk modulus and Debye temperature of all the investigated compounds. The magnitude of Debye temperature is observed to decrease from Si to Pb, and the range of the same indicate the probability of low thermal conductivity. Further the phonon dispersion plot of CaSrSi and CaSrGe are presented in Figure 5.5. The less dispersed phonon modes indicate the probability of lesser thermal conductivity in these materials. The range of frequency, where the acoustic and optical phonon modes interact is found to be decreased from CaSrSi to CaSrGe, and the corresponding frequencies are 70 cm^{-1} to 50 cm^{-1}, implying the low thermal conductivity in these compounds, which is appropriate for TE applications. A unique band profile along Γ -Y direction encourage us to examine the electronic structure in detail, and we have analysied the topological behavior of these studied compounds. All the investigated compounds are invariant under time reversal symmetry, and the topological character of the same can be connected with Z_2 topological invariant. Moreover, the system possesses inversion symmetry and the corresponding space group also fall into non-symmorphic crystalline group. As the consequence of the coexistence of time reversal symmetry and inversion symmetry, Z_2 topological invariant can be connected to the parity of bands in each TRIM point (time reversal invariant momentum) in the Brillouin zone. Here we have to consider the case of three dimensional system, in which the system possess 8 TRIM points, which are (0,0,0), (0.5,0,0), (0.0, 0.5,0.0), (0.0, 0.0, 0.5), (0.5, 0.5, 0.0), (0.5, 0.0, 0.5), (0.0, 0.5, 0.5), and (0.5, 0.5, 0.5). For this purpose we have adapted the method suggested by Liang Fu and Charles L. Kane [277]. The equation for Z_2 topological invariant is, $(-1)^{\nu} = \prod \gamma_i$

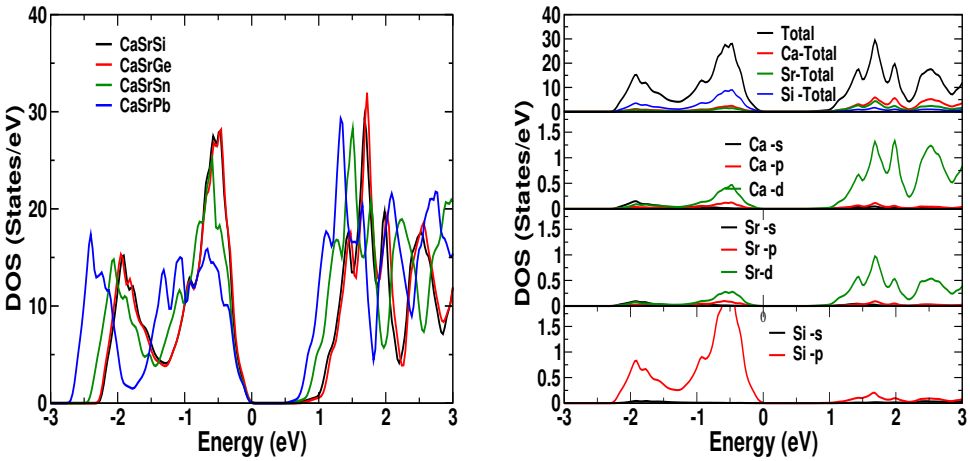

(a) (b)

Figure 5.4: a) Total density of states of all the compounds, b)Total and partial density of states of CaSrSi

, where γ_i are parities of each band. Computed Z_2 topological invariants of all the compounds are represented in Table 5.3. Due to the semiconducting nature of the studied compounds, we have considered all the occupied bands for the calculations, and we have found that at Γ point, parity is -1 and at all the other points the value is +1, and lead to a non zero value for Z_2 parameter. A strong topological character has been observed in all the investigated compounds. Further we have calculated the surface states for all the compounds and presented in figure 5.6. Well linearized Dirac cone like surface bands is observed around Γ high symmetry point, which again confirm the strong topological nature in this compound. In the next paragraph we try to understand the TE properties of these compounds.

Thermopower, electrical conductivity and power-factor as a function of carrier concentrations at different temperatures are studied for all the compounds. Figure 5.7 to 5.10 represent the TE properties of CaSrSi, CaSrGe, CaSrSn and CaSrPb as a function of both hole and electron concentrations at different temperatures. The difference in band dispersion along different crystallographic directions are reflected in thermopower. Around 300 K, thermopower along 'a'-axis has secured the highest value than 'c'-axis value, which is followed by 'b'-axis value. When we move to higher temperature, the difference between 'a'-axis and 'c'-axis values are reducing, and 'b'-axis value remains the lowest. Around 700 K onwards, bi-polar conduction has been observed for low concentration range. Coming to electron doping, the thermopower values are more isotropic and bipolar conduction is observed similar to that of holes. The magnitude of thermopower for electron doping is lesser than the same for hole doping. Figure 5.7 (c,d) present the electrical conductivity for CaSrSi for both holes and electrons at different temperatures. At around 300 K, conductivity along 'b'-axis is found to be more, and 'c' -axis has the lowest value. Up to 700 K the trend is same, and around 900 K at low concentrations, the conductivity is found to be invariant as a function of carrier concentration, and for higher concentration it varies linearly. In the case of electron doping, for all temperatures the b-axis value is higher, and other two axes values are found to be almost same. Figure 5.8 (c,d), 5.9 (c,d) and 5.10 (c,d) reported the electrical conductivity values for CaSrGe, CaSrSn and CaSrPb

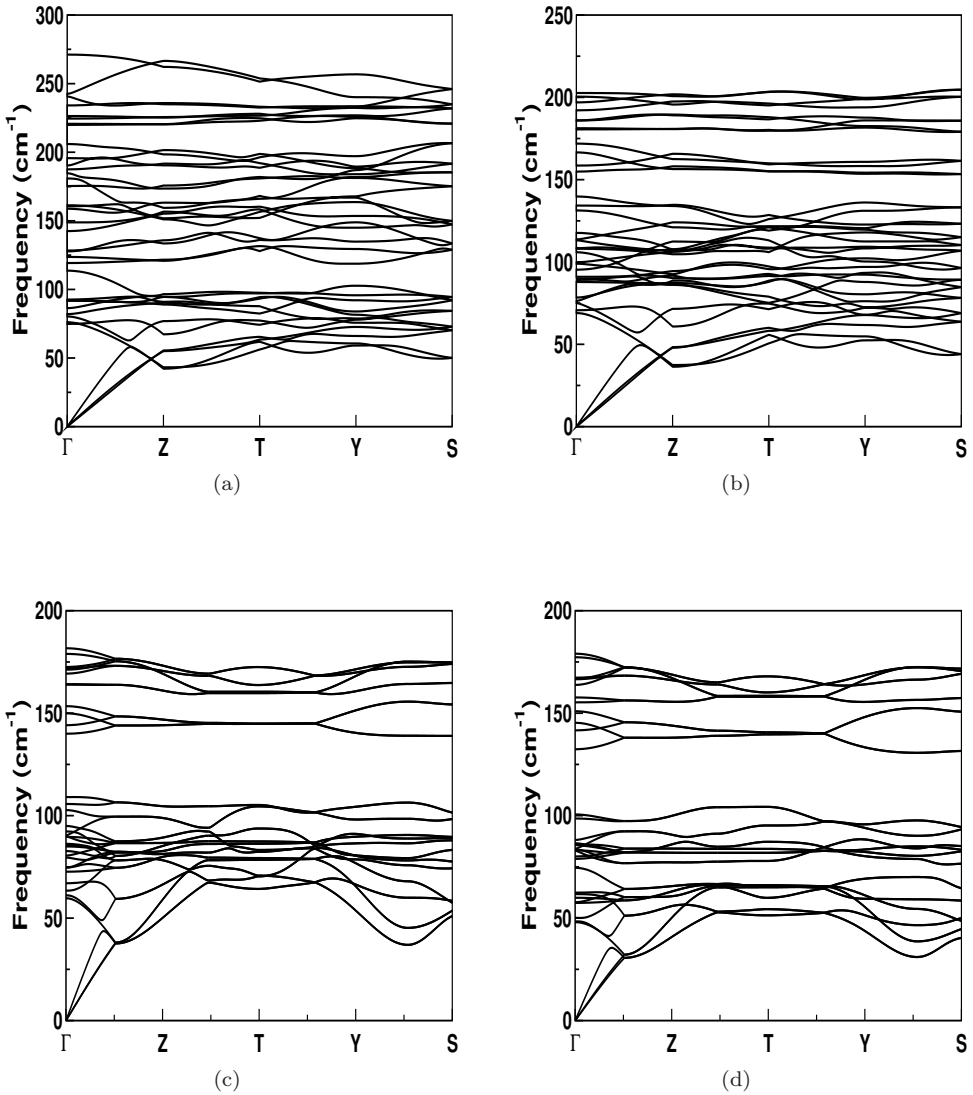

Figure 5.5: a) Calculated phonon dispersion plot for all the investigated compounds a)CaSrSi, b)CaSrGe, c)CaSrSn, d)CaSrPb

respectively. Power factor of CaSrSi is presented in Figure 5.7 (e,f). For hole doping, significant difference is observed between each crystallographic directions, and 'b'-axis is found to have highest value. But for electron doping, we could see little anisotropic character, where b -axis value is higher than 'a' and 'c' axes. Since all the investigated compounds show bipolar conduction at higher temperatures, we have presented the magnitude of thermopower over a temperature range of 100 K to 500 K around the carrier concentration of 10^{18} cm^{-3} for all the compounds in Figure 5.11. From the figure it is quite evident that, all the investigated compounds posses appreciable value of thermopower over the temperature range of 100 K to 500 K. Electrical conductivity and power-factor of other compounds are also found to show similar behaviour as that of CaSrSi, as seen from figures 5.8 to 5.9.

Table 5.2: Calculated Elastic constants of CaSrX (X: Si, Ge, Sn, Pb)

Parameter	CaSrSi	CaSrGe	CaSrSn	CaSrPb
C_{11}(GPa)	68.72	64.58	57.17	53.98
C_{22}(GPa)	77.23	74.64	66.35	61.99
C_{33}(GPa)	73.52	69.37	62.19	59.15
C_{44}(GPa)	35.23	34.02	29.69	28.27
C_{55}(GPa)	28.98	27.89	23.54	22.06
C_{66}(GPa)	34.11	32.58	28.10	26.33
C_{12}(GPa)	19.85	19.01	17.52	16.94
C_{13}(GPa)	19.24	17.83	15.44	14.39
C_{23}(GPa)	22.53	20.23	19.16	17.38
DebyeT(K)	340.79	295.44	253.82	212.41

Table 5.3: Calculated Z_2 topological invariants of CaSrX (X: Si, Ge, Sn, Pb) at ambient

	CaSrSi	CaSrGe	CaSrSn	CaSrPb
ν_0	1	1	1	1
ν_1	0	0	0	0
ν_2	1	1	1	1
ν_3	0	0	0	0

As we mentioned earlier, the figure of merit is an important parameter for thermoelectric materials. The magnitude of power-factor for all the compounds at 300 K around the concentration range

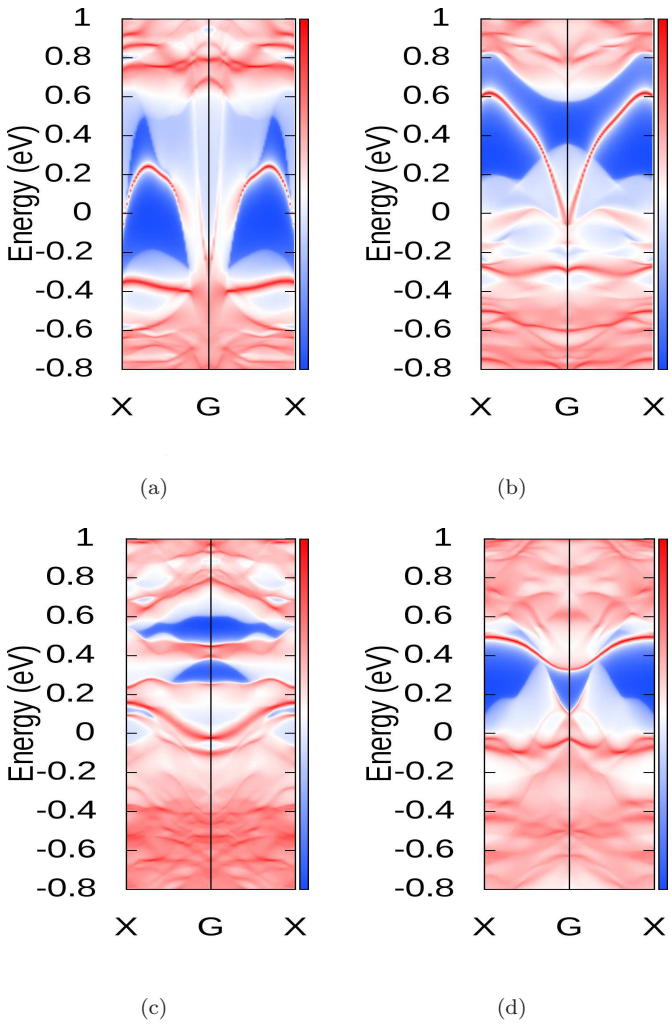

Figure 5.6: a) Calculated surface band structure for all the compounds along (110) surface a)CaSrSi, b)CaSrGe, c)CaSrSn, d)CaSrPb

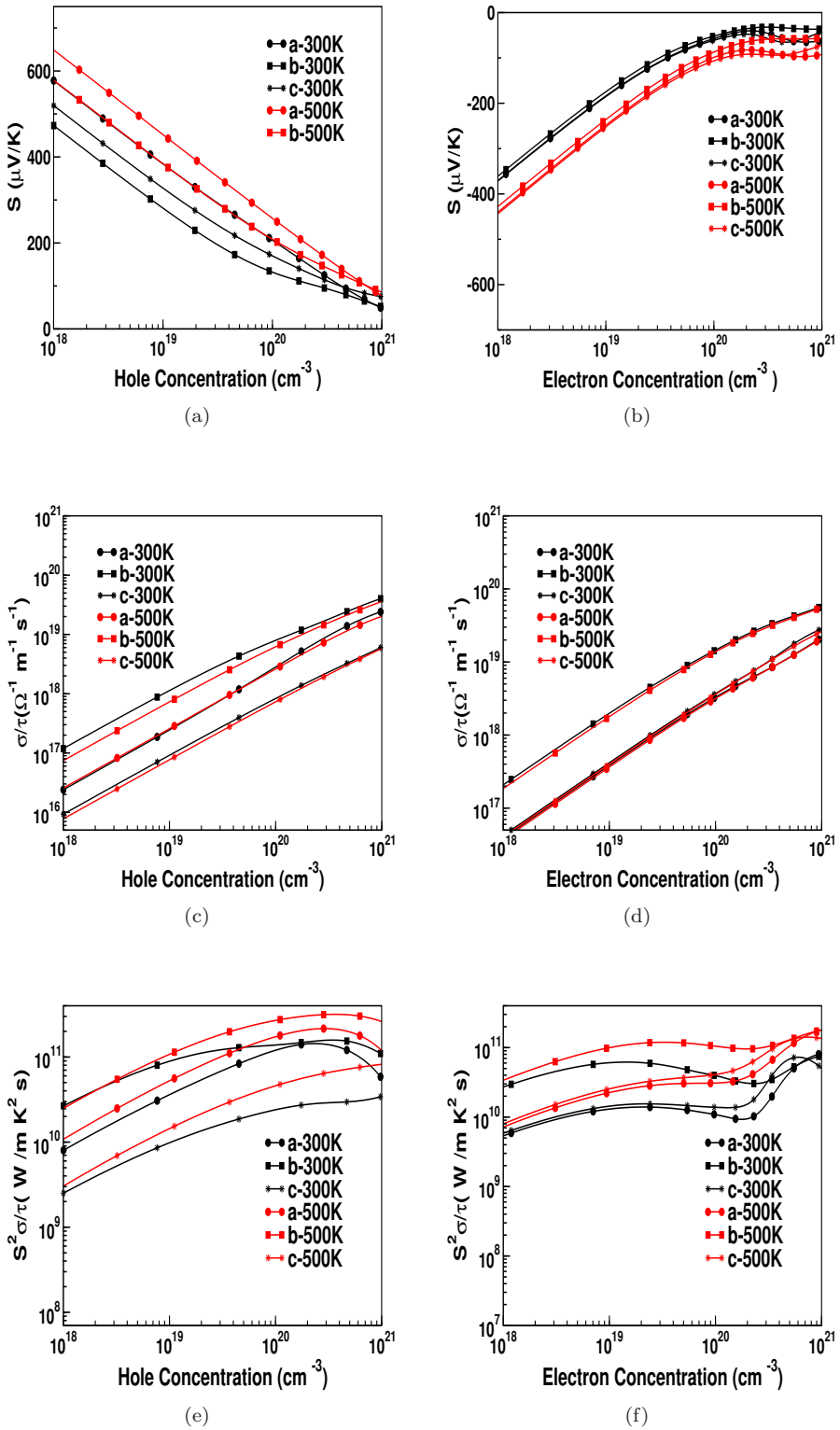

Figure 5.7: Calculated TE properties for CaSrSi at different temperatures (a)thermopower as a function of hole concentration, (b) thermopower as a function of electron concentration, c) electrical conductivity as a function of hole concentration, d) electrical conductivity as a function of electron concentration, e) power factor as a function of hole concentration, f) power factor as a function of electron concentration.

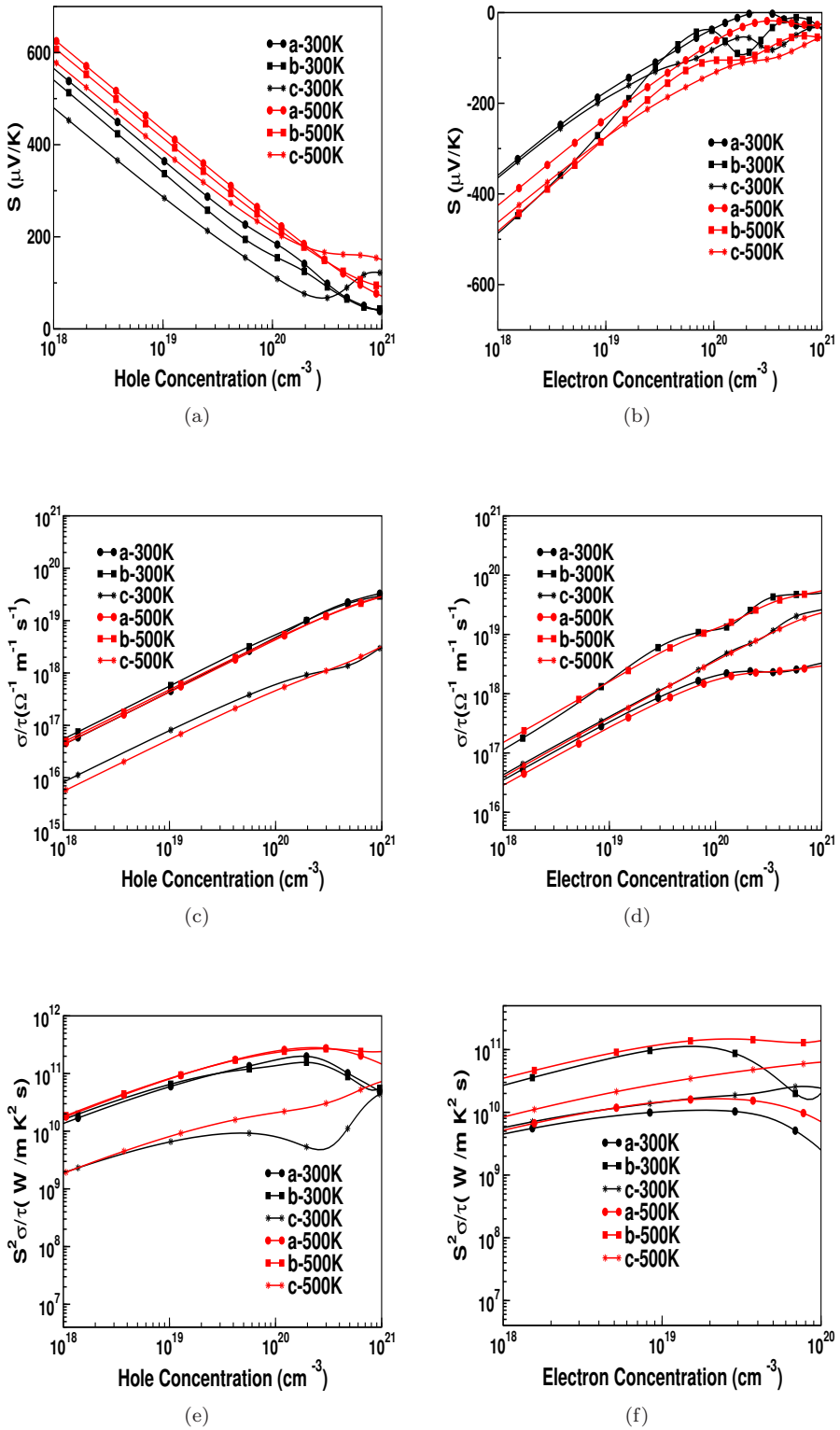

Figure 5.8: Calculated TE properties for CaSrGe at different temperatures (a)thermopower as a function of hole concentration, (b) thermopower as a function of electron concentration, c) electrical conductivity as a function of hole concentration, d) electrical conductivity as a function of electron concentration, e) power factor as a function of hole concentration, f) power factor as a function of electron concentration.

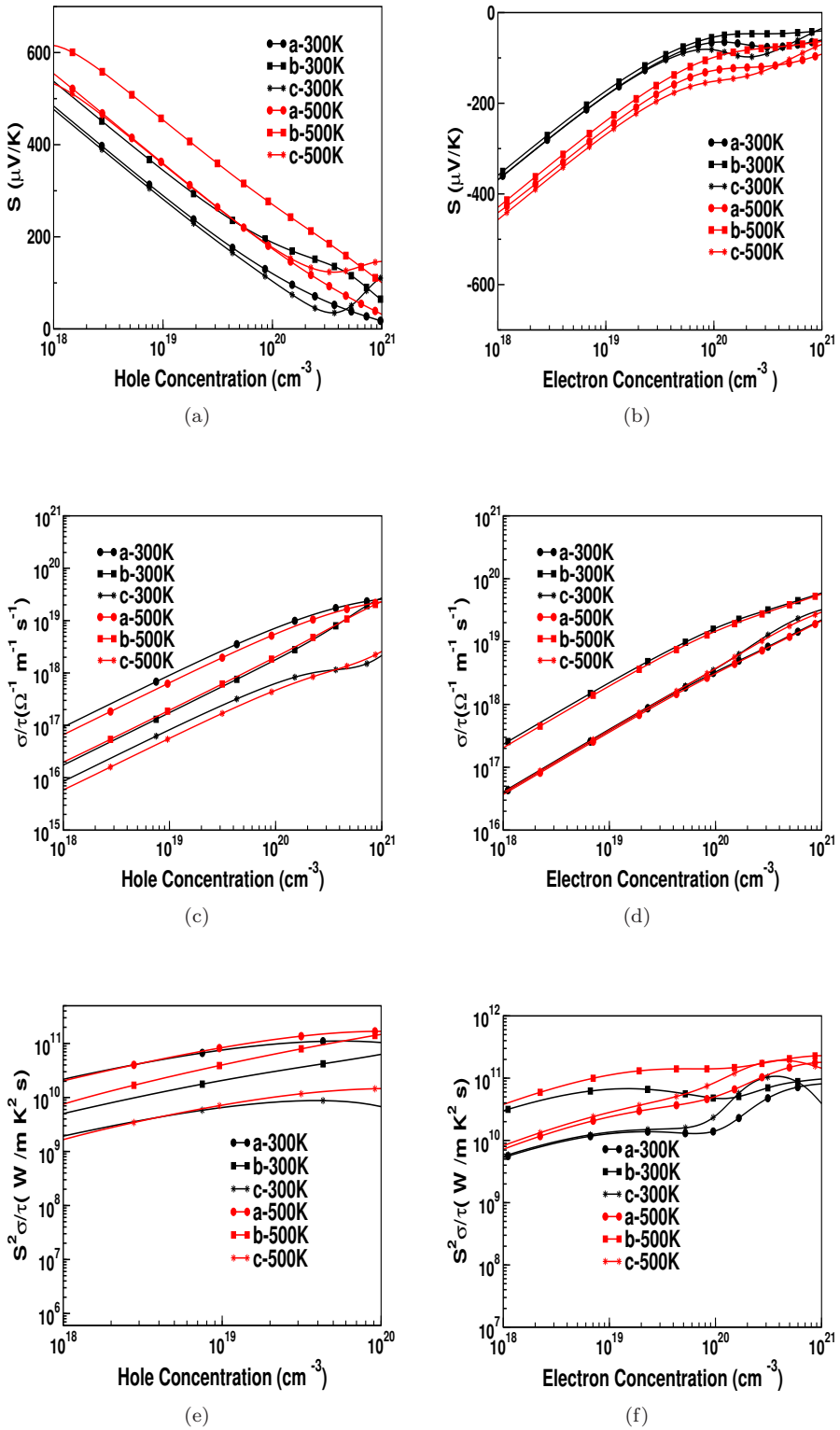

Figure 5.9: Calculated TE properties for CaSrSn at different temperatures (a)thermopower as a function of hole concentration, (b) thermopower as a function of electron concentration, c) electrical conductivity as a function of hole concentration, d) electrical conductivity as a function of electron concentration, e) power factor as a function of hole concentration, f) power factor as a function of electron concentration.

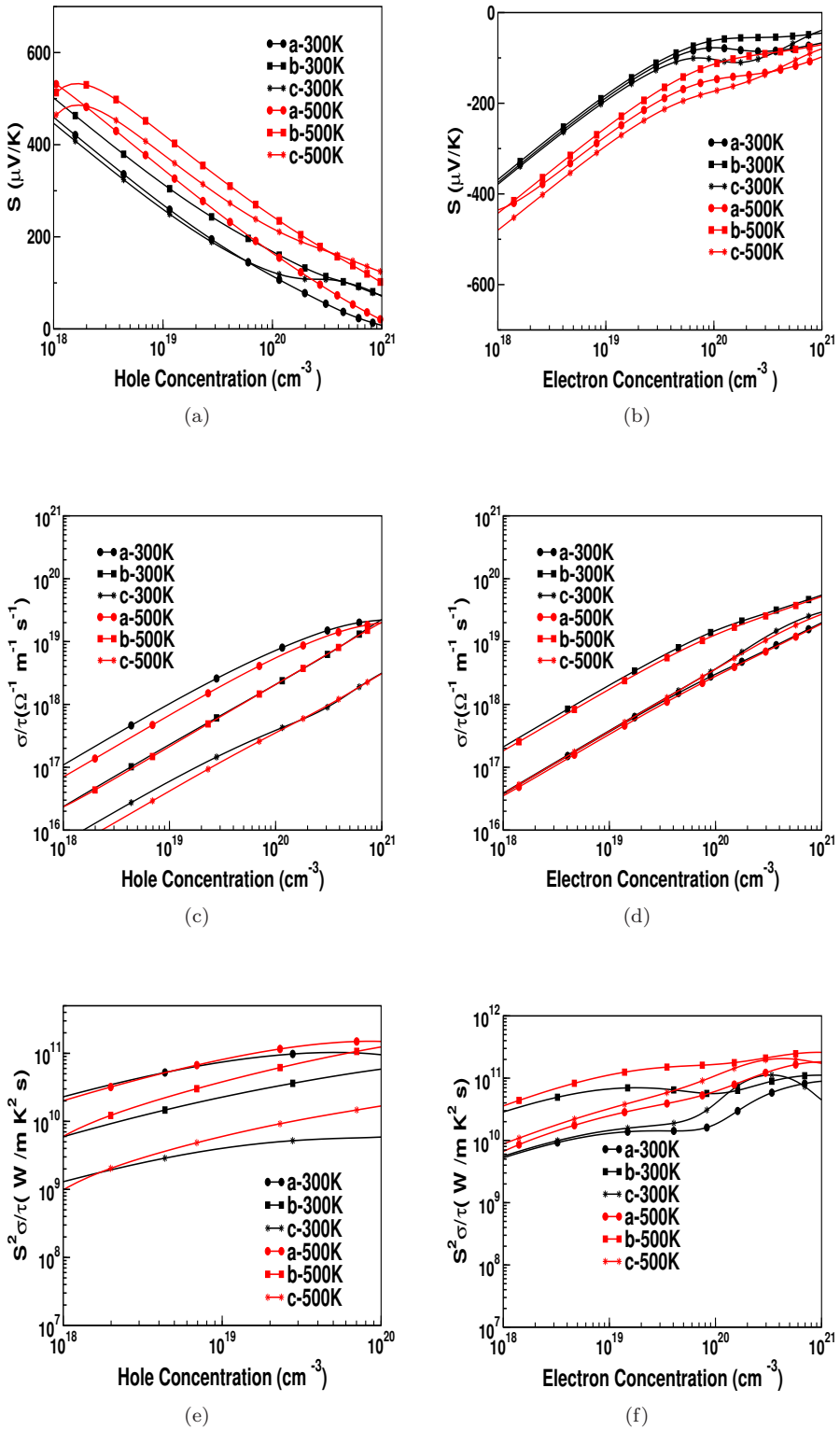

Figure 5.10: Calculated TE properties for CaSrPb at different temperatures (a)thermopower as a function of hole concentration, (b) thermopower as a function of electron concentration, c) electrical conductivity as a function of hole concentration, d) electrical conductivity as a function of electron concentration, e) power factor as a function of hole concentration, f) power factor as a function of electron concentration.

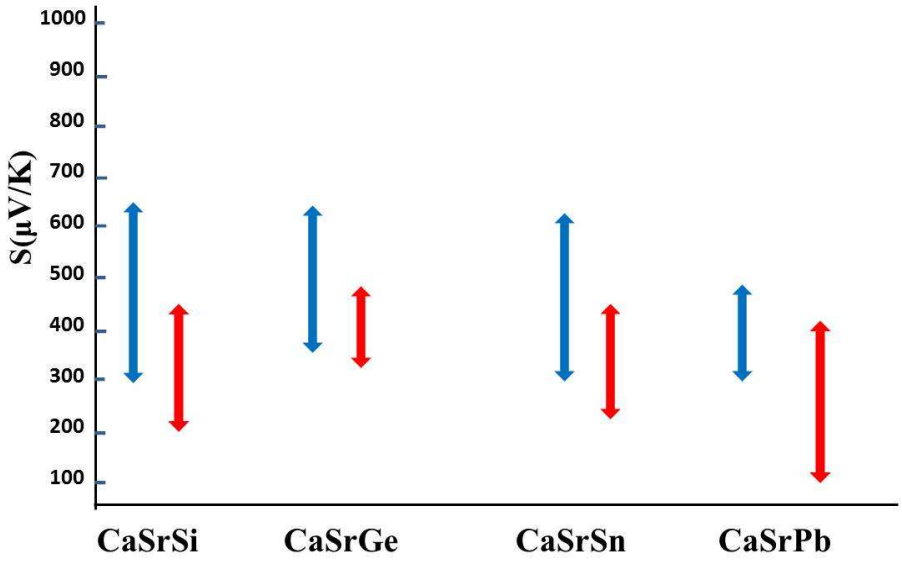

(a)

Figure 5.11: Magnitude of thermopower for both holes and electrons over the temperature range 100 K - 500 K for all the compounds, blue colour represents hole thermopower, red colour represents electron thermopower

10^{19} cm^{-3} is around 1×10^{11}, which is appreciable. Another vital parameter is the thermal conductivity, and here we have calculated the minimum lattice thermal conductivity of all the compounds using Cahill's model[278]. Calculated minimum thermal conductivity for CaSrSi, CaSrGe, CaSrSn and CaSrPb are 0.328, 0.258, 0.222 and 0.192 W/mK respectively. From our earlier discussions, we have mentioned that the low value of Debye temperature and flat phonon bands might lead to low thermal conductivity. Further we have assumed the relaxation time as 10^{-14} s, and calculated the range of figure merit for all the compounds at 300 K. Calculated value of figure of merit at 300 K for CaSrSi, CaSrGe, CaSrSn and CaSrPn are 1.34, 1.5, 1.48 and 1.68 respectively. Altogether the present study reveals the topologically non-trivial states and presented noticeable thermoelectric properties of all the investigated compound at ambient. Subsequently we have analyzed the effect of strain, which is presented in the upcoming section.

5.3.2 Effect of strain

Topological insulators are in general very responsive to external perturbations such as strain/pressure. Here, we have examined the impact of the strain on electronic structure and transport properties of the investigated compounds. Firstly, we have examined the effect of hydrostatic strain, where the percentage of strain along each crystallographic direction is same. The band gap of the studied compounds is found to reduce with compressive strain and increase with tensile strain, where the band profile is found to be preserved. On the other hand, we have observed that the uni-axial strain has drastically changed the band profile of all the studied compounds. Among the three axes, the uni-axial strain applied along 'b' axis is found to have more impact on the electronic structure

and hence on transport properties of the investigated compounds. Starting the discussion with the compressive strain on CaSrSi, a drastic change has been observed in the band profile of CaSrSi. Figure 5.12 (a,b,c,d) represent the band structure along the high symmetry direction T- Γ- Y and U- Γ- X at different compressive strains, The band gap is found to be decreased and closed around 10% strain and then opens again around 12% strain. Here Γ is the centre of the BZ, T is in 'yz' plane (0.0, 0.5, 0.5), Y is along 'y' axis (0.0, 0.5, 0), then the first path T- Γ- Y in 'YZ' plane. Likewise U point is lying in 'xz' plane (0.5, 0, 0.5), and X is along 'x'-axis, and the second path is in 'XZ' plane. As we mentioned earlier the band gap is found to be reduced and band profile has been changed. Let us discuss the case from 6% compressive strain onwards. The ambient and 6% strain are almost same and around 8% strain onwards, the bands gets more linearised and then at 10% strain , highly linearized band is observed. Around 12% strain, the linear dispersive nature has vanished, and a double well kind of band profile along Γ- Y is seen. On the other hand, the high symmetric direction U- Γ- X preserved a parabolic nature as a function of compressive strain and around 10% strain, the conduction and valence band touch each other and then open the band gap around 11% strain. From these analysis we could see that, the band dispersion along YZ plane and ZX plane is completely different. The closing and opening of band gap nature motivate us to verify the Z_2 topological invariant in these strained state. Our calculations suggest that CaSrSi is converting to a normal insulator through b -axis uni-axial compressive strain, where the parity at Γ point has flipped to +1, which give a zero Z_2 value . The projected band structure clearly shows that, the band flipping is happening between Sr-d ans Si -p states (see figure 5.12(e)), which further provides the confirmation for the transformation from a strong topological insulating state to a normal insulating state. Similar behaviour we have observed in CaSrGe also, where the band closing is found around 11% compressive strain, and the band structure of the same is given in figure. 5.13. The remaining compounds CaSrSn and CaSrPb preserve their non-trivial states up to 15% 'b' axial compressive strain. For further strain, these compounds also might show the similar behaviour. With uni-axial tensile strain along 'b' axis, the band gap is found to increase. For compressive strain (uni-axial strain along 'b' axis) around 10 % strain, the band gap is found to be closed and the system turned to a semi-metallic state, and the Fermi surface formed in this state is very interesting (See the Figure 5.12(d)). Extremely small arc has been observed in 'XZ' plane, which is due to the parabolic bands present there. This small arc like Fermi surface further provide the information about the dimensional reduction in the system. It has to be noted that the uni-axial strain along the other two axes are also studied, where we could not observe any interesting properties within the applied strain. For further strain, these directions also might show similar trend.

In the previous section, we have discussed the changes in electronic structure with respect to strain along different direction. Further, we have analysed the TE properties of investigated compounds as a function of hydrostatic and uni-axial strain along different directions. The thermopower for CaSrSi as a function of carrier concentration at different hydrostatic strains is presented in Figure 5.14 (a,b). The magnitude of thermopower is found to be reduced with compressive strain and found to be increased with tensile strain. In the case of electrical conductivity, we can see reverse trend, and for electron doping we can see the anisotropy in electrical conductivity (See Figure 5.14 (c,d)). In Figure 5.15(a), we have shown the thermopower variation as a function of 'b' axis strain. From the electronic structure, we could see that, CaSrSi transfer to a semi-metallic state around 10% compressive strain, and in that state the thermopower is found to be very low. For further strain

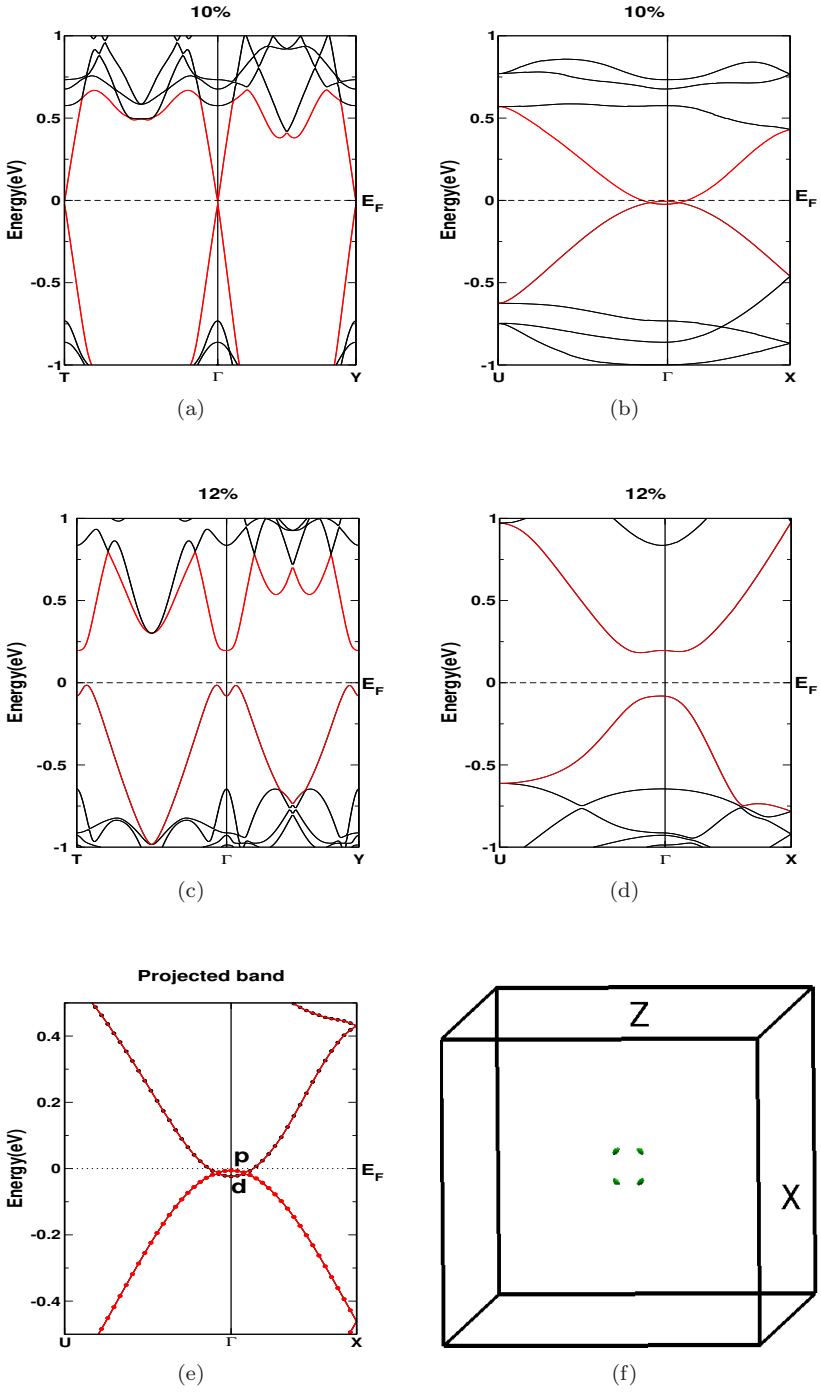

Figure 5.12: a) Band structure of CaSrSi at 10% compressive strain along 'b' axis in T-Γ -Y direction, b) Band structure of CaSrSi at 10% compressive strain along 'b' axis in U-Γ -X direction, c) Band structure of CaSrSi at 12% compressive strain along 'b' axis in T-Γ -Y direction, d) Band structure of CaSrSi at 12% compressive strain along 'b' axis in U-Γ -X direction, e) 'p' and 'd' projected band structure at 10% strain, f) Fermi surface of CaSrSi at 10% compressive strain

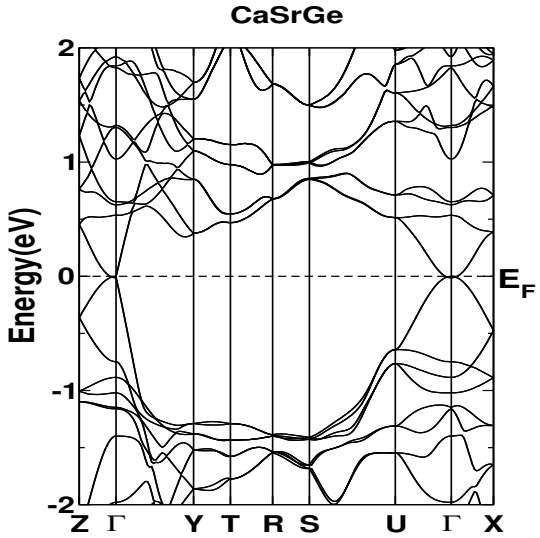

(a)

Figure 5.13: Calculated band structure of CaSrGe at 11% compressive strain

around 12%, the thermopower values are found to increase again, which is according to the band opening in this state. For tensile strain, the magnitude of thermopower is found to be comparable with ambient value , and anisotropy in thermopower is found to be reduced. Electrical conductivity for compressive strain along 'b' axis is found to enhance the magnitude of anisotropy in the system (See Figure 5.15(b)). Above 9.5% strain, the system is found to possess huge anisotropy, where conductivity values along 'b' axes is found to be 2 order higher than 'a' and 'c' axes. This indicate a quasi two dimensional nature in the system. As we discussed in the previous sections, the compressive strained state along 'b' axis (around 10%) has shown several interesting phenomena for CaSrSi. In this state, the system turned to be a metallic, with remarkable electronic structure, which include a highly Dirac cone like band structure along Γ- Y direction, and parabolic bands along the perpendicular plane. The huge difference in the band dispersion along these directions, which is induced by strain is the main reason for peculiar transport properties at this state. We have observed a highly interesting transport responses at these strained state around 10% at low temperatures within the range of 50 K to 150 K along 'b' axis. Here the nature of thermopower along 'a' and 'c' axes are found to be quite normal, and the 'b' axes thermopower shows a highly oscillating variation as a function of chemical potential/carrier concentrations, which is represented in Figure 5.15(c). The small disconnected arc like Fermi surface also support this behaviour. This strained state is the transition state between a strong topological insulator to a normal insulator. As we mentioned in the introduction part, the thermopower fluctuation can originate from several ways with or without magnetic filed[265, 266, 267, 268]. One vital point here is that, at this strained state, system is almost two dimensional, which again gives strong insight to our observation, where these kind of quantum fluctuations in physical quantities can be expected. In the case of CaSrGe also, we could see similar behaviour, which is presented in Figure 5.15(e).

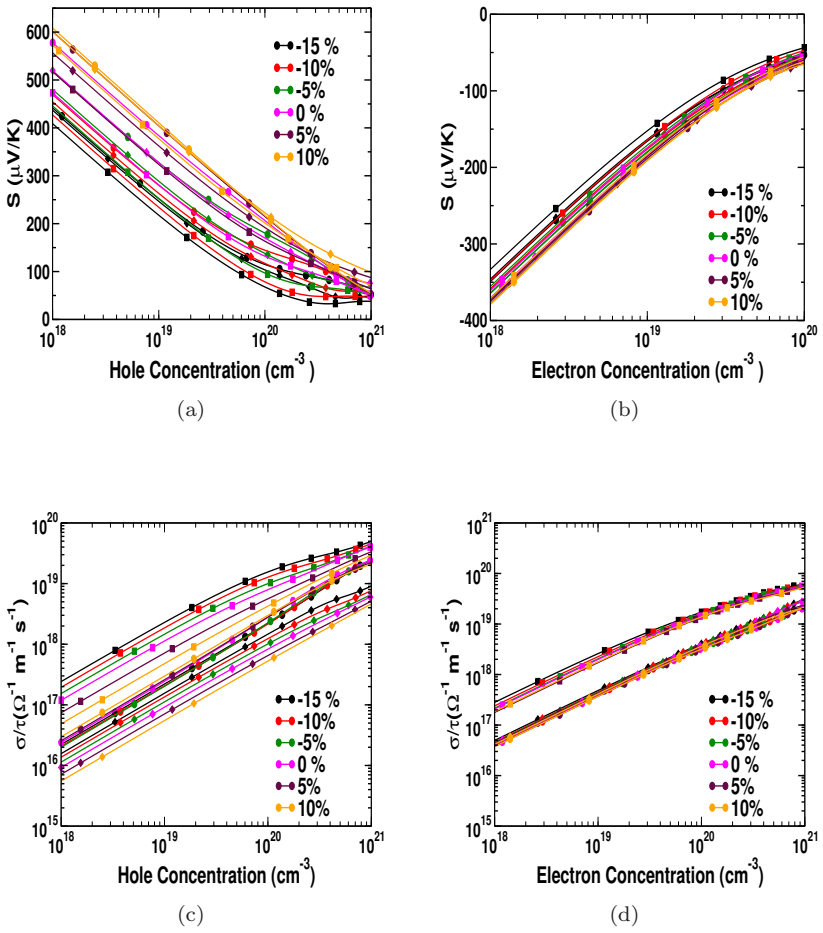

Figure 5.14: Calculated TE properties of CaSrSi at hydrostatic strains a) Variation of thermopower as a function of hole concentration at different hydrostatic strains, b) Variation of thermopower as a function of electron concentration at different hydrostatic strains ,c) Variation of electrical conductivity as a function hole concentration at different strains, d)Variation of electrical conductivity as a function electron concentration at different strains(circle, square and diamond symbols represent 'a', 'b' and 'c' axes respectively)

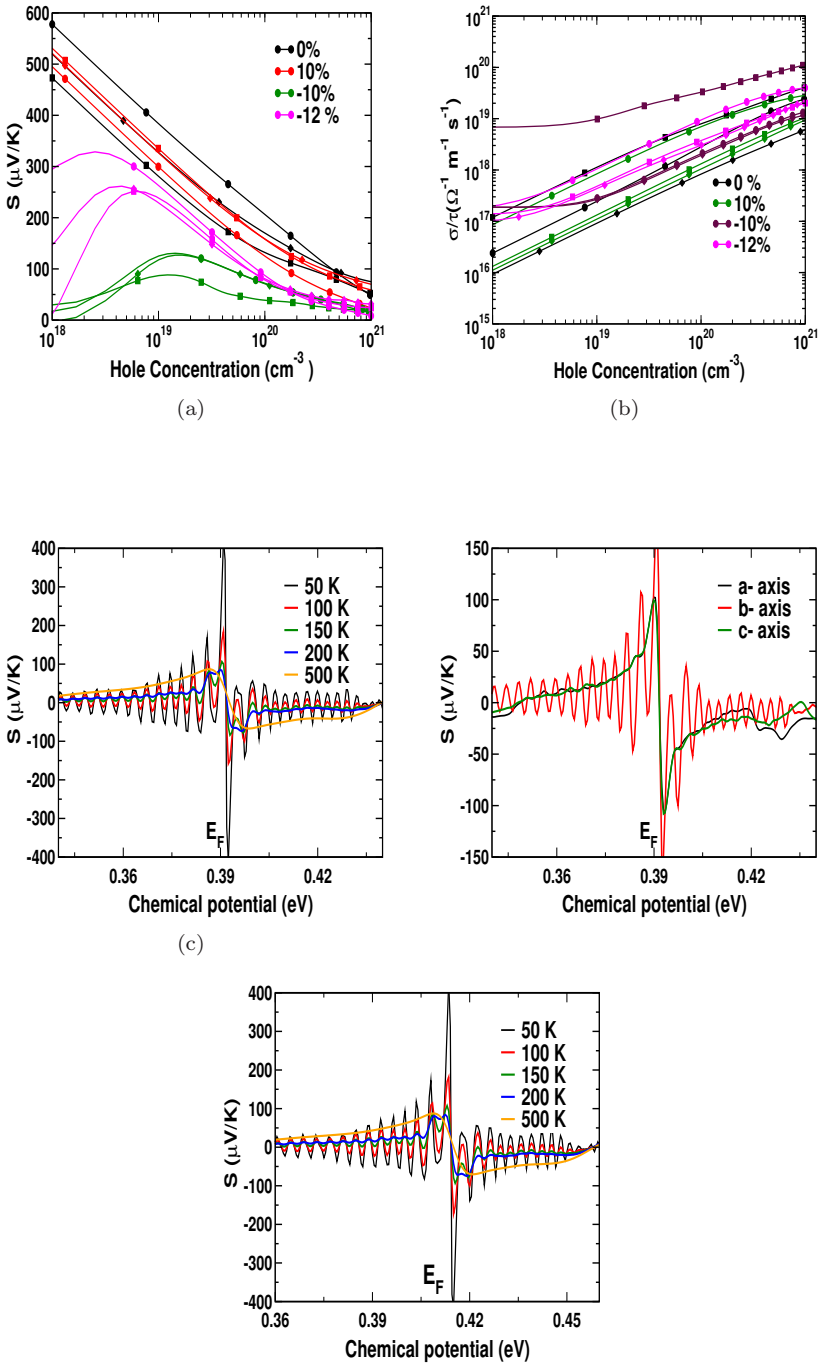

Figure 5.15: a) Variation of thermopower as a function of hole concentration for different strains, b) Variation of electrical conductivity as a function of hole concentration for different strains (circle, square and diamond symbols represent 'a', 'b' and 'c' axes respectively), c) Thermopower variation as a function of chemical potential for CaSrSi at 10% compressive strain along 'b' axis at different temperatures d) Thermopower variation as a function of chemical potential for different crystallographic directions for CaSrSi at 10% compressive strain at 100 K e) Thermopower variation as a function of chemical potential for CaSrGe at 11% compressive strain along 'b' axis at different temperatures

5.4 Conclusions

A systematic analysis of electronic, topological and transport properties were presented, and identified the studied materials as topological insulators at ambient conditions. The potential TE properties were also presented for the investigated compounds. The application of strain in these system gave insight to several interesting phenomena, which include the formation of Dirac semi-metallic state, and enhanced 2D nature, which opens up wide range of applications for the investigated compounds.

Chapter 6

Giant thermopower in p-type OsX_2, and layer independent TE properties of ReS_2

The current chapter deals with the electronic and thermoelectric properties of few transition metal dichalcogenides, which are less investigated. We have chosen pyrite type OsX_2 (X: S, Se, Te) and triclinic ReX_2 (X: S, Se) for the current study. To begin with, we report the electronic structure and thermoelectric (TE) properties of OsX_2 (X: S, Se, Te), and find a giant value of thermopower around 600 μVK^{-1} to 800 μVK^{-1} for a wide temperature range of 100 K - 500 K for hole doping (at 10^{18}cm^{-3}), which is higher than the value found for well established TE materials. The optimized structural parameters are in good agreement with available experimental reports. The mechanical stability of OsX_2 (X: S, Se, Te) is confirmed from the computed elastic constants. The band gap of the investigated compounds is examined by several exchange correlation functionals, and TB-mBJ with modified parameters is found to be the best for OsX_2. The heavy valence bands stimulates the thermopower value for hole doping and light conduction bands intensifies the electrical conductivity values for electron doping, enabling both 'n' and 'p' type doping to be favourable for TE applications at higher concentrations (10^{20}cm^{-3}), which brings out the device application. Study on OsX_2 unveils the possibility of TE applications for all the examined compounds for a wide temperature range (100 K to 500 K), and OsS_2 specifically is quite exceptional with the operating temperature ranging from 100 K - 900 K. Further, we have examined the electronic and thermoelectric properties of ReX_2 (X: S, Se) and revealed the potential thermoelectric properties. Further we have extended the study in ReS_2 by two ways, one is cleaving to free standing monolayer and bilayer and the other is the application of hydrostatic/uni-axial strain. From our study we could show that, ReS_2 is a highly versatile system, which transforms from a semiconductor to a two dimensional metal under uni-axial compressive strain along *'a'* direction in both bulk and monolayer. The 2D nature is realized from highly flat Fermi surfaces and anisotropic transport properties. Moreover the layer independent electronic structure properties are revisited and thermoelectric properties of ReS_2 in bulk, monolayer and bilayer forms reveal the competing thermoelectric (TE) coefficients in each form. The in-plane power-factor (*'a'* and *'b'* axes) shows an enhancement over *'c'* axis value as a function of strain,

which is almost two orders of magnitude. In addition, strain induced tunable in-plane anisotropy of almost one order has been observed in both bulk and monolayer ReS_2 (around 20% strain), which further open up the possibility of TE application as nanowires. Our analysis unveils a wide range of application for ReS_2 in the field of thermoelectrics as bulk and thin films for a large temperature range. The magnitude of TE coefficients are comparable with other well established transition metal dichalocogenides.

6.1 Introduction

Transition metal chalcogenides and pnictides possess diverse structural, electronic properties, and stand in the forefront of various applications[280, 281, 282, 283]. A huge structural varieties can be observed in this family which include layered and non-layered materials with diverse space groups, and among them van der Waals layered structure such as MoS_2 and pyrite FeS_2 type structures are attractive with several properties[284, 285]. The structural and chemical properties of these two series are well investigated. The 2D like materials are quite attractive because of their nano-level applications[286, 287], and significant number of compounds from pyrite/marcasite family have been investigated for their electronic, optical, thermoelectric and photovoltaic applications[288, 289]. Moreover, pyrite to marcasite structural transitions are also observed under pressure in several materials like FeS_2[290]. However, Os based dichalcogenides and dipnictides are less investigated in comparison with other transition metal dichalcogenides (TMD). Crystal structure and Raman spectra of Os based dichalcogenides has been examined in the very early stage, where they confirmed the pyrite structure, whereas, Os based dipnictides are found to crystallize in marcasite structure[291]. The band gap of both Os based dichalcogenides and dipnictides matches with the semiconducting range, and this indicate the possibility of photovoltaic and thermoelectric applications in these compounds. Conventional TMD materials, in general, host a mixture of flat and dispersed bands, which further help for thermoelectric energy conversion. Yet another point to mention is that, OsS_2 (Erlichmanite) is a well known naturally occurring compound, and fall into platinum group minerals. Other pyrite type dichalcogenides like FeS_2 are already realized as a good thermoelectric materials[292], but Os based compounds are less investigated in this family. Since OsX_2 (X: S, Se, Te) are iso-structural with pyrite FeS_2, we believe that OsX_2 (X: S, Se, Te) can be explored further for thermoelectric properties. ReS_2 is one of the transition metal dichalcogenides which stands out with very peculiar properties, and has drawn adequate attention in the recent past. Unlike the other layered transition metal dichalcogenides, ReS_2 crystallizes in triclinic space group. Recent study reveals that the interaction between layers in ReS_2 is negligible implying that the monolayer of ReS_2 might have similar electronic properties as that of bulk, enabling ReS_2 to be the highlight in the last decade[293]. Pressure and strain are the robust tools which can modify the structure and electronic properties of materials, and transition metal dichalcogenides showed considerable response to strain and pressure[294, 295, 296], leading to metallization at high pressure, direct to indirect band gap transitions etc. Optical and electronic properties are also explored for both bulk and layered ReS_2 [297], and this compound has found application in field effect transistors[298, 299]. The inherent structural anisotropy of ReS_2 has further shown an influential response towards pressure and strain, resulting in tuning of in-plane, and through plane anisotropy in several physical properties like resistivity, charge mobility etc, and significant number of studies are dedicated to understand this especially for monolayer ReS_2[300, 301, 302, 303, 304]. Though plethora of literatures are available exploring ReS_2 in several directions, studies addressing the physical properties and its anisotropic behaviour along different crystallographic directions of ReS_2 (where the out of plane component does not represent the other crystallographic direction as the symmetry is triclinic) are less investigated, and one of the earlier study has reported the anisotropy in resistivity along *'b'* and *'c'* axes experimentally, and it is worthy to analyse these properties in detail. In addition, studies related to pressure induced structural transitions and metallization are also reported[305]. Here we would like to explore the effect of uni-axial strain on bulk and few layers of ReS_2 using first principles

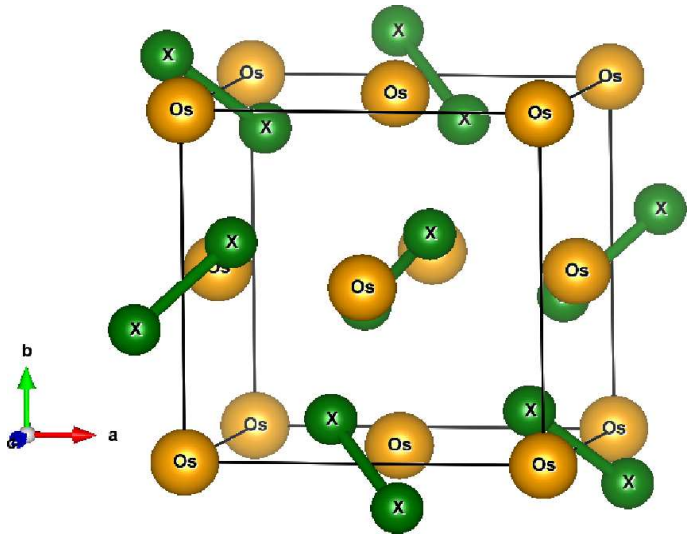

(a)

Figure 6.1: Crystal structure of OsX_2 (X: S, Se, Te).

calculations. The well studied TMD like MoS_2 is already explored for straintronic applications[306], and we expect ReS_2 to be yet another prospective compound.

6.2 Computational details

For structural optimization of OsX_2, we have used pseudo potential method as implemented in Plane Wave self consistent field (Pwscf) program[274], with a plane wave cut-off 140 Ry and convergent criteria of 10^{-5} Ry per formula unit has been used for energy minimization. The optimized lattice parameters are used for further calculations. We have used full potential linearised augmented plane wave (FP-LAPW) method as implemented in Wien2k package [162, 163] to understand the electronic structure properties. To obtain the proper band gap for OsX_2, we have used Tran-Blaha modified Becke-Johnson (TB-mBJ) functional[165, 166] with modified parameters[307]. Due to the presence of heavy elements in the investigated compounds, we have included spin orbit coupling in our calculations. For total energy calculations, band structures and density of states, we have used 1000 k-points in the full Brillouin zone. Transport coefficients such as thermopower and electrical conductivity were calculated using BoltzTraP code[169] with a dense k- mesh of 50×50×50 k-points. We have used the experimental structure parameters for ReS_2 and performed a complete geometry optimization and phonon dispersion using VASP[245, 308]. Since ReS_2 possess a layered structure, we have included van der Waals correction using Tkatchenko -Scheffler method[309]. Further electronic structure properties like band structure, Fermi surface etc were calculated using full potential linearised augmented plane wave (FP-LAPW) method as implemented in WIEN2k package. Different layered structures of ReS_2 were cleaved from the bulk material, and vacuum convergence are performed for each layered structure with a k-mesh of 10×10×9 for bulk and 12×12×3 for layers. The applied vacuum for monolayer and bilayer structures is around 15 angstroms. We have performed super cell calculation to ensure that the properties remain unchanged, and, have continued

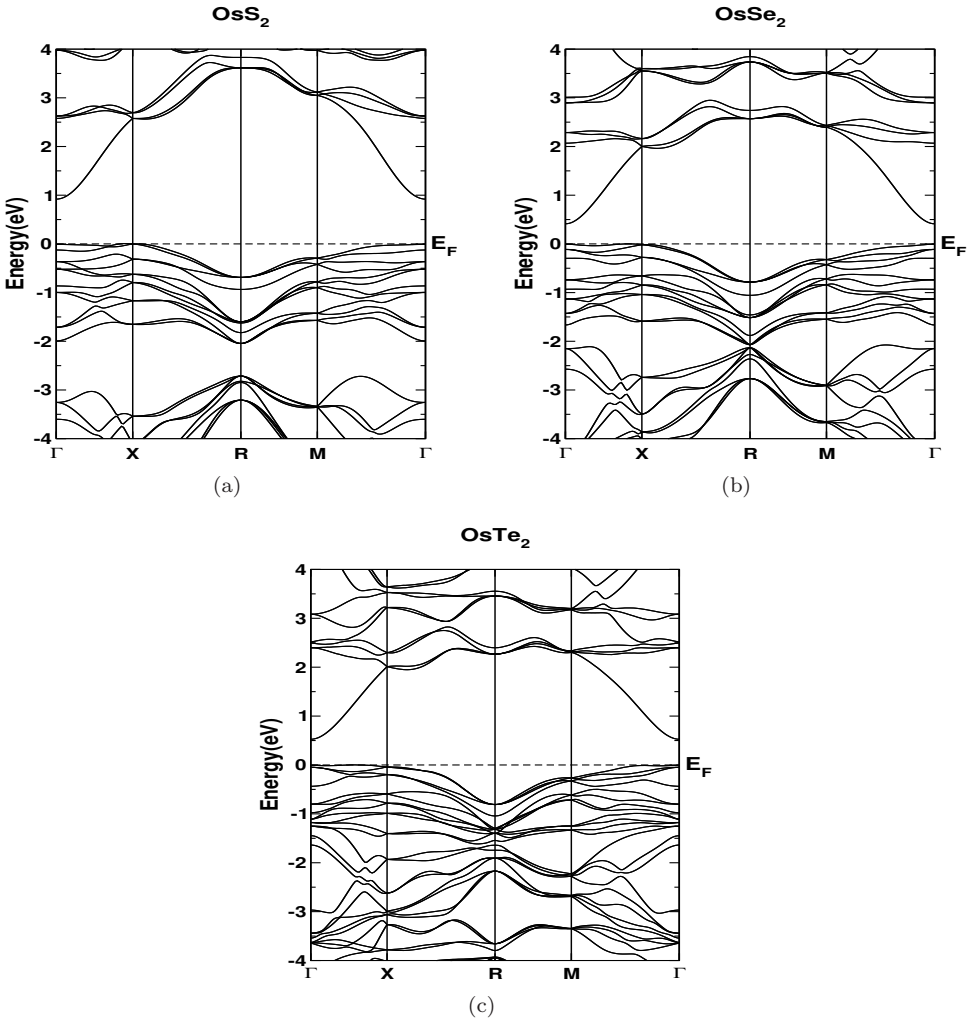

Figure 6.2: Calculated band structure for (a) OsS_2, (b) $OsSe_2$, (c) $OsTe_2$

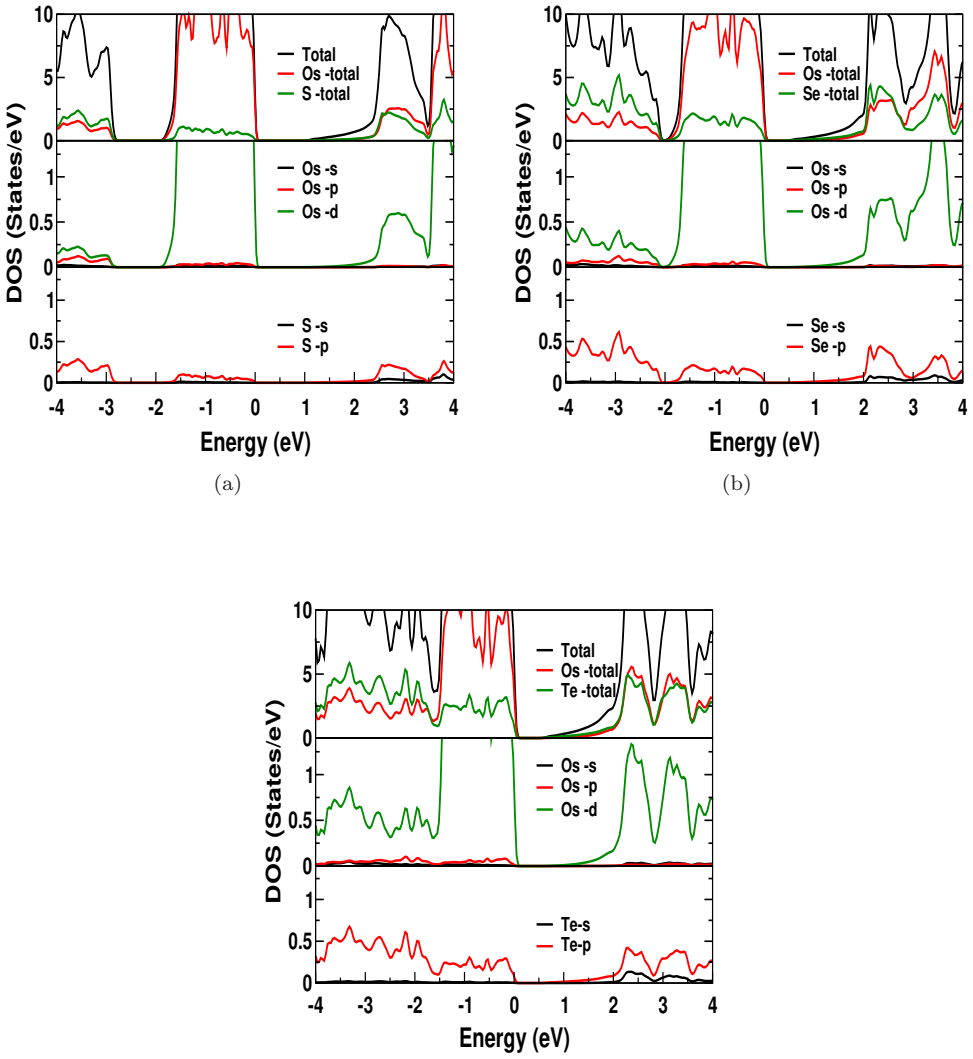

(a) (b)

(c)

Figure 6.3: Calculated total and partial density of states of all the compounds a) OsS_2, b) $OsSe_2$, c) $OsTe_2$

with 4 Re and 8 S atom unit cell only. Presence of heavy elements in the investigated compounds warrants the inclusion of spin orbit coupling in our calculations. Transport coefficients were calculated using BoltzTraP code with a dense k-mesh of the order of 32×36×25 k-points resulting in 14402 k-points in irreducible Brillouin zone. Hydrostatic/uni-axial strain calculations were performed by changing the lattice parameters and we have optimized the atomic position for each strained state. To understand the Fermi surface nesting in the strained state of ReS_2, we have calculated the real and imaginary part of Lindhard function by using Wien2k outputs.

6.3 Results and discussions

6.3.1 Structural and electronic properties of OsX_2 (X: S, Se, Te)

The investigated compounds OsX_2 (X: S, Se, Te) crystallize in pyrite structure with space group $P_a\bar{3}$, as shown in Figure 6.1. Bond lengths and angles of OsX_2 are analysed for all the compounds, and are given in Table 6.1. The bond length between 'Os' and 'X' (X: S, Se, Te) are found to increase from OsS_2 to $OsTe_2$, and both, bond lengths and bond angles are found to be higher than the prototype compound FeS_2[310]. The observed incremental nature in the bond length from OsS_2 to $OsTe_2$ might eventually reduce the interaction between atoms and lead to lesser value of Debye temperature [311], and further provide the possibility of reduced thermal conductivity value. The optimized lattice parameters along with available experimental reports are represented in Table 6.2, and from the table it is clear that optimized values are in good agreement with experimental values, and for further calculations we have used the optimized lattice parameters. Coming to electronic structure analysis, the computed band gap using different functionals are provided in Table 6.3, and band structure along different high symmetry directions using TB-mBJ with modified parameter are presented in Figure 6.2. All the investigated compounds are found to be direct band gap semiconductors with almost similar band profile, and comparable with other prototype compounds. A close analysis of the band structure of OsS_2 reveals, the existence of flat and dispersed bands near Fermi level, and more flat bands are observed near valence band maximum compared to the vicinity of conduction band minimum, which might indicate higher value of thermopower for hole doping, and higher value of electrical conductivity for electron doping. Furthermore, the number of bands near the valence band maximum is higher than that near the conduction band minimum, and this introduces more number of bands within small energy range and will contribute for thermopower, which again gives a hint of favourable thermopower for hole doping. It is worthy to compare the band profile of these pyrite structure with other TMDs. In the case of MoS_2, FeS_2 and Os based pnictides, both valence and conduction bands are found to be similar, and expected to have complementing transport properties. But in the compounds of present study, the band profile of valence and conduction bands are entirely different, and one might expect dissimilar transport properties. This significant difference in the band profile might lead to interesting TE properties of these investigated compounds, and will be discussed in the later section. From the band structure, it is clear that in valence band, along Γ-X, the bands are almost flat, and along R-M the band is dispersive, whereas in the conduction band, the band is highly dispersive along Γ-X, and less dispersive along R-M. The dispersive nature is found to increase from S to Te. This indicates the presence of heavy and light mass carriers in the band structure, which is helpful for thermoelectric properties, where heavy band

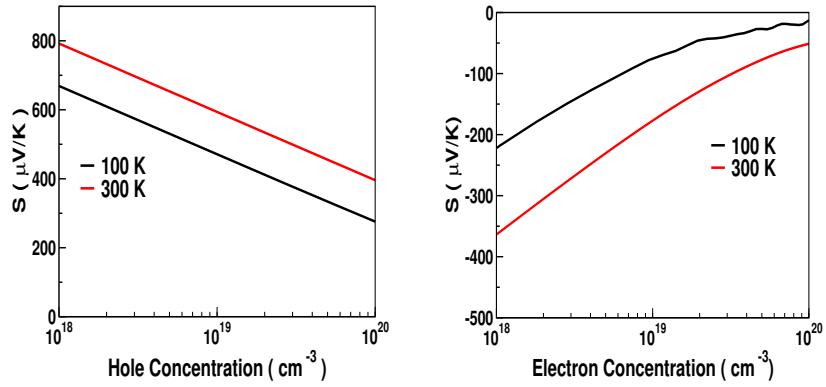

(a)

(b)

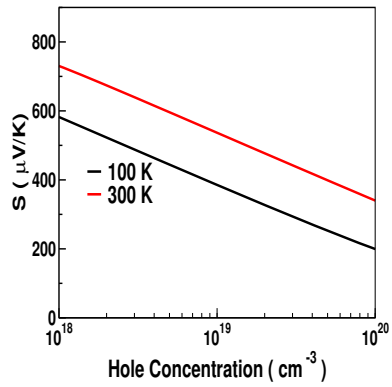

(c)

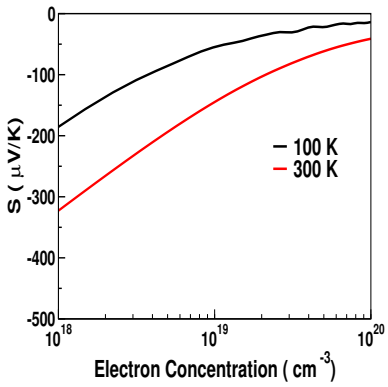

(d)

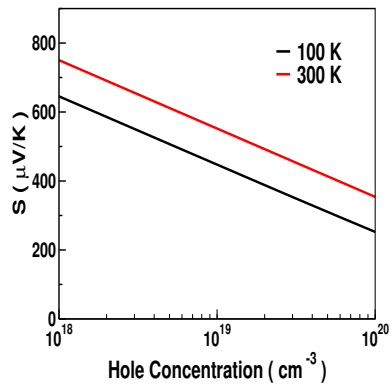

(e)

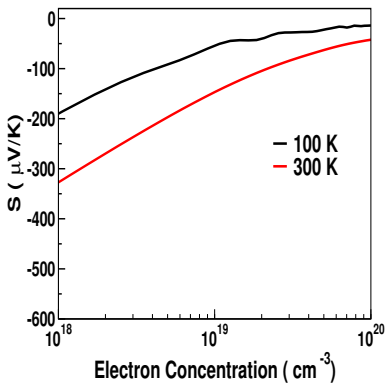

(f)

Figure 6.4: Variation of thermopower as a function of carrier concentration for all the investigated compounds at different temperatures (a, b) OsS_2 (c,d) $OsSe_2$, (e,f) $OsTe_2$

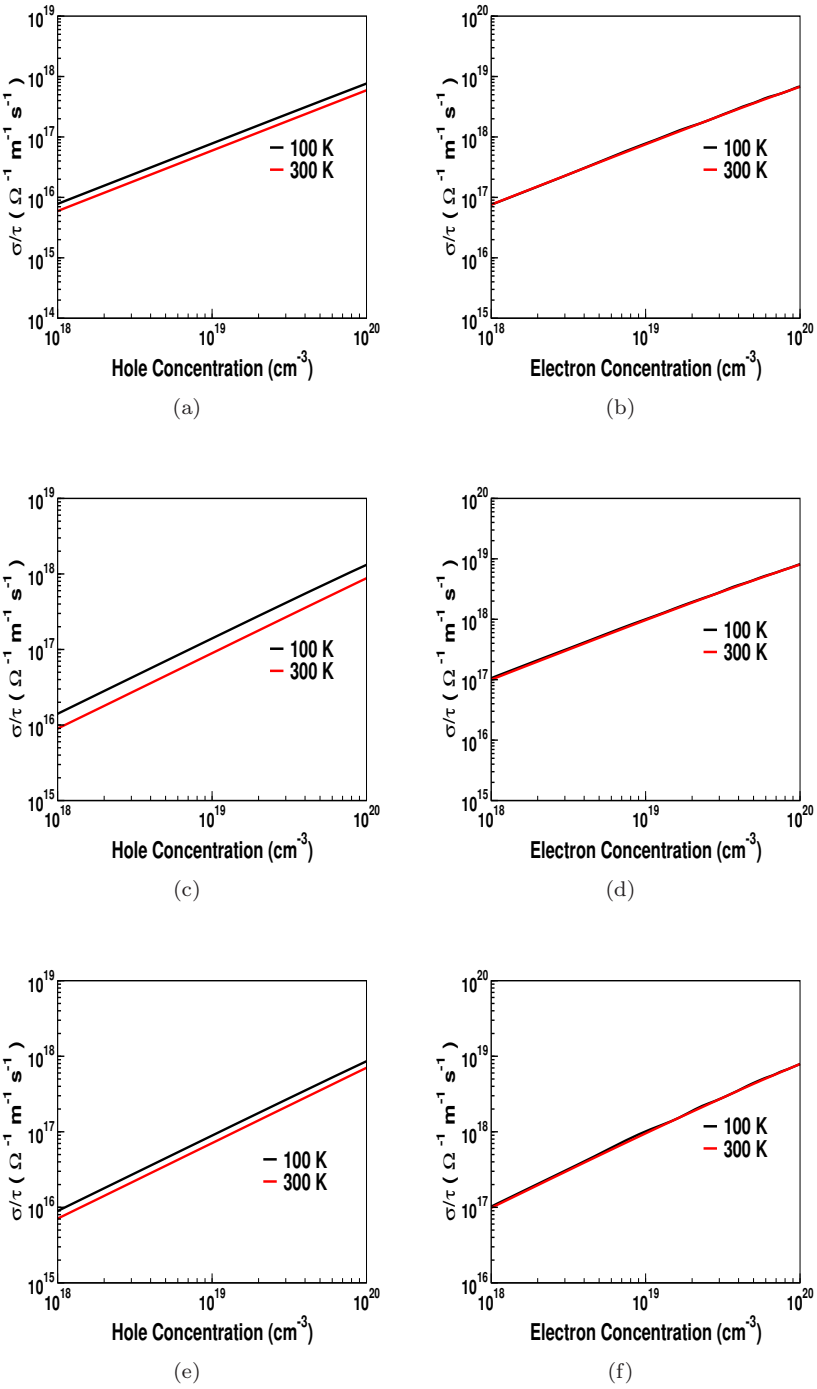

Figure 6.5: Variation of electrical conductivity as a function of carrier concentration for all the investigated compounds at different temperatures (a,b) OsS_2 , (c, d) $OsSe_2$, (e,f) $OsTe_2$

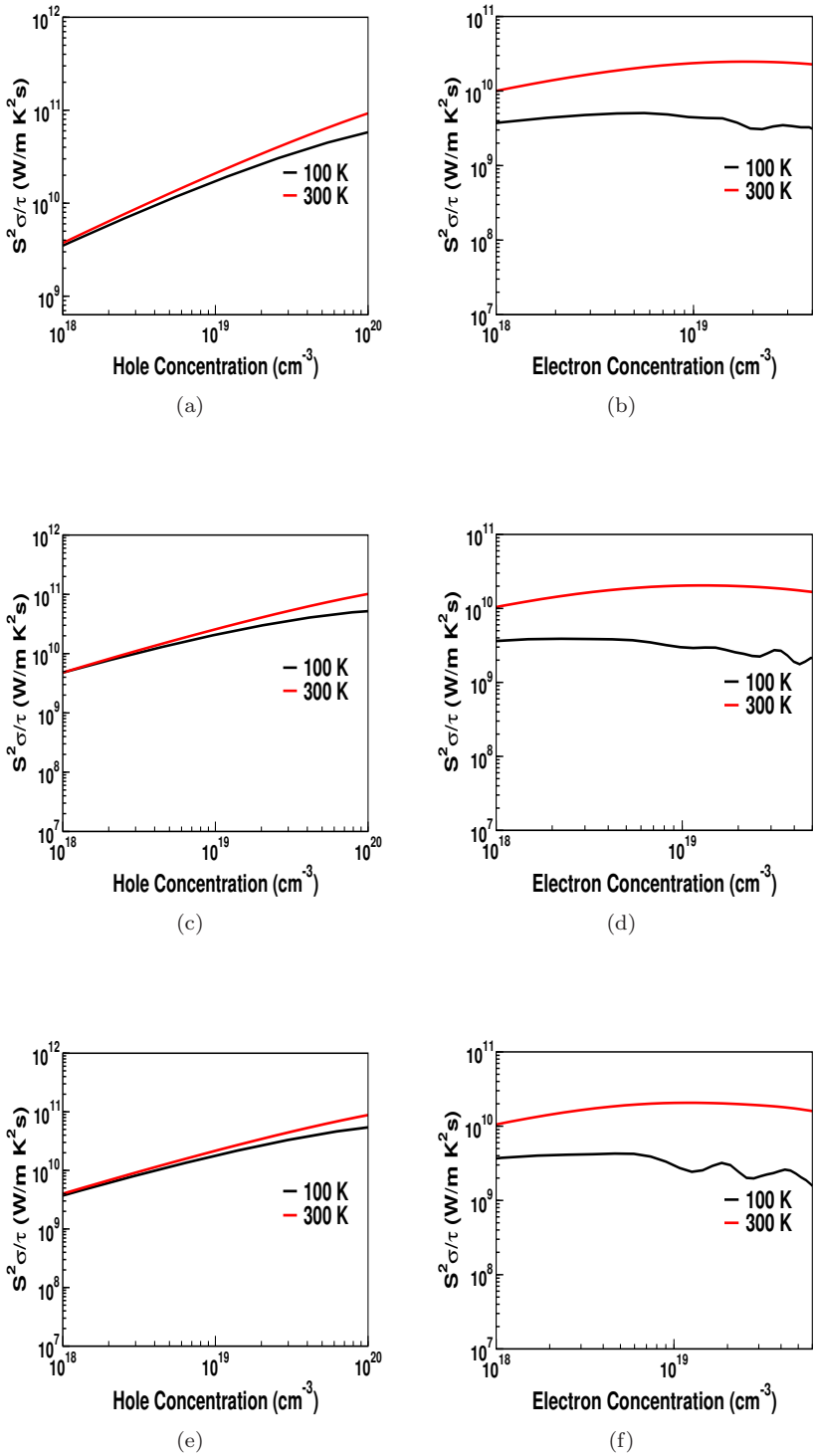

Figure 6.6: Variation of power factor as a function of carrier concentrations for all the compounds at different temperatures (a,b) OsS_2 , (c,d) $OsSe_2$, (e, f) $OsTe_2$

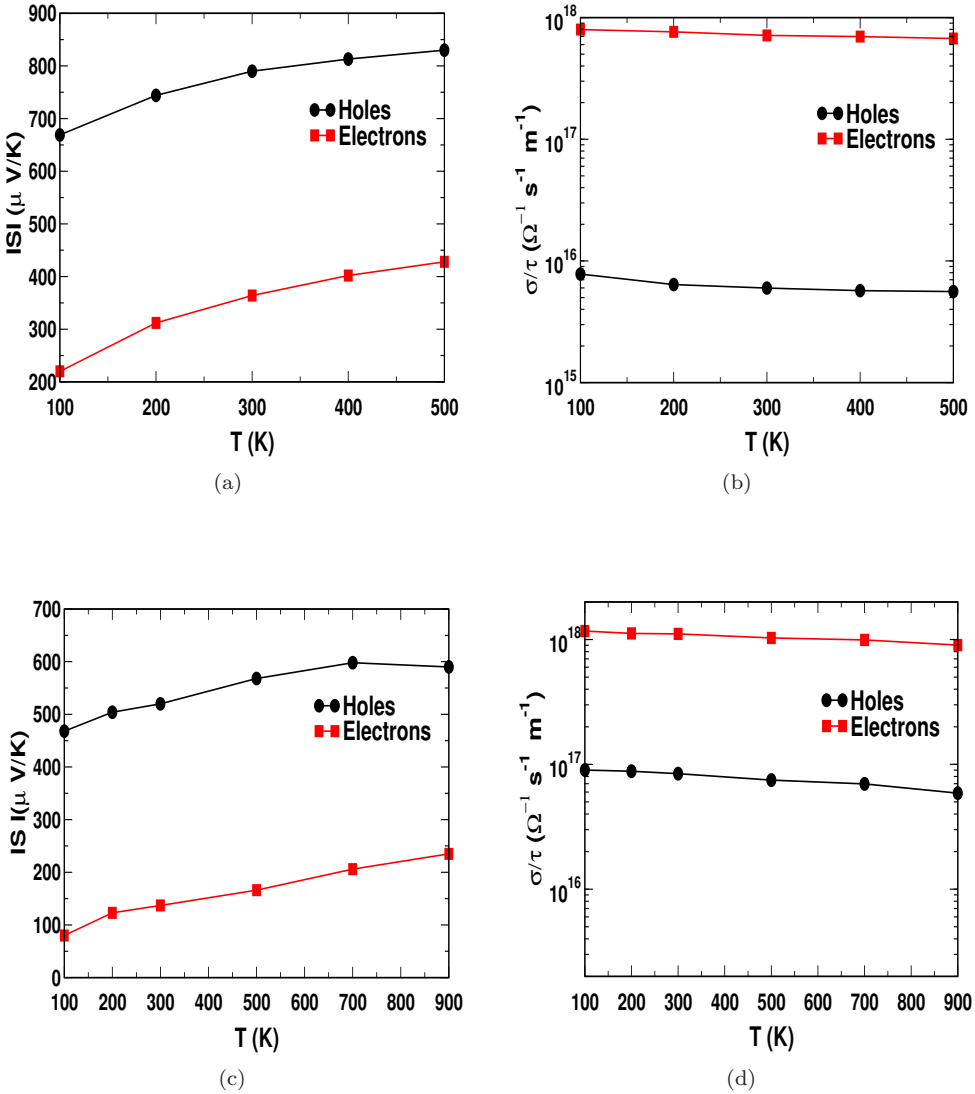

Figure 6.7: Thermopower and electrical conductivity as a function of temperatures for OsS_2 a) thermopower b) electrical conductivity at concentration around 10^{18}cm^{-3} , c) thermopower d) electrical conductivity at concentration around 10^{19}cm^{-3}

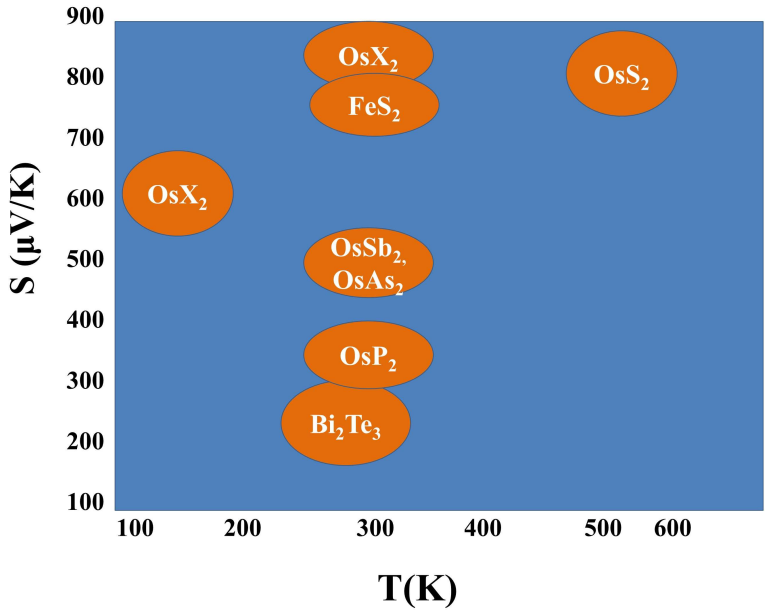

(a)

Figure 6.8: Comparison of thermopower value with other compounds, OsX_2 (X: S, Se, Te), FeS_2[314], Bi_2Te_3[148], $OsSb_2$, $OsAs_2$[291]

mass will contribute for thermopower and light band mass will contribute for electrical conductivity. To understand the dominant states near the Fermi level, we have investigated the total and partial density of states. In Figure 6.3, we have represented the density of states of all the investigated compounds. In the case of OsS_2, valence band states near Fermi level, are dominated by Os, and in conduction band, we can see a hybridisation of Os and S states. While moving from S to Te, we can see the contribution of anion increasing in valence band near Fermi level. Compared to conduction band, we can see a steep increment in density of states in valence band near Fermi level, and this indicates the dominating thermopower nature for hole doping. The extended hybridisation in the conduction band near Fermi level reveals the possibility of enhanced electrical conductivity for electron doped case compared to hole doped case. To confirm the presence of light and heavy band mass in the band structure, we have examined the effective mass in the unit of electron mass along Γ-X for both valence and conduction band, and are given in Table 6.4. From the table it is evident that there exist, one order of magnitude difference in the values between valence and conduction band, which is in line with our band dispersion. In the present compounds, the valence bands are found to be very flat and conduction bands are little dispersed, whereas in other marcasite compounds the band dispersion and hence magnitude of effective mass is almost same for both valence and conduction bands.

To check the mechanical stability of these compounds, we have calculated the elastic constants, and the same is represented in Table 6.5. All the elastic constants for all the compounds are found to be positive and found to satisfy Born elastic stability criteria[312], and this confirms the mechanical stability of these compounds. The C_{11} value of all the compounds are found to be higher than both C_{12} and C_{44}, which indicate the strong resistance for axial compression compared to shear

compressions[313]. In addition, bulk modulus, longitudinal velocity, transverse velocity and Debye temperature are given in Table 6.5. The values of elastic constants are found to be higher in $OsSe_2$ compared to other two compounds. The bulk modulus of all the investigated compounds are found to be comparable with prototype compounds such as FeS_2 and 'Os' based pnictides. Further, the value of Debye temperature of the investigated compounds are found to be lesser than the prototype compound FeS_2[314], indicating the thermal conductivity to be lower in these compounds[315] than FeS_2.

6.3.2 Thermoelectric properties of OsX_2 (X: S, Se, Te)

In this section, we have analyzed the thermoelectric properties such as thermopower, electrical conductivity and power factor as a function of carrier concentrations and temperatures. Figure 6.4(a-f) represents the thermopower as a function of carrier concentrations for both holes and electrons for all the investigated compounds at different temperatures. As anticipated from the band structure, the hole carriers are found to secure higher magnitude of thermopower for all the investigated compounds. A thermopower around 600 μVK^{-1} has been observed at 100 K for hole concentration around 10^{18}cm^{-3} for all the investigated compounds, which is huge compared to well established TE materials. In the case of OsS_2, the variation of thermopower as a function of both holes and electrons are found to be decreased with increasing carrier concentration. A maximum value of 820 μVK^{-1} is found around 600 K for hole doping. In the case of electrons, the magnitude of thermopower is found to be around 200 μVK^{-1} to 400 μVK^{-1} for temperatures ranging between 100 K to 600 K, which is also appreciable. Coming to $OsSe_2$, the trend of thermopower is found to be similar except for the presence of bipolar conduction around 500 K[316, 317]. $OsTe_2$ also showed similar behaviour as that of other compounds. Moving to the electrical conductivity values, Figures 6.5(a-f) represent the electrical conductivity for hole and electron doping for all the investigated compounds. The extremely dispersed bands in the conduction bands provided a favourable conductivity for electron doping over hole doping with almost one order difference in magnitude. This trend is found to be similar for all the compounds. The magnitude of electrical conductivity is found to be increased with carrier concentration. The difference in band profile of valence and conduction bands are reflected in both thermopower and electrical conductivity value for both hole and electron doping. As our attention is towards the net thermoelectric efficiency, we need to look at the parameter called power factor, and the same is given in Figure 6.6(a-f). The enhanced electrical conductivity for electron doping leads to enhanced power factor values for electron doping over hole doping for all the investigated compounds at lower concentrations. The vital point is that at higher concentrations around 10^{20}cm^{-3} and temperature around 600 K, both hole and electron doping secured almost similar value of power-factor, which might lead to device applications.

As discussed in the introduction, it is demanding to explore the TE materials for wide temperature range. In general, the carrier concentrations ranging from 1×10^{18}cm^{-3} to 1×10^{21}cm^{-3} are considerable, and now let us have a close analysis of the transport properties for the allowed range of carrier concentration. In the first part of this section, we point out the presence of bipolar conduction above 600 K for OsS_2, and for the other two compounds its starts at little lower temperatures itself. Now let us take the case of OsS_2, where the thermopower has reduced due to bipolar conduction only at low carrier concentrations around 1×10^{18}cm^{-3}, and for higher concentrations the thermopower values are appreciable. We have examined the thermopower and electrical

conductivity of OsS_2 at around $2.3\times10^{19}cm^{-3}$ for a wide temperature range from 100 K - 900 K, and provided the same in Figure 6.7. For the whole temperature range, holes secured higher value of thermopower and electrons were found to possess higher value of conductivity. From the figures (Figure 6.8 and Figure 6.7) it is quite evident that, OsS_2 might turn to be a potential TE material for a wide temperature range. Figure 6.8, represent the comparison plot of OsX_2 (X: S, Se, Te) with other TE materials, and from the figure it is evident that the investigated compounds possess higher value of thermopower at 100 K and comparable value at room temperature and above.

Huge value of thermopower around 100 K is found with a reasonable electrical conductivity for hole doping in all the investigated compounds. The power factor value of hole doping is found to increase as a function of carrier concentration and reach a magnitude of around 10^{11} (in W/m K^2 s) at higher concentrations of $10^{20}cm^{-3}$, which is comparable with established TE materials. If one can enhance the electrical conductivity, by preserving thermopower, through chemical doping, all the investigated compounds might be promising TE material.

Table 6.1: Calculated bond length and bond angle in OsX_2 (X: S, Se, Te)

paramaters	OsS_2	$OsSe_2$	$OsTe_2$
d(Os-X)(Å)	2.39	2.50	2.70
d(Os-Os)(Å)	4.02	4.25	4.61
(Os-X-Os)(deg)	115.26	116.61	117.30

Table 6.2: Ground state properties of OsX_2 (X: S, Se, Te)

paramaters	OsS_2	$OsSe_2$	$OsTe_2$
a_{pre}(Å)	5.68	6.02	6.53
a_{exp}(Å)	5.6196[318]	5.946[319]	6.397[320]

Table 6.3: Calculated band gaps (in eV) of OsX_2 (X: S, Se, Te)

method	OsS_2	$OsSe_2$	$OsTe_2$
GGA	0.21	0	0
TB−mBJ	0.5	0.02	0
TB−mBJwith parameter	0.98	0.41	0.53

Table 6.4: Calculated effective masses (in the unit of electron mass) of OsX_2 along different high symmetry directions

Directions	OsS_2	$OsSe_2$	$OsTe_2$
VB (valence band)			
Γ-X	6.03	5.76	4.53
CB (conduction band)			
Γ-X	0.36	0.32	0.37

Table 6.5: Calculated elastic constants of OsX_2 (X: S, Se,Te)

parameters	OsS_2	$OsSe_2$	$OsTe_2$
C_{11}(GPa)	449.653	481.477	426.226
C_{12}(GPa)	55.650	57.936	36.464
C_{44}(GPa)	107.321	143.651	151.963
B (GPa)	186.98	199.11	166.38
V_l (in Km/s)	6.33	6.31	6.05
V_t (in Km/s)	3.85	3.98	3.97
θ (in K)	511.54	496.14	454.652

6.3.3 Structural properties of ReX_2(X: S, Se)

The compounds ReS_2 and $ReSe_2$ crystallize in distorted triclinic structure[321, 324] with space group $P\bar{1}$, which is exceptional in TMD. One of the recent study on ReS_2 has reported a structural transition of the compound at around 0.1 GPa, and named the ambient one as distorted 3R and the transformed structure as distorted 1T structure[305]. From our analysis, we have observed the energy difference between these two structures to be negligibly small and one can conclude these to be competing structures, and in this scenario, we have proceeded with calculation using 3R structure which is experimentally reported. The details of the experimental crystal structure, together with present optimized values for both the compounds are given in Table 6.6. The weak interlayer bonding of these compound is well known[293] and we have optimized the structure by adding the van der Waals correction. The cleaved monolayer and bilayer structure also preserve triclinic structure. The two 'Re' chains in the crystal structure generate an anisotropy in several physical properties[325, 326]. The schematic crystal structure of the investigated compounds is presented in Figure 6.9. In the next part, we have discussed the electronic structure of ReX_2 (X: S, Se).

6.3.4 Electronic structure and thermoelectric properties of ReX_2 (X: S, Se) in bulk and layered forms of ReS_2

Computed electronic structure of ReX_2 (X: S, Se) is presented in Figure 6.10. Several previous studies[293, 327, 328, 329, 330, 331] on ReS_2 investigated the nature of band gap in this compound,

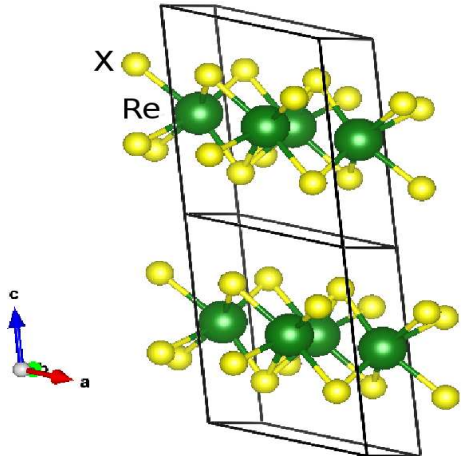

(a)

Figure 6.9: Crystal structure of ReX_2 (X: S, Se) (green colour represent 'Re' and yellow colour represent 'X')

which are contradicting. Among them, few studies proposed indirect band gap of ReS_2[331, 327] from experiment. Very recent study by Echeverry and Gerber theoretically predicted direct band gap in ReS_2 using GW method, and our present study is in good agreement with the same[330]. We have observed a direct band gap nature for bulk ReS_2 with a band gap around 1.2 eV. For $ReSe_2$ also we could see a direct band gap. The band dispersion along different crystallographic directions is found to be different. The overall band profile of these compouds are comparable with other celebrated transition metal dichalcogenids. Figure 6.11 shows the total and partial density of states of these compounds. Dominating Re 'd' states in both valence and conduction band is evident from the density of states plots. Re and X(X: S, Se) 's', 'p' states are found to have similar contributions in both valence and conduction band. In general TMDs are well known for high thermopower[332], and in these compound also, we can observe flat bands aligned in both valence and conduction bands, which might contribute to thermopower. The varying effective mass values in the unit of electron mass along different crystallographic directions, again projects the inherent anisotropy present in the system (see Table 6.7). Further we have analyzed the thermoelectric coefficients such as thermopower, electrical conductivity and power factor for ReX_2(X: S, Te). Similar to the other TMDs, the thermopower value of ReX_2 is found to be appreciable. In Figure 6.12 we have summarized the thermoelectric properties of ReS_2 as a function of both hole and electron doping. Figure 6.12 (a,b) represent the thermopower value for hole and electron doping and from the figure it is clear that magnitude of thermopower for hole doping is enhanced over electron doping by very less value, and this might be due to the similar band dispersion in both valence and conduction bands. Magnitude of thermopower is found to be decreased with increasing carrier concentration for both holes and electrons. Small anisotropy along different crystallographic directions are observed, in accordance with band dispersion anisotropy. For hole doping, the thermopower value along *'a'* axis is found to be little higher than the other two, and for electron doping *'c'* direction values are found to be slightly enhanced. Maximum thermopower for hole doping is found to be 600 μVK^{-1} and for electrons the same is found to be around 540 μVK^{-1} , which is comparable with well-

Table 6.6: Calculated ground state properties of bulk and monolayer ReS_2

Compound	a(Å)	b(Å)	c(Å)
ReS_2-Bulk(with vdW) $_{present}$	6.31	6.53	6.46
ReS_2-Bulk (without vdW)$_{present}$	6.41	6.52	7.00
ReS_2-Bulk$_{exp}$[321]	6.45	6.39	6.4
ReS_2-Bulk$_{exp}$[322]	6.417	5.510	5.461
ReS_2-Mono-layer$_{present}$	6.31	6.49	21.34
$ReSe_2$	6.63	6.60	6.77
$ReSe_2$ (exp)[323]	6.716	6.602	6.728

Table 6.7: Calculated effective mass (in the unit of electron mass) for ReX_2

Compound	Γ-X	Γ-Y	Γ -Z
ReS_2	1.92	1.5	2.18
$ReSe_2$	1.8	1.2	2.02

established $MoSe_2$ and WSe_2, where the 'S' value are found to be 590 μVK^{-1} and 580 μVK^{-1} respectively[334]. In the case of electrical conductivity, we can observe a significant anisotropy between the crystallographic directions, and basal plane values secured the maximum for both holes and electrons, which projects the inherent quasi two dimensional nature, and the magnitude of electrical conductivity for electrons is found to be more than holes. From the power-factor values, it is clearly seen that both holes and electrons are beneficial with electron possessing slightly higher value, and the range of power factor is not very far from well-established TMD based TE materials. The thermoelectric coefficients are found to be promising for a wide range of temperature in the case of ReS_2. In a similar way, we have calculated the thermoelectric properties of $ReSe_2$ and represent the same in Figure 6.13. In line with ReS_2, the magnitude of thermopower is found to decrease with carrier concentration and Figure 6.13 (a,b) show the variation at different temperatures. Almost similar values are observed for hole and electron doping and at higher temperature around 900 K, we have observed bipolar conduction in the low concentration range (around 10^{18}cm^{-3}). Coming to electrical conductivity of $ReSe_2$, the anisotropy along different crystallographic direction is found to be lesser compared to the case of ReS_2. Overall the magnitude power factor of $ReSe_2$ also show appreciable values thereby indicating the potential TE applications.

After analyzing the electronic and thermoelectric properties at ambient conditions, we have further extended our study to improve the thermoelectric properties. For this purpose we have chosen ReS_2, and cleaved into monolayer and bilayer structure. Figure 6.14(a) reveals the band structure for monolayer ReS_2, which is similar to bulk band structure with slightly higher band gap compared to bulk. The band gap of monolayer ReS_2 is observed around 1.42 eV. It is to be noted that in other TMDs band gap nature is found to be different from bulk to monolayer[333]. A close analysis of the band structures of bulk and monolayer form shows that, there is a slight change in the band dispersion along X and Y high symmetry points, and these small layer dependent nature has been reported in the previous study also[330].

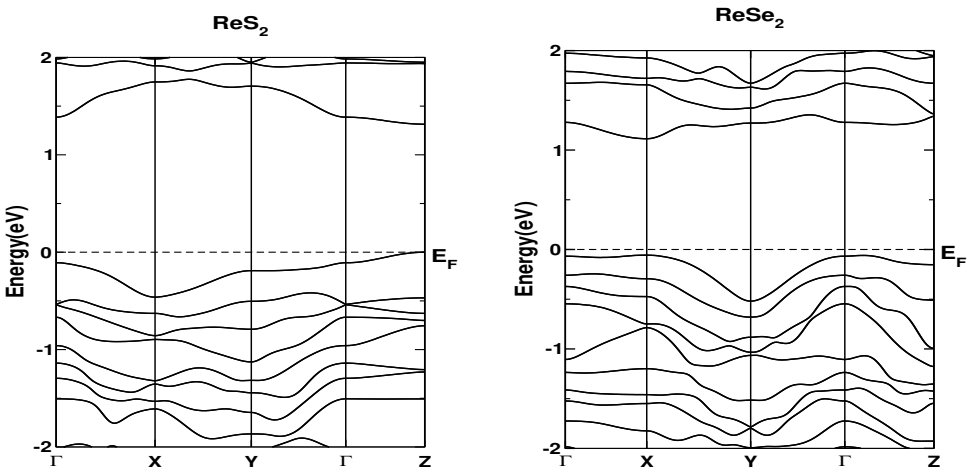

(a) (b)

Figure 6.10: Calculated band structure of a) ReS_2 b) $ReSe_2$ using TB-mBJ functional

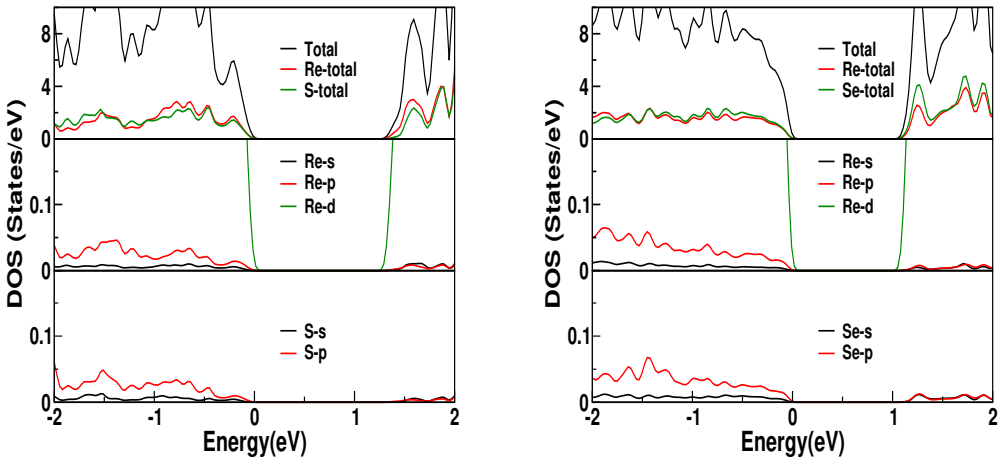

(a) (b)

Figure 6.11: Calculated total and partial density of states a) ReS_2 b) $ReSe_2$ using TB-mBJ functional

Now let us analyse the bilayer band structure (see Figure 6.14(b)), which is also almost identical to bulk and monolayer, with a direct band gap of 1.36 eV. We would also like to mention here that this small layer dependence is not significantly reflected in the thermoelectric properties from our calculations.

Since electronic structure properties are same for both bulk and layered forms for ReS_2, we can expect the same to be reflected in transport properties also. Figure 6.15(a,c) shows the thermopower of monolayer and bilayer, and the magnitude of thermopower is found to be little enhanced in monolayer, than the bulk, but the trend is found to be the same for both monolayer and bilayer. In the case of electrical conductivity (see Figure 6.15 (b,d)), we could see similar behaviour as bulk. Altogether, the thermoelectric properties of bulk and layered forms are found to be similar, implying the layer independent transport properties of ReS_2. Further we were inquisitive to improve the transport properties, and we have applied uni-axial compressive strain along 'a' on bulk and monolayer ReS_2. The upcoming section deals with the effect of uni-axial strain on electronic structure and TE properties.

6.3.5 Effect of uni-axial strain in bulk and monolayer form of ReS_2

As discussed earlier, a systematic analysis of electronic and TE properties are performed under the application of uni-axial compression strain along 'a' direction, which covers up to a wide range of 20% lattice variation. The percentage of uni-axial strain is defined as $((a-a_0)/a_0))\times 100$. The basic strain tensor for three dimensional system is

$$\begin{bmatrix} \epsilon(11) & \epsilon(12) & \epsilon(13) \\ \epsilon(21) & \epsilon(22) & \epsilon(23) \\ \epsilon(31) & \epsilon(32) & \epsilon(33) \end{bmatrix}$$

where $\epsilon(ii)$ are strain along i^{th} direction, and $\epsilon(ij)$ is shear strain.

One of the recent study on ReS_2 has revealed the pressure effects on the electronic structure resulting in metallization at high pressure around 70 GPa, and the same inspired us to investigate the effect of uni-axial strain on ReS_2. First let us analyse the case of bulk ReS_2. The band gap is found to decrease and the band gap nature is found to turn from direct to indirect as a function of compressive strain along *'a'* direction (See Figure 6.16(b)). An appreciable amount of change is observed in band dispersion along different crystallographic directions as a function of *'a'*-axis compressive strain, which eventually is reflected in the anisotropic nature of transport properties. The band structure at different strained states are given in Figure 6.16 (a,b). At around 5 % strain, the compound is almost quasi two dimensional, where the Γ - X and Γ - Y band dispersions are very similar and along Γ - Z, we could see highly flat bands. For further strain around 10%, the scenario is changed completely, where we could see a significant difference in band dispersion within the plane and between basal plane and *'c'* axis. Around 16 % strain, the system metallizes and the band structures at 16% strained state together with the one at ambient are represented in Figure 6.17(a). From the figure it is evident that, apart from metallization the band profile of the compound is drastically changed. At strained state, the dispersion along Γ - X is found to be very high compared to other two directions, which might induce a huge anisotropy in the system resulting in dimension reduction. The calculated effective mass along different crystallographic direction further provide

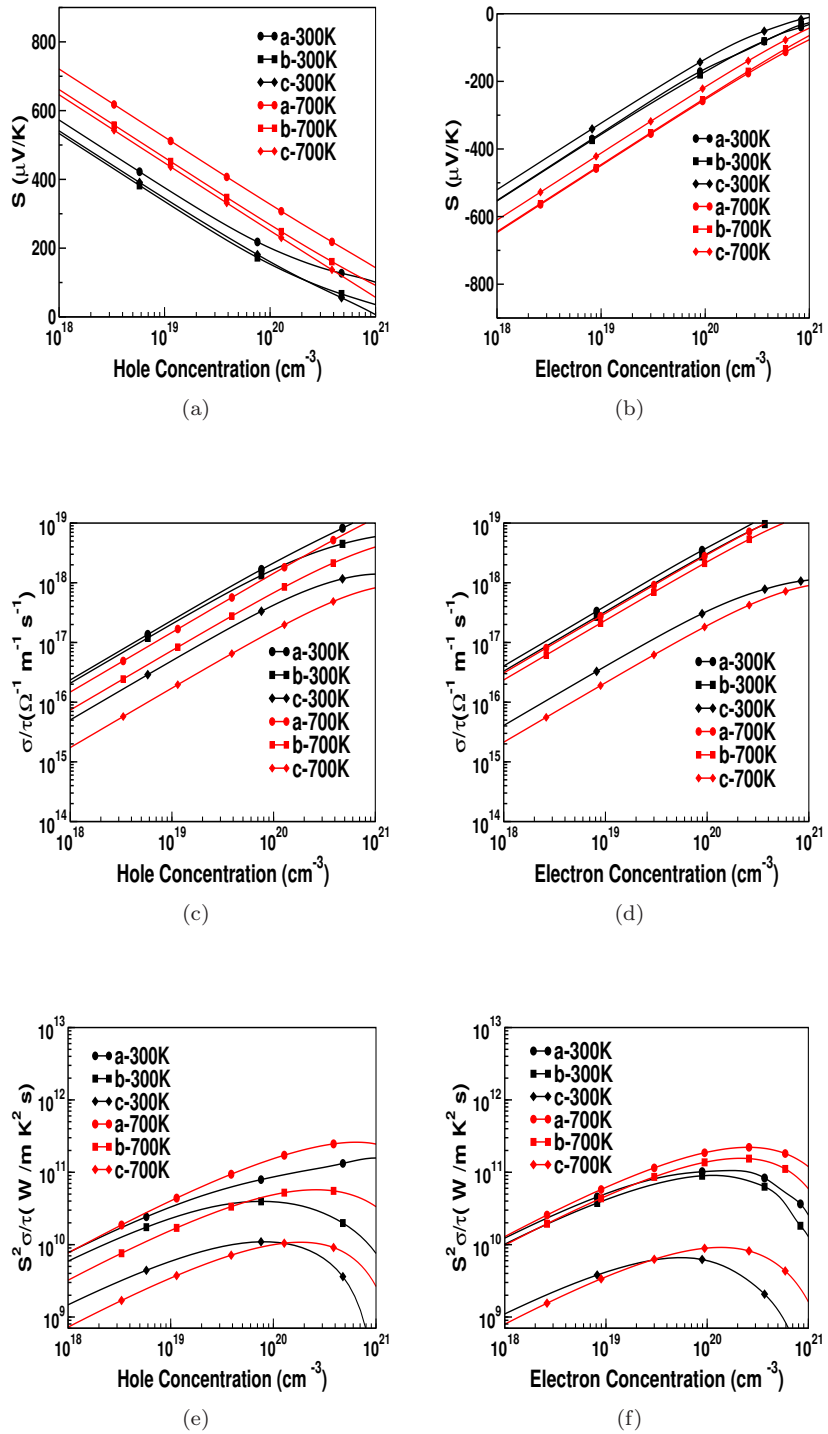

Figure 6.12: Calculated thermopower, electrical conductivity and power factor as a function of hole and electron concentrations for ReS_2

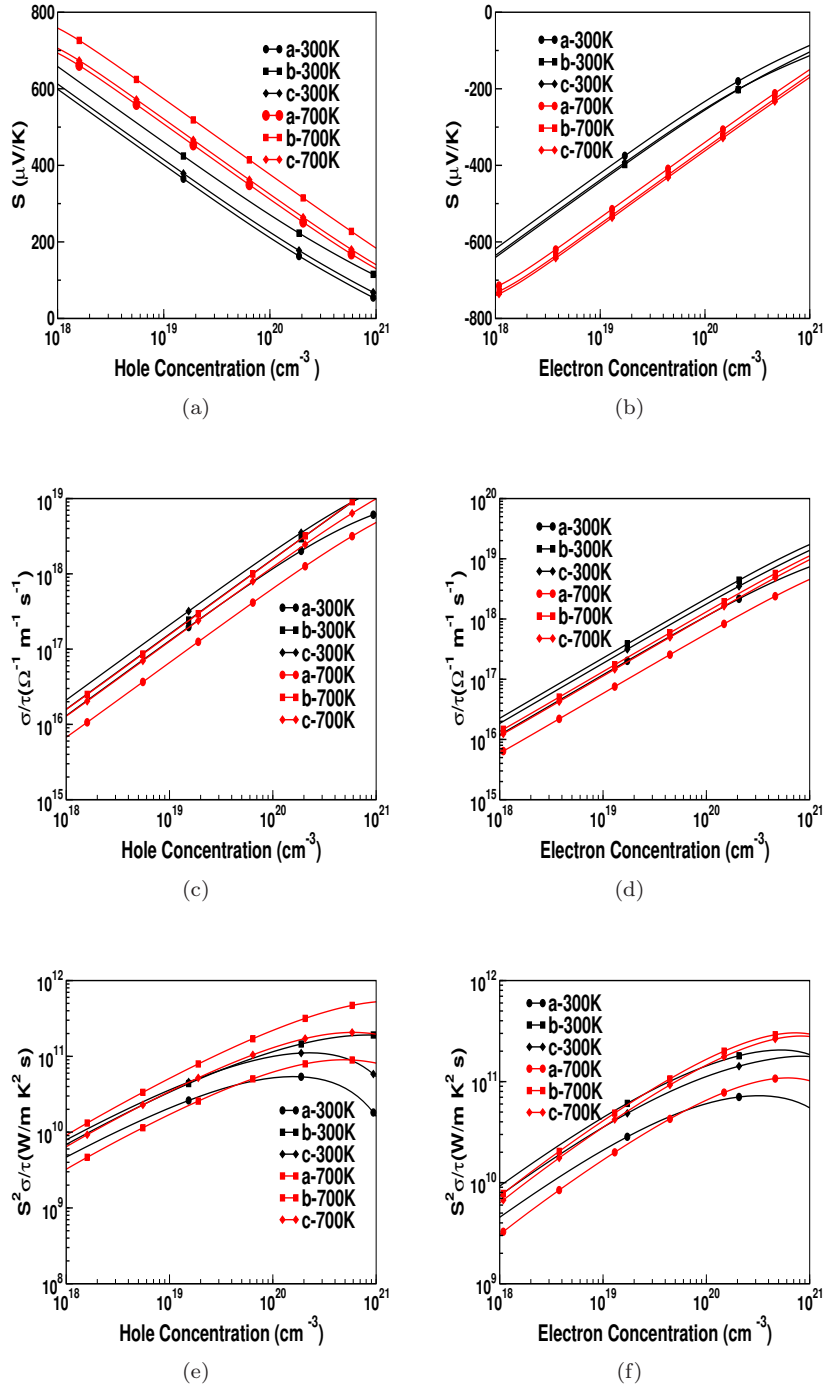

Figure 6.13: Calculated thermopower, electrical conductivity and power factor as a function of hole and electron concentrations for $ReSe_2$

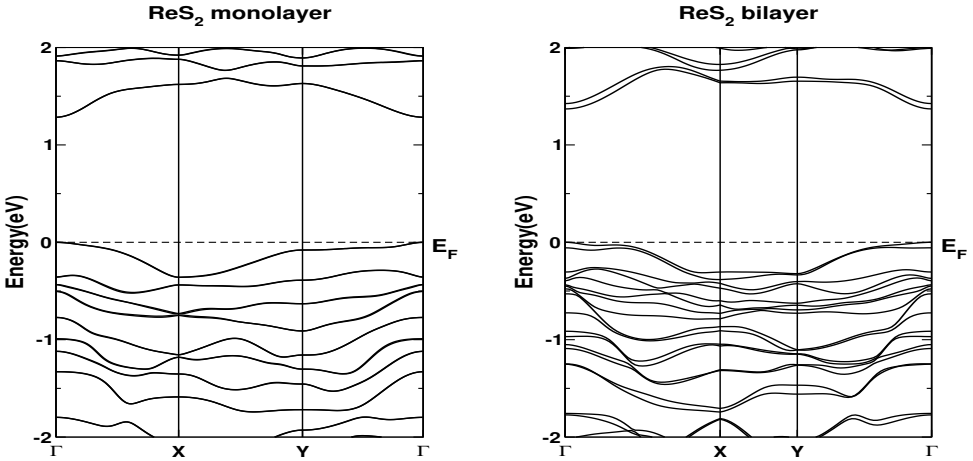

Figure 6.14: Calculated band structure of ReS_2 in a) monolayer form, b) bilayer form

the glimpse of two dimensionality of the system, where effective mass in the unit of 'electron mass' along Γ - X and Γ - Z are 1.92 and 2.18 respectively at ambient and for strained state, it turns out to be 2.49 and 38.3 reflecting the flat bands along the Γ - Z direction. At the metallized state, there are two bands which cross the Fermi level, and that corresponds to two Fermi surfaces, among which, one is a hole like FS and another is an electron like FS (see Figure 6.18(c)). These two surfaces are very thin sheets with different shapes. It is quite evident that the bands along Γ - Y is found to be very flat, and indicate the two dimensional nature of the system. The stability of this strained state is further confirmed by phonon dispersion analysis, and the same is given in Figure 6.17(c). For further strain around 17 %, we could observe more flat nature of bands and highly nested Fermi surface. The hole like FS is represented as FS-1 and electron like FS is named as FS-2 (see the Figure 6.18(c)). From the the Fermi surface plots, one can evidence the nesting of Fermi surface happening in two directions, as represented with arrow marks. To elucidate more about nesting of Fermi surface authentically, we have calculated the real and imaginary part of the generalised susceptibility $\chi(q)$, where q is the wave-vector of FS-1 along the high symmetric direction Γ - Y. The singularity observed in the imaginary part of the susceptibility gave a clear evidence of Fermi surface nesting (See Figure 6.18(d)) along that direction. More prominent flat Fermi surface is observed in the second direction, and due to the lack of high symmetry points along that direction, we did not calculate the $\chi(q)$, but one can always expect higher amount of nesting towards that direction. In the previous study, the pressure induced structural transition (at around 90 GPa) and superconductivity in the transformed structure (around 102 GPa) was reported. Here, the observed peak in density of states (as shown in figure 6.18(b)) at Fermi level and highly nested Fermi surface are throwing light on the possibility of superconducting state and need to be verified[335].In a similar way, superconducting states are observed for both $ReSe_2$ and $ReTe_2$ at higher pressure states[336]. Moreover, the anisotropy in transport property like electrical conductivity gave further evidence for this two dimensional nature in strained bulk ReS_2. In addition, the response of uni-axial strain is examined in monolayer also, and we could see a very similar kind of metallization happening around 16 % strain (see Figure 6.17(b)), which again substantiate the dimension reduction. We

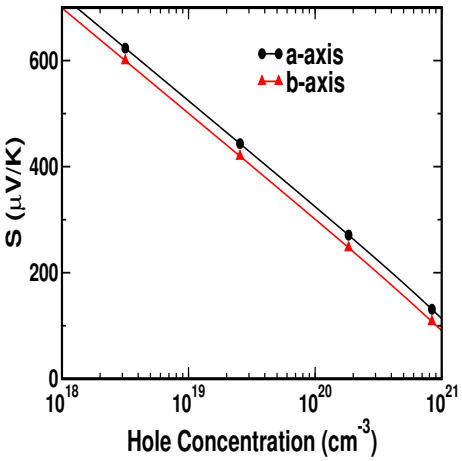
a-axis
b-axis
S (μV/K)
Hole Concentration (cm-3)

(a)

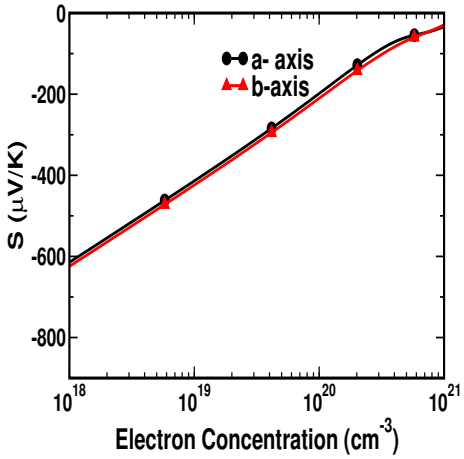
a- axis
b-axis
S (μV/K)
Electron Concentration (cm-3)

(b)

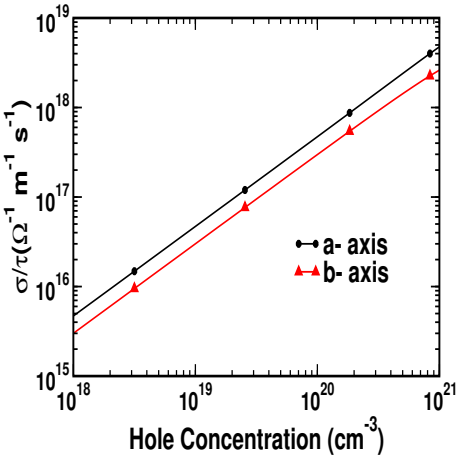
a- axis
b- axis
σ/τ(Ω-1 m-1 s-1)
Hole Concentration (cm-3)

(c)

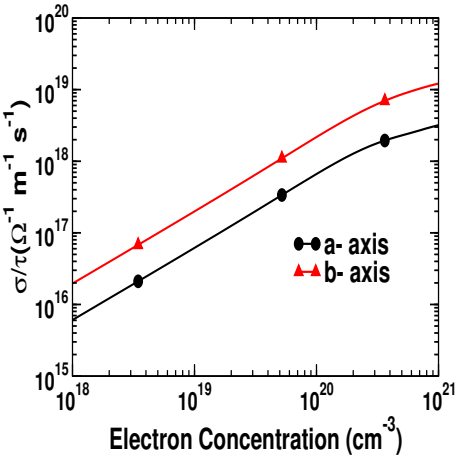
a- axis
b- axis
σ/τ(Ω-1 m-1 s-1)
Electron Concentration (cm-3)

(d)

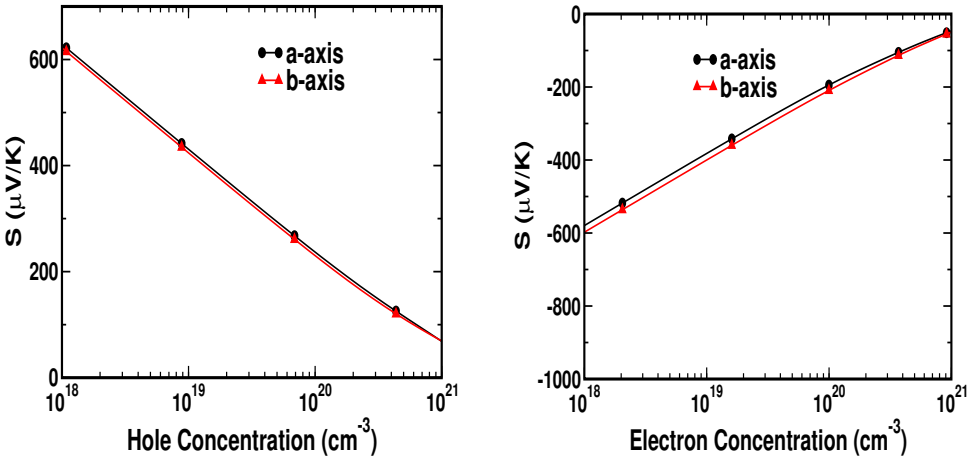

(e) (f)

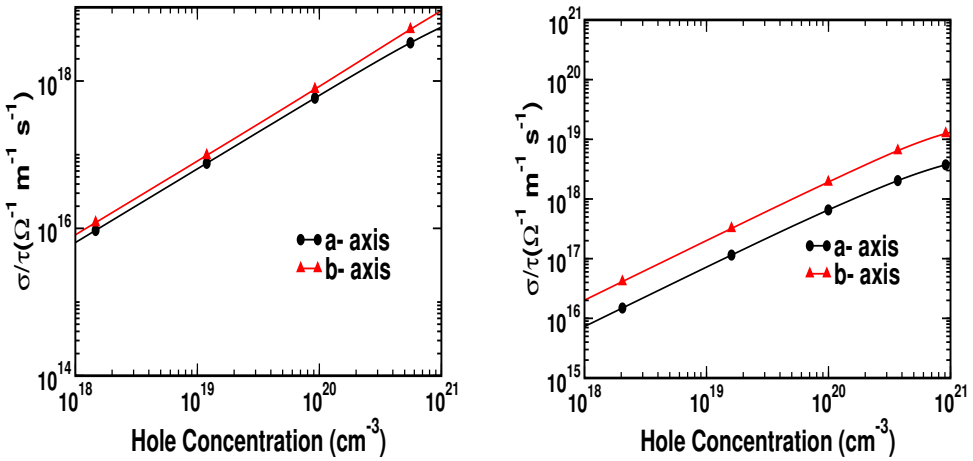

(g) (h)

Figure 6.15: (a,b) Thermopower as a function of hole and electron concentrations for monolayer, (c,d) Electrical conductivity as a function of hole and electron concentrations for monolayer, (e,f) Thermopower as a function of hole and electron concentrations for bilayer, (g,h) Electrical conductivity as a function of hole and electron concentrations for bilayer

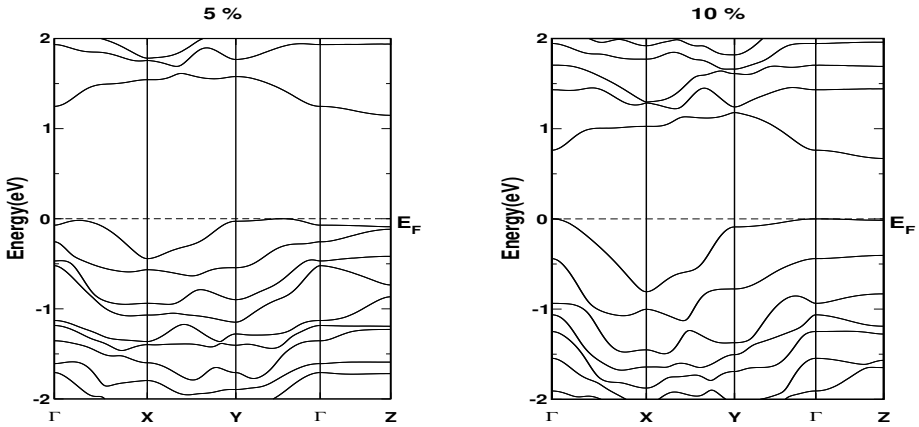

Figure 6.16: Band structure of bulk and monolayer ReS_2 at different compressive strains, a) 5% compressive strain, b) 10% compressive strain

have verified the stability of monolayer ReS_2 at this strained state (16 % strain) by calculating the phonon dispersion, an the same is given in Figure 6.17 (d).

Interesting thermoelectric coefficients are observed as a function of strain, and the anisotropic nature is more pronounced. The anisotropy in the band dispersion as a function of strain is reflected in the transport properties also. The power-factor at different strains are provided in Figure 6.19 (a,b). At 5 % strain, we could see a quasi two dimensional nature, where basal plane properties are almost found to be same and enhanced compared to 'c' axis. Subsequently for 10 % strain, almost one order difference in power factor is observed within the basal plane and between 'a' and 'c' axis, the anisotropy has turned to almost two orders in magnitude. Concentrating on the metallized state (17%), the magnitude of thermopower is found to be reduced as expected due to metallization, and the vital point is, along 'a' direction the value of thermopower is found to be around 40 $\mu V K^{-1}$ for hole doping and for the other two direction we could see the sign change because of carrier flipping. A compensating incremental nature is observed in electrical conductivity which again benefits the net thermoelectric performance. Higher value of electrical conductivity and moderate value of thermopower, result in promising value of power-factor in the basal plane, which is found to be higher than the ambient value at low carrier concentrations. The variation of electrical conductivity and power factor as a function of carrier concentration at 17 % strained state is represented in Figure 6.19 (c,d). The in-plane power factor values are found to be two orders higher than the out of plane power factor, which again supports the two dimensional characteristics of the strained state[337]. A similar in-plane electrical conductivity values are observed for monolayer also. Moreover, the phonon dispersion at the strained state is found to be promising, where the interaction between the acoustic and optical phonons are found to be in low frequency range around 60 cm^{-1}, which might result in low values for thermal conductivity in this state.

In general, the semiconducting states are considered to be more promising for thermoelectric application, but here, we could find a higher value of power factor in the metallized state. At metallization in this strained state, the band dispersions along Γ - X, Γ - Y and Γ - Z are anisotropic, which lead to an asymmetry in density of states as seen in Figure 6.18(b), which further emphasises

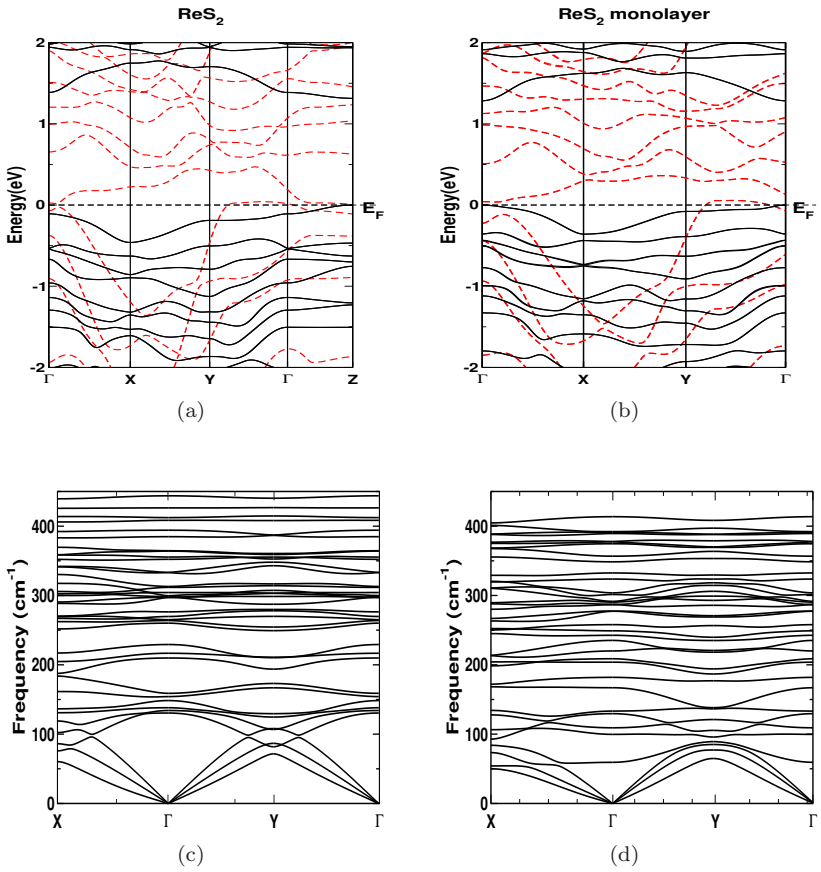

Figure 6.17: Band structure of bulk and monolayer ReS_2 at different compressive strains, black solid line represents the ambient state and red dashed line represents the strained state a) bulk , b) monolayer, c) phonon dispersion for bulk ReS_2 at 16 % strain d) phonon dispersion for monolayer ReS_2 at 16 % strain

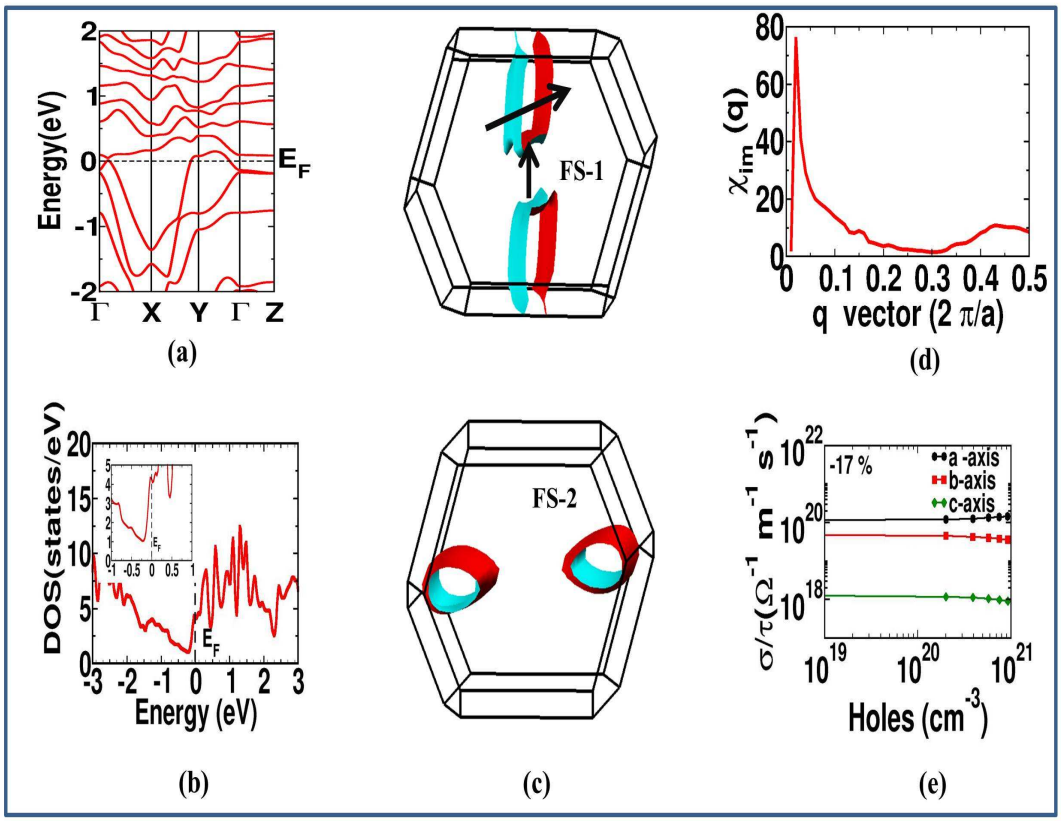

(a)

Figure 6.18: Properties at 17 % compressive strain. a) band structure b) density of states, c) Fermi surface , d) imaginary part of susceptibility, e) electrical conductivity

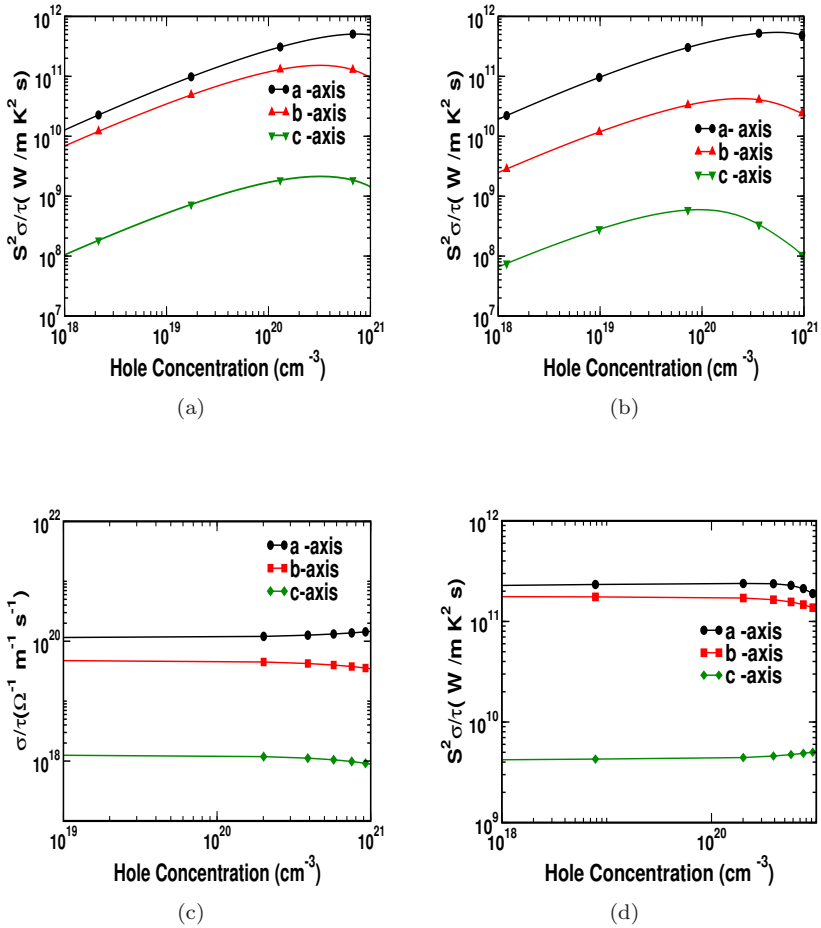

Figure 6.19: a) Power factor at 5% compressive strain, b) power factor at 10% compressive strain, c) electrical conductivity at 17% compressive strain, c) power factor at 17% compressive strain

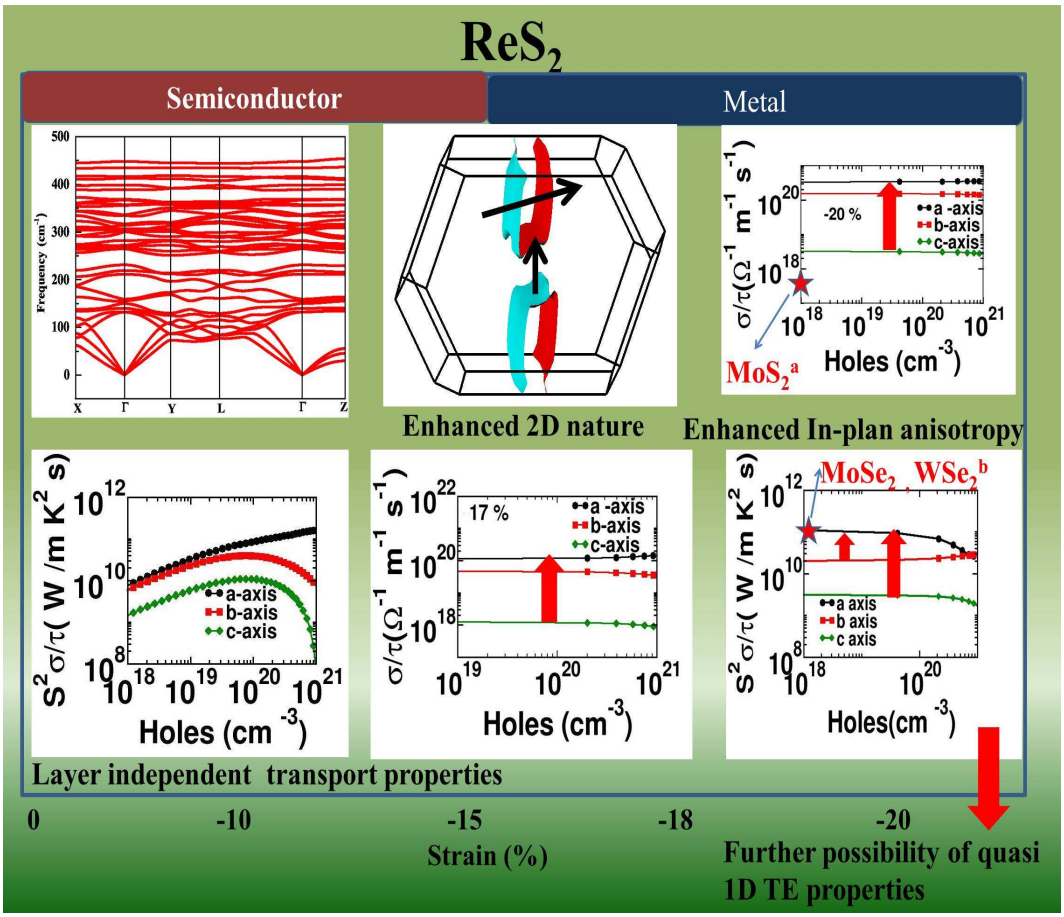

(a)

Figure 6.20: Schematic of ReS_2, and comparison with other established compounds. a:Ref[338], b:Ref:[334]

the fact that holes are more favourable carriers in ReS_2.

While focusing on the power factor plot, one can clearly observe that there is a small in-plane anisotropy in the strained state. For further strain around 20 % we could see more than one order difference between the power factor along 'a' and 'b' axis, and two order difference between 'a' and 'c' axis (included in Figure 6.20). The developed enormous in-plane anisotropy indicates the possibility of using ReS_2 nanowires for TE applications, which has to be taken as future project. Sequence of calculations have provided the clear picture of metallization, increasing anisotropy and an enhancement in power-factor along 'a' direction in the system as an effect of uni-axial strain, and ReS_2 has turned to be an excellent candidate for thermoelectric applications. In Table 6.7, we have represented the effective mass, electrical conductivity and power factor for ambient and strained state of bulk and monolayer, which clearly shows the enhanced anisotropy as a function of strain. Moreover, Figure 6.20 represents the schematic of our overall study together with the comparison of other TMD , and summarize the semi-conductor to metal transition in ReS_2. As a function of strain, the electrical conductivity is found to be enhanced, and the phonon dispersion analysis has further provided the clue for reduction of thermal conductivity. This shows the possibility of better thermoelectric performance in the strained state. In addition, a similar kind of metallization is observed in the monolayer ReS_2 which further shows promising dimension reduction with enhanced electrical conductivity, which certainly projects ReS_2 to be more versatile TMD compared to others. If one can improve the thermopower value, without suppressing the conductivity value, ReS_2 might turn out to be a promising candidate for nanowire TE applications.

6.4 Conclusions

Electronic and thermoelectric properties of OsX_2 are analysed. Huge value of thermopwer is observed at low temperature around 100 K for hole doping for all the investigated compounds, which is found be higher than well established TE materials. The mixture of heavy and light band mass in the band structure is reflected from the band structure. Analysis of thermoelectric properties revealed the potential TE application for a wide temperature range. All the investigated compounds are favourable for electron doping at low concentrations, and for higher concentrations both carriers are preferable, which shows possible device applications for all the compounds. Semiconductor-metal transition together with enhanced 2D nature is predicted in ReS_2 under the application of uni-axial strain in bulk ReS_2. In line with bulk, monolayer ReS_2 also emerges to be a metal at strained state (around 16 %), further emphasising the layer independent properties of ReS_2. The anisotropic property in the strained monolayer opens up the possibility of further dimension reduction in the system which need to be inspected. In addition to that, the thermoelectric properties are also analysed, and are found to be promising in ReS_2 for both bulk and layered forms. Our results indicate the possibility of using ReS_2 as a TE material in different forms.

Chapter 7

Conclusions

Thermoelectric properties of four series of compounds including Zn based pnctides, natural bulk super lattice materials, zintl phase compounds and few transition metal di-chalcogenides were investigated within the frame work of density functional theory and are reported as promising TE materials for a wide temperature range. Ground state properties, electronic structure, mechanical properties were examined systematically. Electronic structure and hence thermoelectric properties were tuned as a function of hydrostatic/uni-axial strain and the enhancement of TE properties are reported. Among the studied compounds, $ZnGeSb_2$ and Ca based zintl phase compounds were systematically examined for topological insulating nature, and our investigation on $ZnGeSb_2$ proposed the benefit of Dirac cone like band structure near the Fermi level for TE applications, and the study on Ca based zintl phase compounds explored the coexistence of strong topological insulating nature and potential TE properties. In the first study, we have chosen few Zn based pnictide compounds in the form $ZnXPn_2$ (X: Si, Ge, Sn; Pn: P, As, Sb), which possess high melting point, high earth abundance, and systematically examined the electronic and thermoelectric properties. Most of the investigated compounds were found to be promising TE material for a wide temperature range from 300 K to 900 K, and showed highly comparable TE performance with existing TE materials. Further we have selected two narrow band gap semiconductors from the above series such as $ZnGeSb_2$ and $ZnSnSb_2$ and examined the effect of hydrostatic strain on electronic and TE properties of the same. Both the compounds were found to be highly sensitive towards the applied strain, and found the gradual phase change from a normal semiconductor to topological semi-metal through Dirac states together with band topology change. Among them $ZnGeSb_2$ secured huge power factor value due to higher electrical conductivity. In the next study, we have chosen few natural bulk super-lattice materials, and these compounds in general possess low thermal conductivity, which is fruitful for TE applications. The quasi two dimensional nature of band structure is identified from band dispersion and effective mass calculations. The calculated thermopower values are found to be higher for all the compounds. Huge anisotropy is observed for electrical conductivity for hole doping, which again confirms the quasi two dimensional nature in these compounds. The transport properties of all the investigated compounds are comparable with the prototype material SrAgSF, which is reported as good TE material. The low value of Debye temperature and highly interacting acoustic and optical phonon modes confirm the possibility of low thermal conductivity in these compounds. Further we have extended our analysis of thermoelectric properties of these materials by calculating a parameter

known as 'A' parameter, which helps to decouple the relaxation time from the calculations. The calculated 'A' parameter have higher values than traditional TE materials, which further confirm the potential thermoelectric properties in this series. In the third study, we have examined CaSrX (X: Si, Ge, Sn, Pb), few zintl phase compounds. A systematic analysis of electronic, topological and transport properties were presented, and identified the studied materials as topological insulators at ambient conditions. The potential TE properties were also presented for the investigated compounds. The application of strain in these system gave insight to several interesting phenomena, which includes the formation of Dirac semi-metallic state with enhanced 2D nature, which opens up wide applications for the investigated compounds. In the last chapter, we have examined the thermoelectric properties of few transition metal dichalcogenides. Firstly, electronic and thermoelectric properties of OsX_2 were analysed. Huge value of thermopower is observed at low temperature around 100 K for hole doping for all the investigated compounds, which is found to be higher than well established TE materials. The mixture of heavy and light band mass in the band structure is reflected from the band structure. Analysis of thermoelectric properties revealed the potential TE application for a wide temperature range. All the investigated compounds are favourable for electron doping at low concentrations, and for higher concentrations both the carriers are preferable, which shows possible device applications for all the compounds. Further, we have examined th electronic and TE properties of ReX_2 (X: S, Se). Semiconductor-metal transition together with enhanced 2D nature is predicted in ReS_2 under the application of uni-axial strain in bulk ReS_2. In line with bulk, monolayer ReS_2 also emerges to be a metal at strained state (around 16 %), further emphasizing the layer independent properties of ReS_2. The anisotropic property in the strained monolayer opens up the possibility of further dimension reduction in the system which need to be inspected. In addition to that, the thermoelectric properties are also analysed, and are found to be promising in ReS_2 for both bulk and layered forms. Our results indicate the possibility of using ReS_2 as a TE material in different forms. Overall, the present thesis explored potential materials for thermoelectric applications for a wide temperature range, and proposed feasible methods for improving the thermoelectric properties of investigated compounds. Few of the investigated compounds such as OsS_2 are shown as promising TE properties for both 'n' and 'p' type doping, which might fetch device applications. $ZnGeSb_2$ secured high power factor value, which can be explored further experimentally, and ReS_2 can be used for bulk/thinfilm TE applications.

While summarizing the present thesis work, it is evident that few of the investigated compounds turned to be very promising TE material from electronic structure point of view. As we already know that the real parameter is figure of merit, which decide the performance of a TE material, we need to have an idea about thermal conductivity, and exact calculations of lattice thermal conductivity is beyond the scope of present thesis, and can be taken up as main future scope of the present study. Yet another interesting phenomena we have experienced in the present thesis is that few of the materials have shown strong topological nature, and found to possess highly linearized Dirac cone like band structure. To understand the influence of these peculiar electronic structure towards TE properties, we have to calculate the surface transport coefficients also, and this is again beyond the scope of present thesis. We strongly believe that the experimental realization of the above mentioned quantities might help to explore promising TE materials from the present study, resulting in device applications.

References

[1] Ashwani Kumar, Kapil Kumar, Naresh Kaushik, Satyawati Sharma, Saroj Mishra, Renewable energy in India: Current status and future potentials, *Renewable and Sustainable Energy Reviews*, 14, (2010) 2434-2442.

[2] Abdeen Mustafa Omer, The Energy Crisis, the Role of Renewable and Global Warming, *Greener Journal of Environment Management and Public Safety*, 1, (2012) 038-070.

[3] A. Mahmoudi, M. Fazli, M.R. Morad, A recent review of waste heat recovery by Organic Rankine Cycle, *Applied Thermal Engineering*, 143, (2018) 660-675.

[4] Hussam Jouhara, Navid Khordehgah, Sulaiman Almahmoud, Bertrand Delpech, Amisha Chauhan, Savvas A. Tassou, Waste heat recovery technologies and applications, *Thermal Science and Engineering Progress*, 6, (2018) 268-289.

[5] B. Orr, A. Akbarzadeh, M. Mochizuki, R. Singh, A review of car waste heat recovery systems utilising thermoelectric generators and heat pipes, *Applied Thermal Engineering*, 101, (2016) 490-495.

[6] Th. J. Seebeck, Magnetische Polarisation der Metalle und Erze Durch Temperatur-Differenz 1822-23 in Ostwald's Klassiker der Exakten Wissenshaften Nr. 70 (1895). Seebeck Biography 1. Seebeck Biography 2.

[7] W. Thomson, On the Dynamical Theory of Heat. *Trans. R. Soc. Edinburgh: Earth Sci.* 3, (1851) 91-98. Thomson Biography.

[8] E. Altenkirch, *Physikalische Zeitschrift* 10, (1909) 560-580 ; *Physikalische Zeitschrift* 12, (1911) 920.

[9] M. V. Vedernikov and E. K. Iordanishvili "A. F. Ioffe and origin of modern semiconductor thermoelectric energy conversion" 17th Int. Conf. on Thermoelectrics vol 1, pp 3742 (1998); A. F. Ioffe "Semiconductor Thermoelements and Thermoelectric Cooling"

[10] H. J. Goldsmid and R. W. Douglas, The use of semiconductors in thermoelectric refrigeration, *British J. Appl. Phys.* 5, (1954) 386.

[11] A. Eucken and G. Kuhn Z. "Ergebnisse neuer Messungen der Wrmeleitfhigkeit fester krystallisierter Stoffe bei 0 und 190 C" *Phys. Chem.*, 134, (1928) 193

[12] L. D. Hicks, M. S. Dresselhaus, Effect of quantum-well structures on the thermoelectric figure of merit, *Phys. Rev. B* 47, (1993) 12727.

[13] Xiao Zhang, Li-Dong Zhao, Thermoelectric materials: Energy conversion between heat and electricity, *Journal of Materiomics* 1 (2015) 92-105.

[14] Ran He, Gabi Schierning, and Kornelius Nielsch, Thermoelectric Devices: A Review of Devices, Architectures, and Contact Optimization, *Adv. Mater. Technol.*, 3, (2018) 1700256

[15] C. Wood, Materials for thermoelectric energy conversion, *Rep. Prog. Phys.*, 51, (1988) 459.

[16] D.M. Rowe, CRC Handbook of thermoelectric materials, CRC Press Published July 14, 1995

[17] GUANGHE LI, Thesis Enhancement of Thermoelectric Properties of Sb-based Bulk Materials by Crystal Structure Design, Graduate School of Engineering, Osaka University, https://doi.org/10.18910/50507

[18] Vijay Kumar Gudelli, V Kanchana, G Vaitheeswaran, Axel Svane, Niels Egede Christensen, Thermoelectric properties of chalcopyrite type $CuGaTe_2$ and chalcostibite $CuSbS_2$, *Journal of Applied Physics*, 114, (2014) 223707.

[19] G. Jeffrey Snyder and Eric S. Toberer, Complex thermoelectric materials, *Nature materials*, 7, (2008) 105.

[20] Y. Pei, H. Wang and G. J. Snyder, Band engineering of thermoelectric materials, *Adv. Mater.*, 24, (2012) 6125.

[21] J. P. Heremans, V. Jovovic, E. S. Toberer, A. Saramat, K. Kurosaki, A. Charoenphakdee, S. Yamanaka and G. J. Snyder, Enhancement of Thermoelectric Efficiency in PbTe by Distortion of the Electronic Density of States, *Science*, 321 (2008) 554.

[22] Y. Pei, X. Shi, A. LaLonde, H. Wang, L. Chen and G. J. Snyder, Convergence of electronic bands for high performance bulk thermoelectrics, *Nature*, 473, (2011) 66.

[23] Sergey V.Ovsyannikov, Natalia V.Morozova,Igor V.Korobeinikov, Lidia N.Lukyanova, Andrey Y.Manakov, Anna Y.Likhacheva, Alexey I.Ancharov, Alexander P.Vokhmyanin, Ivan F.Berger, A.Usov,Vsevolod A.Kutasov,Vladimir A.Kulbachinskii,TakuOkada,and Vladimir V.Shchennikov, Enhanced power factor and high-pressure effects in $(Bi,Sb)_2(Te,Se)_3$ thermoelectrics, *Appl. Phys. Lett.* 106, (2015) 143901.

[24] San-Dong Guo and Jian-Li Wang, Pressure enhanced thermoelectric properties in Mg_2Sn, *RSC.Adv.*, 6, (2016) 31272.

[25] Vassilios Vargiamidis and Neophytos Neophytou, Hierarchical nanostructuring approaches for thermoelectric materials with high power factors, *Phys. Rev. B* 99, (2019) 045405.

[26] M. Sabarinathan, M. Omprakash, S. Harish, M. Navaneethan, J. Archana, S. Ponnusamy, H. Ikeda, T. Takeuchi , C. Muthamizhchelvan, Y. Hayakawa, Enhancement of power factor by energy filtering effect in hierarchical $BiSbTe_3$ nanostructures for thermoelectric applications, *Applied Surface Science*, 418, (2017) 246-251.

[27] P. Pichanusakorn and P. R. Bandaru, Minimum length scales for enhancement of the power factor in thermoelectric nanostructures , *J. of Appl. Phys.* 107, (2010) 074304.

[28] Kubakaddi, S and Basavaraj G, Mulimani and Jali, V M, Thermopower in Quasi-Two-Dimensional Semiconductor Quantum Well Structures, *physica status solidi* 137, (1986) 683-689.

[29] Sunao Shimizu, Mohammad Saeed Bahramy, Takahiko Iizuka, Shimpei Ono Kazumoto Miwa, Yoshinori Tokura, and Yoshihiro Iwasa, Enhanced thermopower in ZnO two-dimensional electron gas, *PNAS*. 113(23) (2016), 6438-6443.

[30] Te-Huan Liu Jiawei Zhoua Mingda Lia, Zhiwei Ding, Qichen Song, Bolin Liao, Liang Fud, and Gang Chena, Electron mean-free-path filtering in Dirac material for improved thermoelectric performance, *PNAS*, 115 (5), (2018) 879-884.

[31] Herwin Ahuja, Bao Yang, PhD Thanh N. Tran - Thermoelectric Technology Assessment: Application to Air Con- ditioning and Refrigeration, *HVACR Research*, 14 (2008) 635-653.

[32] Weishu Liu, Xiao Yan, Gang Chen and Zhifeng Ren, Recent Advances in Thermoelectric Nanocomposites, *Nano Energy*, 1, (2012) 42-56.

[33] S Bhattacharya, A L Pope, R T Littleton IV and T M Tritt - Effect of Sb Doping on the Thermoelectric Properties of Ti - nased Half Heusler Compounds, $TiNiSn_{1-x}$ Sb_x, *Applied Physics Letters*, 77, (2000) 16.

[34] Mishra, S. K., S. Satpathy, and O. Jepsen, Electronic structure and thermoelectric properties of bismuth telluride and bismuth selenide, *J. Phys. Condens. Matter*, 9, (1997) 461.

[35] Thonhauser, T., T. J. Scheidemantel, J. O. Sofo, J. V. Badding, and G. D. Mahan. Thermoelectric properties of Sb_2Te_3 under pressure and uniaxial stress. *Phys. Rev. B*, 68 (2003) 085201.

[36] Hinsche, N. F., B. Yu. Yavorsky, I. Mertig, and P. Zahn. . Influence of strain on anisotropic thermoelectric transport in Bi_2Te_3 and Sb_2Te_3, *Phys. Rev. B*, 84, (2011) 165214.

[37] Y. L. Chen, J. G. Analytis, J.-H. Chu, Z. K. Liu, S.-K. Mo, X. L. Qi, H. J. Zhang, D. H. Lu, X. Dai, Z. Fang, S. C. Zhang, I. R. Fisher, Z. Hussain and Z.-X. Shen, Experimental Realization of a Three-Dimensional Topological Insulator, Bi_2Te_3, *Science*, 325, (2009) 178-181.

[38] Shi, H., D. Parker, M. H. Du, and D. J. Singh. Connecting thermoelectric performance and topological-Behavior: Bi 2 Te 3 and Bi 2 Te 2 Se from first principles. *Phys. Rev. Appl.* 3, (2015) 014004.

[39] Haijun Zhang, Chao-Xing Liu, Xiao-Liang Qi, Xi Dai, Zhong Fang1and Shou-Cheng Zhang, Topological insulators in Bi_2Se_3, Bi_2Te_3 and Sb_2Te_3 with a single Dirac cone on the surface, *Nature Physics*, 5, (2009) 438-442.

[40] Venkatasubramanian R, Siivola E, Colpitts T, O'Quinn B., Thin-film thermoelectric devices with high room-temperature figures of merit, *Nature*. 413, (2001) 597-602.

[41] Lyden, H. A. . Temperature dependence of the effective masses in PbTe. *Phys. Rev.* 135, (1964) 514521.

[42] Tauber, R., A. Machonis, and I. Cadoff, Thermal and optical energy gap in PbTe. *J. Appl. Phys.*, 37, (1966) 4855-4860.

[43] Greig, D, Thermoelectricity and thermal conductivity in the lead sulfide group of semiconductors. *Phys. Rev.*, 120, (1960) 358-365.

[44] Heremans, J. P., V. Jovovic, E. S. Toberer et al. Enhancement of thermoelectric efficiency in PbTe. *Science*, 321, (2008), 554-557.

[45] Hsu, K. F., S. Loo, F. Guo, Wei Chen, Jeffrey S. Dyck, Ctirad Uher, Tim Hogan, E. K. Polychroniadis, Mercouri G. Kanatzidis, Cubic $AgPb_{(m)}SbTe_{(2+m)}$: Bulk thermoelectric materials with high figure of merit. *Science* 303, (2004) 818-821.

[46] Biswas, K, He J, Blum ID, Wu CI, Hogan TP, Seidman DN, Dravid VP, Kanatzidis MG., High-performance bulk thermoelectrics with all-scale hierarchical architectures. *Nature*, 489, (2012) 414-418.

[47] Zhao, L., H. Wu, S. Hao, C. I. Wu, X. Y. Zhou, K. Biswas, J. Q. He, T. P. Hogan, C. Uher, C. Wolverton, V. P. Dravid, M. G. Kanatzidis, All-scale hierarchical thermoelectrics: MgTe in PbTe facilitates valence band convergence and suppresses bipolar thermal transport for high performance. *Energy Environ. Sci.*, 6, (2013) 3346-3355.

[48] Pei, Y., J. LenschFalk, E. S. Toberer, D. L. Medlin, and G. J. Snyder, High thermoelectric performance in PbTe due to large nanoscale Ag_2Te precipitates and La doping. *Adv. Funct. Mater.*, 21, (2011) 241-249.

[49] Kanatzidis, M. G. Nanostructured thermoelectrics: The new paradigm? *Chem. Mater.*, 22, (2009) 648-659.

[50] Poudeu, P. F., J. DAngelo, A. D. Downey, J. L. Short, T. P. Hogan, and M. G. Kanatzidis. High thermoelectric figure of merit and nanostructuring in bulk p-type Na1x Pb m Sb y Te m+2 . *Angew. Chem.* 118, (2006) 3919-3923.

[51] de Boor, J., S. Gupta, H. Kolb, T. Dasgupta, and E. Mller. Thermoelectric transport and microstructure of optimized Mg 2 Si 0.8 Sn 0.2 . *J. Mater. Chem. C.*, 3, (2015) 10467-10475.

[52] Tani, J.-I. and H. Kido, Thermoelectric properties of Sb-doped Mg_2Si semiconductors, *Intermetallics*, 15, (2007) 1202-1207.

[53] Gao, P., I. Berkun, R. Schmidt, Matthew F. LuzenskiXu LuPatricia Bordon SaracEldon D. CaseTimothy P. Hogan, Transport and mechanical properties of high-ZT $Mg_{2.08}Si_{0.4x}Sn_{0.6}Sb_x$ thermoelectric materials, *J. Electron. Mater.*, 43, (2013) 1790-1803.

[54] Zaitsev, V. K., M. I. Fedorov, E. A. Gurieva, I. S. Eremin, P. P. Konstantinov, A. Y. Samunin, and M. V. Vedernikov, Highly effective $Mg_2Si_{1x}Sn_x$ thermoelectrics, *Phys. Rev. B*, 74, (2006) 045207.

[55] Dasgupta, T., C. Stiewe, J. de Boor, and E. Mller. 2014. Influence of power factor enhancement on the thermoelectric figure of merit in $Mg_2Si_{0.4}Sn_{0.6}$ based materials, *Phys. Stat. Solidi*, 21, (2014) 1250-1254.

[56] Wei Liu, Xiaojian Tan, Kang Yin, Huijun Liu, Xinfeng Tang, Jing Shi, Qingjie Zhang, and Ctirad Uher, Convergence of conduction bands as a means of enhancing thermoelectric performance of n-type $Mg_2Si_{1x}Sn_x$ solid solutions, *Phys. Rev. Lett.*, 108, (2012) 166601.

[57] Fedorov, M. I. and V. K. Zaitsev. 2005. Thermoelectrics of transition metal silicides. In Thermoelectrics Handbook: Macro to Nano, ed. D. M. Rowe. CRC Press, Boca Raton, FL.

[58] Ikuto Aoyama, Mikhail I. Fedorov, Vladimir K. Zaitsev, Fedor Yu. Solomkin, Ivan S. Eremin, Aleksandr Yu. Samunin, Mika Mukoujima, Seijiro Sano and Toshihide Tsuji, 2005. Effects of Ge doping on micromorphology of MnSi in MnSi 1.7 and on their thermoelectric transport properties, *Jpn. J. Appl. Phys.*, 44, (2005) 8562.

[59] Voronov, B. K., L. D. Dudkin, and N. N. Trusova, Anisotropy of thermoelectric properties in single crystals of chromium disilicide and higher manganese silicide, *Kristallografia* 12, (1967) 1137.

[60] Ikuto Aoyama, Hiromasa Kaibe, Lutz Rauscher, Toshio Kanda, Mika Mukoujima, Seijiro Sano and Toshihide Tsuji, Doping effects on thermoelectric properties of Higher Manganese Silicides (HMSs, MnSi 1.74) and characterization of thermoelectric generat-ing module using p-type (Al, Ge and Mo)-doped HMSs and n-type $Mg_2Si_{0.4}Sn_{0.6}$ legs, *Jpn. J. Appl. Phys.* 44, (2005) 4275.

[61] Migas, D. B., V. L. Shaposhnikov, A. B. Filonov, V. E. Borisenko, and N. N. Dorozhkin, Ab initio study of the band structures of different phases of higher manganese silicides, *Phys. Rev.B*, 77, (2008) 075205.

[62] Kanibolotskii, D. S. and V. V. Lesnyak, Thermodynamic properties of Mn-Si alloys, *Russ. Metall.*, 2006, (2006) 199-205.

[63] Kaibe, H., L. Rauscher, I. Aoyama et al. 2004. Development of the thermoelectric generating modules using silicide. In Proceedings of the 23rd International Conference on Thermoelectrics, ICT 2004, Adelaide, South Australia, Australia.

[64] Karina R.Tarantik, Jan D. Knig, Martin Jgle, Jana Heuer, Jan Horzella, Andreas Mahlke, Marc Vergez, Kilian Bartholom, Thermoelectric modules based on silicides Development and characterization, *Mater. Today Proc.*, 2, (2015) 588-595.

[65] Kim, J. H., N. L. Okamoto, K. Kishida, K. Takata, and H. Inui, High thermoelectric per- formance of type-III clathrate compounds of the Ba-Ge-Ga system. *Acta Mater.* 54, (2006) 2057-2062.

[66] Saiga, Y., B. Du, S. K. Deng, K. Kajisa, and T. Takabatake, Thermoelectric properties of type-VIII clathrate Ba 8 Ga 16 Sn 30 doped with C, *J. Alloys Compd*, 537, (2012) 303-307.

[67] Koda, S., K. Kishimoto, K. Akai, H. Asada, and T. Koyanagi. Thermoelectric and transport properties of sintered n-type K_8 $Ba_{16}Ga_{40}Sn_{96}$ with type-II clathrate structure, *J. Appl. Phys.* 116, (2014) 023710.

[68] Poon, S. J. . Electronic and thermoelectric properties of half-Heusler alloys, Chapter 2. In: Tritt T. M. (ed.), Semiconductors and Semimetals, Recent Trends in Thermoelectric Materials Research, *Academic Press*, San Diego, 70, (2000) 37-76.

[69] Yu, C., T. J. Zhu, R. Z. Shi, Yun Zhang, Xin-Bing Zhao, Jian He, High-performance half-Heusler thermoelectric materials Hf_{1x} $Zr_xNiSn_{1y}Sb_y$ prepared by levitation melting and spark plasma sintering, *Acta Mater.* 57, (2009) 2757-2764.

[70] Maji, P., N. J. Takas, D. K. Misra et al. Effects of Rh on the thermoelectric performance of the p-type $Zr_{0.5}Hf_{0.5}Co_{1x}Rh_xSb_{0.99}Sn_{0.01}$ half-Heusler alloys, *J. Solid State Chem.*, 183, (2010) 1120-1126.

[71] Yaqub, R., P. Sahoo, J. P. A. Makongo, Takas, Nathan, Poudeu, Pierre F. P, Stokes, Kevin L, Investigation of the effect of NiO nanoparticles on the transport properties of $Zr_{0.5}Hf_{0.5}Ni_{1x}Pd_xSn_{0.99}Sb_{0.01}$ (x = 0 and 0.2). *Sci. Adv. Mater.* 3, (2011) 633-638.

[72] Culp, S. R., J. W. Simonson, S. J. Poon et al. (Zr, Hf)Co(Sb, Sn) half-Heusler phases as high temperature (¿700C) p-type thermoelectric materials. *Appl. Phys. Lett.* 93, (2008) 022105.

[73] Becquerel, A. C. *Ann. Chim. Phys.* 35, (1827) 328.

[74] Becquerel, A. E. *Ann. Chim. Phys.*, 48, (1866) 389.

[75] Brown, D. R., T. Day, T. Caillat, and G. J. Snyder. Chemical stability of $(Ag,Cu)_2Se$: A historical overview, *J. Electron. Mater*, 42, (2013) 2014-2019.

[76] Hinderman, J. D. 1979. Thermoelectric materials evaluation program. Annual technical report for fiscal year (Report No. MMM-2331-0642) (DOE, 1979), Minnesota Mining and Mfg. Co., St. Paul, MN. doi: 10.2172/5741759.

[77] Osmeyer, W. E. 1979. Selenide isotope generator for the Galileo Mission. Program final report (Report no. TES-33009-46) (DOE, 1979), Teledyne Energy Systems, Hunt Valley, Maryland. doi:10.2172/5928964.

[78] Liu, H., X. Shi, F. Xu, Zhang L, Zhang W, Chen L, Li Q, Uher C, Day T, Snyder GJ, Copper ion liquid-like thermoelectrics, *Nat. Mater.* 11, (2012), 422-425.

[79] Xiao, X. X., W. J. Xie, X. F. Tang, and Q. J. Zhang, Phase transition and high temperature thermoelectric properties of copper selenide $Cu_{2x}Se_{(0x0.25)}$, *Chin. Phys. B*, 20, (2011) 087201.

[80] Yu, B., W. S. Liu, S. Chen, Wang, Hui; Wang, Hengzhi; Chen, Gang; Ren, Zhifeng, Thermoelectric properties of copper selenide with ordered selenium layer and disordered copper layer, *Nano Energy*, 1, (2012) 472-478.

[81] Ballikaya, S., H. Chi, J. R. Salvador, and C. Uher, Thermoelectric properties of Ag-doped Cu 2 Se and Cu 2 Te., *J. Mater. Chem. A*, 1, (2013) 12478-12484.

[82] Liu, H. L., X. Yuan, P. Lu, Xun Shi, Fangfang Xu, Ying He, Yunshan Tang, Shengqiang Bai, Wenqing Zhang, ong Chen, Yue Lin, Lei Shi, He Lin, Xingyu Gao, Xingmin Zhang, Hang Chi and Ctirad Uher, Ultrahigh thermoelectric performance by electron and phonon critical scattering in $Cu_2Se_{1x}I_x$, *Adv. Mater.* 25, (2013) 6607-6612.

[83] Zhao, L.-D., V. P. Dravid, and M. G. Kanatzidis. The panoscopic approach to high performance thermoelectrics, *Energy Environ. Sci.*, 7, (2014) 251-268.

[84] Zhao, L.-D., J. He, D. Berardan, Yuanhua Lin, Jing-Feng Li, Ce-Wen Nan, Nita Dragoe, BiCuSeO oxyselenides: New promising thermoelectric materials, *Energy Environ. Sci.*, 7, (2014) 2900-2924.

[85] Schaefer, H, On the problem of polar intermetallic compounds: The stimulation of E. Zintls work for the modern chemistry of intermetallics, *Ann. Rev. Mater. Sci.*, 15, (1985) 1-41.

[86] von Schnering, H. G, Homoatomic bonding of main group elements, *Angew. Chem. Int. Ed.*, 20, (1981) 33-51.

[87] Gascoin, F., S. Ottensmann, D. Stark., M. S. Haile, and G. Snyder, Zintl phases as thermoelectric materials: Tuned transport properties of the compounds $Ca_xYb_{1x}Zn_2Sb_2$. *Adv. Funct. Mater.*, 15, (2005) 1860-1864.

[88] Snyder, G. J., M. Christensen, E. Nishibori, T. Caillat, and B. B. Iversen. . Disordered zinc in Zn_4Sb_3 with phonon-glass and electron-crystal thermoelectric properties, *Nat. Mater.*, 3, (2004) 458-463.

[89] Paik, J.-A., E. Brandon, T. Calliat, R. Ewell, and J. P. Fleurial. 2011. Life testing of $Yb_{14}MnSb_{11}$ for high performance thermoelectric couples, *Nuclear and Emerging Technologies for Space (NETS)* 2011, Albuquerque, NM, February 7-10, 2011.

[90] Kauzlarich, S. M., S. R. Brown, and G. J. Snyder, Zintl phases for thermoelectric devices, *Dalton Trans.*, 21,(2007) 2099-2107.

[91] Toberer, E. S., A. F. May, and G. J. Snyder, Zintl chemistry for designing high efficiency thermoelectric materials. *Chem. Mater.* 22, (2010) 624-634.

[92] Cahill, D., S. Watson, and R. Pohl, Lower limit to the thermal conductivity of disordered crystals. *Phys. Rev. B* 46, (1992) 6131-6140

[93] Zheng XF, Yan YY, Simpson K. A potential candidate for the sustainable and reliable domestic energy generation-thermoelectric cogeneration system. *Appl Therm Eng*, 53, (2012) 305-11.

[94] Ma H-K, Lin C-P, Wu H-P, Peng C-H, Hsu C-C. Waste heat recovery using a thermoelectric power generation system in a biomass gasifier. *Appl Therm Eng*, 88, (2015) 274-279.

[95] Suh I-S, Cho H, Lee M. Feasibility study on thermoelectric device to energy storage system of an electric vehicle. *Energy*, 76, (2014), 436-44.

[96] Weng C-C, Huang M-J. A study of using a thermoelectric generator to harvest energy from a table lamp. *Energy*, 76, (2014) 788-98.

[97] H. J. Wu, L.-D. Zhao, F. S. Zheng, D. Wu, Y. L. Pei, X. Tong, M. G. Kanatzidis and J. Q. He, Broad temperature plateau for thermoelectric figure of merit ZT¿2 in phase-separated $PbTe_{0.7}S_{0.3}$, *Nat. Commun.*, 5, (2014) 4515.

[98] M. Born and R. Oppenheimer, Quantum theory of the molecules, *Ann. der Physik*, 84, (1927) 457.

[99] P. Hohenberg and W. Kohn, Inhomogeneous electron gas, *Phys. Rev.*, 136, (1964) B864.

[100] W. Kohn and L. J. Sham, Self-consistent equations including exchange and correlation effects, *Phys. Rev.* 140(4A), (1965) A1133-A1138.

[101] R. G. Parr and W. Yang, Density functional theory of atoms and molecules, Oxford University, Oxford, 1989.

[102] W. Kohn, Nobel Lecture: Electronic structure of matterwave functions and density functionals, *Rev. Mod. Phys.*, 71, (1998) 1253-1266.

[103] R. O. Jones and O. Gunnarsson, The density functional formalism, its applications and prospects, *Rev. Mod. Phys.*, 61, (1989) 689-746.

[104] W. Koch and M. C. Holthausen, A Chemists guide to density functional theory, WILEY-VCH 2001.

[105] M. R. Dreizler and E. K. U. Gross, Density functional theory : An approach to the quantum many-body problem, Springer, Berlin, 1990.

[106] N. M. Harrison, An introduction to density functional theory, 2002 ($http : //www.ch.ic.ac.uk/harrison/Teaching/DFT_N ATO.pdf$.).

[107] Richard M. Martin, Electronic structure: basic theory and practical methods, Cambridge University Press, Cambridge, UK; New York, 2004. ISBN 0521782856.

[108] Klaus Capelle, A bird's-eye view of density-functional theory, November 2006 ($http : //arxiv.org/abs/cond - mat/0211443v5$).

[109] L. H. Thomas, The calculation of atomic fields, *Math. Proc. Cambridge*, 23, (1927) 542.

[110] E. Fermi, Un Metodo Statistico per la Determinazione di alcune Prioprietá dell'Atomo, *Rend. Accard. Naz. Lincei* 6, (1927) 602.

[111] I. N. Levine, Quantum Chemistry, Prentice-Hall of India Private Limited, 2006.

[112] F. Herman, J. P. Van Dyke, and I. B. Ortenburger, Improved Statistical Exchange Approximation for Inhomogeneous Many-Electron Systems, *Phys. Rev. Lett.*, 22, (1969) 807.

[113] Fabien Tran and Peter Blaha, Accurate Band Gaps of Semiconductors and Insulators with a Semilocal Exchange-Correlation Potential, *Phys. Rev. Lett* 102, (2009) 226401.

[114] Axel D. Becke and Erin R. Johnson, A simple effective potential for exchange, *J. Chem. Phys.* 124, (2006) 221101

[115] P. Blaha, K. Schwarz, G. K. H. Madsen, D. Kvasnicka and J. Luitz, WIEN2k, An augmented plane wave + local orbitals program for calculating crystal properties (Karlheinz Schwarz, Techn. Universit t Wien, Austria), 2001 $< http://www.wien2k.at/ >$. P. Blaha, K. Schwarz, P. I. Sorantin and S. B. Tricky, Full-potential linearinsed augmented plane wave programs for crystalline systems, *Computer. Phys. Commun.*, 59, (1990) 399-415.

[116] P. Giannozzi, S. Baroni, N. Bonini, M. Calandra, R. Car, C. Cavazzoni, D. Ceresoli, G. L. Chiarotti, M. Cococcioni, I. Dabo, et al. QUANTUM ESPRESSO: a modular and open-source software project for quantum simulations of materials. *J. Phys.: Condens. Matter*, 21, (2009) 395502-1-395502-19 ($< http://www.pwscf.org >$).

[117] Liang Fu and C. L. Kane, Topological insulators with inversion symmetry, *Phys. Rev. B* 76, (2007) 045302.

[118] A. A. Mostofi, J. R. Yates, G. Pizzi, Y.-S. Lee, I. Souza, D. Vanderbilt and N. Marzari, An updated version of wannier90: A Tool for Obtaining Maximally-Localised Wannier Functions, *Comput. Phys. Commun.* 185, (2014) 2309.

[119] Nicola Marzari, Arash A. Mostofi, Jonathan R. Yates, Ivo Souza, David Vanderbilt, Maximally localized Wannier functions: Theory and applications, *Rev. Mod. Phys.* 84, (2012) 1419.

[120] J. M Ziman, Electrons and phonons: The theory of transport phenomena in solids, Oxford University Press, USA, 2001.

[121] R. Kubo, Statistical-Mechanical Theory of Irreversible Processes. I. General Theory and Simple Applications to Magnetic and Conduction Problems, *Journal of the Physical society of Japan*, 12, (1957), 570.

[122] G. K. H. Madsen and D.J Singh, BoltzTraP. A code for calculating band-structure dependent quantities, *Comput. Phys. Commun*, 175, (2006) 67-71.

[123] Farahi, N., M. VanZant, J. B. Zhao, Tse JS, Prabhudev S, Botton GA, Salvador JR, Borondics F, Liu Z, Kleinke H, Sb-and Bi-doped Mg_2Si: Location of the dopants, micro- and nanostructures, electronic structures and thermoelectric properties. *Dalton Trans.*, 43, (2014), 14983-14991.

[124] Bourgeois, J., J. Tobola, B. Wiendlocha, L. Chaput, P. Zwolenski, D. Berthebaud, F. Gascoin, Q. Recour, and H. Scherrer, Study of electron, phonon and crystal stability

versus thermoelectric properties in Mg_2X (X = Si, Sn) compounds and their alloys. *Funct. Mater. Lett.* 06, (2013) 1340005.

[125] K. P. Ong, D. J. Singh and P. Wu, Analysis of the thermoelectric properties of n-type ZnO, *Phys. Rev. B*, 83, (2011) 115110.

[126] D. J. Singh and I. I. Mazin, Calculated thermoelectric properties of La-filled skutterudites, *Phys. Rev. B*, 56, (1997) R1650.

[127] J. L. Shay and J. H. Wernick (Auth.)-Ternary Chalcopyrite Semiconductors Growth, Electronic Properties and Applications - Pergamon Press (1975).

[128] M. D. Lind and R. W. Grant, Structural dependence of birefringence in the chalcopyrite structure. Refinement of the structural parameters of $ZnGeP_2$ and $ZnSiAs_2$, *J. Chem. Phys.* 58,(1973) 357-362 .

[129] V. Kumar and S. K. Tripathy, First-principle calculations of the electronic, optical and elastic properties of $ZnSiP_2$ semiconductor, *J. Alloys Compd.* 582, (2014) 101-107.

[130] M. Turowski, G. Margaritondo, M. K. Kelly and R. D. Tomlinson, Photoemission studies of $CuInSe_2$ and $CuGaSe_2$ and of their interfaces with Si and Ge, *Phys. Rev. B*, 31, (1985) 1022-1027.

[131] G. A. Medvedkin and V. G. Voevodin, Magnetic and optical phenomena in nonlinear optical crystals $ZnGeP_2$ and $CdGeP_2$, *J. Opt. Soc. Am. B*, 22, (2005) 1884-1898.

[132] S. Das, Pump tuned wide tunable noncritically phase-matched $ZnGeP_2$ narrow line width optical parametric oscillator, *Infrared Physics and Technology*, 69, (2015) 13.

[133] Y. Xu, Z. M. Ao, D. F. Zou, G. Z. Nie, W. Sheng, D. W. Yuan, Strain effects on the electronic structure of $ZnSnP_2$ via modified BeckeJohnson exchange potential, *Phys. Lett. A*, 379, (2015) 427-430.

[134] A. H. Reshak, Transport properties of mixed $CuAl(S_{1x}Se_x)_2$ as promising thermoelectric crystalline materials, *J. Phys. Chem. Solid*, 78, (2015) 46-52.

[135] B. Yao, J. Yuan, J. Li, T. Dai, X. Duan, Y. Shen, Z. Cui and Y. Pan, High-power Cr2+:ZnS saturable absorber passively Q-switched Ho:YAG ceramic laser and its application to pumping of a mid-IR OPO, *Opt. Lett.*, 40, (2015) 348-351.

[136] Z. Zhang, D. T. Reid, S. C. Kumar, M. E. -Z, P. G. Schunemann, K. T. Zawilski and C. R. Howle, Femtosecond-laser pumped CdSiP2 optical parametric oscillator producing 100MHz pulses centered at 6.2m, *Opt. Lett.*, 38, (2013) 5110-5113.

[137] D. O. Scanlon and A. Walsh, Bandgap engineering of $ZnSnP_2$ for high-efficiency solar cells, *App. Phy. Lett.* 100, (2012) 251911.

[138] J. E. Jaffe and A. Zunger, Theory of the band-gap anomaly in ABC_2 chalcopyrite semiconductors, *Phys. Rev. B*, 30, (1984) 741-756 .

[139] V. Kumar, B. P. Singh and B. P. Pandey, First-principle calculations of the elastic properties of AIIBIVC2V semiconductors, *Comput. Mater. Sci.*, 87, (2014) 227-231.

[140] D. Parker and D. J. Singh, Thermoelectric properties of $AgGaTe_2$ and related chalcopyrite structure materials *Phys. Rev. B*, 85, (2012) 125209 .

[141] V. K. Gudelli, V. Kanchana, G. Vaitheeswaran, A. Svane and N. E. Christensen, Thermoelectric properties of chalcopyrite type $CuGaTe_2$ and chalcostibite $CuSbS_2$, *J. Appl. Phys.* 114, (2013) 223707

[142] V. K. Gudelli, V. Kanchana and G. Vaitheeswaran, $CuAlTe_2$: A promising bulk thermoelectric material, *J. Alloys Compd.* 648, (2015) 958-965.

[143] T. Plirdpring, K. Kurosaki, A. Kosuga, T. Day, S. Firdosy, V. Ravi, G. J. Snyder, A. Harn- wunggmoung, T. Sugahara, Y. Ohishi, H. Muta and S. Yamanaka, Chalcopyrite $CuGaTe_2$: A HighEfficiency Bulk Thermoelectric Material, *Adv. Mater.* 24, (2012) 3622-3626

[144] K.MasumotoS.IsomuraW.Goto, The preparation and properties of $ZnSiAs_2$, $ZnGeP_2$ and $CdGeP_2$ semiconducting compounds, Journal of Physics and Chemistry of Solids, 27, (1966), 1939-1947.

[145] Brian Piccione, Daniel S. Gianola, Tunable thermoelectric transport in nanomeshes via elastic strain engineering, *Appl. Phys. Lett*, 106, (2015) 113101.

[146] V. Sergey, Ovsyannikov, V. Natalia, Morozova, V. Igor, Korobeinikov, N. Lidia, Lukyanova, Y. Andrey, Manakov, Anna Y. Likhacheva, I. Alexey, Ancharov, P. Alexander, Vokhmyanin, F. Ivan, Berger, A. Oleg, Usov, A. Vsevolod Kutasov, A. Vladimir, Kulbachinskii, Taku Okada, Vladimir V. Shchennikov, Enhanced power factor and high-pressureeffects in (Bi,Sb)2(Te,Se)3 thermoelectrics, *Appl. Phys. Lett*, 106, (2015) 143901

[147] Lukas M uchler, Frederick Casper, and Binghai Yan, Topological insulators and thermoelectric materials, *Physica Status Solidi Rapid Research Letters*, 7, (2013) 91-100.

[148] Hongliang Shi, David Parker, Mao-Hua Du, and David J. Singh, Connecting Thermoelectric Performance and Topological-Insulator Behavior: Bi_2Te_3 and Bi_2Te_2Se from First Principles *Physical Review Applied*, 3, (2015), 014004.

[149] D. L. Miller, K. D. Kubista, G. M. Rutter, Ming Ruan, W. A. de Heer, P. N. First and Joseph A. Stroscio, Observing the Quantization of Zero Mass Carriers in Graphene, *Science* 324, (2009), 924.

[150] Yan Lu, Ying Song, Fuping Wang, Thermoelectric properties of graphene nanosheets-modified polyaniline hybrid nanocomposites by an in situ chemical polymerization, *Materials Chemistry and Physics*, 138, (2013) 238-244.

[151] Y Chen, T Jayasekera, A Calzolari, K W Kim and M Buongiorno Nardelli, Thermoelectric properties of graphene nanoribbons, junctions and superlattices, *J. Phys.: Condens. Matter,* 22, (2010) 372202.

[152] Junxi Duan, Xiaoming Wang, Xinyuan Lai, Guohong Li, Kenji Watanabe, Takashi Taniguchi, Mona Zebarjadi, Eva Y. Andrei, High thermoelectricpower factor in graphene/hBN devices, *PNAS*, 113 (50), (2016) 14272-14276.

[153] Takafumi Sato, Kouji Segawa, Hua Guo, Katsuaki Sugawara, Seigo Souma, Takashi Takahashi and Yoichi Ando, Direct Evidence for the Dirac-Cone Topological Surface States in the Ternary Chalcogenide $TlBiSe_2$, *Phys. Rev. Lett.* 105, (2010) 136802 .

[154] Haijun Zhang, Chao-Xing Liu, Xiao-Liang Qi, Xi Dai, Zhong Fang and Shou-Cheng Zhang, Topological insulators in Bi_2Se_3, Bi_2Te_3 and Sb_2Te_3 with a single Dirac cone on the surface, *Nature Physics*, 5, (2009) 438 .

[155] Liu. Z. K, B. Zhou, Y. Zhang, Z. J. Wang, H. M. Weng, D. Prabhakaran, S.-K. Mo, Z. X. Shen, Z. Fang, X. Dai, Z. Hussain and Y. L. Chen,Discovery of a Three-Dimensional Topological Dirac Semimetal, Na_3Bi, *Science*, 343, (2014) 864.

[156] Madhab Neupane, Su-Yang Xu, Raman Sankar, Nasser Alidoust, Guang Bian, Chang Liu, Ilya Belopolski, Tay-Rong Chang, Horng-Tay Jeng, Hsin Lin, Arun Bansil, Fangcheng Chou and M. Zahid Hasan, Observation of a three-dimensional topological Dirac semimetal phase in high-mobility Cd_3As_2, *Nat. Commun*, 5, 2014, 3786.

[157] Borisenko. S, Quinn Gibson, Danil Evtushinsky, Volodymyr Zabolotnyy, Bernd Bchner and Robert J. Cava, Experimental Realization of a Three-Dimensional Dirac Semimetal, *Phys. Rev. Lett.* 113, (2014) 027603.

[158] B. A. Assaf, T. Phuphachong, V.V. Volobuev, A. Inhofer, G. Bauer, G. Springholz, L.A. de Vaulchier and Y. Guldner, Massive and massless Dirac fermions in $Pb_{1x}Sn_xTe$ topological crystalline insulator probed by magneto-optical absorption, *Sci Rep.* 6, (2016) 20323.

[159] Kyu Won Lee and Cheol Eui Lee., Extreme sensitivity of the electric-field-induced band gap to the electronic topological transition in sliding bilayer graphene, *Sci Rep.*, 5, (2015) 17490.

[160] A. Varykhalov, J. Snchez-Barriga, D. Marchenko, P. Hlawenka, P. S. Mandal and O. Rader, Tunable Fermi level and hedgehog spin texture in gapped graphene, *Nat. Commun.* 2015, 6, 7610.

[161] Rex Lundgren, Pontus Laurell and Gregory A. Fiete, Thermoelectric properties of Weyl and Dirac semimetals, *Phys. Rev. B*, 90, (2014) 165115

[162] P. Blaha, K. Schwarz, G. K. H. Madsen, D. Kvasnicka and J.Luitz. $WIEN2k$, An augmented plane wave +local orbitals program for calculating crystal properties, Karlheinz Schwarz, Techn. Universitat Wien, Austria (2001).

[163] P. Blaha, K. Schwarz, P. I. Sorantin and S. B. Tricky, Full-potential, linearized augmented plane wave programs for crystalline systems, *Comput. Phys. Commun.* 59, (1990) 399 .

[164] J. P. Perdew, K. Burke and M. Ernzerhof, Generalized Gradient Approximation Made Simple, *Phys. Rev. Lett.* 77, (1996) 3865.

[165] A. D. Becke and E. R. Johnson, A simple effective potential for exchange, *J. Chem. Phys.* 124, (2006) 221101.

[166] F. Tran, P. Blaha, Accurate Band Gaps of Semiconductors and Insulators with a Semilocal Exchange-Correlation Potential, *Phys. Rev. Lett.* 102, (2009) 226401.

[167] D. J. Singh, Electronic structure calculations with the Tran-Blaha modified Becke-Johnson density functional, *Phys. Rev. B* 82, (2010) 205102.

[168] D. Koller, F. Tran and P. Blaha, Merits and limits of the modified Becke-Johnson exchange potential, *Phys. Rev. B*, 83, (2011) 195134.

[169] G. K. H. Madsen and D.J Singh, BoltzTraP. A code for calculating band-structure dependent quantities, *Comput. Phys. Commun*, 175, (2006) 67-71.

[170] T. J. Scheidemantel, C. Ambrosch-Draxl, T. Thonhauser, J. V. Badding and J.O. Sofo, Transport coefficients from first-principles calculations, *Phys. Rev. B*, 68, (2003) 125210.

[171] L. Jodin, J. Tobola, P. P echeur, H. Scherrer and S. Kaprzyk, Effect of substitutions and defects in half-Heusler FeVSb studied by electron transport measurements and KKR-CPA electronic structure calculations, *Phys. Rev. B*,70, (2004) 184207.

[172] L. Chaput, P. Pecheur, J. Tobola and H. Scherrer, Transport in doped skutterudites: Ab initio electronic structure calculations, *Phys. Rev. B*, 72, (2005) 085126.

[173] K. P. Ong, D. J. Singh and P. Wu, Analysis of the thermoelectric properties of n-type ZnO, *Phys. Rev. B*, 83, (2011) 115110.

[174] D. J. Singh and I. I. Mazin, Calculated thermoelectric properties of La-filled skutterudites, *Phys. Rev. B*, 56, (1997) R1650.

[175] D. Parker and D. J. Singh, High-temperature thermoelectric performance of heavily doped PbSe, *Phys. Rev. B*, 82, (2010) 035204.

[176] G. K. H. Madsen, K. Schwarz, P. Blaha and D. J. Singh, Electronic structure and transport in type-I and type-VIII clathrates containing strontium, barium, and europium, *Phys. Rev. B*, 68, (2003) 125212 .

[177] L. Zhang, M. -H. Du and D. J. Singh, Zintl-phase compounds with SnSb4 tetrahedral anions: Electronic structure and thermoelectric properties, *Phys. Rev. B*, 81, (2010) 075117.

[178] Paolo Giannozzi, Stefano Baroni, Nicola Bonini, Matteo Calandra, Roberto Car, Carlo Cavazzoni, Davide Ceresoli, Guido L Chiarotti, Matteo Cococcioni, Ismaila Dabo, Andrea Dal Corso, Stefano de Gironcoli, Stefano Fabris, Guido Fratesi, Ralph Gebauer, Uwe Gerstmann, Christos Gougoussis, Anton Kokalj, Michele Lazzeri, Layla Martin-Samos, Nicola Marzari, Francesco Mauri, Riccardo Mazzarello, Stefano Paolini, Alfredo Pasquarello, Lorenzo Paulatto, Carlo Sbraccia, Sandro Scandolo, Gabriele Sclauzero, Ari P Seitsonen, Alexander Smogunov, Paolo Umari and Renata M Wentzcovitch, *J. Phys.: Condens. Matter*, 21, (2009) 395502.

[179] S. Limpijumnong, W. R. L. Lambrecht and B. Segall, Electronic structure of $ZnGeP_2$: A detailed study of the band structure near the fundamental gap and its associated parameters, *Phy.Rev.B*, 60, (1999) 8087.

[180] A. S. Verma, B. K. Sarkar, S. Sharma, R. Bhandari and V. K. Jindal, Models for lattice thermal expansion and thermal conductivity for ternary (ANB2+NC27N) tetrahedral semiconductors, *Materials. Chem. Phy.*, 127, (2011) 74.

[181] S. K. Mishra, S. Satpathy and O. Jepsen. Electronic structure and thermoelectric properties of bismuth telluride and bismuth selenide, *J. Phys.: Condens. Matter* 9, (1997) 461-470.

[182] N. Taghizade, G. Rashedi, Z. Nourbakhsh and M. Farahi, Three dimensional topological insulators of $Cu_xAu_{1x}InTe_2$ alloys, *J. Alloys Compd.*, 593, (2014) 235.

[183] S. Hebert, D. Flahaut, C. Martin, S. Lemonnier, J. Noudem, C. Goupil, A. Maignan, J. Hejtmanek, Thermoelectric properties of perovskites: Sign change of the Seebeck coefficient and high temperature properties, *Progress in Solid State Chemistry*, 35, (2007) 457.

[184] V. V. Maslyuk, S. Achilles, L. Sandratskii, M. Brandbyge and I. Mertig, Thermopower switching by magnetic field: First-principles calculations, *Phys. Rev. B*, 88, (2013)081403(R).

[185] D. Kim, K. Kurosaki, Y. Ohishi, H. Muta and S. Yamanaka, Reduction in Lattice Thermal Conductivity of InSb by Formation of the ZnIn18GeSb20 Alloy, *Material Transactions*, 53, (2012) 1976.

[186] H. Peña-Pedraza, S. A. Lopez-Rivera, J. M. Martin, J. M. Delgado and Ch. Power, Crystal and phonon structure of $ZnSiP_2$, a II-IV-V2 semiconducting compound, *Mater.Sci. Eng. B,* 177, (2012) 1465.

[187] B. R. Pamplin, T. Kiyosawa and K. Masumoto, Ternary chalcopyrite compounds, *Prog. Crystal Growth Charact.*,1, (1979) 331.

[188] F. Boukabrine, F. Chiker, H. Khachai, A. Haddou, N. Baki, R. Khenata, B. Abbar and A. Khalfi, Ab initio calculation of $ZnSiAs_2$ and $CdSiAs_2$ semiconductor compounds, *Physica B*, 406, (2011) 169.

[189] S. Sharma and A. S. Verma, Structural, electronic, optical, elastic and thermal properties of $ZnXAs_2$ (X = Si and Ge) chalcopyrite semiconductors, *Eur. Phys. J. B*, 87, (2014) 159.

[190] Aaron D.Martinez, Emily L. Warren, Prashun Gorai, Kasper A. Borup, Darius Kuciauskas, Patricia C. Dippo, Brenden R. Ortiz, Robin T. Macaluso, Sau D. Nguyen, Ann L. Greenaway, Shannon W. Boettcher, Andrew G. Norman, Vladan Stevanovi, Eric S. Toberer, and Adele C. Tamboli, Solar energy conversion properties and defect physics of $ZnSiP_2$, *Energy Environ. Sci.*, 9, (2016) 1031.

[191] A. Mackinno, Numerical data and functional relationships in science and technology, in: O. Madelung (Ed.), Landolt-Brnstein New Series, Group III, vol. 17, Pt. h, Springer, Berlin, 1985, 9.

[192] F. Boukabrine, F. Chiker, H. Khachai, A. Haddou, N. Baki, R. Khenata, B. Abbar, A Khalfi, Ab initio calculation of ZnSiAs2 and $CdSiAs_2$ semiconductor compounds, *Physica B*, 406 (2011) 169-176.

[193] Mohnish Pandey, Korina Kuhar, and Karsten W. Jacobsen, IIIVV 2 and IIIIIIV 2 Polytypes as Light Absorbers for Single Junction and Tandem Photovoltaic Devices, *J. Phys. Chem. C*, 121, 2017) 17780-17786.

[194] G.C. Xing, K.J. Bachmann, J.B. Posthill and M.L. Timmons, ZnGeP2: A Wide Bandgap Chalcopyrite structure semiconductor for nonlinear Optical Applications, *Mat. Res. Soc. Symp. Proc.*, 162, (1990) 615.

[195] A. Janotti, Su-Huai Wei, S. B. Zhang, and Sarah Kurtz, Structural and electronic properties of $ZnGeAs_2$, *Phys. Rev. B*, 63, 195210.

[196] J. L. Shay, B. Tell, E. Buehler and J. H. Wernick, Band Structure of $ZnGeP_2$ and $ZnSiP_2$ Ternary Compounds with Pseudodirect Energy Gaps, *Phys. Rev. Lett.*, 30, (1973) 983.

[197] J. C. Rife, R. N. Dexter, P. M. Bridenbaugh and B. W. Veal, Optical properties of the chalcopyrite semiconductors $ZnGeP_2$, $ZnGeAs_2$, $CuGaS_2$, $CuAlS_2$, $CuInSe_2$, and $AgInSe_2$, *Phys. Rev. B*, 16, (1977) 4491.

[198] H. S. Saini, M. Singh, A. H. Reshak and M. K. Kashyap, Effect of cation substitution on electronic band structure of $ZnGeAs_2$ pnictides: A mBJLDA approach, *J. Alloys Compd.* 518, (2012) 74.

[199] N. A. Goryunova, M. L. Belle, L. B. Zlatkin, G. V. Loshakova, A. S. Poplavnoi and V. A. Chaldyshev, *Fiz. Tekh. Poluprovodn.*, 2, (1968) 1344.

[200] S. Mishra and B. Ganguli, Effect of pd hybridization, structural distortion and cation electronegativity on electronic properties of $ZnSnX_2$ (X=P, As, Sb) chalcopyrite semiconductors, *J. Solid State Chem.*, 200, (2013) 279.

[201] Y. V. Rud, V. Sovolev, S. N. Shestatskii, *Fiz. Tekh. Poluprovodn.*, 2, (1968) 893.

[202] David O. Scanlon and Aron Walsh, Bandgap engineering of $ZnSnP_2$ for high-efficiency solar cells, *Appl. Phys. Lett.* 100, (2012) 251911.

[203] W. M. Ducan, A.F. Schreine, S.M. Bedair, M.A.Littlejohn, Electronic structure of the LPE grown semiconductor, p-ZnSnAs2, explored by newly-observed laser-excited photoluminescence, *Journal of Luminescence*, 21, (1980) 137-146.

[204] Walter Scott, Preparation and some properties of ZnSnSb2, *Journal of Applied Physics*, 44, (1973) 5165.

[205] Ami Nomura, Seongho Choi, Manabu Ishimaru, Atsuko Kosuga, Thomas Chasapis, Saneyuki Ohno, G. Jeffrey Snyder, Yuji Ohishi, Hiroaki Muta, Shinsuke Yamanaka, and Ken Kurosaki, Chalcopyrite ZnSnSb2: A Promising Thermoelectric Material, *ACS Appl. Mater. Interfaces*, 2018, 10, 43682-43690.

[206] W. Scott, Preparation and some properties of $ZnSnSb_2$, *J. Appl. Phys.* 44, (1973) 5165-5166.

[207] J. E. Jaffe and A. Zunger, Theory of the band-gap anomaly in ABC2 chalcopyrite semiconductors, *Phys. Rev.B*, 29, (1984) 4.

[208] Charles Kittel *1*986, Introduction to Solid State Physics, John Wiley Sons, Inc. New York.

[209] W. Feng, Di Xiao, Jun Ding and Yugui Yao, Three-Dimensional Topological Insulators in IIIIVI2 and IIIVV2 Chalcopyrite Semiconductors, *P*hys. Rev. Lett. 2011 106, 016402.

[210] Li Bin Guo, Yuan Xu Wang, Yu Li Yan, Gui Yang, Jue Ming Yang, and Zhen Zhen Feng, Electronic structure and thermoelectricproperties of orthorhombic SrLiAs, *Journal of Applied Physics*,116, (2014) 033705.

[211] R. R. Reddy, Y. N. Ahammed, K. R. Gopal and D V Raghwam, *Indian Journal of Pure and Applied Physics*, 1999, 37, 25-28.

.

[212] Alexander J. Samuels and J. David Carey, Engineering Graphene Conductivity for Flexible and High-Frequency Applications, *ACS Appl. Mater. Interfaces* 2015 **7**, 22246.

[213] Gianluca Giovannetti, Petr A. Khomyakov, Geert Brocks, Paul J. Kelly and Jeroen van den Brink, Substrate-induced band gap in graphene on hexagonal boron nitride: Ab initio density functional calculations, *Phys. Rev. B*, 76, (2007) 073103.

[214] Lanqing, Yongping Zheng and Jin-Cheng Zheng, Thermoelectric transport properties of PbTe under pressure, *Phys. Rev. B* 82, (2010) 195102.

[215] Tian Liang, Quinn Gibson, Mazhar N. Ali, Minhao Liu, R. J. Cava and N. P. Ong, Ultrahigh mobility and giant magnetoresistance in the Dirac semimetal Cd_3As_2, *Nature Materials,* 2015, **1**4, 280-284.

[216] Dmitry V. Fedorov, Martin Gradhand, Sergey Ostanin, Igor V. Maznichenko, Arthur Ernst, Jaroslav Fabian, and Ingrid Mertig, Impact of Electron-Impurity Scattering on the Spin Relaxation Time in Graphene: A First-Principles Study, *Phy. Rev. Lett,* 2013 **1**10, 156602.

[217] Ming Tan, Yanming Hao, Gangzhi Wang, *Journal of Solid State Chemistry*,2014, **2**15, 219- 224.

[218] Li-Dong Zhao, Shih-Han Lo, Yongsheng Zhang, Hui Sun, Gangjian Tan, Ctirad Uher, C. Wolverton, Vinayak P. Dravid, Mercouri G. Kanatzidis, Ultralow thermal conductivity and high thermoelectric figure of merit in SnSe crystals, *Nature*,508, (2014) 373-377.

[219] X. J. Tan, H. Z. Shao, J. He, G. Q. Liu, J. T. Xu, J. Jiang, H. C. Jiang, Band engineering and improved thermoelectric performance in M-doped SnTe (M = Mg, Mn, Cd, and Hg), *Phys. Chem. Chem. Phys.*, 18, (2016) 7141-7147.

[220] Giri Joshi, Xiao Yan, Hengzhi Wang, Weishu Liu, Gang Chen, and Zhifeng Ren. Enhancement in Thermoelectric Figure-Of-Merit of an N-Type Half-Heusler Compound by the Nanocomposite Approach, *Adv. Energy Mater.* 2011, 1, 643-647.

[221] Koushik Pal, Shashwat Anand and Umesh V. Waghmare, Thermoelectric properties of materials with nontrivial electronic topology, *J. Mater. Chem. C,*, 3, (2015) 12130.

[222] Gangjian Tan, Li-Dong Zhao, and Mercouri G. Kanatzidis, Rationally Designing High-Performance Bulk Thermoelectric Materials, *Chem. Rev.,*, 116 (19),(2016) 12123 - 12149

[223] L. D. Hicks and M. S. Dresselhaus, Effect of quantum-well structures on the thermoelectric figure of merit, *Phys. Rev. B*, 47(1993) 12727.

[224] K. Kuroki and R. Arita, Pudding Mold Band Drives Large Thermopower in $NaxCoO_2$, *J. Phys. Soc. Jpn.* 76 (2007) 083707.

[225] I. Terasaki, Y. Sasago and K. Uchinokura, Large thermoelectric power in NaCo2O4 single crystals, *Phys. Rev. B 56 (1997)12685.*

[226] D.J. Singh, Electronic structure of $NaCo2O_4$, *Phys. Rev. B*, 61 (2000) 13397.

[227] Hidetomo Usui, Kazuhiko Kuroki, Seiya Nakano, Kazutaka Kudo, and Minoru Nohara, Large Seebeck effect in electron-doped $FeAs_2$ driven by a quasi-one-dimensional pudding-mold-type band, *Phys. Rev. B*, 88 (2013) 075140.

[228] Y. Kamihara, T. Watanabe, M. Hirano and H. Hosono, Iron-Based Layered Superconductor La[O1-xFx]FeAs (x = 0.050.12) with Tc = 26 K, *J. Am. Chem. Soc.*, 130 (2008) 3296.

[229] F. Han, X. Zhu, G. Mu, P. Cheng and H.H. Wen, SrFeAsF as a parent compound for iron pnictide superconductors, *Phys. Rev. B*, 78 (2008) 180503

[230] M. Palazzi, S. Jaulmes, Structure du conducteur ionique (LaO)AgS, *Acta Crystallogr. B*, 37 (1981)1337-1339.

[231] S. K. Saha, Exploring the origin of ultralow thermal conductivity in layered BiO-CuSe,*Phys. Rev. B*, 92 (2015) 041202(R).

[232] V. K. Gudelli, V. Kanchana, G. Vaitheeswaran, David J. Singh, A. Svane, N. E. Christensen and S. D. Mahanti, Electronic structure, transport, and phonons of SrAgChF (Ch = S, Se, Te): Bulk superlattice thermoelectrics, *Phys. Rev B*, 92 (2015) 045206.

[233] P. Blaha, K. Schwarz, G. K. H. Madsen, D. Kvasnicka, and J. Luitz, WIEN2K, *An augmented plane wave + local orbitals program for calculating crystal properties.* (Karlheinz Schwarz, Techn. Universität Wien, Austria), 2001.

[234] J. P. Perdew, K. Burke, M. Ernzerhof, Generalized Gradient Approximation Made Simple, *Phys. Rev. Lett.,*, 77 (1996) 3865-3868.

[235] F. Tran, and P. Blaha, Accurate Band Gaps of Semiconductors and Insulators with a Semilocal Exchange-Correlation Potential, *Phys. Rev. Lett.*, 102 (2009) 226401.

[236] G. K. H. Madsen, and D. J. Singh, BoltzTraP. A code for calculating band-structure dependent quantities, *Comput. Phys. Commun.* 175 (2006) 67-71.

[237] D. I. Bilc, S. D. Mahanti, and M. G. Kanatzidis, Electronic transport properties of PbTe and $AgPb_mSbTe_{2+m}$ systems, *Phys. Rev. B*, 74 (2006) 125202.

[238] J. M. Ziman, *Electrons and Phonons: Theory of Transport Phenomena in Solids* (Oxford University Press, London, UK, 1960).

[239] B. R. Nag, *Electron Transport in Compound Semiconductors* (Springer-Verlag, Berlin, 1980).

[240] D. J. Singh, and I. I. Mazin, Calculated thermoelectric properties of La-filled skutterudites, *Phys. Rev. B*, 56 (1997) R1650.

[241] D. J. Singh, Thermopwer of SnTe from Boltzmann transport calculations, *Funct. Mat. Lett.*, 3 (2010) 223-226.

[242] D. Parker, and D. J. Singh, Thermoelectric properties of AgGaTe2 and related chalcopyrite structure materials, *Phys. Rev. B*, 85 (2012) 125209.

[243] K. P. Ong, D. J. Singh, and P. Wu, Analysis of the thermoelectric properties of n-type ZnO, *Phys. Rev. B*, 83 (2011) 115110.

[244] P. Giannozzi, S. Baroni, N. Bonini, M. Calandra, R. Car, C. Cavazzoni, D. Ceresoli, G. L. Chiarotti, M. Cococcioni, I. Dabo, A. Dal Corso, S. Fabris, G. Fratesi, S. de Gironcoli, R. Gebauer, U. Gerstmann, C. Gougoussis, A. Kokalj, M. Lazzeri, L. Martin-Samos, N. Marzari, F. Mauri, R. Mazzarello, S. Paolini, A. Pasquarello, L. Paulatto, C. Sbraccia, S. Scandolo, G. Sclauzero, A. P. Seitsonen, A. Smogunov, P. Umari, R. M. Wentzcovitch, *J.Phys.:Condens.Matter*, 21, 395502 (2009)

[245] G. Kresse and J. Hafner, Ab initio molecular dynamics for liquid metals, *Phys. Rev. B*, 47 (1993) 558.

[246] S. K. Saha and G. Dutta, Elastic and thermal properties of the layered thermoelectrics BiOCuSe and LaOCuSe, *Phys. Rev. B*, 94 (2016) 125209.

[247] A. Zakutayev, R. Kykyneshi, G. Schneider, D. H. McIntyre, and J. Tate, Electronic structure and excitonic absorption in BaCuChF (Ch=S, Se, and Te), *Phys. Rev. B*, 81 (2010) 155103.

[248] T. Takeuchi, Conditions of Electronic Structure to Obtain Large Dimensionless Figure of Merit for Developing Practical Thermoelectric Materials, *Mater. Trans.*, 50 (2009) 2359.

[249] Y. Katsura and H. Takagi, MgSrSi-Type Compounds as a Possible New Family of Thermoelectric Materials, *Journal of Electronic Materials*, 42 (2013) 1365-1368

[250] R. Hill, The Elastic Behaviour of a Crystalline Aggregate, *Proc. Phys. Soc.*,, Sect. A, 65 (1952) 349-354.

[251] Li-Dong Zhao, Shih-Han Lo, Yongsheng Zhang, Hui Sun, Gangjian Tan , Ctirad Uher, C. Wolverton, Vinayak P. Dravid Mercouri G. Kanatzidis, Ultralow thermal conductivity and high thermoelectric figure of merit in SnSe crystals, *Nature*, 508 (2014) 373-377.

[252] G. A. Slack, Nonmetallic crystals with high thermal conductivity, *J. Phys. Chem. Solids*, 34 (1973) 321-335.

[253] D.G. Cahill, S.K. Watson, R.O. Pohl, Lower limit to the thermal conductivity of disordered crystals, *Phys. Rev. B*, 46 (1992) 6131.

[254] Hiroshi Yanagi, Janet Tate, Sangmoon Park, Cheol-Hee Park, Douglas A. Keszler, Masahiro Hirano and Hideo Hosono, Valence band structure of BaCuSF and BaCuSeF, *J. of Appl. Phys.*, 100 (2006) 083705.

[255] Cheol-Hee Park, Robert Kykyneshi, Alexandre Yokochi, Janet Tate, Douglas A. Keszler, Structure and physical properties of BaCuTeF, *Journal of Solid State Chemistry*, 180, (2007) 1672-1677.

[256] P. M. Palazzi and S. Jaulmes, Structure du conducteur ionique (LaO)AgS, *Acta Cryst. B*, 37 (1981) 1337-1339.

[257] Minping Zhang, Wei, Junhong; Wang, Guangtao, Thermoelectric and topological properties of half-Heusler compounds ZrIrX(As, Sb, Bi), *Physics Letters A*, 382, 2018, 673

[258] Gang Yang, Junwei Liu, Liang Fu, Wenhui Duan, and Chaoxing Liu, Weak topological insulators in PbTe/SnTe superlattices, *Phys. Rev. B*, 89, 2014, 085312

[259] Yong Xu, Thermoelectric effects and topological insulators, *Chinese Physis B*, 25 2016, 11

[260] VijayKumarGudelli, VKanchana and GVaitheeswaran, Predicted thermoelectric properties of olivine-type Fe2GeCh4 (Ch=S, Se and Te), *J. Physics: Condens. Matter.*,, 28, 2016, 025502

[261] Tao Fan, Congwei Xie, Shiyao Wang, Artem R. Oganov and Laifei Cheng, First-principles study of thermoelectric properties of Mg_2SiMg_2Pb semiconductor materials, *RSC Adv.*, 8, 2018,17168

[262] Yandong Ma, Ying Dai, Liangzhi Kou, Thomas Frauenheim, and Thomas Heine, Robust Two-Dimensional Topological Insulators in Methyl-Functionalized Bismuth, Antimony, and Lead Bilayer Films, *Nano Lett.*,, 15, 2015, 1083

[263] Masayuki Ochi, Ryotaro Arita, Nandini Trivedi, and Satoshi Okamoto, Strain-induced topological transition in $SrRu_2O_6$ and $CaOs_2O_6$, *Phys. Rev, B*, 93, 2016, 195149

[264] Min Zhang, Xiangqi Wang1, Azizur Rahman, Qunsong Zeng, Da Huang, Rucheng Dai, Zhongping Wang, and Zengming Zhang, Pressure-induced topological phase transitions and structural transition in 1T-$TiTe_2$ single crystal, *Appl. Phys. Lett.,*, 112, 2018, 041907

[265] Ramzy Daou, Raymond Frsard, Sylvie Hbert, Antoine Maignan, Impact of short-range order on transport properties of the two-dimensional metal $PdCrO_2$, *Phys. Rev. B,* 92, 2015, 245115

[266] Yonatan Dubi, Possible origin of thermoelectric response fluctuations in single-molecule junctions, *New Journal of Physics*, 15, 2013, 105004

[267] Yong Lu and Bruce R Patton, Fluctuation thermopower above the superconducting transition temperature, *Phys.: Candens. Matter,* 7, 1995, 9247

[268] B. L. Gallagher, T. Galloway,P. Beton,J. P. Oxley,S. P. Beaumont,S. Thoms, and C. D. W. Wilkinson, *Phys. Rev. Lett*, 64, 1990, 2058

[269] Marcin Matusiak, J.R. Cooper Dariusz Kaczorowski, Thermoelectric quantum oscillations in ZrSiS, *Nature Communications volume*, 8, 2017, 15219

[270] Tianyu Liu, D. I. Pikulin, and M. Franz, Quantum oscillations without magnetic field, *Phys. Rev. B*, 95, 2017, 041201(R)

[271] E. Rossi, J. H. Bardarson, M. S. Fuhrer, and S. Das Sarma, Universal Conductance Fluctuations in Dirac Materials in the Presence of Long-range Disorder, *Phys. Rev. Lett,*, 109, 2012, 096801

[272] Li Bin Guo, Yuan Xu Wang, Yu Li Yan, Gui Yang, Jue Ming Yang, and Zhen Zhen Feng, Electronic structure and thermoelectric properties of orthorhombic SrLiAs, *J. Appl. Phy*, 116, 2014, 033705

[273] Saleem Ayaz Khan, A.H. Reshak, Optoelectronic and transport properties of Zintl phase KBa2Cd2Sb3 compound, *Computational Materials Science*, 95, 2014, 328

[274] S. Baroni, S. D. Gironcoli and A. dal Corso et al, 2008. ¡ http : //www.pwscf.org ¿

[275] M. P. L. Sancho, J. M. L. Sancho and J. Rubio, Quick iterative scheme for the calculation of transfer matrices: application to Mo (100), *J. Phys. F: Met.Phys.,* 14, 1984, 1205.

[276] W. QuanSheng, S. N. Zhang, H.-F. Song, M. Troyer and A. A. Soluyanov, 2017, arXiv:1703.07789v2 [physics.comp-ph].

[277] Liang Fu, C.L. Kane, Topological insulators with inversion symmetry, *Phys. Rev. B*, 76, 2007, 045302

[278] D.G. Cahill,S.K.Watson,R.O.Pohl, Lower limit to the thermal conductivity of disordered crystals, *Phys.Rev.B*, 46, 1992, 6131.

[279] A. Saoudi, et. al, First principles study of the structural, elastic, electronic and optical properties of CaSrTt (Tt=Si, Ge, Sn and Pb), *Solid State Communications*, 152, 2012, 1800-1806

[280] Wen-Hui Xie, Ya-Qiong Xu, Bang-Gui Liu and D. G. Pettifor,Half-Metallic Ferromagnetism and Structural Stability of Zincblende Phases of the Transition-Metal Chalcogenides, *Phys. Rev. Lett*, 91, (2003), 037204.

[281] Thomas Heine, Transition Metal Chalcogenides: Ultrathin Inorganic Materials with Tunable Electronic Properties, *A*cc. Chem. Res, 48, (2015), 65

[282] Wen-Hui Xie, Bang-Gui Liu and D. G. Pettifor,Half-metallic ferromagnetism in transition metal pnictides and chalcogenides with wurtzite structure, *P*hys. Rev. B, 68, (2003) 134407

[283] Deep Jariwala, Vinod K. Sangwan, Lincoln J. Lauhon, Tobin J. Marks, and Mark C. Hersam, Emerging Device Applications for Semiconducting Two-Dimensional Transition Metal Dichalcogenides, *A*CS Nano, 8 (2), (2014), 1102.

[284] XiaoLi,HongweiZhu, Two-dimensional MoS2: Properties, preparation, and applications, Journal of Materiomics, 1, (2015),

[285] Dmitry Ovchinnikov, Adrien Allain, Ying-Sheng Huang, Dumitru Dumcenco, and Andras Kis*, Electrical Transport Properties of Single-Layer WS2

[286] Yifei Yu, Guoqing Li, Lujun Huang, Andrew Barrette, Yong-Qing Cai, Yiling Yu, Kenan Gundogdu, Yong-Wei Zhang, and Linyou Cao, Enhancing Multifunctionalities of Transition-Metal Dichalcogenide Monolayers via Cation Intercalation, ACS Nano, 11, (2017), 9390

[287] Hang Chen, Tianjiao Liu, Zhiqiang Su, Li Shang and Gang Wei,2D transition metal dichalcogenide nanosheets for photo/thermo-based tumor imaging and therapy, *N*anoscale Horiz, 3, (2018), 74.

[288] Dong Gwon Moon, Rehan, Shanza; Lim, Soo Yeon; Nam, Dahyun; Seo, Ilwan; Gwak, Jihye; Cheong, Hyeonsik; Cho, Yong Soo; Lee, Yunsang; Ahn, SeJin Structural, optical and electrical impacts of marcasite in pyrite thin films, *S*olar Energy, 159, (2018) 930.

[289] Wen, Xiangli; Liang, Yuxuan; Bai, Pengpeng; Luo, Bingwei; Fang, Teng; Yue, Luo; An, Teng; Song, Weiyu; Zheng, ShuqiFirst-principles calculations of the structural, elastic and thermodynamic properties of mackinawite (FeS) and pyrite (FeS2), *P*hysica B: Condensed Matter, 15, (2017) 119.

[290] Vijay Kumar Gudelli, et. al, 2013, Phase Stability and Thermoelectric Properties of the Mineral FeS2: An Ab Initio Study, *J*. Phys. Chem. C, 117, (2013) 21120.

[291] Daniel E. Bugaris, Christos D. Malliakas, Daniel P. Shoemaker, Dat T. Do, Duck Young Chung, Subhendra D. Mahanti, and Mercouri G. Kanatzidis, Crystal Growth and Characterization of the Narrow-Band-GapSemiconductors $OsPn_2$ (Pn = P, As, Sb), *I*norg. Chem., 53, (2014) 9959-9968.

[292] Vijay Kumar Gudelli, V. Kanchana, G. Vaitheeswaran, M. C. Valsakumarc and S. D.Mahantid, Thermoelectric properties of marcasite and pyrite FeX_2 (X= Se, Te): a first principle study, **R**SC Adv., 4, (2014) 9424.

[293] S. Tongay, Hasan Sahin, Changhyun Ko, Alex Luce, Wen Fan, Kai Liu, Jian Zhou, Ying-Sheng Huang, Ching-Hwa Ho, Jinyuan Yan, D. Frank Ogletree, Shaul Aloni, Jie Ji, Shushen Li, Shushen Li, Jingbo Li, F. M. Peeters, Junqiao Wu, Monolayer behaviour in bulk ReS_2 due to electronic and vibrational decoupling, Nature Communications, 5 (2014) 3252.

[294] Zhao Zhao, Haijun Zhang, Hongtao Yuan, Shibing Wang, Yu Lin, Qiaoshi Zeng, Gang Xu, Zhenxian Liu, G. K. Solanki, K. D. Patel, Yi Cui, Harold Y. Hwang Wendy L. Mao, Pressure induced metallization with absence of structural transition in layered molybdenum diselenide, *Nature Communications*, 6 (2015) 7312.

[295] S. Song, Dong Hoon Keum, Suyeon Cho, David Perello, Yunseok Kim, and Young Hee Lee, Room Temperature SemiconductorMetal Transition of $MoTe_2$ Thin Films Engineered by Strain, *Nano Lett.* 16 (2016) 188.

[296] X. Wang, Xuliang Chen, Yonghui Zhou, Changyong Park, Chao An, Ying Zhou, Ranran Zhang, Chuanchuan Gu, Wenge Yang Zhaorong Yang, Pressure-induced iso-structural phase transition and metallization in WSe_2, *Scientific Reports*, 7 (2017) 46694.

[297] K. Friemelt, M.Ch. LuxSteiner, and E. Bucher, Optical properties of the layered transitionmetaldichalcogenide ReS_2: Anisotropy in the van der Waals plane, *Journal of Applied Physics*, 74 (1993) 5266.

[298] E. Zhang, Yibo Jin, Xiang Yuan, Weiyi Wang, Cheng Zhang, Lei Tang, Shanshan Liu, Peng Zhou, Weida Hu Faxian Xiu, ReS2Based FieldEffect Transistors and Photodetectors, *Advanced Functional materials*, 25 (2015) 4076.

[299] Chris M. Corbet, Connor McClellan, Amritesh Rai, Sushant Sudam Sonde, Emanuel Tutuc, and Sanjay K. Banerjee, Field Effect Transistors with Current Saturation and Voltage Gain in Ultrathin ReS_2, *ACS Nano*, 9 (2015) 363.

[300] Yan-ling Li, Yunguo Lib, Chunlin Tang, Strain engineering and photocatalytic applicationof single-layer ReS_2, *International Journal of hydrogen energy* , 42 (2017) 161-167.

[301] Y.M.Min, A.Q.Wang X. M.Ren L.Z.LiuX.L.Wu, Defect formation and electronic structure regulated by strain engineering in ReS_2, *Applied surface sciences*, 427 (2018) 942.

[302] Wen Wen, Yiming Zhu, Xuelu Liu, HungPin Hsu, Zhen Fei, Yanfeng Chen, Xinsheng Wang, Mei Zhang, KuanHung Lin, FeiSheng Huang, YiPing Wang, YingSheng Huang, ChingHwa Ho, PingHeng Tan, Chuanhong Jin, Liming Xie, Anisotropic Spectroscopy and Electrical Properties of 2D ReS2(1x)Se2x Alloys with Distorted 1T Structure, *small*, (2017) 1603788.

[303] D. A. Chenet, O. Burak Aslan, Pinshane Y. Huang, Chris Fan, Arend M. van der Zande, Tony F. Heinz, and James C. Hone, In-Plane Anisotropy in Mono- and Few-Layer ReS2 Probed by Raman Spectroscopy and Scanning Transmission Electron Microscopy *Nano Lett.*, 15 (2015) 5667.

[304] Yung-Chang Lin, Hannu-Pekka Komsa, Chao-Hui Yeh, Torbjrn Bjrkman, Zheng-Yong Liang, Ching-Hwa Ho, Ying-Sheng Huang, Po-Wen Chiu, Arkady V. Krasheninnikov, and Kazu Suenaga, Single-Layer ReS2: Two-Dimensional Semiconductor with Tunable In-Plane Anisotropy, *ACS Nano*, 9 (2015) 11249.

[305] Dawei Zhou, Yonghui Zhou, Chunying Pu, Xuliang Chen, Pengchao Lu, Xuefei Wang, Chao An, Ying Zhou, Feng Miao, Ching-Hwa Ho, Jian Sun, Zhaorong Yang Dingyu Xing, Pressure-induced metallization and superconducting phase in ReS_2, *npj Quantum Materials*, 2 (2017) 19.

[306] S. Bhattacharyya, Tribhuwan Pandey and Abhishek K Singh, Effect of strain on electronic and thermoelectric properties of few layers to bulk MoS_2, *Nanotechnology*, 25, (2015) 465701.

[307] Radi A. Jishi, Oliver B. Ta, and Adel A. Sharif, 2014, **P**hys. Chem. C, **1**18, 28344.

[308] G. Kresse, J. Furthmuller, Comput. Mater. Sci. 6 (1996) 15.

[309] A. Tkatchenko, R. A. Di Stasio, R. Car, and M. Scheffler, Accurate and Efficient Method for Many-Body van der Waals Interactions, *Phys. Rev. Lett.*, 108 (2012) 236402.

[310] Mette S. Schmkel, Lasse Bjerg, Simone Cenedese, Mads R. V. Jrgensen, Yu-Sheng Chen, Jacob Overgaard and Bo B. Iversen, *C*hem. Sci., 5, (2014) 1408.

[311] Tetsur Nakamura, Influences of Mass and Bond Length on the Debye Temperatures of Ionic and Covalent Substances, *Japanese Journal of Applied Physics*, 20, 1981, L653-L565.

[312] M. Born, K. Huang, Dynamical Theory of Crystal Lattices, Clarendon, Oxford, 1954.

[313] E. Guler and M. Guler, 2015 , *C*HINESE JOURNAL OF PHYSICS, *5*3, 2.

[314] Vijay Kumar Gudelli, V. Kanchana, S. Appalakondaiah, G. Vaitheeswaran and M. C. Valsakumar, Phase Stability and Thermoelectric Properties of the Mineral FeS2: An Ab Initio Study, *J.* Phys. Chem. C , 117, (2013) 21120.

[315] T NaKamura, 1981, *J*apanese Journal of applied Physics, **2**0, 9.

[316] Je-Hyeong Bahk and Ali Shakouri, Minority carrier blocking to enhance the thermoelectric figure of merit in narrow-band-gap semiconductors, *P*hys. Rev. B, 93 (2016) 165209

[317] Tribhuwan Pandey and Abhishek K. Singh, Origin of enhanced thermoelectric properties of doped CrSi2, *P*hys. Chem. Chem. Phys, 17, (2015) 16917

[318] Sutarno, , Osvald Knop, and , K.I.G. Reid, Chalcogenides of the transition elements. V. Crystal structures of the disulfides and ditellurides of ruthenium and osmium, *C*an. J. Chem. 45, (1967) 1391-1400.

[319] W. N. STASSEN and R. D. HEYDING, Crystal structures of RuSe2, OsSe2, PtAs2, and -NiAs2, *C*anadian Journal of Chemistry, 46, (1968) 2159

[320] Sandip Dey and Vimal K. Jain, Platinum Group Metal Chalcogenides, *P*latinum Metals Rev., 48, (2004) 16.

[321] C H Ho, Y S Hauang, K K Tiong and P C Liao, In-plane anisotropy of the optical and electrical properties of layered ReS2 crystals, *J. Phys:, Condens. Mater*, 11 (1999) 5367 .

[322] H.H. Murray, et al., *Inorg. Chem.* 33 (1994) 4418.

[323] Wildervanck J and Jellinek F *J. Less-Common Met.* 24 (1971) 7381

[324] Bhakti Jariwala, Arumugum Thamizhavel and Arnab Bhattacharya, ReSe2: a reassessment of crystal structure and thermal analysis, J. Phys. D: Appl. Phys. 50 (2017) 044001.

[325] C. H. Ho and Y. S. Huang,J. L. Chen and T. E. Dann, K. K. Tiong, Electronic structure of ReS2 and ReSe2 from first-principles calculations, photoelectron spectroscopy, and electrolyte electroreflectance, *Phys. Rev. B*, 60 (1999) 766 .

[326] Daniel Wolverson, Simon Crampin, Asieh S. Kazemi, Adelina Ilie, and Simon J. Bending, Raman Spectra of Monolayer, Few-Layer, and Bulk ReSe2: An Anisotropic Layered Semiconductor, *ACS Nano*, 2014, 8, 11, 11154-11164.

[327] Ozgur Burak Aslan, ,Daniel A. Chenet, Arend M. van der Zande, James C. Hone, and Tony F. Heinz, Linearly Polarized Excitons in Single- and Few-Layer ReS_2 Crystals, *ACS Photonics*, 3, (2016), 96.

[328] D. Biswas, Alex M. Ganose, R. Yano, J. M. Riley, L. Bawden, O. J. Clark, J. Feng, L. Collins-Mcintyre, M. T. Sajjad, W. Meevasana, T. K. Kim, M. Hoesch, J. E. Rault, T. Sasagawa, David O. Scanlon, and P. D. C. King, Narrow-band anisotropic electronic structure of ReS_2, *Phys. Rev. B*, 96, (2017), 085205

[329] James L. Webb, * Lewis S. Hart, and Daniel Wolverson, Chaoyu Chen, Jose Avila, and Maria C. Asensio, Electronic band structure of ReS2 by high-resolution angle-resolved photoemission spectroscopy, *Phys. Rev. B*, 96, (2017) 115205

[330] J. P. Echeverry and I. C. Gerber, Theoretical investigations of the anisotropic optical properties of distorted 1TReS2 and ReSe2 monolayers, bilayers, and in the bulk limit, *Phys. Rev. B*, 97, (2018), 075123

[331] Ignacio Gutirrez-Lezama, Bojja Aditya Reddy, Nicolas Ubrig and Alberto F Morpurgo, Electroluminescence from indirect band gap semiconductor ReS2, *2D Mater.* 3 (2016) 045016

[332] C. Lee, Jisook Hong, Myung-Hwan Whangbo, and Ji Hoon Shim, Enhancing the Thermoelectric Properties of Layered Transition-Metal Dichalcogenides 2H-MQ2 (M = Mo, W; Q = S, Se, Te) by Layer Mixing: Density Functional Investigation, *Chem. Mater.*, 25 (2013) 3745 .

[333] Jason K. Ellis, Melissa J. Lucero,and Gustavo E. Scuseria, The indirect to direct band gap transition in multilayered MoS2 as predicted by screened hybrid density functional theory, *Applied Physics Letters*, 99 (2011) 261908 .

[334] S. Kumar and U. Schwingenschlo , Thermoelectric Response of Bulk and Monolayer MoSe2 and WSe2, *Chem. Mater.*, 27 (2015) 1278

[335] S. Chandra, S. Mathi Jaya and M.C. Valsakumar, Electronic structure of Li 2Pd 3B and Li 2Pt 3B, *Physica C* 432 (2005) 116

[336] Jurong Zhang, Ermiao Sun, Xiaolei Feng, Hanyu Liu, Simon A. T. Redfern, V. Kanchana, Guangtao Liu and Hongbo Wang, Phase transition and superconductivity in ReS 2 , ReSe 2 and ReTe 2, *Phys. Chem. Chem. Phys.*, 2018, 20, 29472

[337] V. K. Gudelli, V. Kanchana, G. Vaitheeswaran, D. J. Singh, A. Svane and N. E. Christensen and Subhendra D. Mahanti, Electronic structure, transport, and phonons of SrAgChF (Ch = S, Se, Te): Bulk superlattice thermoelectrics, *Phys. Rev. B*, 92 (2015) 045206

[338] G. Huai-Hong, Yang Teng, Tao Peng, and Zhang Zhi-Dong, Theoretical study of thermoelectric properties of MoS_2, *Chin. Phys. B*, 23 (2014) 017201.

List of Publications

Refereed journal papers

1. Sreeparvathy P. C., V. Kanchana and G. Vaitheeswaran, Thermoelectric properties of zinc based pnictides semiconductors, *J. of Applied Physics*, 119, (2016) 085701

2. Sreeparvathy P. C., V. Kanchana, G.Vaitheeswaran, and N. E. Christensen, $ZnGeSb_2$: A promising thermoelectric material with tunable ultra-high conductivity, *Phys. Chem. Chem. Phys*, 18, (2016) 26275-26283

3. Sreeparvathy P. C., V. Kanchana, Novel natural super-lattice materials with low thermal conductivity for thermoelectric applications: A first principles study, *Journal of Physics and Chemistry of Solids* 111, (2017) 5462.

4. Sreeparvathy P. C., V. Kanchana, Quantum fluctuation in thermopower at the topological phase transition in CaSrX (X: Si, Ge, Sn, Pb) studied from first principles theory, *J. Phys.: Conden. Matter*, 31, (2019), 095501

5. Sreeparvathy P. C., V. Kanchana, Giant thermopower in p type OsX_2 ((X: S, Se. Te) for a wide temperature range: A first principles study, *J. Phys.: Conden. Matter*, 30, (2018) 295501

6. Sreeparvathy P. C., V Kanchana, P Anees, G Vaitheeswaran, Emergence of Strain Induced Two Dimensional Metallic State in ReS_2, *Journal of Solid State Chemistry*, 269, (2019) 138-144

7. V. Rajaji, Utpal Dutta, P. C. Sreeparvathy, Saurav Ch. Sarma, Y.A. Sorb, B. Joseph, Subodha Sahoo, Sebastian C. Peter, V. Kanchana, Chandrabhas Narayana, Structural vibrational and electrical properties of 1T-$TiTe_2$ under hydrostatic pressure: Experiments and Theory, *Phys. Rev. B*, 97, (2018) 085107

8. Sanchayita Mondal, Chandan Mazumdar, R Ranganathan, Eric Alleno, PC Sreeparvathy, V Kanchana, G Vaitheeswaran, Ferromagnetically correlated Ru_2NbAl clusters in semimetallic Heusler alloy and its thermoelectric propertie, *Phy. Rev. B*, 98, 205130, (2018)

9. Anoop K. Chandran, Vijay Kumar Gudelli, Sreeparvathy P. C. and V. Kanchana, Structural and thermoelectric properties of Zintl-phase CaLiPn (Pn=As, Sb, Bi), *J. Sold State Chemistry*, 243, 198-206, (2016).

Conference papers

1. Sreeparvathy P. C., Vijay Kumar Gudelli, V. Kanchana, G. Vaitheeswaran, A. Svane and N. E. Christensen, Thermoelectric properties of binary LnN (Ln=La and Lu): First Principles Study, AIP Conference Proceedings, 1665, 110008 (2015)